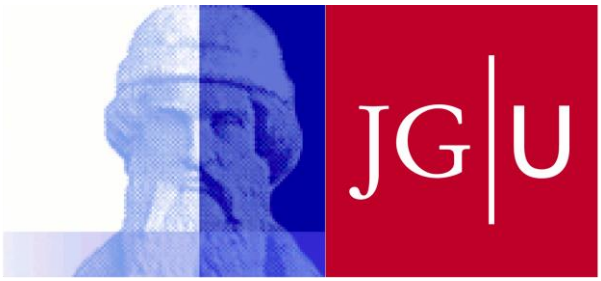

JOHANNES GUTENBERG
UNIVERSITÄT MAINZ

Role of the anterior *Hox* genes in segment-specific NB7-3 lineage development in the embryonic central nervous system of *Drosophila melanogaster*

Dissertation
zur Erlangung des Grades
Doktor der Naturwissenschaften

Am Fachbereich Biologie
der Johannes Gutenberg-Universität Mainz

Sudha Rani. Myneni
Mainz, May 2016

Chapter index

1. Introduction

Over a century of research has been invested in answering the fundamental question of how a single diploid cell constructs a whole organism consisting of complex organs with different tissues. Various pattern-forming genes usually restrict the developmental choices of groups of embryonic cells and allow formation of different tissues. Understanding the molecular mechanisms that control many developmental aspects of specification, proliferation and differentiation poses many challenges. Sequential activation of a complex cascade of patterning genes such as maternal-effect, gap and pair-rule genes in the *Drosophila melanogaster* cellular embryo establishes the anteroposterior (AP) and dorsoventral (DV) body axes. These events progressively drive segment polarity, columnar and homeotic (*Hox*) gene expression in the gastrulating embryo, which subdivide the embryo into ordered segments of the head, three gnathal, three thoracic and ten abdominal segments. *Hox* genes assign differential positional cues to the different body parts along the AP axis during development. The *Drosophila* embryonic central nervous system (CNS) serves as an excellent model system to clarify the developmental mechanisms that link positional information provided by *Hox* genes to cell-type specification. The aim of current research is to investigate the role of *Hox* genes in developmental patterning of the CNS that leads to segment-specific neuronal diversity.

1.1. *Drosophila* embryonic CNS development

The *Drosophila* CNS comprises the brain and the ventral nerve cord (VNC). In the early embryo, subsets of neural stem cell precursors called neuroblasts (NB) are derived from the ventral region of the ectoderm (Hartenstein and Campos-Ortega, 1985). The NBs arising from the ventral neurogenic region (vNR) generate the VNC and the ones from the procephalic neurogenic region (pNR) give rise to the brain (Fig. 1A, C). The dorsal epidermal ectoderm (dEpi) produces only ectodermal cells. The vNR is composed of mesoectoderm and neuroectoderm regions (Fig. 1B). From the mesoectoderm a specialized population of cells called midline precursors arises, from which the midline (ML) neurons and glia are generated (Bossing and Technau, 1994). The midline divides the neuroectoderm into two bilateral halves.

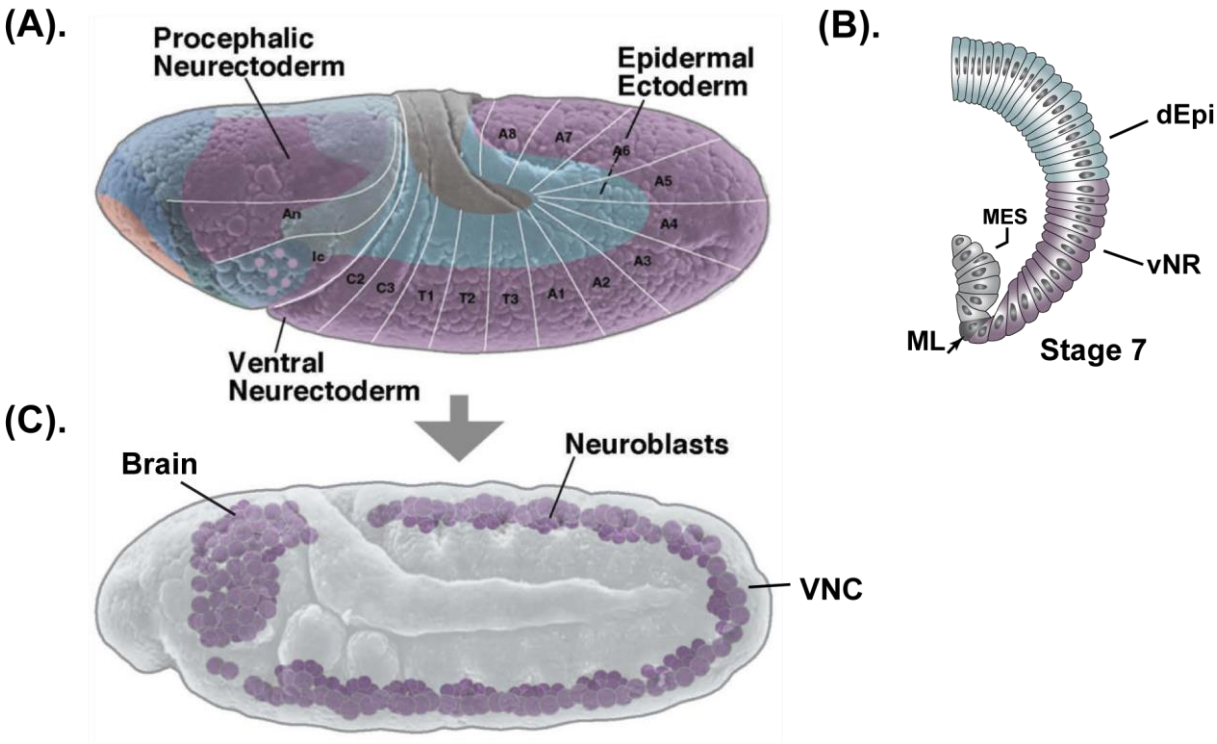

Fig. 1. Development of the *Drosophila* embryonic central nervous system.
(A) Lateral view of *Drosophila* embryo before NB formation. The outer ectoderm is divided into the ventral neuroectoderm and dorsal epidermal ectoderm (dEpi) regions, which are shaded in purple and blue, respectively. Black letters indicate the segments and the white lines represent the segment boundaries. (B) Cross-section of a gastrulating embryo showing dEpi (blue) and two regions of the ventral neuroectoderm: the mesoectoderm (MES, grey) and the ventral neurogenic region (vNR, purple). The mesoectoderm gives rise to midline (ML) cells. (C) Lateral view of *Drosophila* embryo after NB formation. The NBs formed from the vNR and procephalic neuroectoderm subsequently generate the VNC and the brain, respectively. Scheme adapted from Hartenstein and Wodarz, 2013.

Each half of the segmental neuromere is called the hemineuromere. Altogether, the VNC region is separated into repeated units of six gnathal, six thoracic and twenty abdominal hemineuromeres. The graded action of NF-kB, bone morphogenetic protein (BMP) and epidermal growth factor receptor (EGFR) signaling pathways establish the DV pattern by initiating expression of the columnar genes in three rows (Fig. 2A) (Skeath, 1998, 1999; Bhat, 1999; Ohlen and Doe, 2000). This sub-division activates the specific combination of so-called proneural genes, which are known to provide neural competence (Fig. 2B). Altogether, within each hemineuromere, superimposition of segment-polarity and dorsoventral patterning gene activities, in conjunction with specific *Hox* gene expression combination provides unique positional information to the neural precursors.

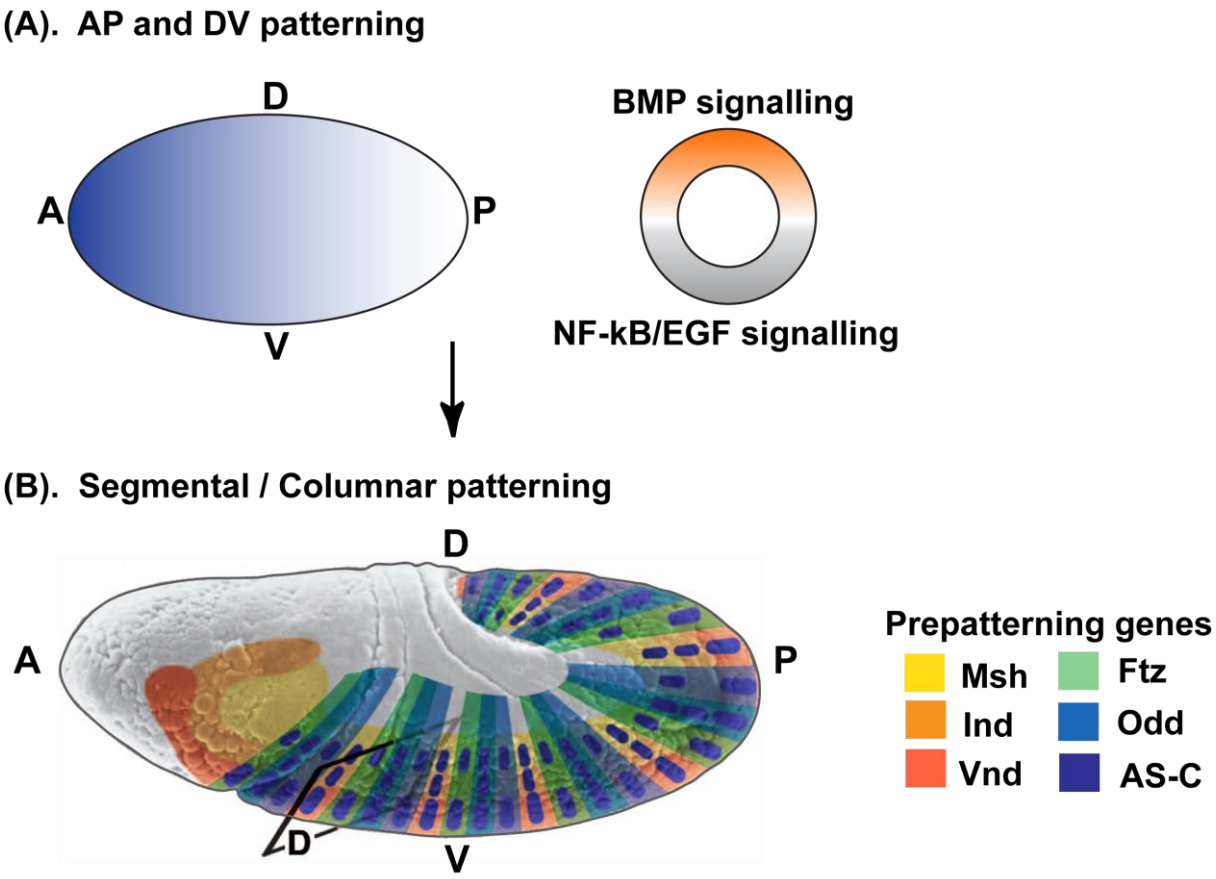

Fig. 2. Prepatterning of the early *Drosophila* neuroectoderm.
(A) Scheme depicting the early developmental events. The embryo is divided into anterior, posterior, dorsal and ventral poles (A, P, D, V). In the early embryo, complex networks of maternal effect genes and BMP signalling cascades act in gradients along the AP and DV axis, respectively. (B) Lateral view of a *Drosophila* embryo with a subdivided pattern of the ventral neuroectoderm. The initial patterning events activate segment-polarity, pair-rule (represented by fushi tarazu (Ftz) and odd skipped (Odd) expression) and columnar gene (Vnd, Ind and Msh) expression in four transverse and three longitudinal stripes in each segment including the neuroectoderm. The combinatorial expression of segment-polarity and columnar genes in each hemisegment activates the specific combination of proneural genes called *achete-scute* complex (*AS-C*) initially in 10 groups of cells. Scheme adapted from Skeath and Thor, 2003; Hartenstein and Wodarz, 2013.

The process of neurogenesis in the *Drosophila* embryonic VNC takes place in three basic steps - the formation of a neuroblast, specifying the identity of the neuroblast and elaboration of a neuroblast lineage. Each of these steps during neurogenesis requires a strict coordination of cell-cycle progression and specific cell fate acquisition that plays a crucial role in ultimately generating a complex nervous system. My thesis deals with the first step, the formation of a neuroblast, which is described in the next chapter.

1.2. Neuroblast Formation

The neuroectoderm is a monolayer of bipotent cells, which have to choose between the two alternative fates of development, neurogenesis versus epidermogenesis. The patterned neuroectoderm activates the specific combination of proneural gene expression in a cluster of cells called neural equivalence groups. From each equivalence group, a single cell attains the neural precursor identity and delaminates into the interior. The designated neural precursors internalize from the monolayer and divide asymmetrically like stem cells to produce the neural primordium inside the embryo. The neuroectodermal cells that do not adopt the neural fate remain at the surface and subsequently generate epidermal structures. Two groups of genes called proneural and neurogenic genes regulate the separation of neural and epidermal progenitors from the bipotent neuroectoderm (Brand and Campos-Ortega, 1988). The proneural genes include members of the *achaete-scute* complex (*AS-C*), *daughterless*, *atonal*, *ventral nervous condensation defective* (*vnd*) and probably other yet unidentified genes (Jimenez and Campos-Ortega, 1979, 1987, 1990; White, 1980; White et al., 1983; Caudy et al., 1988a). The *AS-C* includes *achaete* (*ac*), *scute* (*sc*), *lethal of scute* (*l'sc*) proneural genes and the neural precursor gene *asense*. Most known proneural genes encode basic Helix-Loop-Helix (bHLH) transcription factors. The products of AP and DV patterning genes combinatorially act on a large array of cis-regulatory regions of *AS-C* genes and initiate their expression. A segmentally repeated stereotyped expression pattern of single or a combination of proneural genes in a cluster of 5 to 7 neuroectodermal cells, called proneural clusters, are initiated (Fig. 3A). Proneural gene expression becomes restricted from a group of cells in the cluster to just one, the future NB (Cabrera, 1990; Cubas et al., 1991; Martin-Bermudo et al., 1991; Skeath and Carroll, 1992). Genetic and cell ablation experiments suggest that the proneural clusters are groups of equipotent cells, all of which can adopt the neural fate (Taghert et al., 1984; Doe and Goodman, 1985; Simpson, 1990). This competence appears to be conferred to all cells in the equivalence group by proneural gene expression. The dynamics of the proneural gene pattern directly reflects cell fate restriction (Cabrera et al., 1987). In a second step, the Notch signaling pathway mediated by the neurogenic genes eventually restricts this potential to a single cell. In the context of VNC development, neurogenic genes include *Notch* (*N*), *Delta* (*Dl*), *bigbrain* (*bib*), *mastermind* (*mam*), *neuralized* (*neur*) and *Enhancer of splits* Complex (*E(spl)-C*). Epistasis and transplantation

experiments suggest that the function of each of these genes appears to be dependent on another member of the group. If the function of any neurogenic gene is lost, the function of the entire chain is perturbed. These experiments placed the *Enhancer of split* locus at the endpoint of the Notch pathway during embryonic neurogenesis (Technau and Campos-Ortega, 1987; de la Concha et al., 1988; Lieber et al., 1993). As an exception, *bib* functions in a parallel pathway, independent of other *Notch* loci. The neurogenic genes *N*, *bib* and *Dl* encode membrane proteins (Wharton et al., 1985; Kidd et al., 1986; Vaessin et al., 1987; Kopczynski et al., 1988; Rao et al., 1990). The other neurogenic genes *mam*, *neur* and *E(spl)-C* code for nuclear proteins (Knust et al., 1987; Preiss et al., 1988; Klambt et al., 1989; Smoller et al., 1990; Boulianne et al., 1991). The neurogenic gene expression is initially activated in all ectodermal cells (Fig. 3B). The proneural proteins in a cluster refine this pattern by directly activating the transcription of *Dl* (Kunisch et al., 1994). The proteins encoded by *N* and *Dl*, two neurogenic genes, interact directly on the membranes of 5 to 7 contiguous cells, which leads to cleavage of the intracellular domain of Notch (N^{intra}). The cleaved products in a given cell activate the transcription of *E(spl)-C* genes. A slight imbalance in the AS-C protein expression in one of the cells of the cluster elevates the expression of *Dl.* The cell with a higher amount of Dl sends a stronger inhibitory signal to the neighboring cells through cleavage of N (Fig. 3C). This mechanism is defined as lateral inhibition. The signal obtained in these cells by the N^{intra} protein, augments the expression of the E(spl)-C, which in turn inhibit transcription of the *AS-C* genes resulting in down-regulation of Dl expression in the receiving cells. The initial imbalance is thus amplified until one cell within the cluster expresses exclusively the AS-C, while the others express E(spl)-C proteins (Fig. 3D). The expression pattern of all the genes in the *E(spl)-C* appear similar and complement neuroblast segregation (Knust et al., 1992; Tata and Hartley, 1995). *N* loss of function disrupts the lateral inhibitory signal. Thus, all cells in the proneural cluster adopt the neural fate and result in extreme hypertrophy of the embryonic nervous system (Lehmann et al., 1983; Brand and Campos-Ortega, 1988; Skeath and Carroll, 1992). Conversely, expression of an activated form of the N protein or even its downstream factor E(spl) proteins prevents all cells, including the presumptive neuroblast, from adopting the neural fate (Lieber et al., 1993; Struhl et al., 1993; Nakao and Campos-Ortega, 1996). In *N*, *Dl* and *neur* mutants, E(spl) bHLH proteins do not accumulate (Knust et al., 1992). Activation of bHLH repressors by

Notch signaling is therefore a general strategy for preventing equipotent cells from acquiring the same fate.

1.3. Neuroblast specification

In *Drosophila*, after fertilization, 13 rapid synchronous nuclear divisions occur without cytokinesis and detectable gap phases, resulting in the formation of a syncytium (Foe, 1989). Following gastrulation, NB formation in each hemisegment occurs from a monolayer of neuroectodermal cells. Segmentation genes including the signalling molecules Wingless (Wg) and Hedgehog (Hh), the transmembrane receptor Patched (Ptc) and genes which interact with these signalling pathways such as *naked* (*nkd*), *smoothened* (*smo*), gooseberry (*gsb*) and *engrailed* (*en*) dissect the neuroectoderm of each hemisegment into four transverse row of cells along the AP axis (Chu-LaGraff and Doe, 1993; Zhang et al., 1994; Skeath et al., 1995; Bhat, 1996; Bhat and Schedl, 1997; McDonald and Doe, 1997). Three columnar genes *Ventral nerve cord defective* (*vnd*), *Intermediate nerve cord defective* (*ind*) and *muscle-specific homeobox gene* (*msh)* subdivide the early neuroectoderm into a parallel array of three adjacent longitudinal columns of ventral, intermediate and lateral columns, respectively (Skeath et al., 1994; Ishiki et al., 1997; McDonald et al., 1998; Weiss et al., 1998). The different combinations of columnar and segment polarity genes then direct the activation of a unique set of genes (e.g. the proneural genes, *seven-up*, *runt*, *huckebein*) within individual proneural clusters. Nearly 30 NBs sequentially delaminate invariantly in five temporal waves from thoracic to abdominal hemisegments (Doe, 1992). The segregated precursors in the VNC divide asymmetrically and generate fixed amounts of neurons and glial populations. Within the orthogonal subdivided pattern of four anteroposterior (AP) cell rows and three mediolateral columns, initially 10 individual AS-C expressing clusters are formed (Fig. 4A). From these clusters, the first 10 S1 phase NBs delaminate into the VNC. Shortly thereafter, five S2 proneural clusters arise at specific locations and segregate NBs, which interdigitate between S1 NBs (Fig. 4B). Divisions 14-16 within the ectoderm layer occur after gastrulation (Edgar et al., 1994). The S1 and S2 NB formation occur from a cellularized neuroectodermal cells arrested at G2 of cycle 14. Subsequently, 16 S3-S5 NBs arise at invariant positions within this pattern.

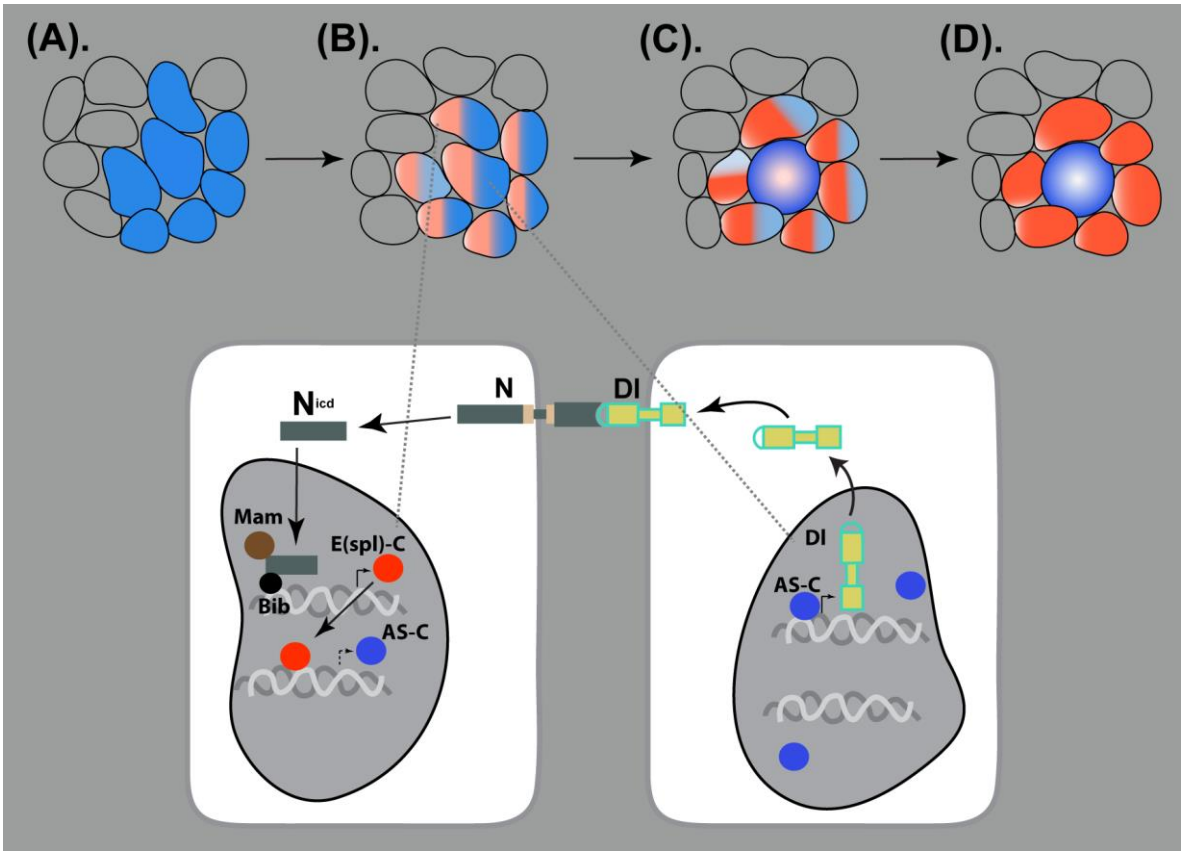

Fig. 3. Notch-mediated NB selection within the *Drosophila* VNC.
Schematic drawing of neuroectodermal cells and nuclei depicting the proneural and neurogenic gene expression patterns. (A) Combined action of segment polarity and columnar patterning genes activate AS-C (blue) expression in 5 to 7 neuroectodermal cells. (B) The neurogenic gene cascade terminally activates *E(spl)-C* gene expression ubiquitously in all cells of neuroectoderm, which is further refined by the Notch-activated cascade. The cell with a slightly higher level of AS-C expression activates more *Dl* expression in that cell compared to others. The interaction of extracellular domains of Dl and N leads to cleavage of the intracellular domain of Notch (N^{intra}), which when translocated to the nucleus initiates the *E(spl)-C* gene expression along with other factors like Mam and Bib. E(spl)-C proteins bind to DNA and inhibit the proneural gene expression. (C) This loop of the Notch-mediated cascade ends with the selection of one single cell as NB with strong proneural gene expression. The surrounding cells in the cluster have elevated E(spl)-C expression. (D) Finally, the highest AS-C accumulation in the NB completely represses the *E(spl)-C* expression in that cell. Conversely, the stronger E(spl)-C protein expression in other cells of the cluster represses proneural gene expression.

However, the combination of proneural genes that give rise to S3, S4 and S5 NBs has not been described in detail to date (Hartenstein et al., 1994). After S3 phase, the neuroectodermal cells enter and finish a single post blastodermal mitotic division, cycle 14 (Foe, 1989; Edgar and Farrell, 1990). This division always results in two cells of different fates, an epidermoblast and a neuroblast (Schmidt et al., 1997). Nevertheless, the neuroblast fate is independent of neuroectodermal divisions taking place in neuroectodermal progenitors (Berger et al., 2001). The patterns of delamination and mitosis are closely correlated:

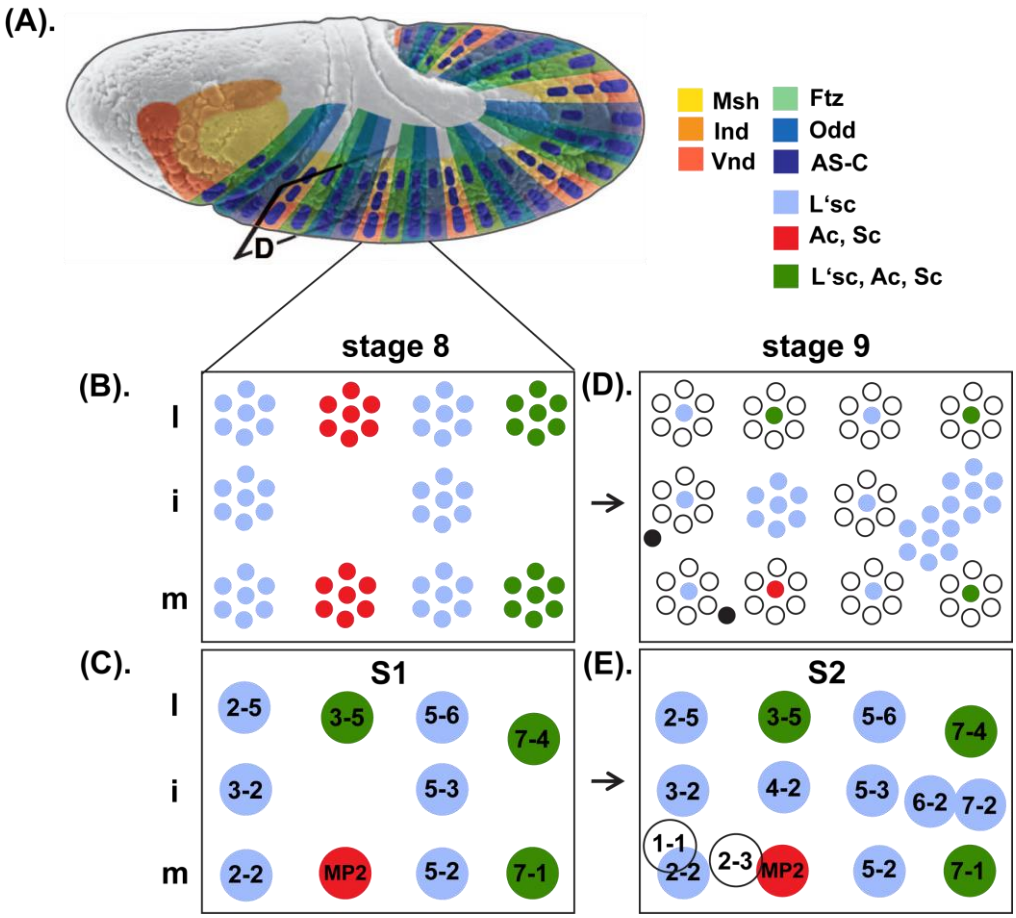

Fig. 4. NB specification in the embryonic VNC.
(A) Lateral view of stage 8 embryo depicting ten early proneural clusters (blue, red and green dots) formed in each hemisegment. (B) Schematic representation of specific combinations of AS-C protein expression in early ten proneural clusters formed in each hemisegment at a particular position. (C) From each proneural cluster, the first 10 S1 NBs are formed. (D) Additional S2 proneural clusters formed at stage 9 mostly in the intermediate row. (E) Five S2 NBs are formed at late stage 9. Scheme taken from Skeath, 1994 and Hartenstain and Wodarz, 2013.

delamination occurs either immediately after a cell has divided or shortly before the division (Hartenstein et al., 1994). Thus, each of 30 delaminated NBs in each hemisegment is named and can be identified unambiguously based on position and temporal phase of its delamination, along with the specific combination of markers it expresses (Doe, 1992). NBs delaminating from the same position in each hemisegment are called serial homologs (Fig. 4C). Upon delamination from the vNR, the NBs undergo series of asymmetric divisions and generate secondary neural precursors called ganglion mother cells (GMC). GMCs can divide only once and produce either two neurons or two glia cells or a combination of a neuron and glia (Fig. 4D) (Hartenstein et al., 1987). The lineage produced by each NB in the serial homolog pattern is an almost invariant combination of neuronal and/or glial progeny.

Intersegmental variations in NB formation and specification imposed by *Hox* genes are described in the following section.

1.4. *Hox* genes in *Drosophila*

Drosophila features a single *Hox* gene cluster which has been split into two groups, the *Antennapedia* complex (ANT-C) and the *bithorax* complex (BX-C) (Lewis, 1978; Scott et al., 1983; Kaufman et al., 1990). The ANT-C includes *labial* (*lab*), *proboscipedia* (*pb*), *Deformed* (*Dfd*), *Sex combs reduced* (*Scr*) and *Antennapedia* (*Antp*) genes, which specify the head and the anterior thoracic segments. The body parts in the posterior thorax and abdominal segments are specified by BX-C genes *Ultrabithorax* (*Ubx*), *abdominal-A* (*abd-A*) and *Abdominal-B* (*Abd-B*). The alignment of *Hox* genes along the chromosome mirrors the order of the structures they specify along the AP axis (McGinnis and Krumlauf, 1992), a phenomenon called spatial colinearity (Fig. 5A). A unique combination of gap and pair-rule genes initiates *Hox* gene expression in the cellular embryo (Harding and Levine, 1988; Irish et al., 1989). Once established, *Hox* gene expression in *Drosophila* is regulated at three levels: transcriptional regulation by segmentation genes, by the Polycomb / trithorax group (PcG / trxG) of proteins and by Hox proteins themselves (Hafen et al., 1984; Harding et al., 1985; Struhl and White, 1985; Martinez-Arias and White, 1988; Simon and Tamkun, 2002). The PcG proteins maintain a repressive state of homeotic gene expression, while the trxG proteins maintain *Hox* gene activity. The expression pattern of homeotic proteins is observed either in distinct parasegments or in an overlapping fashion along the neuroectoderm (Fig. 5B) and later in the CNS (Hirth et al., 1998). The essentiality of *Hox* genes for the determination of segmental identity is explained by examples of *Hox* gain- and loss-of-function mutations. Posterior *Hox* genes manifest a dominance phenomenon termed posterior prevalence, in which loss-of-function of any BX-C gene leads to transformation of those segment identity to an anterior segment identity through extension of anterior *Hox* gene expression (Lewis, 1978). Thus, loss of function studies often does not explain the role of a missing gene. Anterior *Hox* gene loss-of-function manifests either anterior prevalence or a *Hox* less ground state, which is a ground state independent of the *Hox* gene function (Wakimoto and Kaufman, 1981; Merill et al., 1987, 1989; Gehring et al., 2009).

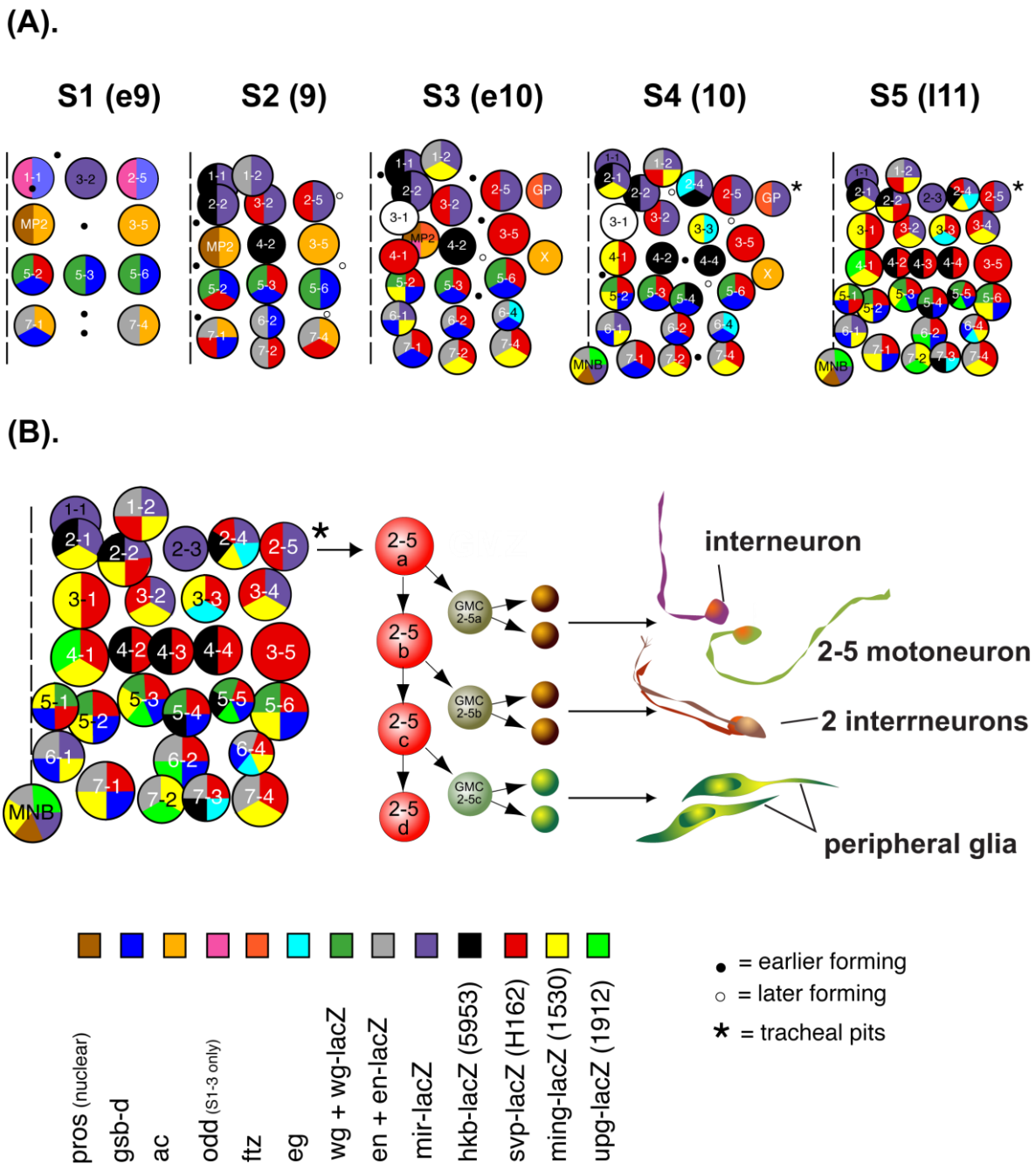

Fig. 5. Segregation mode of embryonic VNC NBs.
(A) Cartoon depicting 5 segregation waves of NB delamination from stage 9 to stage 11 in the VNC of the *Drosophila* embryo. Each delaminated NB can be identified by the specific combination of molecular marker gene expression. (B) The NB division mode is exemplified using NB2-5. The delaminated NB divides asymmetrically several times and makes intermediate precursors called GMCs, which divide once and generate specific motoneurons, interneurons or glia cells. Scheme after C.Doe, 1992 and kindly provided by C. Rickert, C. Berger.

Hox genes encode transcription factors that contain a 60 aa homeodomain (HD). The homeodomain is a basic helix-loop-helix protein motif present in many eukaryotic transcription factors (McGinnis et al., 1984; Scott and Weiner, 1984). The biological function of Hox transcription factors often requires an interaction with two other

homeodomain containing transcription factors: Homothorax (Hth) and Extradenticle (Exd) to improve their DNA-binding ability (Mann et al., 2009). The molecular interaction of various HDs with predicted DNA binding sites has been precisely dissected *in vitro* and *in vivo* (Grienenberger et al., 2003; Gebelein et al., 2004; Walsch and Carroll, 2007). Despite being active in a very large number of cells, Hox proteins affect target gene expression in precisely defined sub-domains (Vachon et al., 1992; Capovilla et al., 1994; Hersh and Carroll, 2005). In the most extreme case the regulation of a Hox target gene can be limited to a single cell (Brodu et al., 2002)

1.5. Establishing early embryonic intersegmental variations in VNC by *Hox* genes

Hox genes are expressed in broad and partially overlapping domains along the AP axis in the *Drosophila* VNC (Hirth et al., 1998; Sprecher et al., 2004). Numerous studies unraveled the role of *Hox* genes in patterning the *Drosophila* embryonic VNC in NB formation and in functions related to cell fate specification and apoptosis. An initial step in the development of the CNS is the delamination of a stereotype population of NBs from the neuroectoderm. The formation of serially homologous NBs described in the previous section is invariant in all thoracic and 8 abdominal segments. However, the *Hox* gene *Abd-B* together with the transcription factor caudal inhibits formation of certain NBs in the terminal abdominal segments. Thus, in A9 and A10 segments only 23 and 11, NBs respectively are observed (Birkholz et al., 2013a, b). 7 of the 30 serially homologous embryonic lineages have been shown to include different subsets of cells in the thoracic and abdominal segments, mediated by *Hox* genes. The tagma-specific differences involved were either in cell types produced in NB1-1, NB2-2 and NB6-4 or in cell number generated in NB2-4, NB3-1, NB5-4 and NB5-6 (Udolph et al., 1993; Bossing et al., 1996; Schmidt et al., 1997; Schmid et al., 1999). At the neuroectodermal level, the thoracic identity of NB1-1 is probably determined being the “ground” state, as it requires no *Hox* gene input. The expression of *Ubx* and *abd-A* in the neuroectoderm of the corresponding abdominal region is necessary and sufficient for NB1-1 to generate different lineage in the abdominal segments (Prokop and Technau, 1994). Thus, NB1-1T produces 2 motoneurons and 10 interneurons, whereas its abdominal counterpart gives rise to 1 motoneuron, 6 interneurons and 3 glial cells (Fig. 7A).

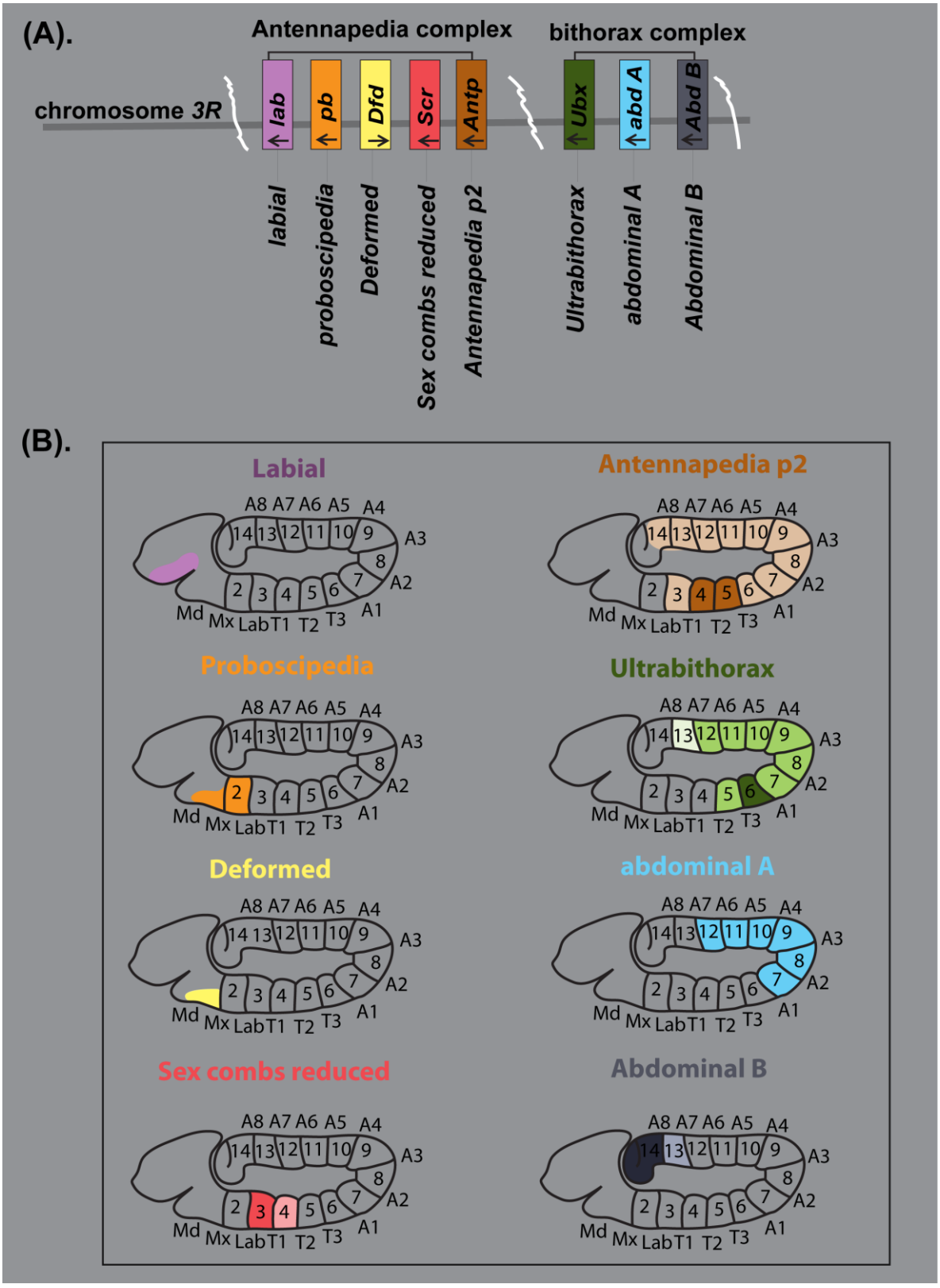

Fig. 6. *Drosophila Hox* gene complex genomic organization and expression pattern.
(A) Scheme of *Drosophila Hox* genes clusters (not to scale) in the order of their presence on the chromosome *3R*. Genes are colored to differentiate between *Hox* family members. (B) Lateral view of stage 10 embryos showing the parasegmental expression pattern of each Hox protein in the neuroectoderm. Numbering specify the segments and parasegments. The weak expression is shown with light color code. Scheme modified after Alberts et al., Molecular Biology of the cell, 4th edition.

At the level of the neuroblast, it has been shown for the NB6-4 lineage that *Hox* gene products specify the formation of different progeny in the thoracic and abdominal segments. Thoracic NB6-4 induces the formation of both neurons and glial cells from their respective neural and glial precursor, whereas its abdominal counterpart generates only glial cells. The cell-cycle regulator gene *Cyclin E (CycE)* and the *Hox* genes *abd-A* and *Abd-B* establish these differences in the abdominal region NB6-4 to the thoracic ground state (Berger et al., 2005, 2010; Kannan et al., 2010). Segment-specific cell number variations in the lineage were achieved either through regulating more cell divisions or the NBs cell cycle exit process or by apoptosis of NB (Cenci and Gould, 2005; Tsuji et al., 2008; Karlsson et al., 2010). For example, in thoracic NB3-3, the *Hox* gene *Antp* is responsible for inducing quiescence, a non-proliferative state that extends to the end of the first larval stage, earlier than in homologous abdominal segments neuroblasts expressing *abd-A* (Tsuji et al., 2008). Similarly, in NB5-6, *Antp* promotes more cell divisions in thoracic segments, while *Ubx* and *abd-A* regulate fewer divisions in abdominal segments (Karlsson et al., 2010). Majority of abdominal NBs are normally removed by apoptosis after they have generated their embryonic progeny (Bray et al., 1989; White et al., 1994; Peterson et al., 2002), whereas in the thoracic neuromeres most of the NBs enter quiescence at the end of embryogenesis and continue dividing as postembryonic NBs in larval stages (Truman and Bate, 1988).

1.6. *Hox* genes segment-specifically sculpt the terminal embryonic lineages in the VNC

At the postmitotic level in the VNC, the *Hox* genes also contribute to the segment-specific refinement of the neural lineages in terminal embryonic development (Rogulja-Ortmann et al., 2008; Suska et al., 2011). One of the key aspects of functional nervous systems is the restriction of particular neural subtypes to specific regions, which permits the establishment of differential segment-specific neuromuscular networks. *Hox* genes role in pruning of late embryonic neural lineages along the AP axis was illustrated in prior studies. Specifically, one motoneuron of NB2-4 and NB7-3 lineages undergoes late embryonic segment-specific apoptosis through *Hox* gene involvement (Fig. 7B, C) (Rogulja-Ortmann and Technau, 2008). The thoracic NB2-4 lineage comprises 8 to 12 neurons whereas the abdominal

segments lineage possess 7 to 8 neurons, two of which are motoneurons (MNa, p) (Schmidt et al., 1997; Schmid et al., 1999). Only in segment T3, the anterior NB2-4t motoneuron (MNa) underwent Caspase-dependent apoptosis at late stage 16 (Fig. 7C) (Rogulja-Ortmann and Technau, 2008).

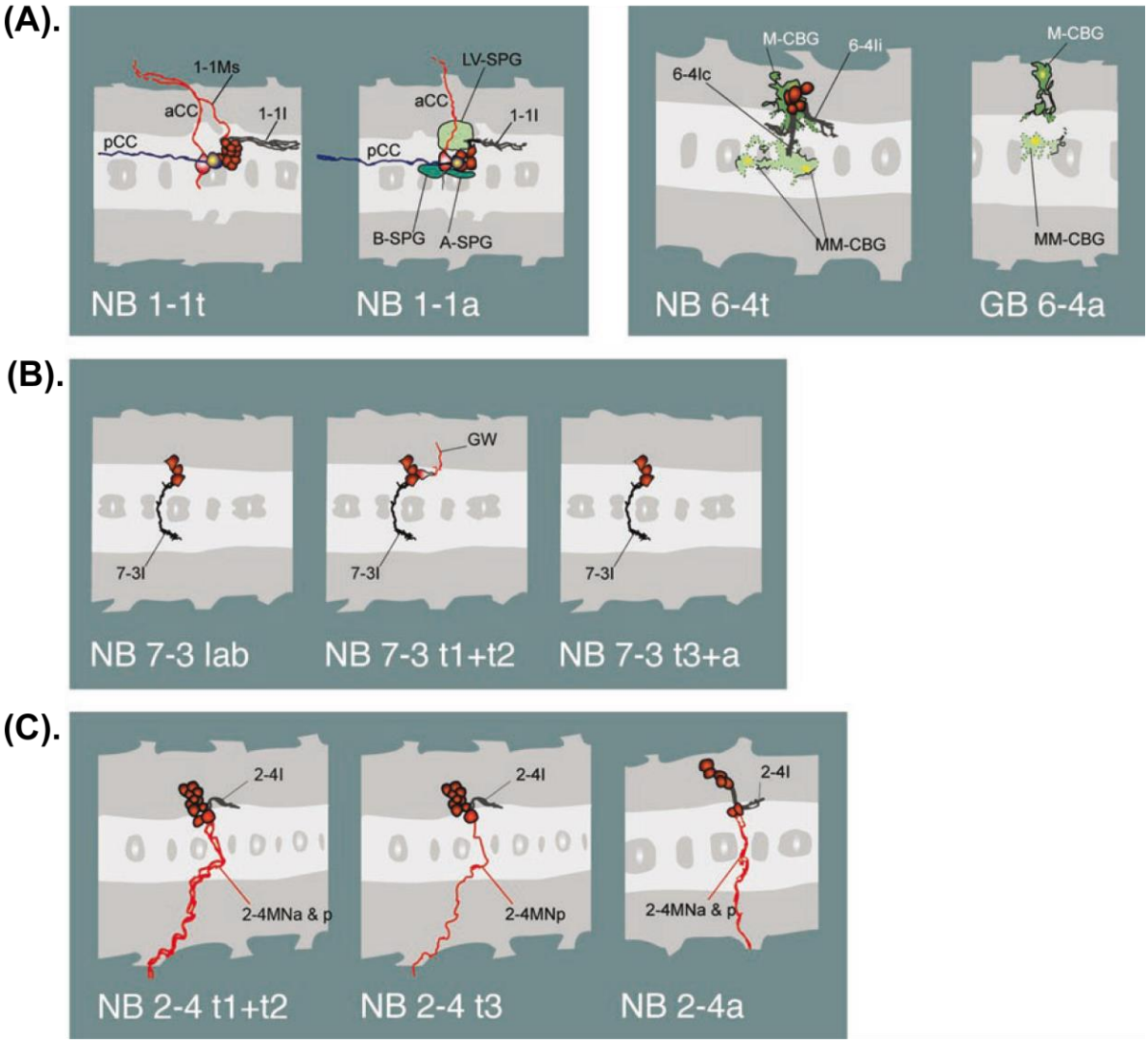

Fig. 7. *Hox* genes regulate intersegmental lineage variations.
Each group shows the schematic illustration of Wt lineages that show segmental differences in late embryonic stages. Glia cells are depicted in green, motoneurons in light red and interneurons in dark red. (A) Tagma-specific thoracic versus abdominal lineage variations arises by imposing *Hox* gene activity in the abdominal segments either within the neuroectoderm (for NB1-1) before NB delamination or thereafter (for NB6-4). (B) *Hox*-gene dependent segment-specific refinement of the terminal embryonic 7-3 lineage. The GW motoneurons of Labial and T3-A6 segments undergo apoptosis. It survives only in T1 and T2 segments. (C) Apart from thoracic vs abdominal-specific cell number variations within the NB2-4 lineage, specific removal of one of the motoneurons (MNa) by *Ubx* in the T3 segment occurs in late embryonic stages. Image taken from Rogulja-Ortmann and Technau, 2008.

NB7-3 lineages retain four neurons by late embryonic development. Of which, one is a motoneuron called GW (Lundell and Hirsh, 1992; Bossing et al., 1996; Higashijima et al., 1996; Dittrich et al., 1997; Lundell and Hirsh, 1998; Schmid et al., 1999; Isshiki et al., 2001; Novotny et al., 2002). Strong upregulation of Ubx expression in late embryonic stage 14 or 15 activates apoptotic gene reaper (*rpr*) in GW neuron of NB7-3 lineage from T3 to A7 segments, which leads to apoptosis of this neuron in these segments at late stage 16. While the strong expression of Antp in T1 and T2 segments rescue this neuron from apoptosis (Rogulja-Ortmann et al., 2008). Similarly, the GW neuron of Labial segment also has been shown to undergoes apoptosis (Rogulja-Ortmann and Technau, 2008). In the process of above studies Rogulja-Ortmann et al., 2008 noted enlarged thoracic NB7-3 lineage in *Antp*^{25},*Ubx*^{1} double mutant. However, those lineages were not elaborated further. Hence, I carried out my study to analyze the enlarged thoracic NB7-3 lineage in *Antp*^{25},*Ubx*^{1} double mutant and the role of *Hox* genes in causing this phenotype were evaluated.

1.7. Aim

Hox genes play a major role in shaping the *Drosophila* CNS along the anterior-posterior body axis during embryonic development. They encode transcription factors that control the expression of downstream target genes through a common 60 aa domain, the homeodomain, which is involved in DNA-binding. They contribute to cellular diversity at different levels and at different times in development. *Hox* genes also act in a more permissive manner in that the effects of their actions vary and depend on the cellular context of each cell and the precise time in development. Their roles in cell specification at the level of the neuroectoderm, neuroblast and/or postmitotic progeny in the embryonic VNC was uncovered through several prior studies. In this study, I have characterized the enlarged NB7-3 lineage phenotype observed in thoracic segments of the *Antp*^{25},*Ubx*^{1} double mutants (Rogulja-Ortmann et al., 2008). The individual roles of *Hox* genes *Antp* and *Ubx* in causing this particular phenotype were evaluated in detail. The mechanism how this phenotype arises in specific-*Hox* mutants was dissected. DNA-binding dependent and independent functional roles of homeotic proteins in segment-specific lineage patterning was carried out using NB7-3 lineage.

2. Materials and Methods

2.1. *Drosophila* stocks

The *Drosophila* stocks used in the course of study are listed in Table-2.1. Recessive lethal mutations were maintained over a balancer chromosome that carries a β-galactosidase (lacZ) or green fluorescent protein (GFP) reporter. The reporter genes are carried on P-elements that drive the expression of lacZ or GFP under the control of a specific promoter. Thus, a homozygous mutation in an embryo could be identified by lack of lacZ or GFP expression following antibody staining.

Table-2.1

Name	Genotype	Source
Antp^{1}	*Antp^{1} red^{1} e^{1} / TM3, Sb^{1}*	Bloomington 2293
Antp^{10}	*Antp^{10} p^{p} / TM3, Ser^{1}*	Bloomington 2287
Antp^{11}	*Antp^{11} P^{p} / TM3, Tb^{1}, Sb^{1}*	Bloomington 2286
Antp^{14}	*Ki^{1} Antp^{14} rn^{roe-1} p ^{p}/ TM3, Sb^{1}*	Bloomington 2277
Antp^{17}	*T(2;3)Antp^{17}, Antp^{17} red^{1} e^{1} / TM3, Sb^{1}Ser^{1}*	Bloomington 2299
Antp^{2}	*Df(3R)Antp^{2}, Antp^{2} e^{1} / TM3, Sb^{1}*	Bloomington 1941
Antp^{23}	*Antp^{23} red^{1} e^{1} / TM6B, Tb^{1}*	Bloomington 290
Antp^{25}	*Antp^{25} red^{1} e^{1} / TM3, Sb^{1}*	Bloomington 3020
Antp^{25},Ubx^{1}	*Ki^{1} Antp^{25} p^{p} Ubx^{1} e^{1} / TM6B, Tb^{1}*	Bloomington 2031
Antp^{3}	*Antp^{3} red^{1} e^{1} / TM3, Sb^{1}*	Bloomington 2309
Antp^{6}	*Df(3R)Antp^{6}, Antp^{6} red^{1} e^{1} / TM3, Sb^{1} Ser^{1}*	Bloomington 1938
Antp^{7}	*Df(3R)Antp^{7}, red^{1} e^{1} / TM3, Sb^{1}*	Bloomington 1833
CycE^{AR95}	*CycE^{AR95} / Cyo*	C. Berger
Df(3R)4SCB	*Df(3R)4SCB / TM3, Sb^{1} Ser^{1}*	Bloomington 3360
Df(3R)9A99	*Df(3R)9A99, Diap1^{1} st^{1} cp^{1} in^{1} kni^{ri-1} cu^{1} e^{s} ca^{1} / TM3, Ser^{1}*	Bloomington 3363
Df(3R)Antp-A41	*Df(3R)Antp-A41, red^{1} e^{1} / TM3, Sb^{1}*	Bloomington 1886
Df(3R)Antp-X1	*Df(3R)Antp-X1, Ki^{1} red^{1} / TM3, Sb^{1}*	Bloomington 2013
Df(3R)Antp^{17}	*Df(3R)Antp^{17} / TM3, Sb^{1} Ser^{1}*	Bloomington 1842
Df(3R)Hu	*w^{118};Df(3R)Hu, Antp^{Hu-rv1} / TM3, p(HZR+6.8Xb)JG1, Sb^{1}*	Bloomington 2019
Df(3R)roe	*Df(3R)roe / TM3, Ser^{1}*	Bloomington 3354
Df(3R)Scx2	*Df(3R)Scx2, red^{1} e^{1} / TM3, Sb^{1}; Dp(3;Y)Antp^{+}, y^{+}*	Bloomington 2006
Dfd^{16}	*Dfd^{16} red^{1} e^{1} / TM3, Sb^{1} Ser^{1}*	Bloomington 2325
Dfd^{16}, Scr^{4}	*Dfd^{16}, Scr^{4} / TM6, abdA lacZ*	Bloomington 3032

en^{58}	*en*^{58} / *Cyo*	AG Technau
ey$^{J5.71}$	*y1 w*; ey*$^{J5.71}$ / *In(4)ci*^{D}, *ci*^{D} *pan*^{ciD} *sv*$^{spa-pol}$	AG Technau
hkb^{2}	*hkb*^{2} *P*^{p} / *TM3*	AG Technau
Scr^{17}	*Scr*^{17} / *TM6, abdA lacZ*	Bloomington 3400
Scr^{4}	*w*^{118}*; Scr*^{4} *red*^{1} *e*^{1} / *TM6B, Tb*^{1}	Bloomington 2188
Ubx^{1}	*Ubx*^{1} / *TM6, Tb, Sb, e, Dfd-lacZ*	AG Technau
Ubx$^{6.28}$	*Ubx*$^{6.28}$ / *TM6, Tb, Sb, e, Dfd-lacZ*	AG Technau
Ubx$^{9.22}$	*Ubx*$^{9.22}$ *Sb*$^{sbd-1}$ / *TM1*	Bloomington 3474
Wt	*Oregon R*	Bloomington 5
GAL4 stocks		
en GAL4	w*; *en* GAL4	AG Technau
sca GAL4	w*; *sca* GAL4	AG Technau
UAS stocks		
UAS *Antp*	w; UAS *Antp*	Bloomington 7301
UAS *AntpA50;A51*	w;UAS *AntpA50;A51*	S. Plaza
UAS *AntpK50*	w; UAS *AntpK50*	S. Plaza
UAS *CycE(II)*	w*;UAS *CycE*	AG Berger
UAS *ey*	y^{1}w*;UAS *ey*	Bloomington 6294
UAS *hkb(III)*	w^{118};UAS *hkb*	D. J. Andrew
UAS *l(1)sc(II)*	w*;UAS *l(1)sc;W*$^{+}$	S. Crews
UAS *mCD8::GFP*	UAS *mCD8::GFP*	O. Vef
UAS *UbxIa*	w*;UAS *UbxIa*	AG Technau
Balancer stocks		
abdA lacZ	*TM3* / *TM6b, iab-2* lacZ	O. Vef
Dfd EYFP	*w;;Df(3L)H99* / *TM6b, Sb, Antp*^{Hu}, *Tb, Dfd*-EYFP	O. Vef
Dfd lacZ	*Dr* / *TM6b,Tb, Sb, e, Dfd*-lacZ	O. Vef
Twist GFP	*w*^{1118}*-*;; *Dr* / *TM3Twi* GAL4 UAS GFP, *Sb*^{1} *Ser*^{1}	Bloomington 6663
Twist lacZ	w;*; TM3 ftz lacZ* / *TM6c,Tb, Sb, Twist*-lacZ	O. Vef
Twist lacZ*; abdA* lacZ	*w;pm* / *CyoTwist*-lacZ*;cxd* / *TM6b iab-2* lacZ*, e, Antp*^{Hu}	O. Vef

Deficiency	Mapped location	Bloomington Reference
Df(3R)BSC422	84A5-84B2	24926
Df(3R)BSC633	84B2-84C3	25724
Df(3R)ED7665	84B4-84E11	8685
Df(3R)BSC221	84C1-84D2	9698
Df(3R)BSC548	84C8-84D3	25076
Df(3R)Exel6146	84C8-84D9	7625

Df(3R)BSC423	84D1-84D5	24927
Df(3R)BSC465	84D3-84F9	24969
Df(3R)BSC466	84E1-85A10	24970
Df(3R)ED5296	84F6-85C3	9338
Df(3R)BSC666	85C2-85D11	26518
Df(3R)BSC476	85D16-85D24	24980
Df(3R)ED5429	85D19-85F8	8919
Df(3R)ED5454	85E5-85F12	9080
Df(3R)ED5474	85F11-86B1	9082
Df(3R)BSC479	86A3-86C7	24983
Df(3R)ED5518	86C7-86E13	9084
Df(3R)BSC469	86D8-87A2	24973
Df(3R)ED5559	86E11-87B11	8920
Df(3R)BSC486	87B10-87E9	24990
Df(3R)ED5623	87E3-88A4	37537
Df(3R)ED5642	87F10-88C2	9279
Df(3R)ED5644	88A4-88C9	9090
Df(3R)ED10555	88C9-88D8	23714
Df(3R)BSC635	88D2-88E3	26505
Df(3R)ED5664	88D1-88E3	24137
Df(3R)ED10566	88E2-88E5	24138
Df(3R)BSC741	88E8-88F1	26839
Df(3R)ED5705	88E12-89A5	9152
Df(3R)BSC515	88F6-89A8	25019
Df(3R)Exel7327	89A8-89B1	7982
Df(3R)BSC728	89A8-89B2	26580
Df(3R)Exel7328	89A12-89B6	7983
Df(3R)BSC887	89B6-89B16	30592
Df(3R)ED10639	89B7-89B18	9481
Df(3R)ED10642	89B17-89D5	9482
Df(3R)Exel6270	89B18-89D8	7737
Df(3R)BSC748	89E5-89E11	26846
Df(3R)Exel6176	89E11-89F1	7655
Df(3R)ED5780	89E11-90C1	8104
Df(3R)BSC565	90A2-90D1	26826
Df(3R)BSC566	90C2-90F6	25389
Df(3R)ED5815	90F4-91B8	9208
Df(3R)BSC509	91A3-91D5	25013
Df(3R)ED5938	91D4-92A11	24139
Df(3R)BSC475	91F12-92B4	24979

2.1.1. Fly stock maintenance

The stocks were maintained at 25°C in vials containing the standard *Drosophila* food media. For embryo collections, the flies were placed into food vials containing Apple juice agar medium.

2.2. Genetic crosses

For generating the required fly stock from two genotype fly strains, freshly eclosed female virgins from one fly strain were crossed to males of the other strain and allowed to lay eggs. The F1 progeny obtained from this cross were selected for required genotypes.

2.2.1. Embryo collection

The flies were allowed to lay eggs for scheduled time points or overnight based on the desired developmental stages. The flies were subsequently flipped to a new Apple agar medium vial and the embryos processed accordingly.

2.2.2. Fixation of embryos

The embryos on the Apple agar medium were dechorionated by adding 6% bleach (Sodium hypochlorite) for two min and collected into a funnel with mesh. The embryos were thoroughly rinsed and transferred to an Eppendorf vial consisting of fixation buffer, two-phased solution, for 25 min with vigorous shaking. After the phases separated, the lower phase containing formaldehyde was carefully removed and substituted with an equal amount of methanol. Vigorous vortexing for one min on a vortexer at this stage lets the devitellinized embryos sink to the bottom of the vial. The procedure was repeated for a second time until all the embryos were devitellinized. Then the embryos were rinsed four times with methanol to remove any traces of heptane. Finally, the embryos were used for staining procedure or stored in methanol at -20°C.

2.3. Antibody staining

Embryos which have been fixed and stored in methanol were rinsed with 0.3% PBTX several times. Primary antibodies of appropriate dilution in 0.3% PBTX were added and incubated overnight at 4°C, with gentle shaking. Primary antibodies that can be

rescued were stored at 4°C. The embryos were washed three times with 0.3% PBTX for 12 min each followed by an incubation of appropriately diluted secondary antibodies coupled with a fluorescent dye. The incubation was carried out either for 2 hrs at room temperature (RT) or overnight at 4°C followed by washes with PBTX for three times 12 min each. Next, the embryos were washed in 1x PBS for two times 5 min each and stored at 4°C in 70% glycerol.

Table-2.2. Antibodies

Primary Antibody	Animal	Dilution	Source
Achaete	rat	1:2	DSHB
Antennapedia (8C11)	mouse	1:20	DSHB
Antennapedia (4C3)	mouse	1:100	DSHB
β-Galactosidase	rabbit	1:1000	Promega
β-Galactosidase	mouse	1:1000	Promega
CycE	mouse	1:50	Christain Berger
Deadpan	guineapig	1:250	Jürgen Knoblich
Deadpan	rabbit	1:500	Jürgen Knoblich
Digoxygenin-AP	goat	1:500	Roche
Digoxygenin-POD	goat	1:500	Roche
Eagle	mouse	1:100	Chris Doe
Eagle	rabbit	1:500	Joachim Urban
Engrailed	rabbit	1:100	Santa Cruz
Enhancer of split	mouse	1:2	Sarah Bray
Even-skipped	guineapig	1:500	John Reinitz
Eyeless	rabbit	1:1000	Uwe Walldorf
Huckebein	rat	1:100	Johannes Jaeger
Hunchback	guineapig	1:800	Joachim Urban
Invected (ID4)	mouse	1:10	DSHB
Krupple	rabbit	1:250	Joachim Urban
Krupple	guineapig	1:500	Joachim Urban
Lethal of scute	guineapig	1:500	Stephan Crew
Sex combs reduced	mouse	1:20	DSHB
Zfh1	mouse	1:250	James Skeath
Zfh2	rat	1:100	Joachim Urban
Ultrabithorax	rabbit	1:1000	L.S.Sashidhara
Secondary antibodies			
Mouse-Alexa488	Donkey	1:500	Life Technologies
Mouse-Alexa568	Goat	1:500	Life Technologies
Mouse-Alexa647	Donkey	1:500	Life Technologies

Mouse-DyLight488	Donkey	1:250	Jackson Labororaties
Mouse-DyLight549	Donkey	1:250	Jackson Labororaties
Mouse-DyLight649	Donkey	1:250	Jackson Labororaties
Mouse-POD	Donkey	1:250	Dianova
Rabbit-Alexa488	Donkey	1:500	Life Technologies
Rabbit-Alexa546	Donkey	1:500	Life Technologies
Rabbit-Alexa568	Donkey	1:500	Life Technologies
Rabbit-Alexa647	Donkey	1:500	Life Technologies

2.3.1. Flat preparation

For analysis of the staining, stained embryos were transferred to a clean microscopic slide and flatted. Flat preparations were made using needles to remove the gut material so that the CNS was exposed for imaging. The preparations were covered with 70% glycerol, subsequently covered with a coverslip and sealed with nail polish. The stained flat CNS preparations were imaged either using fluorescence or a confocal microscope.

2.4. Ectopic gene expression

For a number of rescue and overexpression experiments, the Gal4-UAS system (Brand and Perrimon, 1993) was used for tissue specific targeted expression. This system consists of two components-the flies that express the yeast transcriptional activator Gal4 under the regulation of an endogenous promoter (driver stock), and the flies that carry a transgene of interest whose expression is regulated by the Gal4 Upstream Activation Sequence (UAS, UAS stock). When the driver and UAS stock were crossed together, the transgene of interest was expressed in the same pattern as the Gal4 protein (Fig. 8). Thus, ectopic expression of the transgene depends on the enhancer that regulates Gal4 expression. Using an appropriate driver stock in this method allows analysis of the function of a gene of interest in a specific tissue and at a specific developmental stage.

2.5. Complementation analysis

This method is used to identify or narrow down the region of the chromosome, where an unknown recessive lethal mutation is located. The principle behind this method lies in that the unknown mutation has to be homozygous lethal. In this analysis, fly stocks carrying a chromosomal deletion in an identified region of the chromosome is

crossed to the unknown mutation. If no progeny from the resulting cross with the mutation over the deletion is obtained, then the mutation is situated in the known region of the chromosomal deletion.

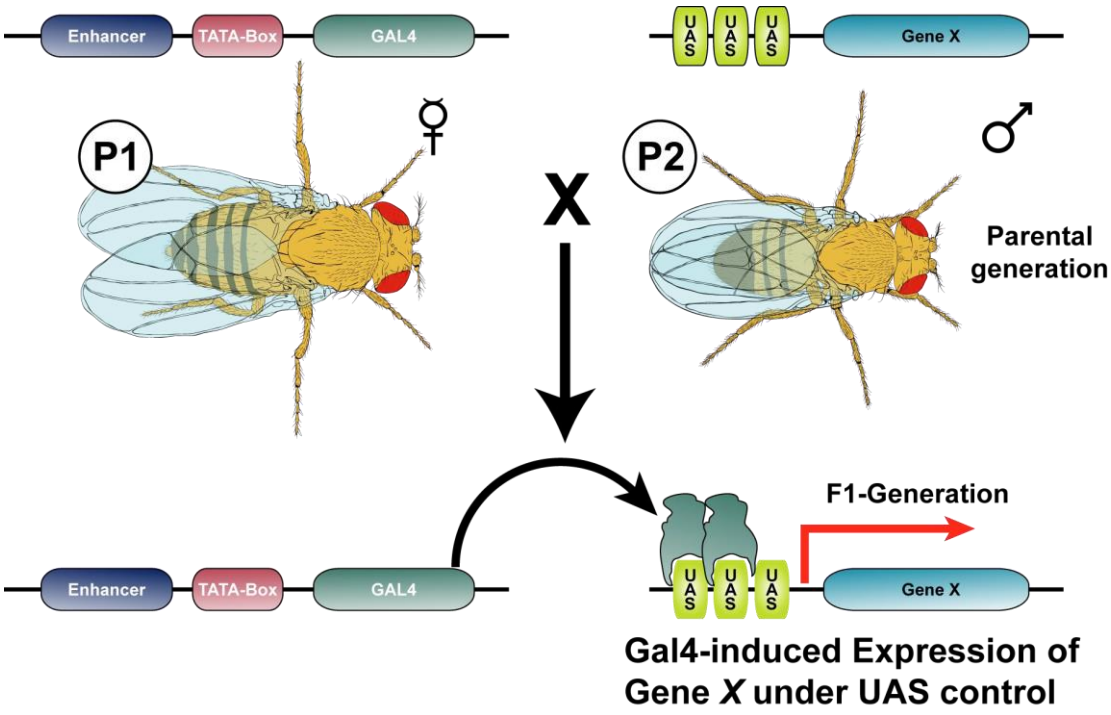

Fig. 8. The Gal4/UAS system.
Flies of the Gal4-strain (P1) express Gal4 under control of an endogenous enhancer. These flies are crossed with flies of the UAS strain (P2), which carry the transgene of interest downstream of several UAS sequences. In the progeny (F1 generation), the Gal4 protein can bind to the UAS sequences and sdrive transcription of gene *X* in the spatio-temporal pattern of endogenous enhancer expression. Image kindly provided by C. Rickert.

2.6. Genetic recombination and segregation

During meiosis, recombination occurs through cross over between identical sequences on nonsister chromatids of homologous chromosomes. In this process, exchange of genes between the chromosomes results in a different genetic combination and ultimately to the formation of unique genotypes with chromosomes that are different from those in parental genotypes. Through the recombination process, two mutations lying on the same chromosome can be recombined. Thereby, a cumulative effect of two or more mutations can be studied in the offspring with a genetic recombination. Conversely, in the segregation process, two mutations lying on the same chromosome are separated by recombination. Therefore, the single isolated mutations can be studied individually.

2.7. RNA *in situ* hybridization

For detecting mRNA transcripts in fixed embryos, labelled anti sense RNA probes were made. Solutions, glassware and pipette tips used in this method must be RNAse-free. Thus, all solutions used were treated with diethylpyrocarbonate (DEPC). The probes and their dilution used in this work were listed in Table-2.3.

Table-2.3. RNA probes

DIG-RNA probe	Dilution	Source
*dSer*T	1:500	Joachim Urban
ind	1:100	Rolf Urbach
hkb	1:1000	Georg Vogel
Antp (P1)	1:250	self made
Antp (P2)	1:250	self made

2.7.1. Generation of *Antp*-Promoter 1 (P1) specific RNA probe

The bacterial colony containing the 846 bp of *Antp* exon1 in pBluescript plasmid (DGRC EST clone GM05003) was cultured in an LB medium. Plasmid was isolated using Qiagen Miniprep kit. The isolated plasmid was linearized with the restriction endonuclease *Eco*RI, purified using Qiagen QIA quick Gel Extraction Kit and eluted in DEPC-treated water. The antisense RNA probe was synthesized using DIG-RNA labeling Mix, Roche with T7 RNA polymerase. The reaction was set according to the manufacturers guidelines and the finally synthesized probe was dissolved in hybridization (hyb) buffer. The *Antp*-promoter 1 specific probe was tested in different dilutions on Wt embryos.

2.7.2. Generation of *Antp*-Promoter 2 (P2) specific RNA probe

For generating *Antp*-promoter2 (P2) specific RNA probe, a part of exon3 encoding 1237 bp product from DGRC clone LD33666 was amplified by PCR and cloned into the pDrive vector using Qiagen PCR Cloning kit. Three clones were confirmed positive with PCR. The plasmid from one of the clones was linearized with *Bam*HI and DIG labelled using SP6 polymerase. The synthesized RNA probe was tested in different dilutions in Wt embryos.

2.7.3. Prehybridization

Freshly fixed or stored embryos were rehydrated with 0.3% PBT, and then incubated in a 1:1 mixture of PBT and prehybridization buffer for 10 min with gentle shaking at RT. The solution was replaced with a prehybridization buffer for 10 min. The prehybridization solution was added to the embryos and incubated for 2 hrs at 62°C.

2.7.4. Hybridization

The digoxygenin (DIG)-labelled probes were diluted in hyb solution, heated for 5 min at 95°C and cooled on ice for few minutes. The prehybridization solution in the embryos was replaced with the probe solution and incubated overnight at 55°C. The probe was removed and stored at -20°C for future reuse and the embryos were washed in hyb buffer, two times for 30 min each at 62°C. Later the embryos were washed once with 1:1 mixture of 0.3% PBT / hyb buffer and later with 0.3% PBT alone each 30 min at 65°C.

2.7.5. Signal detection

Following the hybridization procedure, the embryos were washed with 0.3% PBT at RT for 20 min and then blocked in TNB buffer for 5 min. The blocked embryos were incubated in an anti-DIG-POD antibody, diluted 1:500 in TNB buffer for 2 hrs at RT. The embryos were washed three times with 0.3% PBT for 10 min each and then washed with TNT buffer for 5 min each. For signal amplification, Perkin-Elmer TSA kit was used. The embryos were incubated for 10 min in Tyramide-Cy5, diluted 1:50 in amplification diluent provided in the kit. Immediately, the embryos were rinsed and washed with TNT buffer for four times 10 min each, and then with 0.3% PBT for two times. The embryos were checked under the fluorescence microscope. At this step, the embryos were processed further for antibody staining or stored at 4°C in 70% glycerol.

2.8. Image detection and documentation

The Leica TCS SPII and SPV confocal microscopes were used for fluorescence imaging and the images were processed using Leica confocal software and Adobe Photoshop. The final images were grouped and labelled using Adobe Illustrator. Statistical significance was performed using Chi square test in Graph Pad Prism5 software.

2.9. Sequencing analysis

For identifying the mutation in *Antp* mutants, I performed sequencing analysis from Wt, *Antp*^{25} / TM3 *Twist* GFP and *Antp*^{25},*Ubx*^{1} / TM6 *Dfd* YFP genotypes. The non-coding RNA CR43252, *Antp* promoter sequence and 3' UTR regions were sequenced using genomic DNA. The coding region of *Antp* is amplified from cDNA. The PCR products amplified from cDNA and genomic DNA of the three genotypes were given for sequencing at Starseq Company. The obtained sequences were compared with the FlyBase *Antp* transcript sequences using EMBL-EBI pairwise nucleotide align program. The procedure for cDNA preparation and genomic DNA sequencing is described below.

2.9.1. cDNA preparation from Wt and homozygous *Antp*^{25} mutant embryos

Non-fluorescent homozygous mutant embryos at developmental stage 15 or older were picked under the fluorescence microscope and dechorionated mechanically with a needle on Apple juice agar medium. The dechorionated embryos were immediately moved to an Eppendorf cap and shock frozen in liquid nitrogen. Using High Pure RNA Tissue kit from Roche, the total RNA was extracted from frozen embryos and the amount estimated with the NanoDrop. The cDNA was reverse transcribed from the extracted RNA using Bio-Rad iScript cDNA synthesis Kit.

2.9.2. Genomic DNA extraction from embryos

For DNA isolation procedure, the embryos were homogenized in 400 µl of Buffer A, incubated at 65°C for 30 min. A mixture of 800 µl of Buffer B solution was added and incubated on ice for 10 min, centrifuged for 10 min at RT. The supernatant was transferred to a new Eppendorf, 600 µl of cold isopropanol was added and centrifuged for 15 min at RT. The supernatant washed with cold 70% alcohol, centrifuged, dried the pellet and resuspended in distilled water.

2.9.3. Amplification of *Antp* coding region, promoter and 3' UTR sequences

The *Antp* transcript sequences were amplified from the complete cDNA with Quiagen Q5 Hot start Hi-Fidelity DNA Polymerase. The PCR products were purified with Quiagen PCR purification Kit. The promoter and 3' UTR region of *Antp* were amplified from genomic DNA with *Taq* polymerase and purified with Quiagen PCR purification Kit.

2.9.4. Amplification of non-coding RNA CR43252

1231 bp product of non-coding RNA, CR 43252, was amplified from genomic DNA of three genotypes using the *Taq* DNA polymerase, purified with Quiagen PCR purification kit.

2.10. Gateway cloning of the truncated *Antp* ORF

The 122 aa coding *Antp* ORF from plasmid amplified from DGRC clone LD33666 using primer sets with *CACC* sequence added at the 5' end of the forward primer and and the *Taq* DNA polymerase. To remove the 3'-poly (A) overhangs that the *Taq* DNA polymerase generates on the amplified products, T4 DNA polymerase from Life Technologies was used. The blunt-ended PCR product was cloned into the TOPO Entry vector using the strategy of the directional TOPO Entry Cloning Vector from Life Technologies. Few bacterial colonies were selected and amplified, and the plasmids were prepared with Qiagen Miniprep Kit. Through double digest restriction enzyme analysis using *Eco*RV and *Sma*I, followed by sequencing analysis confirmed the right vectors. Finally, the LR recombinase reaction from Life Technologies was used to clone the truncated *Antp* gene sequence into the destination vector, pUASg.*att*B sequence (Fig. 9A) (kindly provided by Johannes Bischof, Bischof et al., 2007). The recombination reaction permitted the replacement of the *ccd*B domain of destination vector with the gene of interest. The destination plasmid UASg_*Antp-1-123*.*att*B clones were confirmed by sequencing and restriction enzyme analysis using *Eco*RV enzyme (Fig. 9B).

2.11. Generation of transgenic flies carrying the truncated Antp protein coding sequence

The confirmed destination plasmid vector was amplified in large scale and isolated using Qiagen Plasmid Midi Kit. The plasmid eluted in distilled water was sent to BestGene services to microinject in the embryos of the fly strain *M{3xP3-RFP.attP'} ZH-22A (with M{vas-int.Dm}ZH-2A)*, which carries the *att*P sites on the second chromosome at the estimated cytosite of *ZH 22A*, through phic31 integrase method (Bateman et al., 2006). The received five individual transformant transgenic fly strains were balanced using second chromosome balancer stock and maintained.

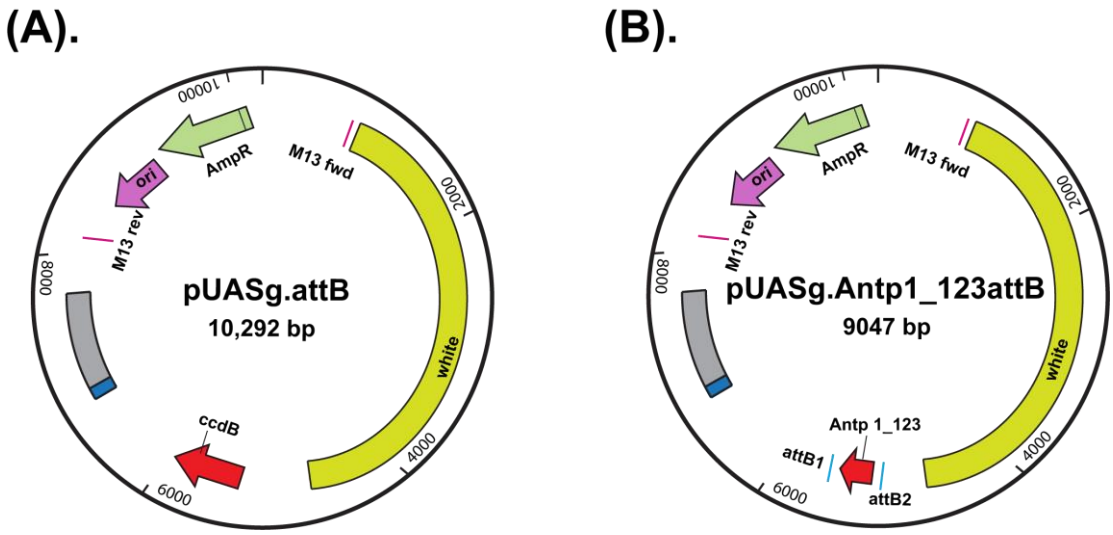

Fig. 9. Schematic vector maps of destination vector pUASg.*attB* and pUASg_*Antp1-123.attB*. (A) Destination vector contains the *attB* and lethal *ccdB* domain sites. (B) LR recombination replaces the *ccdB* (red) domain of destination vector with the truncated ORF of *Antp*.

2.12. *Drosophila* S2R+ cell culture

2.12.1. Transfection

The *Drosophila* S2R+ cells seeded with a dilution of 5-6x10^3 cells / ml per well in 3 ml of Shields and Sang M3 insect medium (Sigma) mixed with antibiotics was used for transfections. 24 hrs after seeding, the cells were transfected with the following vectors: Act-GAL4 vector (62.5 ng/µl) (plasmid kindly provided by J.Urban), pUAS_*Antp1-123_attB* vector (125 ng/µl), control pUAST Histone GFP (125 ng/µl) (plasmid kindly provided by J.Urban). The vectors were diluted in M3 medium without antibiotics to make up to 45 µl per well. For this mixture, finally 2 µl of FuGENE Transfection reagent from Promega was added and incubated for 5 min. For each well, 50 µl of transfection mixture was added slowly from one corner and gently mixed. The cells were incubated at 28°C for 48 hrs and checked under the fluorescence microscope for GFP expression to confirm the transfection has worked.

2.12.2. Antibody staining of S2R+ cells

The transfections were carried out with the Act-GAL4, pUASg_*Antp1-123_attB* vector and pUAST Histone GFP vectors and control transfection reactions with only Act-GAL4 vector and pUAST Histone GFP. After 48 hrs of transfection, the medium from the cells was carefully removed and washed three times with 1x PBS for 5 min each.

The cells were fixed in a 1:1 mix of 8% paraformaldehyde and PBS for 20 min and washed shortly with 0.1% PBT. The cells were incubated separately in diluted primary antibodies 8C11 and 4C3 overnight at 4°C. The primary antibody was washed three times, 5 min each at RT with a gentle shaking. The appropriately diluted secondary antibody was added, incubated for 2 hrs at RT, washed three times with a PBT and rinsed with PBS. Finally 15 µl of Vectashield and DAPI was added to each well and scanned using confocal microscope.

2.12.3. Protein extraction from S2R+ cells

After transfection of Act-GAL4 vector, pUAS_Antp1-123_*attB* vector, and pUAS mCherry (plasmid kindly provided by C. Hessinger) and for control experiment with Act-GAL4 vector and pUAS mCherry, the cells were collected in a falcon tubes and centrifuged at 4000 rpm for 10 min at 4°C. The medium was removed carefully and the pellet dissolved in cold 1x PBS. The cell mixture was transferred to Eppendorf tubes and centrifuged to pellet the cells. The pellet was dissolved in few µl of RIPA buffer from Bio-Rad, containing a mix of protease and phosphatase inhibitors and homogenized with a disposable micro tissue homogenizer for few minutes. A final centrifugation was performed at 10,000 rpm for 10 min at 4°C. The protein concentration was estimated using Bradford reagent from Bio-Rad Laboratories by Bradford assay method.

2.13. Detection of Antp protein

For resolving whether the observed Antp protein in *Antp* mutant embryos is truncated or full length, I performed Western blot analysis using the embryonic nuclear extracts from *Antp*^{25} mutant embryos and Wt embryos.

2.13.1. Nuclear protein extraction from embryos

Homozygous mutant embryos from the *Antp*^{25}/TM3 *Twist* GFP fly strain were picked under a fluorescence microscope. The Wt and mutant embryos were dechorionated with bleach, washed, and the excess water blotted from the embryos. To minimize protein degradation, all the steps from this point were carried out on ice. Solutions and glassware were pre-chilled before use. The embryos were homogenized in cold homogenization buffer using a glass tube and pestle, the extract was centrifuged at

4°C for 10 min at 8000 rpm. The pellet of cells settled at the bottom of the Eppendorf cap was used for nuclear protein extraction. The supernatant and a thin fatty layer above the pellet were carefully removed and the pellet resuspended in high salt buffer for 2 hrs at 4°C with gentle shaking, followed by centrifugation for 1 hr at 13,000 rpm and 4°C. The nuclear extract protein concentration in the supernatant was estimated using Bradford reagent from Bio-Rad Laboratories by Bradford assay method. Nuclear extract aliquots containing an estimate of 100 µg protein were stored at -80°C.

2.13.2. Western blot analysis

100 µg of embryonic nuclear protein extracts from Wt and *Antp*^{25} embryos and 30 µg of protein from S2R+ cell extracts transfected individually with UAS *Antp1-123* and UAS mCherry were denatured in denaturation buffer for 6 min at 98°C, loaded on 14% SDS-PAGE gel along with a prestained marker from Pierce and run at 100V in running buffer. When the marker reached the bottom of the gel, I removed the gel from the plates and washed it in cold transfer buffer. The proteins from the gel were transferred to a nitrocellulose membrane through wet transfer in transfer buffer at 4°C. For testing whether the transfer has worked, Ponceau staining was performed on the membrane and the gel was stained with Coomassie Blue buffer. The staining on the membrane was washed with water several times and incubated in 10% milk powder for 1 hr with shaking at RT. The Antp 4C3 antibody was diluted in 1:250 of 0.3% TBST buffer and incubated overnight with gentle shaking at 4°C. The blot was washed 3 times with 0.3% TBST buffer for 10 min each, followed by incubation in secondary anti mouse-POD antibody in 1:10,000 dilution at RT and three washes with 0.3% TBST buffer for 10 min each. Finally, the blot was washed in TBS for 10 min and developed using BM Chemiluminescence Western Blotting Kit, Roche and the signal was detected with Bio-Rad imager.

2.14. Media, chemicals and solutions

<u>*Drosophila* medium</u>

Agar-Agar	230 g
Yeast	700 g
Soya flour	250 g

Corn flour	1500 g
Malt extract	2200 g
Suger beet molasses	1100 g
Nipagin	70 g
Propionic acid	130 ml
distilled water	42 L

All the ingredients are mixed, except Nipagin and Propionic acid, and cooked.

Apple agar medium

Agar	28 g
Apple juice	1000 ml

The above mixture was boiled in a microwave oven until agar completely dissolved and poured into vials.

Fixation buffer

PBS	450 µl
Formaldehyde (37%)	50 µl
Heptane	500 µl

20x PBS (pH 7.4)

NaCl	151.94 g
Na2HPO4 · 2 H2O	19.88 g
NaH2PO4 · 1 H2O	8.28 g
distilled water	1000 ml

0.3% PBTX

PBS	1x
Triton-x-100	0.3%

70% Glycerol

Glycerol	7 ml
PBS	3 ml

DEPC water

0.1% of DEPC was added to double distilled water, leave overnight in a fume hood with stirring and then autoclaved.

0.3% PBT

PBS	1x
Tween 20	0.3%

Prehybridization buffer

Hybridization buffer	990 µl
ssDNA (10 mg/ml)	10 µl

Hybridization buffer

Formamide	20 ml
20x SSC	12.5 ml
DEPC water	17.5 ml
Tween 20	50 µl

TNB buffer

1M Tris (pH7.5)	10 ml
5M NaCl	3 ml
Blocking reagent	0.5 g (Perkin Elmer)
distilled water	87 ml

Stir for several hours at 60°C on a magnetic stirrer until the blocking reagent is completely dissolved. Filter, then aliquot and store at -20°C.

TNT buffer

2M NaCl	3.76 ml
1M Tris (pH 7.5)	5 ml
Tween 20	25 µl
distilled water	41.24 ml

LB medium

Tryptone	10 g
Yeast extract	5 g
NaCl	10 g
distilled water	1000 ml

The above components were dissolved and autoclaved.

M3 medium (1Liter)

Shields and Sang powdered	39.36 g (Sigma S-8398)
KHCO3	0.5 g

Adjust the pH to 6.6

Yeast extract	10 g (Sigma Y-1000)
Bactopeptone	25 g (Difco 211677)

Filtered with normal filter paper and then with a sterile filter of 0.2 µm pore size. 50 ml of the medium was stored separately for transfections. To the remaining 950 ml medium, 1% of pencillin/streptomycin (Sigma P4333) and 4% of serum was added.

4% serum

Fetal calf serum was used from HyClone. Serum stored at –20°C was thawed, warmed to room temperature, and then heated in a 56°C water bath for 30-60 min, and stored finally at 4°C.

0.1% PBT

PBS	1x
Tween 20	1%

Homogenization Buffer

Tris (pH 7.6)	50 Mm
KCl	10 mM
MgCl2	1.5 mM
EDTA (pH 8)	0.1 mM
Sucrose	350 mM
DTT	1 mM

Complete protease and phosphatase inhibitors mix 2 x (Roche)

High salt Buffer

Tris (pH 7.6)	50 mM
NaCl	0.42 M
MgCl2	1.5 mM
EDTA (pH 8)	0.1 mM
Tween 20	0.1%
Glycerol	10%
DTT	1 mM

Complete protease and phosphotase inhibitors mix 2 x (Roche)

Denaturation Buffer

Tris (pH 6.8)	0.225 M
Glycerol	100%
Bromophenolblue	0.05% (w/v)
DTT	0.25 M

Buffer A

Tris-HCl (pH 7.5)	100 mM
EDTA (pH 8)	100 mM
NaCl	100 mM

SDS	0.5 %
RNAse	10 µg/ml

Buffer B

KCH_3COO	5M
LiCl	6M

KCH_3COO and LiCl in 1 : 2.5 makes the Buffer B.

SDS-Separating gel (14%)

distilled water	2.6 ml
1.5M Tris (pH 8.8)	2.5 ml
10% SDS	100 µl
30% Acrylamide	4.7 ml
10% APS	100 µl
TEMED	10 µl

SDS-Stacking gel

distilled water	3.4 ml
1M Tris (pH 6.8)	2.5 ml
10% SDS	50 µl
30% Acrylamide	830 µl
10% APS	50 µl
TEMED	5 µl

The 14% SDS-PAGE gel was prepared according to the instructions of Bio-Rad gel casting apparatus.

Running buffer (1x)

Tris-HCl	3.02 g
Glycine	14.4 g
SDS	1 g
distilled water	1000 ml.

Adjust the pH to 8.3.

Transfer buffer

Tris-HCl	3.03 g
Glycine	14.4 g
distilled water	1000 ml

Adjust the pH to 8.5.

Ponceau solution S stock (10x)

Ponceau S w/v	2%

Trichloro acetic acid w/v	30%

The working concentration of 1:10 was diluted in distilled water.

Coomassie blue staining buffer

Coomassie-Blue (R-250)	1.25 g
Isopropanol	227 ml
Aceticacid	46 ml
distilled water	227 ml

The gel was soaked in Coomassie Blue buffer for one hour at RT on a shaker and then the excess staining was removed by washing with destaining buffer.

Coomassie-destaining buffer

Isopropanol	75 ml
Acetic acid	50 ml
distilled water	875 ml

1xTBS

Tris	3 g
NaCl	8 g
KCl	0.2 g
Distilled water	1000 ml

Adjust the pH to 7.5.

0.3% TBST

TBS	1x
Tween20	0.3%

2.15. Primers

All the primers used in this work were listed in the Table-2.4.

Table-2.4.

Primer	Sequence
Exon3-F	CGCCGCTCGATTCGCACTT
Exon3-R	AATTGTGGTGTAAAAGTCGGTGCC
RM1F	CATCACACAACAAAGCACTCG
RM1R	AGCTCATTTGCAGCACAGTC
RM2F	CGCGCGTTTCTTTTTATGAT
RM2R	TTGAAACTCTTTTGCGTTGC
RM3F	AAGCGCACGTTATTGGATTT
RM3R	TAGTGCCCATGATGCATGTC
RM4F	ATCAGCAGACGCTGAGGAAG
RM4R	GTCATCTGGGCGTTCATGT
RM5F	TTGGTGGACTGGGTATGGTT
RM5R	GGTGTTATCTCGTCGCCTTC
RM6F	ACGGAGCGCCAGATAAAGAT
RM6R	ACTTATGACGCGTAGATCTAATGTT
RM7F	CAAAACCAACTCATGTGACCTC
RM7R	GCATAAATATCCACTTGCGAGTTT
RM8F	GCAAGAGATTGGCCAACTTAAA
RM8R	ATGGGATTTCTGGGGAATTT
RM9F	GAGGACGGAATGGCAAACTA
RM12R	TCGACGTGAAAGCTGACATC
RM0F(promoter)	AGTTCTCGCTGGGATTTTCA
RM0R(promoter)	CCGAATACCGTTATGCTGCT
RH1F	ATGAATGGACGTGCCAAAT
RH1R	GAACGAGCCCAACGAAAAT
RH2F	CGGCAGCAACATTGAACTT
RH2R	TCATACTTCGAATTTCCCGATT
RH3F	CGCCCAAATTGTGATTGTA
RH3R	CCGCGTGCTTTTAGCTACT
RH4F	GAACAGCAAAGCGAAAATC
RH4R	CTGTTGCTGCTGGTTCTGC
RH5F	AGCAGCACCAGGTCTACTCC
RH5R	TTCGCATCCAGGGATACAGT
RH6F	GACATCCTGGCCAACACAC
RH6R	TTTCAAGCGACAAGGTAGGTT
RH7F	CCCTCTTCGCTTTTCAATTTT
RH7R	CCAGCCCTCATTAGTTACGC
RH0F(promoter)	ACAATGCCGCCATTTATCAT
RH0R(promoter)	GAACCGAACGGAACTAAACG
Antp1_123F	CACCATGACGATGAGTACAAAC
Antp1_123R	TTGCTACTGGTTCTGCGAG
CR43252F	GAGCAACGTGAAGCACAAAA
CR43252R	TTGTGTAATTCAGCGTTTCTTATTT

3. Results

In the *Drosophila* embryonic ventral nerve cord (VNC), the zinc-finger protein Eagle (Eg) is expressed in the delaminated NB7-3 and its progeny along with three other lineages NB2-4, NB3-3 and NB6-4 (Higashijima et al., 1996; Dittrich et al., 1997). After delamination at stage 11, NB7-3 asymmetrically divides and generates three ganglion mother cells (GMC-1, GMC-2 and GMC-3), which generally divide only once and produce a total of 6 neurons (Fig. 10A). The terminal NB7-3, after generating the three GMCs, undergoes apoptosis at mid embryonic development (Karcavich and Doe, 2005). The dorsomedial position clearly demarks NB7-3 from the other Eg-positive lineages. A unique combination of molecular marker genes such as the temporal transcription factors Hunchback (Hb) and Kruppel (Kr), the Zinc-finger homeodomain protein1 (Zfh1), Zinc-finger homeodomain protein2 (Zfh2) and the *Drosophila* Serotonin transporter (dSerT), along with Eg, allows unambiguous identification of the six neurons generated by NB7-3 (Fig. 10A) (Lundell and Hirsh, 1992, 1998; Isshiki et al., 2001; Novotny et al., 2002). In *Df(3L)H99* (*H99*) embryos, a deficiency which removes pro-apoptic genes *grim*, *head involution defective* (*hid*) and *reaper* (*rpr*) genes causes an absence of cell death (White et al., 1994), shows 9 to 10 cells in NB7-3 lineage (Rogulja-Ortmann et al., 2007). A Notch-mediated apoptotic process removes the sibling (sib) neurons of EW2 and EW3 at mid embryonic development (Lundell et al., 2003) (Fig. 10A). Exceptionally, the EW2sib neuron of anterior thoracic segments often observed until late embryonic stages (Rogulja-Ortmann et al., 2008). In addition, specific expression of homeotic (*Hox*) genes refines the late embryonic NB7-3 lineages in a segment-specific manner (Rogulja-Ortmann et al., 2008). The *Hox* gene *Ultrabithorax* (*Ubx*) removes the GW neuron from the third thoracic to the seventh abdominal segments (T3-A7) in the late embryonic stages through activation of apoptosis. Conversely, high *Antennapedia* (*Antp*) expression levels rescue it from apoptosis in anterior thoracic segments T1 and T2. Similarly, the GW neuron from NB7-3 lineages of the Labial (Lab) segment is removed by late embryonic stages (Rogulja-Ortmann and Technau, 2008). Hence, NB7-3 lineages in anterior thoracic segments of late embryos commonly show four neurons GW, EW1, EW2 and EW3, but most often the fifth neuron EW2sib is also observed. Contrarily, the 7-3 lineages of Lab and T3-A7 segments at the end of embryogenesis possess only three neurons EW1, EW2 and

EW3 (Fig. 7B, 10B). As part of the above *Hox*-mediated NB7-3 lineage refinement studies, Rogulja-Ortmann et al., 2008, noted enlarged thoracic NB7-3 lineages in the *Antp*^{25},*Ubx*^{1} double mutant. In order to further characterize the function of *Hox* genes in segment-specific development of NB7-3, the thoracic lineages were closely analyzed using available antibody markers in single *Antp*^{25} and in the *Antp*^{25},*Ubx*^{1} double mutants. An in-depth analysis was carried out to understand how this phenotype is arising in specific-*Hox* mutants.

3.1. *Antp* mutation affects the NB7-3 lineages of labial anterior thoracic segments

Close analysis of the late embryonic NB7-3 lineages using Eg and Hb antibody markers in single *Antp*^{25} and *Antp*^{25},*Ubx*^{1} double mutants uncovered two segment-specific phenotypes. The phenotypes were observed in Lab and T1-T2 segments of single *Antp*^{25} mutant embryos and from Lab to T3 segments of the *Antp*^{25},*Ubx*^{1} double mutant embryos. The GW neurons of Wt 7-3 lineages in Lab and T3-A7 segments undergo segment-specific apoptosis in late embryonic stages (Rogulja-Ortmann and Technau, 2008). Due to this variability in the composition of 7-3 lineages of Lab and T1-T2 segments at developmental stage 16 (Fig. 10B), I restricted the statistical analysis to T1-T2 hemisegments only. In Wt anterior thoracic segments, the NB7-3 lineage of stage 16 embryos retains 4 to 5 Eg-positive cells, including two Hb co-expressing neurons, GW and EW1 (Fig. 10C, C1, C1'). In contrast, 34.28% (n = 70) T1-T2 hemisegments of the single *Antp*^{25} mutant possess 6 to 7 neurons with typical two Hb co-expressing cells (Fig. 10D, D2, D2'). Moreover, in 12.85% (n = 70) of the hemisegments, a very enlarged NB7-3 lineage comprising 8 to 12 Eg-positive neurons with four Hb co-expressing cells instead of two was observed (Fig. 10D, D1, D1'). The two phenotypes observed could be fully distinguished based on the number of Hb co-expressing cells and total Eg-positive neurons in the lineage. Analysis of the NB7-3 lineages in *Antp*^{25}*,Ubx*^{1} double mutant embryos, in which an additional posterior *Hox* gene *Ubx* mutation, *Ubx*^{1} (Castelli-Gair et al., 1990), is carried along with *Antp*^{25} mutation, surprisingly revealed the enlarged 8 to 12 neuron phenotype (Fig. 10E, E1, E1') with an expressivity of 91.07% (n = 56), and the 6 to 7 neuron phenotype (Fig. 10E, E2, E2') was noted in remaining 8.92% of the hemisegments.

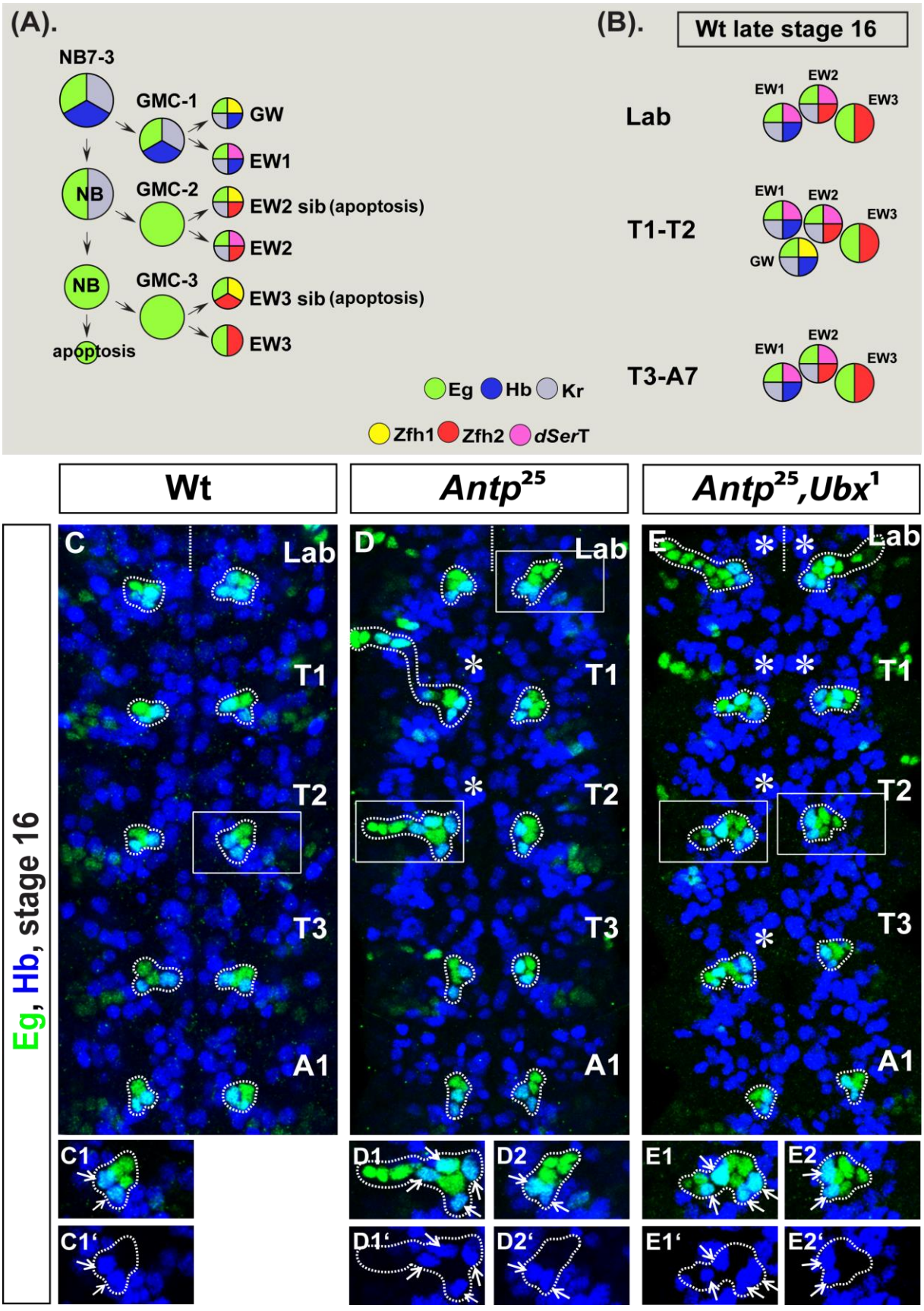

Fig. 10. Segment-specific NB7-3 lineages in *Antp* mutants.
(A) Schematic showing the Wt NB7-3 division mode, including the molecular markers, to differentiate neurons of the lineage in late embryonic VNC. The terminal NB and the sibling neurons of EW2 and EW3 undergo early apoptosis. (B) By late embryonic stages in Wt, the GW neuron undergoes

apoptosis in Lab and T3-A7 segments, but not in the T1-T2 segments. (C, D, E) Late embryonic confocal sections of Eg and Hb staining focusing on NB7-3 lineage (outlined) from Lab to A1 segments in Wt (C), *Antp*^{25} (D) and *Antp*^{25},*Ubx*^{1} (E) mutants. Anterior is up in all images. Dotted straight line marks the midline and the segments in view are always indicated on the right hand side of the image. Magnified single scan of the representative hemisegment (rectangle) lineage of each genotype is shown below. The Hb-positive cells in the magnified sections are indicated with arrows. Hemisegments with duplicated Hb-positive cells are marked with an asterisk (*). (B, B1, B1') The 7-3 lineages of anterior thoracic hemisegments in Wt show 4 to 5 Eg-positive cells, including two Hb co-expressing cells. (C) Certain NB7-3 lineages of Lab to T2 hemisegments of *Antp*^{25} mutants display either one or two additional cells with typical two Hb-positive cells (C2, C2') or a very enlarged cluster of 8 to 12 cells with four Hb co-expressing cells (C1, C1'). (D) In *Antp*^{25},*Ubx*^{1} double mutants, the duplicated Hb co-expressing neuron phenotype (D1, D1') is strongly penetrant from Lab to T3 segments, whereas in the remaining hemisegments, 6 to 7 cell lineages (D2, D2') are seen. Both phenotypes are extended to T3 hemisegments of double mutant embryos.

Both NB7-3 lineage phenotypes observed in anterior thoracic segments of single *Antp*^{25} mutant were also observed in T3 segment of the *Antp*^{25},*Ubx*^{1} double mutant (Fig. 10E). This observation is consistent with the described transformation in *Ubx* mutants, in which the T3 segment attains the identity of anterior T1 or T2 segment (Carroll et al., 1986). The T3 segment NB7-3 lineages of the *Antp*^{25},*Ubx*^{1} double mutant also exhibit the 8 to 12 neuron phenotype with a frequency of 88% (n = 18). Together, the Hb and Eg expression analysis in single *Antp*^{25} and *Antp*^{25},*Ubx*^{1} double mutants clearly suggests that the Hb-positive neurons were doubled in very enlarged NB7-3 lineage. The T3 segment NB7-3 lineages in *Antp*^{25},*Ubx*^{1} double mutants transformed to either T1 or T2 identity and exhibited both phenotypes. On the other hand, only one or two extra Eg-positive cells were seen in 6 to 7 neuron phenotype compared to the characteristic anterior thoracic Wt NB7-3 lineages. To characterize the supernumerary cells in the two observed NB7-3 lineage phenotypes of *Antp* mutants, expression of other molecular markers (Zfh1, Zfh2, Kr and *dSer*T) was analyzed.

The Zfh1 expression is initiated from embryonic developmental stage 13 or 14 and is restricted to GW, EW2sib and EW3sib neurons of the NB7-3 lineage (Lundell and Hirsh, 1998; Isshiki et al., 2001; Karcavich and Doe, 2005; Lee and Lundell, 2007). However, Notch-mediated apoptotic process removes Zfh1-expressing cells EW3sib and EW2sib neurons by stage 16 (Lundell et al., 2003). Thus, the Zfh1-positive cell observed in the NB7-3 lineage at stage 16 is the GW neuron (Fig. 10A, B). Expression analysis of Zfh1 along with Hb and Eg in Wt NB7-3 lineages at stage 16 confirms the presence of GW and the EW2sib cell, which typically survives longer in anterior thoracic segments (Fig. 11A, A', A'', A'''). Among the 6 to 7 Eg-positive

neurons in anterior thoracic 7-3 lineages of *Antp* mutants, three Zfh1 expressing cells were observed (Fig. 11B, B', B", B"'). Hb co-expression confirms that one neuron is the GW. Of the remaining two Zfh1-positive cells, one is EW2sib, which survives longer. The other smaller cell is most likely the EW3sib, which generally undergoes apoptosis by stage 16. In NB7-3 lineages of *Antp* mutants with 8 to 12 Eg-positive neurons, the number of cells expressing Zfh1 varies from 4 to 6. Importantly, among the 4 to 6 Zfh1-positive neurons in the lineage, two cells co-express Hb (Fig. 11C, C', C", C"'). This observation clearly substantiates the assertion that the number of GW neurons among the four Hb expressing neurons is doubled in the enlarged 8 to 12-cell NB7-3 lineage. Other 2 to 4 Hb-negative cells suggest the duplication and survival of EW2sib and EW3sib neurons.

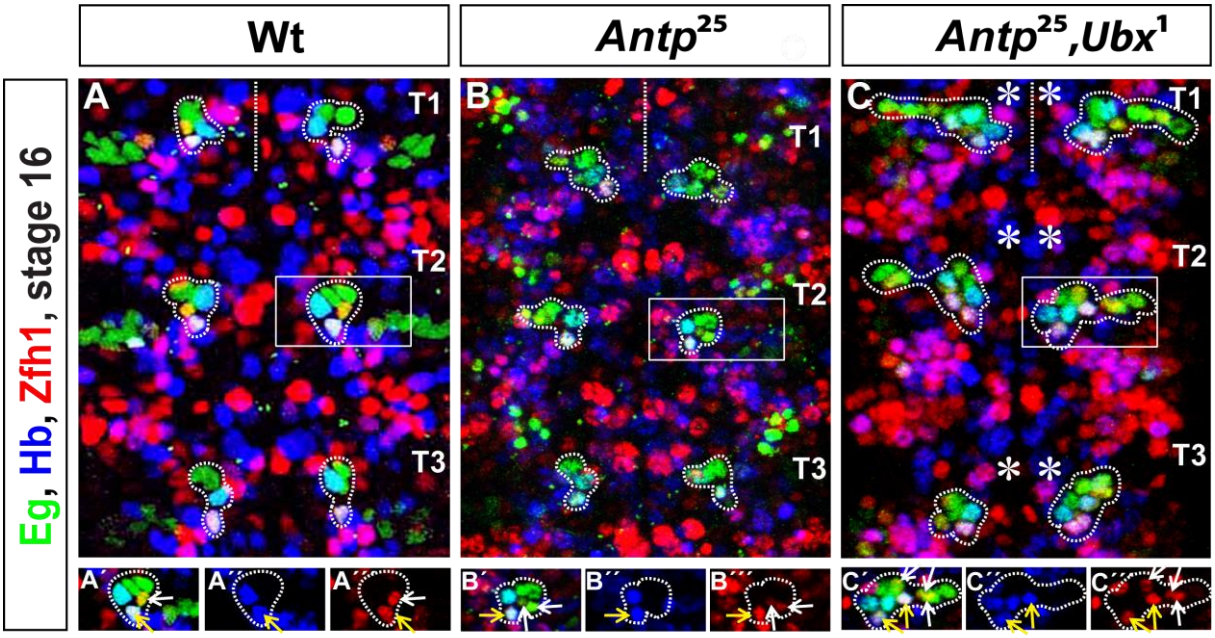

Fig. 11. Duplication of Zfh1 expressing cells in enlarged 7-3 lineages of *Antp* mutants.
(A-C) Confocal sections of Eg, Hb and Zfh1 co-staining focusing on 7-3 lineages (outline) of Wt (A), *Antp*^{25} (B) and *Antp*^{25},*Ubx*^{1} (C) mutants. Anterior is up in all images. Dotted line marks the midline and the segments in view are always indicated on the right hand side of the image. Hemisegments with duplicated Hb-positive cells are marked with an asterisk (*). Magnified single scan of the representative hemisegment (rectangle) of each genotype is shown below. The single channels of Hb and Zfh1 expression are shown for magnified images. The co-labeling with Zfh1 and Hb in NB7-3 lineages discriminates the GW neuron (yellow arrows) from EW2sib and EW3sib neurons (white arrows). (A, A', A", A"') Anterior thoracic 7-3 lineages in Wt at stage 16 retain the Zfh1-positive cell, GW, and very often EW2sib neuron as well. (B, B', B", B"') In 6-7 neuron lineage of *Antp* mutants, three Zfh1 neurons are observed. Hb co-expression identifies one cell as the GW neuron (yellow arrow), whereas the remaining two are most likely the surviving EW2sib and EW3sib neurons. (C, C', C", C"') In 8-12 cell NB7-3 lineage, 4 to 6 Zfh1-positive cells are noted, of which Hb and Zfh1 co-expression identifies two GW neurons.

Zfh2 is expressed from embryonic stage 14 onwards in four post-mitotic NB7-3 progeny cells (EW2, EW2sib, EW3 and EW3sib) generated from GMC-2 and GMC-3 (Lundell and Hirsh, 1992, 1998; Isshiki et al., 2001; Karcavich and Doe, 2005; Lee

and Lundell, 2007). However, only EW2 and EW3 neurons survive until late embryonic stages (Lundell et al., 2003) (Fig. 10A, B). The Zfh2 co-staining, along with the presence of Eg in Wt embryos at stage 16 shows only three Zfh2-positive cells in anterior thoracic segments, which clarifies that either EW2sib or EW3sib neuron was removed by that stage (Fig. 12A, A', A"). In *Antp* mutants, four Zfh2-positive cells were noted in a 6 to 7 cell NB7-3 lineage (Fig. 12B, B', B"). It again suggests the prolonged survival of EW3sib neuron along with EW2sib cell. In the 8 to 12 cell NB7-3 lineage of *Antp* mutants, the Zfh2-expressing cell number was doubled and showed 6 to 8 cells (Fig. 12C, C', C"). This finding indicates that EW2, EW3 and their sibling neurons are duplicated in an enlarged 7-3 lineage.

The acquisition of the temporal factor Kr expression is restricted to the progeny generated from GMC-1 and GMC-2 (GW, EW1, EW2 and EW2sib) (Fig. 10A) (Isshiki et al., 2001; Karcavich and Doe, 2005). Co-expression analysis of Kr and Eg confirms the presence of four double positive cells in anterior thoracic segments of stage 16 embryos (Fig. 12D, D', D"). The Kr-positive neuronal number in a 6 to 7 cell NB7-3 lineage was not altered in *Antp* mutants (Fig. 12E, E", E"). It strongly suggests a duplication of the pertinent neurons and the survival of EW2sib in enlarged NB7-3 lineage (Fig. 12F, F', F").

The dSerT expression is initiated exclusively in EW1 and EW2 neurons at late embryonic stages in the VNC (Fig. 10A) (Lundell and Hirsh, 1994; Dittrich et al., 1997). Analysis of *dSer*T mRNA expression in stage 16 Wt embryos confirms two positive cells in anterior thoracic segments (Fig. 12G). In a 6 to 7 cell NB7-3 lineage, only two *dSer*T- positive cells were noted (Fig. 12H). Among the 8 to 12 cell NB7-3 lineage of *Antp* mutants, four *dSer*T expressing cells were noted (Fig. 12I). This finding confirms that the EW1 and EW2 neurons are duplicated in enlarged NB7-3 lineages of *Antp* mutants. Combining the analysis of Hb, Kr, Zfh1, Zfh2 and *dSer*T expression in *Antp* mutants distinguished the two phenotypes, one as a survival of early dying neurons and another as a complete lineage doubling phenotype. Thus, the two phenotypes observed in *Antp* mutants were classified and hereafter referred to as a ''cell survival phenotype'' and "the duplication phenotype", respectively (Fig. 13). The duplicated lineage was occasionally located in an anterolateral position (Fig. 10D, T1-left hemisegment).

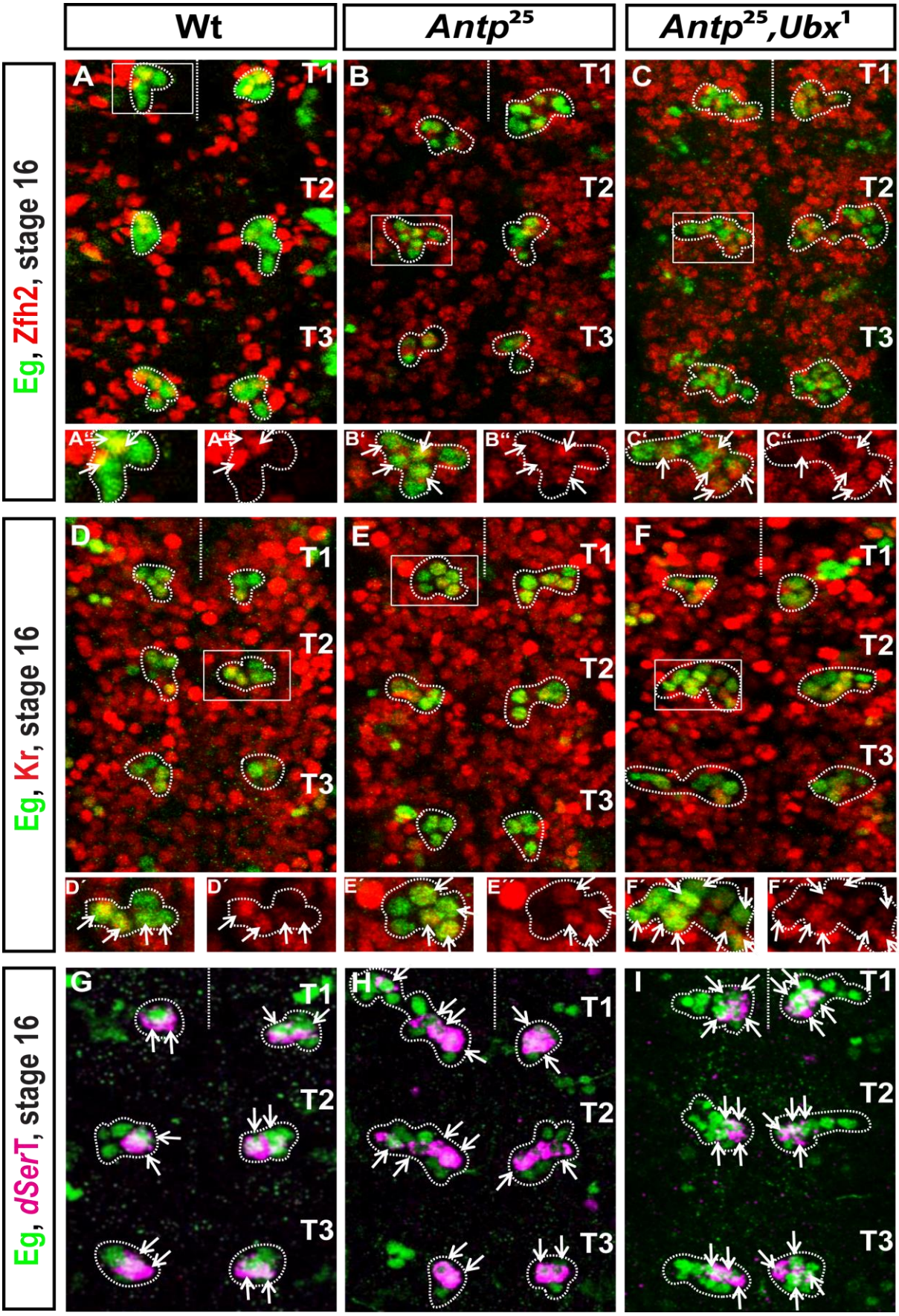
Wt
Antp25
Antp25,Ubx1
Eg, Zfh2, stage 16
Eg, Kr, stage 16
Eg, dSerT, stage 16
A
B
C
D
E
F
G
H
I
T1
T2
T3

Fig. 12. Molecular marker analysis of supernumerary cells in 7-3 lineages of *Antp* mutants.
(A-C) Co-staining of Eg and Zfh2 focusing on the NB7-3 lineage (outline) of Wt (A), *Antp*^{25} (B) and *Antp*^{25},*Ubx*^{1} (C) mutants. Anterior is up in all images. Dotted line marks the midline and the segments in view are always indicated on the right hand side of the image. Hemisegments with enlarged NB7-3 lineages are marked with an asterisk (*). In the magnified image of the representative hemisegment (rectangle), the co-expressed cells are pointed with an arrow. The single channel of Zfh2 expression is shown in magnified images. (A, A', A") Depending on the EW2sib apoptosis, anterior thoracic NB7-3 lineages in Wt possess two or three Zfh2-expressing cells (arrows). (B, B', B") Of the 6 cells in the NB7-3 lineage of *Antp*^{25} mutants at stage 16, four Zfh2-expressing cells are sustained. (C, C', C") In 8 to 12 cell NB7-3 lineage of *Antp* mutants, 6 to 8 Zfh2-positive cells are noted. (D-F) Co-staining of Eg and temporal factor Kr focusing on the NB7-3 lineage (outline) of Wt (D), *Antp*^{25} (E) and *Antp*^{25},*Ubx*^{1} (F) mutants. The single channel of Kr expression is shown in magnified images. (D, D', D") The Wt anterior thoracic segments most often show three or four Kr expressing cells at stage 16. (E, E', E") In NB7-3 lineages of *Antp* mutants with six cells, four Kr-positive cells are observed. (F, F', F") Kr-expressing cell number is increased to eight in enlarged NB7-3 lineages of *Antp* mutants. (G-I) Confocal sections stained for Eg and fluorescent *in situ* hybridization for *dSer*T focusing on the NB7-3 lineage (outline) of Wt (G), *Antp*^{25} (H) and *Antp*^{25},*Ubx*^{1} (I) mutants. The *dSer*T-positive cells are highlighted with an arrow. (G) *dSer*T expression is initiated in late embryonic stages, exclusively in EW1 and EW2 cells in Wt. (H, I) Four *dSer*T expressing cells are seen in *Antp* mutant hemisegments possessing 8 to 12 neurons.

The results noted above also revealed that, within the duplicated NB7-3 lineage, the EW3sib neuron could survive until late embryonic stages. On the other hand, it is surprising how the posteriorly expressed *Hox* gene *Ubx* mutation in *Antp*^{25},*Ubx*^{1} double mutant enhances the NB7-3 lineage duplication frequency in anterior thoracic segments compared to the single *Antp*^{25} mutation. In order to evaluate the role of the *Ubx* mutation in enhancing the duplication phenotype frequency in *Antp*^{25},*Ubx*^{1} double mutant, genetic strategies such as rescue experiments, segregation of *Antp* mutation from the double mutant and recombination of single *Antp* and *Ubx* mutants, were undertaken. The observations are discussed in the next section.

3.2. The loss of *Antp* alone causes the NB7-3 lineage duplication

In order to evaluate the contribution of the *Ubx* mutation to high NB7-3 lineage duplication frequency in anterior thoracic segments of the *Antp*^{25},*Ubx*^{1} double mutant, rescue experiments were performed. The overexpression experiments were carried out under control of the *en* GAL4 driver, which drives the expression in the posterior segment region within the neuroectoderm and in the VNC (Kassis, 1990). These experiments revealed that *Antp* overexpression significantly suppressed the duplication phenotype in anterior thoracic lineages from 91.07% (n = 56) to 6% (n = 50) in the double mutant (Fig. 14A, A'). It also rescued the duplication phenotype

completely in T3 and Lab segments due to transformation to anterior thoracic identity (Fig. 14A, A') (Schneuwly et al., 1987).

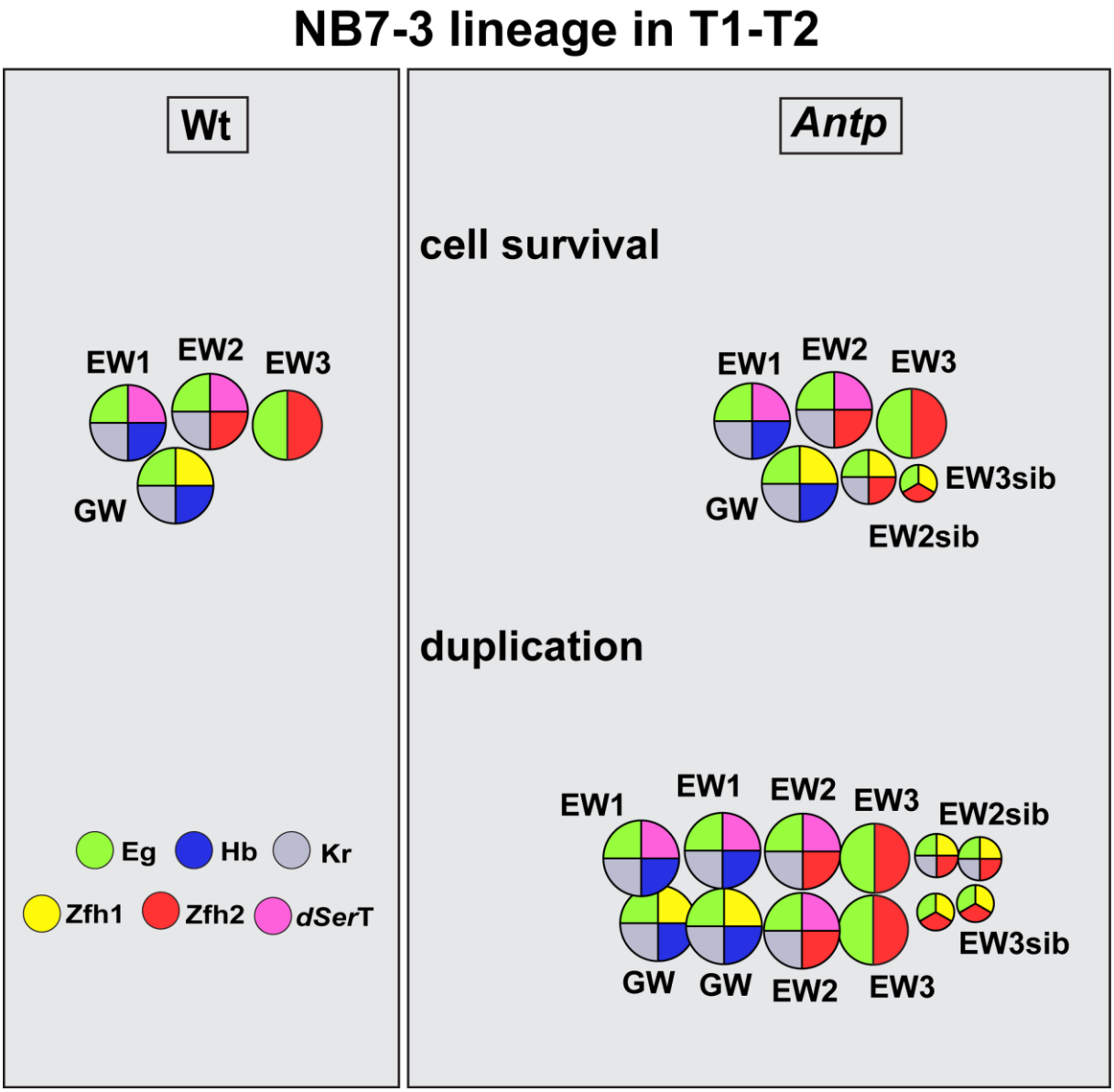

Fig. 13. Summary of two phenotypes in *Antp* mutants.
NB7-3 lineage marker analysis of anterior thoracic hemisegments in Wt and *Antp* mutants at stage 16 confirms the cell survival and duplication of the NB7-3 lineage in *Antp* mutants.

These observations clarify that the early *Antp* expression can suppress the occurrence of the NB7-3 lineage duplication in Lab and anterior thoracic segments. In similar rescue experiments using *Ubx* overexpression, the duplication phenotype was rescued owing to identity transformation in all segments towards the T3 segment identity (Gonzales-Reyes and Morata, 1990) (Fig. 14B, B'). This transformation

resulted in smaller 7-3 lineages and frequent removal of the GW neuron from anterior thoracic segment lineages (Rogulja-Ortmann et al., 2008). Due to the transformation effect, the exact impact of the *Ubx* mutation in increasing the duplication phenotype was not possible to evaluate using the overexpression strategy.

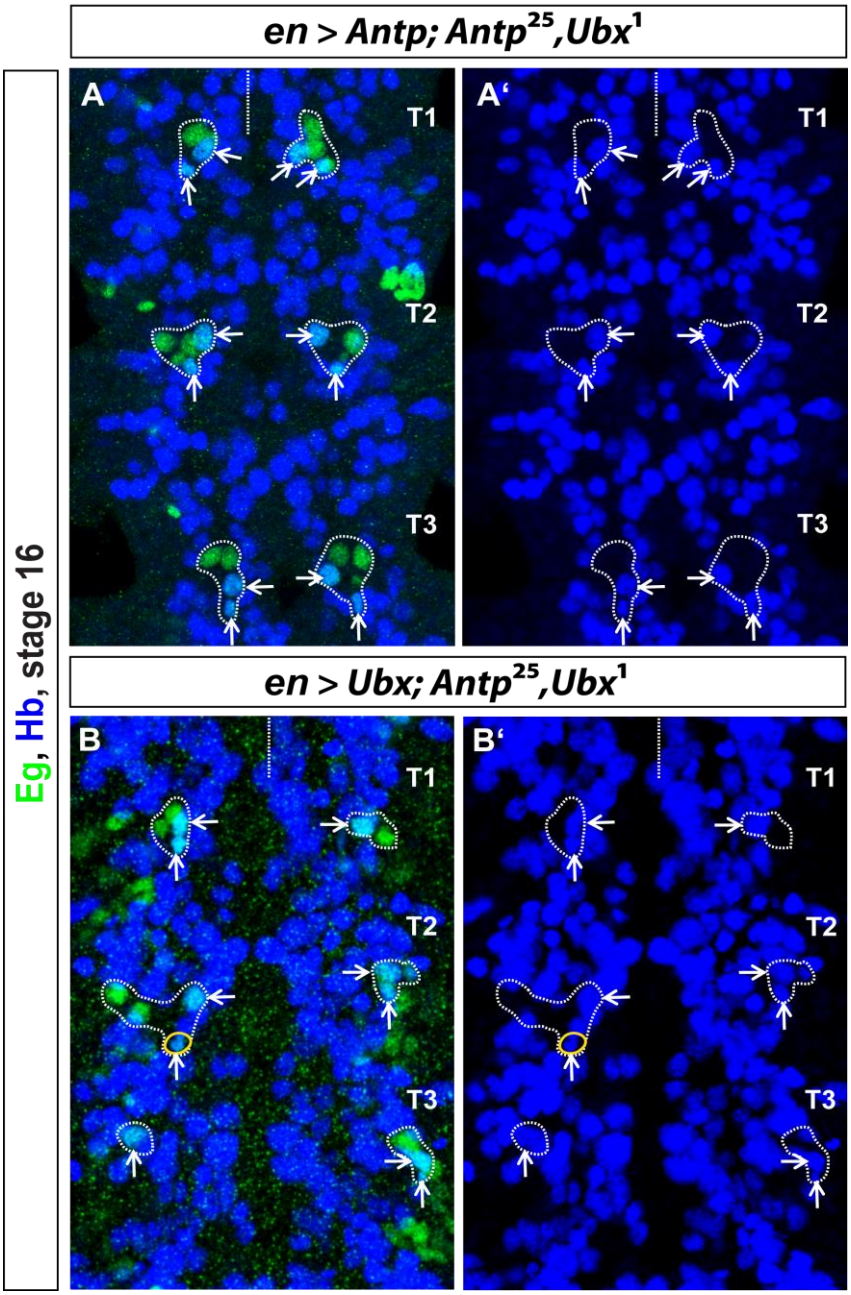

Fig. 14. Overexpression of *Antp* and *Ubx* rescues the duplication phenotype.
Confocal sections of late embryos stained for Eg and Hb focusing on the NB7-3 lineage (outlined). Anterior is up in all images. Dotted straight line marks the midline and the segments in view are always indicated on the right hand side of the image. Hb-positive cells of 7-3 lineages are shown with arrows in both single and double channels. (A, A') Overexpression of *Antp* using *en* GAL4 driver in $Antp^{25}$,Ubx^{1} mutants rescued the duplication phenotype. (B, B') Overexpression of *Ubx* using *en* GAL4 rescues the duplication of NB7-3. The GW neuron was removed from T1 right hemisegment NB7-3 lineage due to transformation of anterior thoracic 7-3 lineages to the T3 identity. A very small probably dying GW neuron in T2 left hemisegment is outlined in yellow.

To circumvent this issue, the *Antp*^{25} mutation was segregated from the *Antp*^{25},*Ubx*^{1} double mutant through segregation. The duplication frequency was determined in eight single *Antp*^{25} segregation mutants (from here on referred to as *Antp*$^{25\ seg}$) (Fig. 15A). In all eight mutants, it was significantly higher than in the single *Antp*^{25} mutation with an average expressivity of 60% ($p<0.0001$) (Table-3.1). Since the wild-typic Ubx expression is restored in all the *Antp*$^{25\ seg}$ mutants, the phenotypes were lost from T3 segment lineages, suggesting that *Ubx* mutation imposes its effect on the T3 segment only (Fig. 15B, B'). Moreover, the higher duplication frequencies in all the *Antp*$^{25\ seg}$ mutants derived from the *Antp*^{25},*Ubx*^{1} double mutant strongly suggest that the duplication phenotype was arising from a mutation in *Antp* alone. To evaluate this assertion, further single *Antp* mutants and deficiencies were analyzed, and the duplication phenotype occurrence determined. The results revealed that several *Antp* mutants and three cytologically mapped deficiencies tested also exhibit the duplication phenotype in two ranges (Table-3.1). The strength of duplication displayed by *Antp*^{11}, a loss of function allele (Johnston et al., 1998), and the three cytologically mapped deficiencies were comparable to those noted in the single *Antp*^{25} mutation (Fig. 16A, Table-3.1). Notably, the *Antp*^{14} mutation, which is a reciprocal translocation of second and third chromosomes (Scott et al., 1983; Abbott and Kaufman, 1986), exhibited a duplication frequency similar to that of the *Antp*$^{25\ seg}$ mutations (Fig. 16B, Table-3.1). Importantly, three single amorphic *Ubx* mutants *Ubx*^{1}, *Ubx*$^{9.22}$ and *Ubx*$^{6.28}$ (Weinzierl et al., 1987) did not display the duplication of NB7-3 lineages in any of the three thoracic segments (Table-3.1). These observations strongly suggest that only the *Antp* mutation causes the duplication of NB7-3 lineages in the labial and anterior thorax. In order to better understand the contribution of the *Ubx* mutation in causing the duplication frequency, the single *Antp* and the *Ubx* mutants were recombined to generate double mutants. The single *Antp*^{25} and *Antp*^{11} mutants with a duplication frequency of 12.85% and 16%, respectively, were recombined with two different *Ubx* mutations, *Ubx*^{1}, and *Ubx*$^{9.22}$ and the duplication frequency determined. The duplication frequency in the recombined *Antp*^{25},*Ubx*^{1} double mutant that I generated (lab) is observed in 21.87% of the cases (n = 32), which is not significant ($p=0.0940$) increase compared to the single *Antp*^{25} mutant (Fig. 15C).

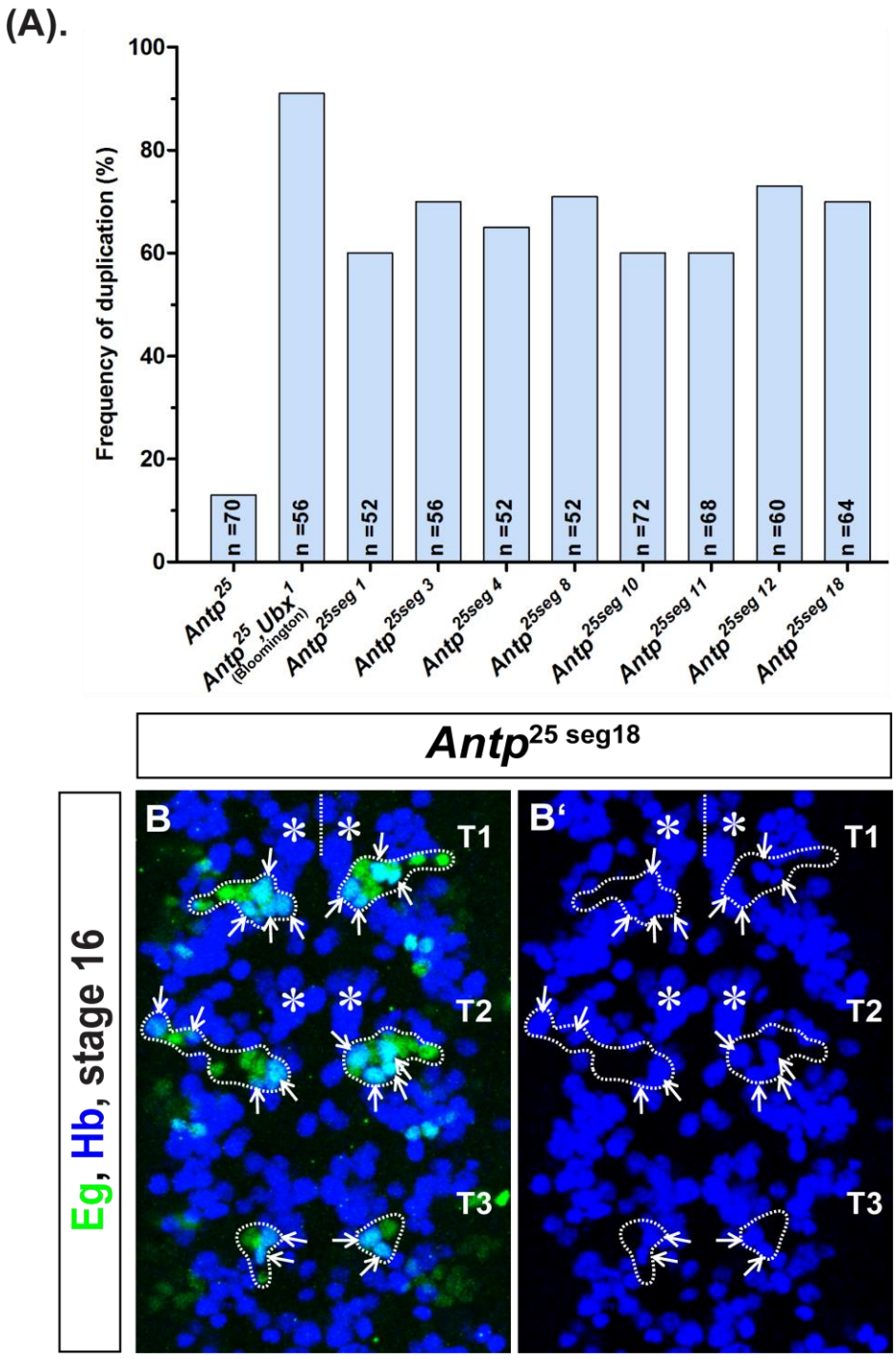

Fig. 15. *Antp*$^{25\ seg}$ mutants segregated from the *Antp*^{25},*Ubx*^{1} double mutant exhibit high duplication frequencies.

Graphic representation of duplication frequency in T1-T2 hemisegments of the single *Antp*^{25} and the double *Antp*^{25},*Ubx*^{1} (Bloomigton) mutant, as well as eight segregated *Antp*$^{25\ seg}$ mutants. All the segregation mutants exhibit significantly higher duplication frequencies compared to the single *Antp*^{25} mutant. The number of hemisegments analyzed in each genotype is denoted with n. (B, B') Confocal sections of a late *Antp*$^{25\ seg18}$ embryo stained for Eg and Hb focusing on the NB7-3 lineage (outlined). Anterior is up in both images. Dotted straight line marks the midline and the segments in view are always indicated on the right hand side of the image. Hb-positive cells of 7-3 lineages are shown with arrows in both single and double channels, whereas hemisegments with duplicated Hb-positive cells are marked with an asterisk (*). In the segregated single *Antp*$^{25\ seg18}$ mutants, the NB7-3 duplication phenotype is seen only in Lab, T1 and T2 segments, but not in T3.

The frequency exhibited by *Antp*^{25},*Ubx*^{1} (lab) double mutant is not comparable to the 91.07% of the *Antp*^{25},*Ubx*^{1} double mutant that was obtained from the Bloomington stock collection (hereafter referred to as *Antp*^{25},*Ubx*^{1} (Bloomington)). Similarly, the duplication frequency in the *Antp*^{11},*Ubx*^{1} and *Antp*^{11},*Ubx*$^{9.22}$ double mutants did not display any significant increase in frequency compared to the single *Antp*^{11} mutations (Fig. 15C, Table-3.1). The duplication phenotype was extended to T3 segment in the recombined double mutants, which was ascribed to segmental transformation. These observations clearly suggest that the *Ubx* mutation neither causes the duplication phenotype nor enhances its frequency in anterior thoracic segments. Hence, the nearly complete duplication phenotype rescue by *Antp* overexpression in *Antp*^{25},*Ubx*^{1} (Bloomington) double mutant, combined with a lack of phenotype enhancement in the newly recombined *Antp* and *Ubx* double mutants, ruled out the *Ubx* role in causing the duplication phenotype in anterior thoracic NB7-3 lineages. This assertion is supported by the high frequency of NB7-3 duplications in all the segregated *Antp*$^{25\ seg}$ mutations and in the single *Antp*^{14} mutant, none of which carry the *Ubx* mutation.

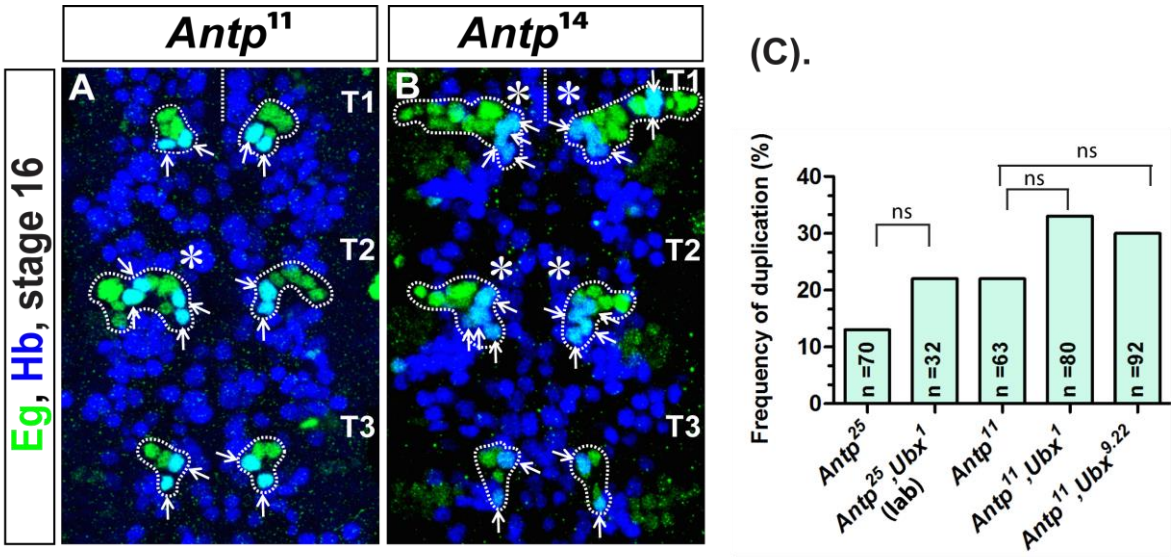

Fig. 16. The *Ubx* mutation does not have significant impact on the duplication frequency caused by *Antp* mutation.
(A, B) Confocal sections of late embryos stained for Eg and Hb focusing on the NB7-3 lineages (outlined) in *Antp*^{11} and *Antp*^{14} mutants. Anterior is up in both images. The midline is marked with a dotted straight line and the segments in view are always indicated on the right hand side of the image. Hb-positive cells of 7-3 lineages are pointed with arrows and the hemisegments with duplicated Hb-positive cells are marked with an asterisk (*). Both the segment-specific duplication phenotype and the cell survival phenotype are seen in single *Antp* mutants. (C) Graphical representation of duplication phenotype frequency in embryos where *Ubx* mutations were recombined with single *Antp* mutants. The number of hemisegments analyzed in each genotype is denoted with n value. Duplication frequencies of single *Antp* mutants have not increased significantly by recombining with *Ubx* mutation. The Chi-squared test (χ^2) was applied for statistical significance analysis and it shows not significant (ns) p values (Table-3.1).

Genotype	Mutation	Frequency (%)	n	χ2 p
Antp^{25}	amorph	12.85%	70	
Antp^{25},*Ubx*^{1} (Bloomington)	double mutant	91.07%	56	
Antp$^{25\ seg1}$	*Antp*^{25} segregation	59.61%	52	<0.0001
Antp$^{25\ seg3}$	*Antp*^{25} segregation	69.64%	56	<0.0001
Antp$^{25\ seg4}$	*Antp*^{25} segregation	65.38%	52	<0.0001
Antp$^{25\ seg8}$	*Antp*^{25} segregation	71.15%	52	<0.0001
Antp$^{25\ seg10}$	*Antp*^{25} segregation	59.72%	72	<0.0001
Antp$^{25\ seg11}$	*Antp*^{25} segregation	60.29%	68	<0.0001
Antp$^{25\ seg12}$	*Antp*^{25} segregation	73.33%	60	<0.0001
Antp$^{25\ seg18}$	*Antp*^{25} segregation	70.31%	64	<0.0001
Antp^{1}	hypomorph	0%	24	
Antp^{11}	loss of function	22.22%	63	
Antp^{14}	translocation	65.62%	32	
Antp^{11}/ *Antp*^{14}	transheterozygotes	52.77%	36	
Antp^{17}	hypomorph	0%	40	
Antp^{2}	deficiency	0%	20	
Antp^{23}	hypomorph	0%	24	
Antp^{6}	deficiency	6.25%	32	
Antp^{7}	deficiency	22.50%	40	
Df(3R)Antp-A41	deficiency	11.53%	52	
Df(3R)roe	deficiency	19.23%	52	
Ubx^{1}	loss of function	0%	20	
Ubx$^{6.28}$	amorph	0%	20	
Ubx$^{9.22}$	amorph	0%	40	
Antp^{25},*Ubx*^{1} (lab)	double mutant	21.87%	32	0.0940
Antp^{11},*Ubx*^{1} (lab)	double mutant	32.50%	80	0.0815
Antp^{11},*Ubx*$^{9.22}$ (lab)	double mutant	30.43%	92	0.1972

Table-3.1. Duplication frequencies of various *Antp* and *Ubx* mutants analyzed.
The number of anterior thoracic hemisegments analyzed for each genotype is denoted with n. The Chi-squared test (χ^2) was applied for statistical significance analysis.

Taken together, these data provide clear evidence for the exclusive role of *Antp* in controlling NB7-3 duplication. Apart from identity transformations, such phenotypes were not identified in embryos mutant for posterior *Hox* genes (Rogulja-Ortmann et al., 2008; Birkholz et al., 2013b). It prompted further investigation aiming to establish whether the phenotypes in *Antp* mutants resulted from any posterior prevalence effect (Duboule and Morata, 1994), i.e., an identity transformation of Lab to T2 segments to anteriorly lying gnathal segments in *Antp* loss of function mutants.

3.3. Duplication of NB7-3 lineage is unique to anterior *Hox* gene mutants

In order to evaluate whether or not the posterior prevalence phenomenon causes the phenotypes in *Antp* mutants, the Wt NB7-3 lineage pattern in the anteriorly positioned maxillary (Mx) and mandibular (Md) segments of the gnathal body region was analyzed. The observations revealed segment-specific more late embryonic refinements in the 7-3 lineages of these segments (Fig. 17A). Co-staining of Eg and Hb revealed that the 7-3 lineage of the Md segment possess only two neurons in late embryos (Fig. 17B, B2, B2'), whereas in the Mx segment three cells were observed, similar to the Lab and T3-A7 segments (Fig. 17A, B, B1, B1'). These observations clearly excluded the possible transformation of Lab and anterior thoracic 7-3 lineages in *Antp* mutants to Mx or Md segment identity. Very small, likely apoptotic cells in the 7-3 lineages of Mx and Md segments were noted from stage 14 to early stage 16 of Wt embryos. The Hb-positive GW neuron in these segments was removed from the 7-3 lineage much earlier than in the posterior segments, in which it undergoes apoptosis at late stage 16 or stage 17 (Rogulja-Ortmann et al., 2008). To establish whether similar *Hox*-mediated segment-specific NB7-3 lineage patterning observed in posterior segments is noted in Md and Mx segments, mutants for *Deformed* (*Dfd*) and *Sexcombs reduced* (*Scr*), the *Hox* genes that specify the Md and Mx segments (Martinez Arias et al., 1987), respectively, were analyzed. Interestingly, analysis of Dfd^{16}, a loss of function allele, revealed an occasional duplication phenotype in Md hemisegments of NB7-3 lineages in 3.13% (n = 36) and a cell survival phenotype in 83.33% of the cases (Fig. 17C, C1, C1', C2, C2'). This observation suggests that *Dfd* regulates the late embryonic NB7-3 lineage patterning and duplication occurrence in the Md segment. In order to evaluate the role of *Scr* in the Mx segment, two loss-of function alleles, Scr^{17} and Scr^{4} were analyzed. Apart from the cell survival phenotype, in 3.84% (n = 26) of analyzed hemisegments in Scr^{17} mutant embryos exhibit the duplication phenotype. In the Scr^{4} mutant, the duplication phenotype is observed in 16% (n = 32) of Mx hemisegments (Fig. 17D, D1, D1', D2, D2'). The duplication phenotype in the double mutants of Dfd^{16},Scr^{4} was observed at a frequency of 21.05% (n = 38) in Mx hemisegments, which is consistent with the findings pertaining to the single Scr^{4} mutant. An occasional duplication was also observed in Lab hemisegments of Scr^{17} and Scr^{4} mutants.

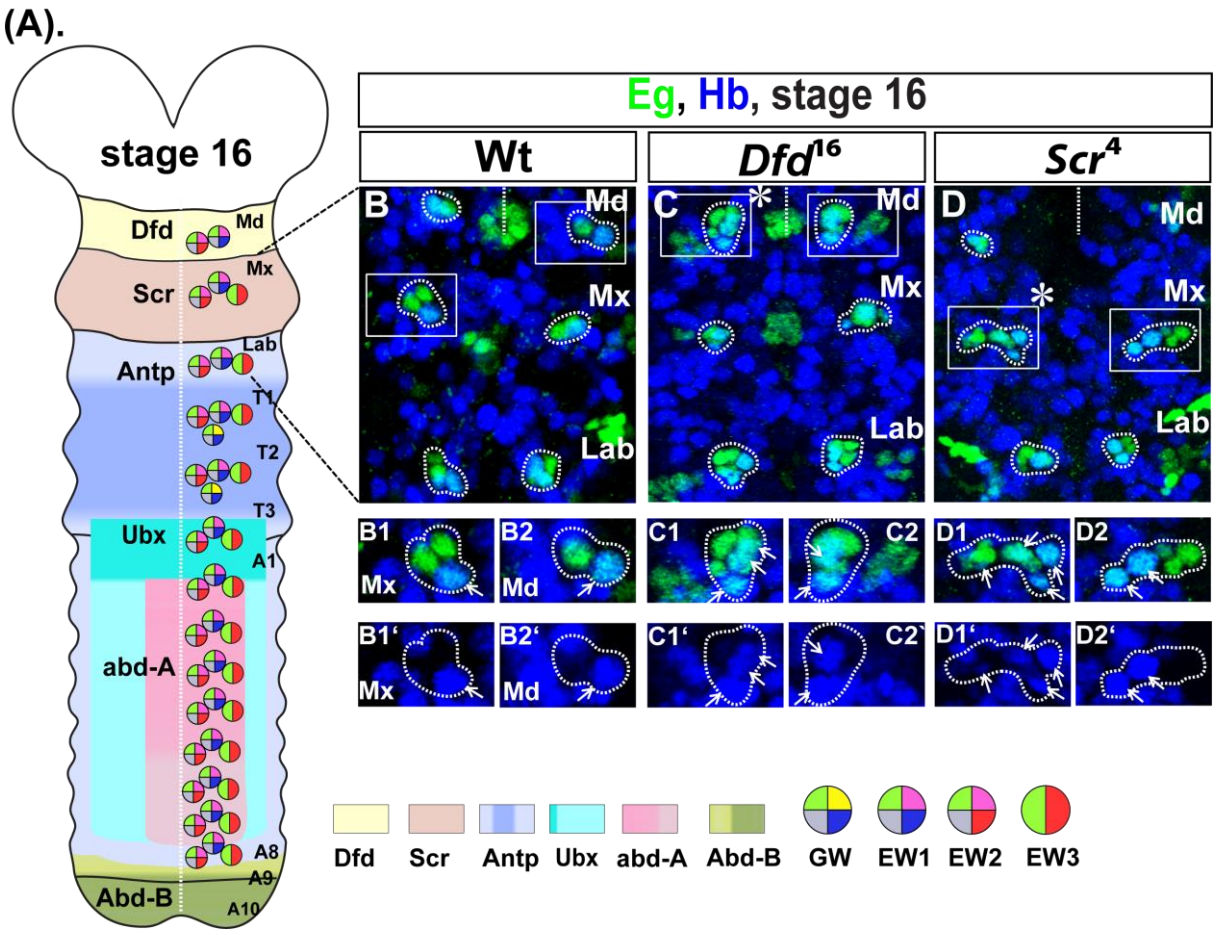

Fig. 17. NB7-3 lineage phenotypes are unique to anterior *Hox* mutants.
(A) Schematic of late embryonic CNS depicting NB7-3 lineage patterning and the Hox expression pattern from Md to A8 segments in Wt. (B, C, D) Confocal sections of late embryos stained for Eg and Hb focusing on the NB7-3 lineages (outlined) in Wt (B), *Dfd*^{16} (C) and *Scr*^{4} (D) mutants. Anterior is up in all images. The midline is marked with a dotted straight line and the segments in view are always indicated on the right hand side of the image. The hemisegments with duplicated Hb-positive cells are marked with an asterisk (*). The magnified images of the representative hemisegment (rectangle) are shown for each genotype below. Hb-positive cells of 7-3 lineages in magnified sections are indicated with arrows in both single and double channels. (B) In the Wt Md segment, the cell number in the 7-3 lineage is reduced to two, with one cell co-expressing Hb (B2, B2'). In the Mx segment, three Eg-positive cells are observed, including one Hb-positive cell (B1, B1'). (C) Only in Md hemisegments of *Dfd* mutants, the duplication phenotype (C1, C1') and cell survival phenotype (C2, C2') are seen. (D) In the Mx hemisegments of *Scr* mutants, both duplication (D1, D1') and cell survival phenotypes of NB7-3 (D2, D2') are clearly evident.

The observed cell survival phenotype in *Dfd*, *Scr* and *Antp* mutants thus provides strong evidence for *Antennapedia* complex (ANT-C) genes being important for inducing apoptosis of EW2sib and EW3sib neurons of Md to T2 segments and GW neuron only in Md, Mx and Lab segments. Most interestingly, in addition to their role in segment-specific refinement in the terminal embryonic 7-3 lineages, they all regulate duplication of the lineage.

The *Ubx* mutation in *Antp*, *Ubx* double mutant embryos transformed the NB7-3 lineages in the T3 segment to anterior thoracic segments identity and shows the *Antp* mutant specific phenotypes. This observation is also in agreement with the anteriorization hypothesis of transformation to anterior segment identity in loss of any segment-specifying *Hox* gene function (Wakimoto and Kaufman, 1981; Gehring et al., 2009). In contrast, the NB7-3 lineages in the respective segments of *Antp*, *Scr* and *Dfd* mutants were not transformed to their posterior or anterior segmental identities. To understand whether this is also true at the level of protein expression in the neuroectoderm and VNC, antibody staining against Ubx and Scr was analyzed in various *Antp* mutants. Ubx is strongly expressed from posterior T3 to anterior A1 segments and specifies these segmental domains (White and Wilcox, 1985). In Wt embryos, the stronger expression domain of Ubx protein within the neuroectoderm at stage 11 was observed from the posterior part of the T3 segment to anterior A1 segment. Apart from that, weak expression of the Ubx protein was also noted from the posterior T2 to anterior T3 segmental domain (Fig. 18A, A'). Ubx expression analysis within the En-positive neuroectoderm of $Antp^{25}$ and $Antp^{25\ seg18}$ mutants at stage 11 confirmed that the expression was not altered and extended to the anterior segments neither in strong nor in weak penetrant *Antp* mutants (Fig. 18B, B', C, C').

After gastrulation, the Scr protein is expressed initially from the posterior Mx segment to anterior Lab segment, which then extends until first thoracic segment (Kuroiwa et al., 1985). The spatial restriction of Scr within the neuroectoderm and CNS is correlated with differential timing of expression in the ectoderm of the Lab and T1 segment. Until the anterior part of Lab ectoderm, the *Scr* RNA accumulates prior to segregation of the neuroblasts while expression in the ectoderm of the T1 segment occurs after neuroblast segregation (Mahaffey and Kaufman, 1987). Consistent with earlier reports, in Wt embryos, the Scr expression within the En-positive neuroectoderm was noted to be restricted from posterior Mx to anterior Lab segment until stage 10. However, En-positive row 6 neuroectodermal cells in Lab segment were also Scr-positive at this stage (Fig. 19A). At stage 11, the Scr expression domain in the Wt was expanded weakly until anterior part of T1 segment (Fig. 19B). The extended expression domain gets stronger by stage 12 (Fig. 19C). No significant differences in the Scr expression pattern and levels in the $Antp^{25}$ (Fig. 19D), $Antp^{25\ seg18}$ (Fig. 19G) and $Antp^{25}$,Ubx^{1} (Bloomington) (Fig. 19J) double mutants were observed at stage 10. Different from Wt at stage 11, in both single *Antp* mutants and

in *Antp*^{25},*Ubx*^{1} (Bloomington) double mutants embryos, the expression domain of Scr extended until neuroectodermal rows 1 and 2 in the anterior half of T2 segment (Fig. 19E, H, K).

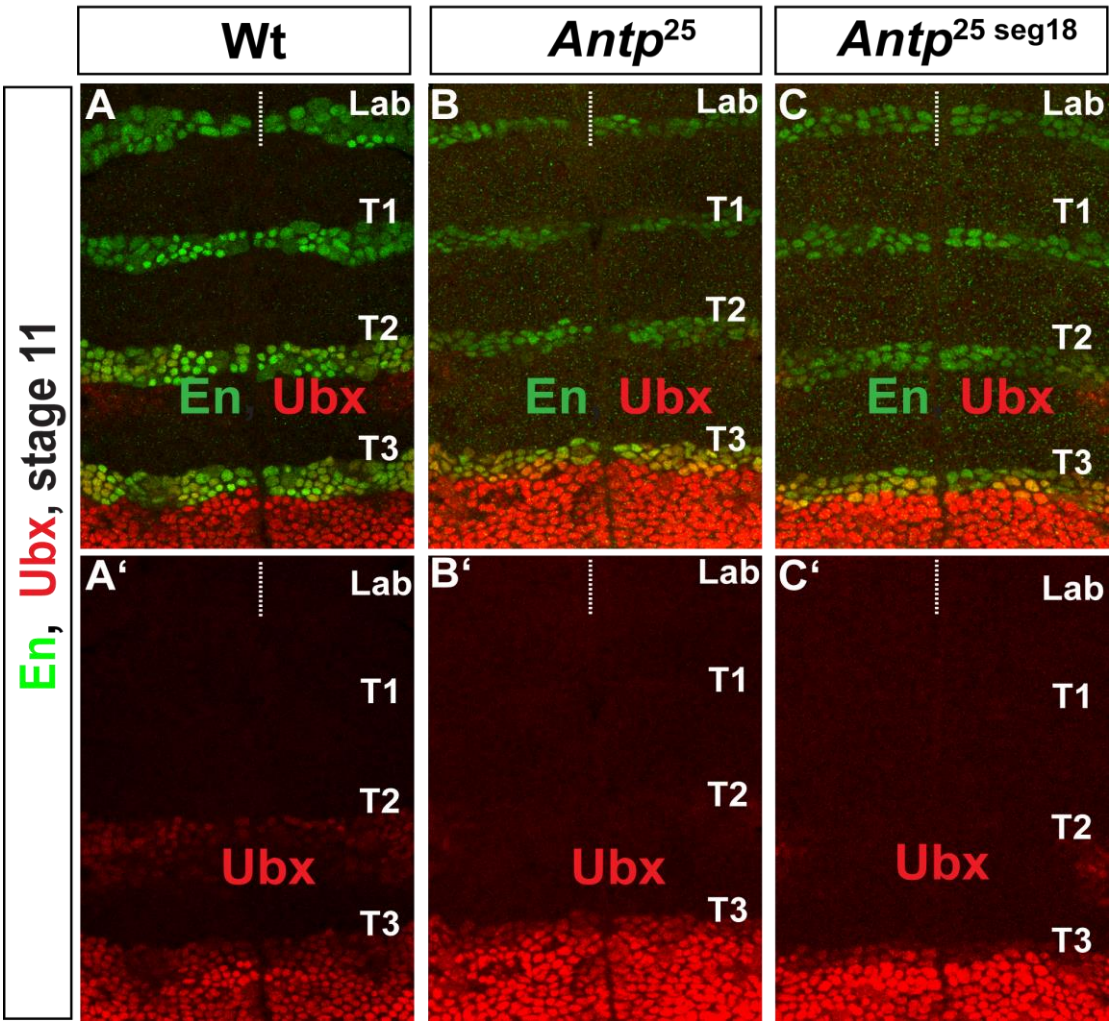

Fig. 18. Ubx expression is unaltered in *Antp* mutants.
Confocal sections of embryos at stage 11 stained for En and Ubx focusing on the neuroectoderm in Wt (A), *Antp*^{25} (B) and *Antp*$^{25\ seg18}$ (C) mutants. Anterior is up in all images. The midline is marked with a dotted straight line and the segments in view are indicated on the right hand side. En staining marks the posterior cell rows in each segment. Ubx expression is shown in a single channel for each image. (A, A') Stronger Ubx expression is present from posterior T3 of the neuroectoderm, whereas weak expression is seen in the posterior En-positive domain of T2 as well. (B, B') The weakly penetrant *Antp*^{25} mutant exhibits a pattern similar to that noted in Wt. (C, C') Ubx expression is invariant from Wt in the strongly penetrant *Antp*$^{25\ seg18}$ mutant.

The extended Scr expression within the neuroectoderm of all mutants gets stronger by stage 12 (Fig. 19F, I, L). However, Scr expression in the En-positive neuroectoderm of Lab and T1 segments in *Antp* mutants could not rescue the duplication phenotype. This finding suggests that Scr regulates NB7-3 identity only in the Mx segment. Together, these observations confirmed that the 7-3 lineage

phenotypes observed in mutants of ANT-C genes *Dfd*, *Scr* and *Antp* were due to respective *Hox* gene function loss only.

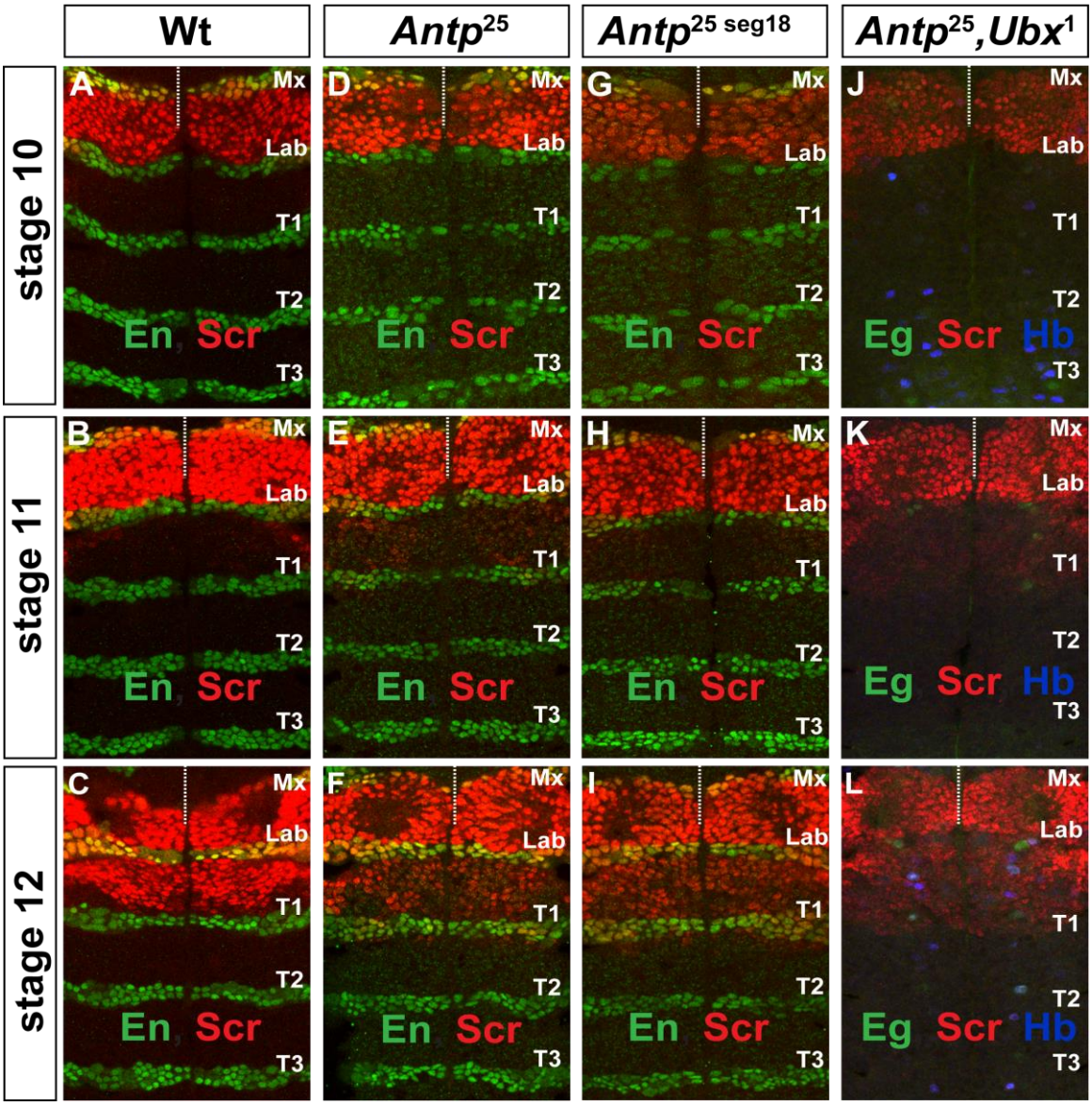

Fig. 19. Scr is not extended to the complete Antp expression domain within the neuroectoderm of *Antp* mutants.
Confocal sections of stages 10, 11 and 12 embryos stained for En and Scr or Eg, Scr and Hb, focusing on the neuroectoderm in Wt (A, B, C), *Antp*^{25} (D, E, F), *Antp*$^{25\ seg18}$ (G, H, I) and *Antp*^{25},*Ubx*^{1} (Bloomington) (J, K, L) mutants. Anterior is up in all images. The midline is marked with a dotted straight line and the segments in view are always indicated on the right hand side of the image. (A, B, C) In Wt embryos, the Scr expression is restricted from posterior Mx to anterior Lab segment at stage 10, but it extends very weakly until anterior T1 by stage 11, which is strongly noticed at stage 12. (D, G, J) At stage 10 of weakly and strongly penetrant *Antp* mutants, the expression domain of Scr was similar to that noted in Wt. (E, H, K) At stage 11 of tested *Antp* mutants, very faint Scr expression crossed the posterior T1 segment and extended until row 2 of anterior T2 segment. (F, I, L) At stage 12, strong expression of Scr is observed from posterior Mx to row 2 of anterior T2 segment is all mutants.

The mechanisms involved in NB7-3 lineage duplication and the functional roles of anterior *Hox* complex genes in segmental patterning of NB lineages were studied further using *Antp* mutants. The findings are presented in the following sections.

3.4. Duplicated 7-3 lineages develop from two neuroblasts

The enlarged, 8 to 12 cell duplicated NB7-3 lineages of *Antp* mutants could arise through abnormal divisions either of the NB or of its progeny, or they could be due to a misspecification mechanism or a lack of terminal NB apoptosis. The neuron number observed in the enlarged lineage of *Antp* mutants correlates with the observed numbers of 9 to 10 cells in NB7-3 clones of *H99* mutant embryos, in which apoptosis is lacking (Fig. 20A, B) (Rogulja-Ortmann et al., 2007). In order to determine whether the enlarged NB7-3 lineages of *H99* mutants are similar to the lineages of *Antp* mutants, marker analysis was performed. *H99* mutant embryos exhibited large 7-3 lineages with an average of 8 to 10 Eg-positive cells in anterior thoracic segments, although only two Hb co-expressing cells were noted (Fig. 20C, C', C"). This finding excludes extended NB survival as the cause of 7-3 lineage duplication in *Antp* mutants. In order to discern how the duplication occurs, early development of the NB7-3 lineage was studied. Considering the fact that expression of the early temporal factor Hb is restricted to two cells within this lineage, staining for Eg and Hb was used. In addition, to distinguish the neuroblast from the GMCs and neurons, Deadpan (Dpn), a marker for NBs was used (Bier et al., 1992). In Wt, the delaminated 7-3 neuroblast expressing Eg, Hb and Dpn can be identified in the VNC at stage 11 (Fig. 21A, A'). Upon delamination, the first asymmetric division of the NB7-3 generates GMC-1, which inherits Hb and Kr expression. Immediately upon the first NB division, Hb expression is downregulated in the NB, whereas the subsequent temporal cascade gene Kr is maintained (Karcavich and Doe, 2005) (Fig. 21B, B'). The GMC-1 divides once and produces only two post-mitotic Hb-positive progeny GW and EW1. The Hb expression in these two progeny cells is maintained throughout embryonic development and allows distinction of these two cells from other 7-3 progeny (Isshiki et al., 2001; Novotny et al., 2002; Mettler et al., 2006). In order to elucidate the origin of four Hb-positive progeny in the duplicated NB7-3 lineage of *Antp* mutants, the possibility of abnormal NB or GMC divisions was investigated in $Antp^{25}$,Ubx^{1} (Bloomington) double mutant embryos.

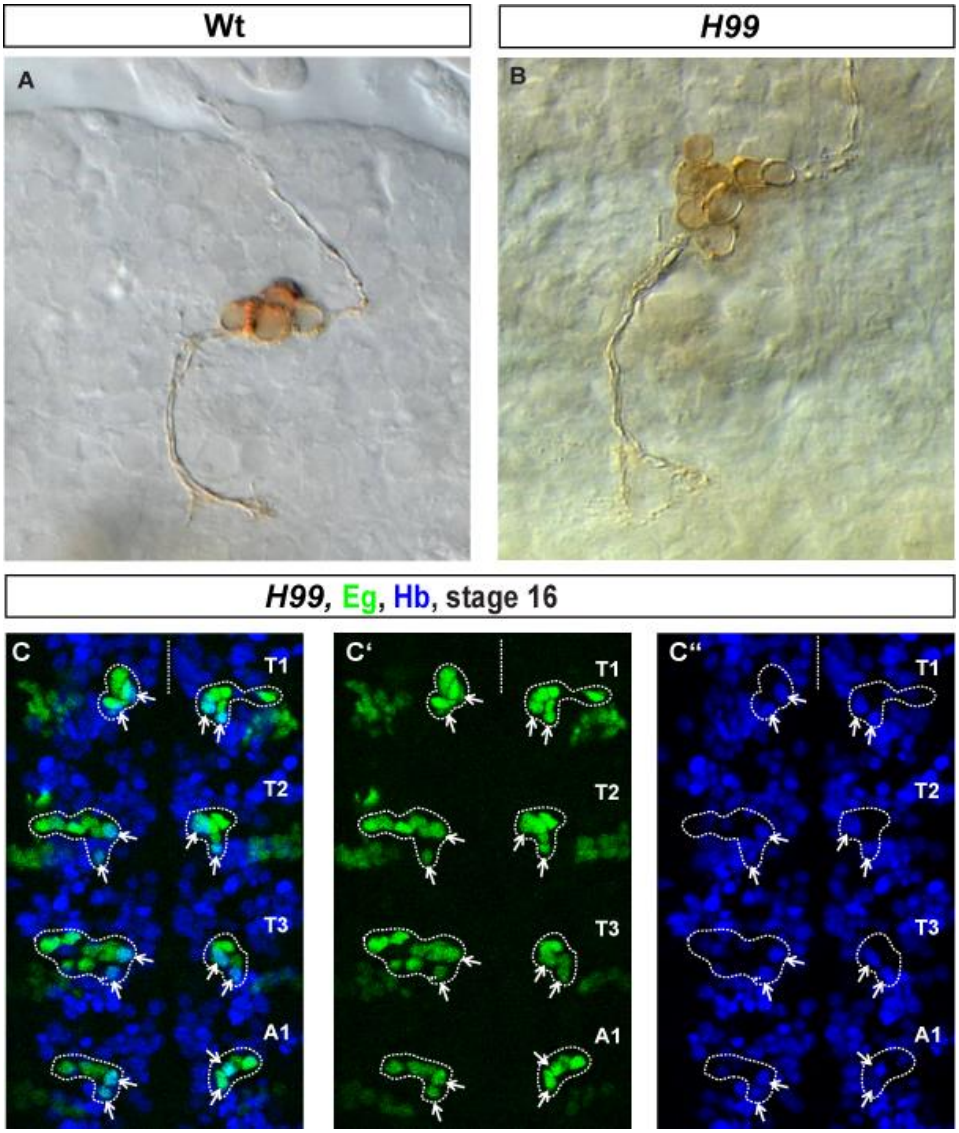

Fig. 20. NB7-3 is not duplicated in *H99* mutants.
(A, B) DiI labelling of NB7-3 lineage performed in Wt (A) and *H99* mutants (B) at late embryonic stages. The Wt 7-3 lineage at stage 16 retains 4 cells, whereas in *H99* mutant embryos it possesses 8 to 10 neurons. The images are taken from the Diploma thesis of Janina Siebert. (C, C', C'') Confocal sections of *H99* mutant embryos focusing on the thoracic NB7-3 lineages stained for Eg and Hb. Anterior is up in all images. The midline is marked with a dotted straight line and the segments in view are indicated on the right hand side of the image. Hb-positive cells of 7-3 lineages are indicated with arrows in both single and double channels. The 7-3 lineages in the thoracic segments of *H99* mutant embryos show 8 to 10 Eg-positive cells, including only 2 Hb-expressing cells.

Like in Wt, one Eg- and Hb-positive NB7-3 was observed at stage 11, which divided asymmetrically to produce one smaller Hb-positive cell, GMC-1 (Fig. 22A, A'). Hb expression was also downregulated after the first asymmetric division of the thoracic NB7-3.

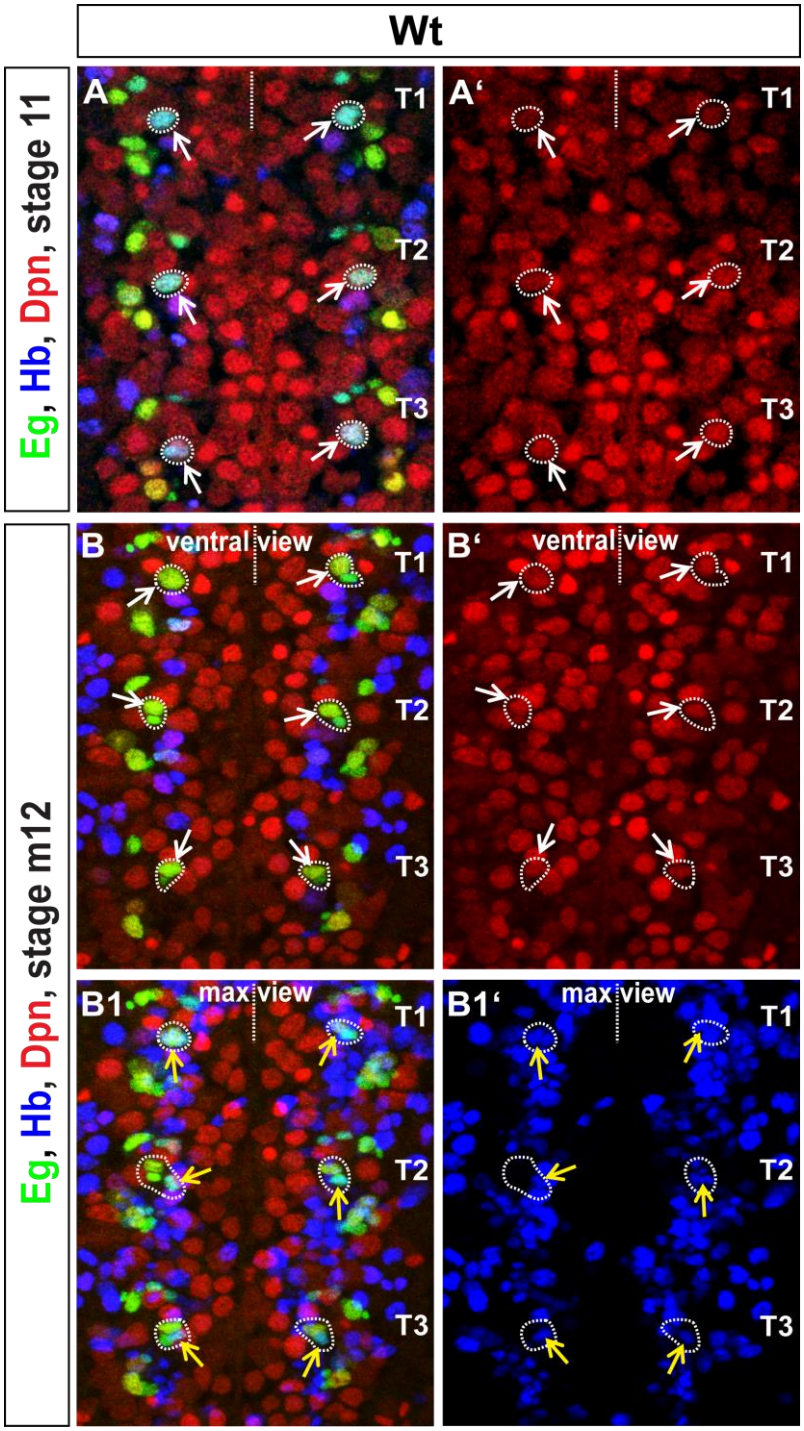

Fig. 21. Identification of 7-3 NB in early embryonic stages of Wt.
Flat preparations of Wt embryos at developmental stages 11 (A) and mid 12 (B) stained for Eg, Hb and Dpn. Anterior is up in all images. The segments in view are always indicated on the right hand side of the image and the midline with a dotted straight line. The neuroblast marker Dpn expression is shown in a single channel for stage 11 and stage mid 12 ventral view images, whereas Hb expression is shown in a single channel for mid-stage 12 maximum projection views (max view). White arrows indicate 7-3 neuroblasts, yellow arrows denote Hb-positive progeny generated from the primary NB. (A, A') At stage 11 in Wt, the Hb-positive 7-3 NB is found in the ventral focal planes. (B, B'). At stage mid 12, the NB has down-regulated Hb and can be observed with Deadpan staining in the ventral focal planes. (B1, B1') The maximum projection view allows the more dorsal Hb-positive progeny to be seen.

At mid-stage 12, when a part of the NB7-3 lineage has already been generated, a second Eg-, Hb- and Dpn-expressing NB was observed ventrally in thoracic hemisegments of the *Antp*^{25},*Ubx*^{1} (Bloomington) double mutant (Fig. 22B, B'). The second NB7-3 and its first descendant GMC-1 in the ventral focal planes at stage 12 could be discriminated from the primary NB due to downregulation of Hb expression in the primary NB (Fig. 22B, B'). At stage 12, two Hb-positive progeny generated by the primary NB were always seen in the dorsal focal planes like in Wt (Fig. 21B1, B1', 22B1, B1'). This observation confirms that first abnormal symmetric division of NB after delamination is not the cause for encountering two NBs in *Antp* mutants. An occasional lateral positioning of the second NB7-3 and its lineage confirmed that the two neuroblasts generate complete lineages. Analysis of duplicated Hb progeny in early developmental stages of *Antp* mutants thus clarified that two temporally distinguishable NBs generate the duplicated NB7-3 lineage.

The segment-polarity genes *en*, *hedgehog* (*hh*), *gooseberry* (*gsb*) and *naked cuticle* (*nkd*) are involved in NB7-3 formation. In loss of function mutants of these genes, NB7-3 formation is affected in various degrees. The combined function of these genes leads to the expression of *eg, eyeless* (*ey*) and *huckebein* (*hkb*) in NB7-3 (Matsuzaki and Saigo, 1996, Lundell et al., 1996; Dittrich et al., 1997; McDonald and Doe, 1997; Deshpande et al., 2001). NB7-3 arise from the posterior row of En expression domain and in embryos that are deficient for *en* and *invected* (*inv*), a homeobox gene that has some functional redundancy to *en*, show that NB7-3 is missing in all segments (Deshpande et al., 2001). Missing NB7-3 lineage in 20% of hemisegments in *hkb* mutants shows its early function in NB7-3 development (Dittrich et al., 1997). Current analysis of NB7-3 lineage in *en*^{58} and *hkb*^{2} mutants showed similar results like in prior reports. Eg expression at NB7-3 position is not observed in *en*^{58} mutants, whereas NB7-3 formation is not affected in *hkb*^{2} mutants. The temporal differences in the appearance of the two 7-3 neuroblasts could be due to a possible misspecification of Eg-positive NB6-4 to a second NB7-3, as was observed in *gsb* mutants (Deshpande et al., 2001). A careful comparative inspection of Eg expression in the VNC of Wt (Fig. 23A, A', B, B') and *Antp*^{25},*Ubx*^{1} (Bloomington) mutant embryos (Fig. 23C, C', D, D') at late stages eliminated the possible misspecification of Eg-positive NB6-4, NB2-4 or NB3-3 to a second NB7-3.

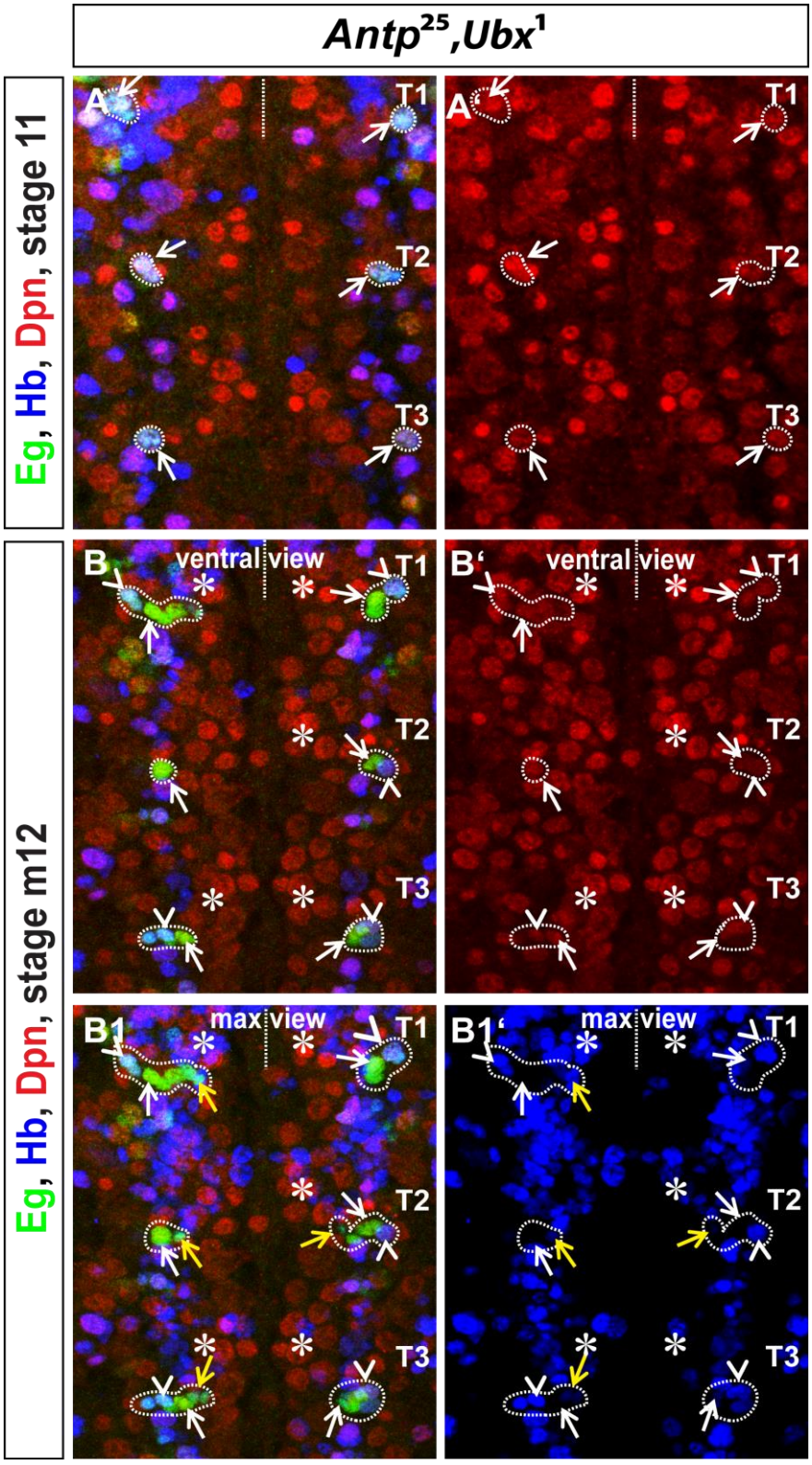

Fig. 22. Two 7-3 NBs appear sequentially in *Antp* mutants.
Flat preparations of *Antp*^{25},*Ubx*^{1} (Bloomington) mutants embryos at developmental stages 11 (A) and mid 12 (B) stained for Eg, Hb and Dpn. Anterior is up in all images. The segments in view are always indicated on the right hand side of the image and the midline with a dotted straight line. The hemisegments with duplicated Hb-positive cells are marked with an asterisk. The neuroblast marker Dpn expression is shown in a single channel for stage 11 and stage mid 12 ventral view images, whereas Hb expression is shown in a single channel for mid-stage 12 maximum projection views (max

view). White arrows and arrowheads indicate 7-3 neuroblasts, yellow arrows denote Hb-positive progeny generated from the primary NB. (A, A') At stage 11 of *Antp*^{25},*Ubx*^{1} (Bloomington) double mutants, one Hb-positive NB7-3 is observed. In T1-left and T2-right hemisegments, the first asymmetric division of NB7-3 produced smaller Hb-positive GMC-1. (B, B') At mid-stage 12 of *Antp*^{25},*Ubx*^{1} mutants, a second Hb-positive 7-3 NB (arrow head) is observed in the ventral view of thoracic hemisegments. The primary NB, which has already down-regulated Hb expression (arrow) is lying next to it. (B1, B1') The Hb-positive progeny generated by the primary NB are found in the more dorsal positions and can be seen in the maximum projection views.

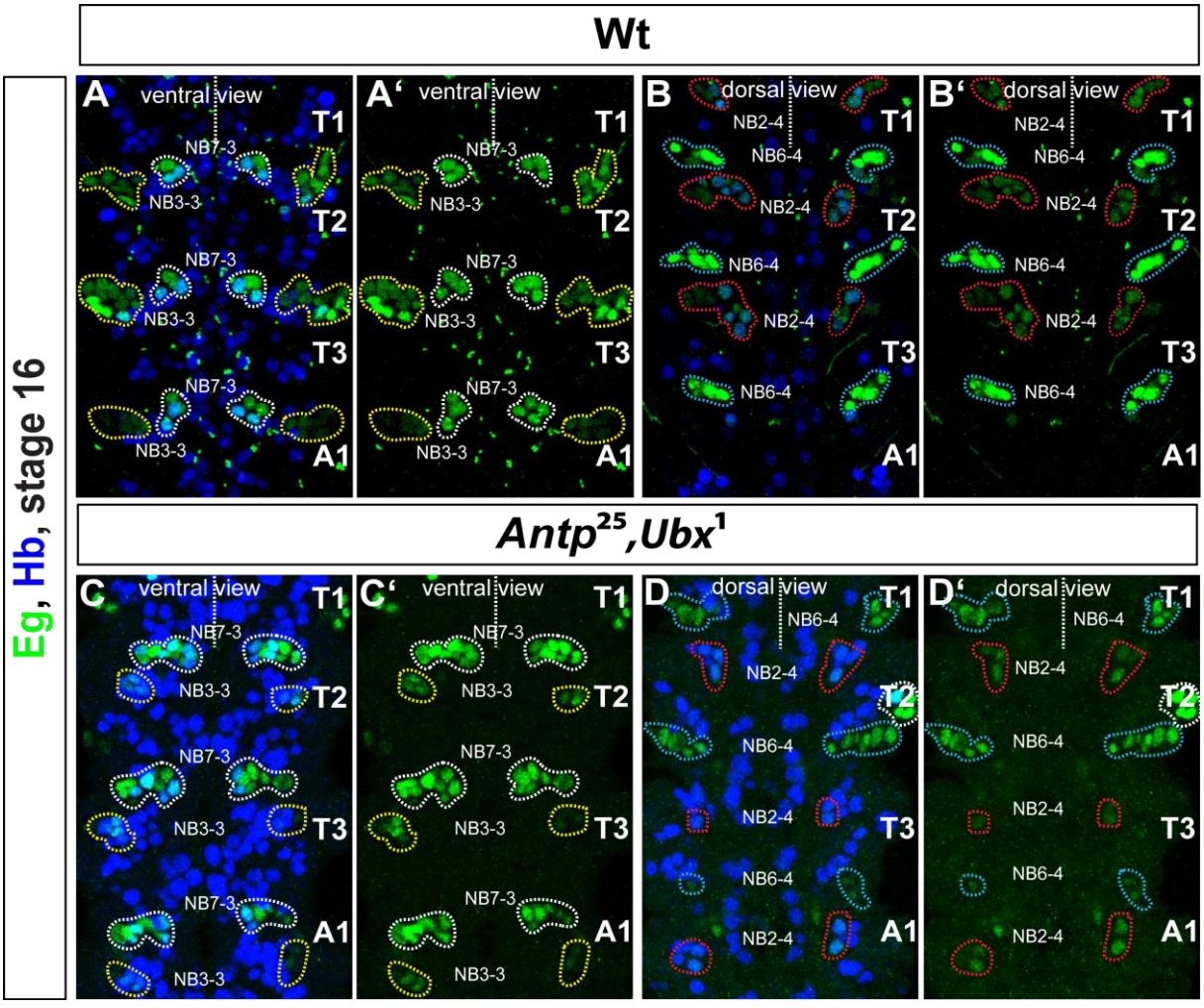

Fig. 23. Other Eg-positive NBs are not misspecified to second NB7-3 in *Antp* mutants.
Confocal sections focusing on the thoracic Eg-positive lineages of Wt (A, B) and *Antp*^{25},*Ubx*^{1} (C, D) (Bloomington) double mutant embryos stained for Eg and Hb. Anterior is up in all images. The midline is marked with a dotted straight line and the segments in view are always indicated on the right hand side of the image. Eg expression is shown in a single channel for each image. The ventral and dorsal sectional views of the same embryo are shown for each case. (A, A') The ventral sectional views of Eg and Hb co-staining in Wt embryos at stage 16 shows the NB7-3 lineage (white outline) medially and the NB3-3 lineage laterally (outlined in yellow). (C, C') At stage 16 in *Antp*^{25},*Ubx*^{1} (Bloomington) double mutant embryos, the duplicated NB7-3 lineage (white outline) and the laterally positioned NB3-3 lineage (outlined in yellow) are observed. (B, B') In the dorsal sectional views of Wt embryos at stage 16, NB6-4 (outlined in blue) and NB2-4 (outlined in red) lineages are observed. (D, D') In *Antp*^{25},*Ubx*^{1} (Bloomington) double mutant embryos, normally positioned NB6-4 (outlined in blue) and NB2-4 (outlined in red) lineages are observed.

Further, to identify any NB7-3 specific gene expression differences between the two 7-3 NBs at stage 12 in *Antp* mutants, the expression of En and Ey protein, as well as *intermediate neuroblast defective* (*ind*) and *hkb* mRNA was analyzed in double mutant embryos. En expression in the VNC is limited to all NBs and their lineages derived from row 6 and 7 cells in the neuroectoderm, and to NB1-2 (Doe, 1992). At mid-stage 12 in the VNC of $Antp^{25}$,Ubx^{1} (Bloomington) mutants, En expression is observed in dorsally lying Hb- and Eg-positive primary 7-3 lineage part and also in the delaminated second 7-3 NB, which can be identified in the ventral layers (Fig. 24A, A', A1, A1'). This finding suggests that the second NB7-3 also arise from the En-positive neuroectoderm. However, segement-specifically lower En expression was observed within the neuroectoderm of the mutants. Among the columnar patterning genes, RNA expression of *ind*, that specifies the intermediate row of NBs (Weiss et al., 1998) was noted in the primary NB7-3 lineage. Similarly, *ind* RNA expression was observed in the Eg- and En-positive second NB7-3 in $Antp^{25}$,Ubx^{1} (Bloomington) mutants (Fig. 24B, B', B1, B1'). This observation suggests that the second NB7-3 in *Antp* mutants segregates from the intermediate neuroectodermal region. Ey expression is observed in NB7-3 and its complete lineage (Deshpande et al., 2001). At stage 12, there is no difference in Ey co-expression between the ventrally and dorsally lying Eg-positive cells of NB7-3 lineage in thoracic segments of the double mutants, suggesting that Ey expression is not variable (Fig. 24C, C', C1, C1'). The expression of *hkb* is restricted to NB7-3 neuroectodermal clusters, along with the complete lineage in En stripe (Chu-LaGraff et al., 1995; McDonald and Doe, 1997). RNA *in situ* analysis for *hkb* expression also affirmed that the second NB7-3 in ventral layers of thoracic segments in $Antp^{25}$,Ubx^{1} (Bloomington) mutants was indeed *hkb*-positive (Fig. 24D, D', D1, D1'). Together, these results confirm the sequential delamination of two 7-3 neuroblasts in *Antp* mutants. Protein and RNA expression analysis to identify NB7-3 clarified that the observed two 7-3 neuroblasts in *Antp* mutants were indistinguishable in their specific gene expression.

3.5. The NB7-3 proneural cluster is maintained in *Antp* mutants in a segment-specific manner

Detecting En, *ind* and *hkb* RNA expression in the second NB7-3 of *Antp* mutants suggests that it is also delaminating from the neuroectoderm that specifies the primary NB7-3.

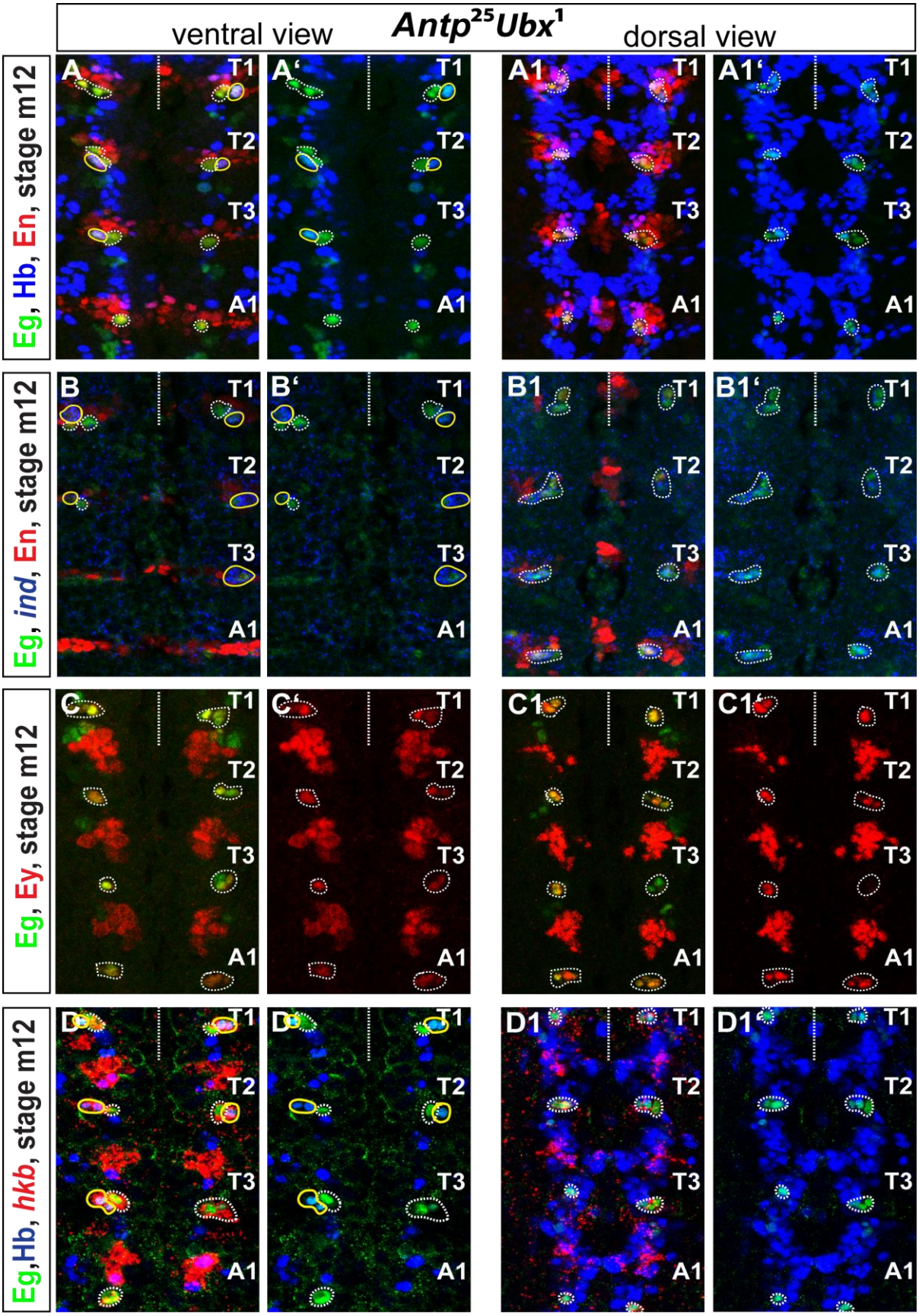

Fig. 24. The two 7-3NBs in *Antp* mutants express the same molecular markers.
Confocal sections focusing on the ventral and dorsal sectional views of same embryos at stage 12 in *Antp*^{25},*Ubx*^{1} (Bloomington) double mutant embryos. Anterior is up in all images. The midline is marked

with a dotted straight line and the segments in view are always indicated on the right hand side of the image. The abdominal segment, in which the duplication phenotype is not observed, represents the wild-typic pattern and helps for comparison. (A, A', A1, A1') At mid-stage 12, En expression is visible in the Eg- and Hb-positive second NB7-3 (outlined in yellow) in thoracic hemisegments and in the primary NB and its progeny (outlined in dotted white). (B, B', B1, B1') RNA expression of the columnar gene *ind* is observed in En and Eg co-expressing cells in the ventral second NB (outlined in yellow) and the primary NB and its lineage in the dorsal focal planes of the double mutant. While *ind* expression is not observed in the first abdominal segment ventral sectional view. (C, C', C1, C1') In the double mutant at stage 12, Ey expression is observed in both ventrally and dorsally lying Eg-positive cells of the thoracic 7-3 lineage (outlined in dotted white). (D, D', D1, D1') The delaminated Eg- and Hb-positive second NB7-3 (outlined in yellow) in ventral view is also positive for *hkb* expression, similar to the primary NB7-3 and its lineage (outlined in dotted white), which is lying in the dorsal sectional views.

To confirm this, *hkb* expression in the En-positive neuroectoderm was compared at developmental stages 11 and 12 of Wt and $Antp^{25}$,Ubx^{1} (Bloomington) double mutant embryos. At stage 11, *hkb* RNA expression was detected in a 5 to 7 cell cluster similar to proneural gene expression within the En-positive neuroectoderm of Wt and $Antp^{25}$,Ubx^{1} (Bloomington) double mutant embryos (Fig. 25A, A', B, B'). The cell with a stronger *hkb* expression in the cluster, the NB7-3, delaminates into the VNC at late stage 11. The Hkb protein expression is maintained in the NB7-3 and its complete lineage in the VNC (Mc Donald and Doe, 1997). After delamination of the NB, *hkb* RNA expression was downregulated almost completely in all cells of the neuroectodermal cluster in Wt embryos at early stage 12 (Fig. 25C, C'). Interestingly, in $Antp^{25}$,Ubx^{1} (Bloomington) double mutant embryos, *hkb* RNA expression in the En-positive neuroectoderm at early stage 12 was still observed specifically in Lab to T3 segments (Fig. 25D, D'). Analysis of *hkb* RNA expression in single mutants $Antp^{25}$, $Antp^{11}$ and $Antp^{14}$ showed similar segment-specific maintenance. This observation strongly suggests that the second NB7-3 neuroblast in *Antp* mutants delaminates from the maintained *hkb*- and En-positive neuroectodermal cluster. To examine whether this is also the case for proneural genes, which provide neural identity to a cluster of ectoderm cells, their expression was analyzed. Among the *Achete-scute* complex (*AS-C*) proneural genes, I tested for Achaete (Ac) and Lethal of Scute (L'sc) protein expression within the Hkb-positive proneural cluster of NB7-3 and could confirm that L'sc was the only proneural gene it expressed. L'sc expression in the proneural cluster is much more dynamic than HKb expression. At embryonic stage 11 in Wt, among 5 to 7 Hkb- and L'sc co-expressing cells within the En-positive neuroectodermal region, a single cell begins expressing higher levels of L'sc and Hkb and delaminates into the VNC (Fig. 26A).

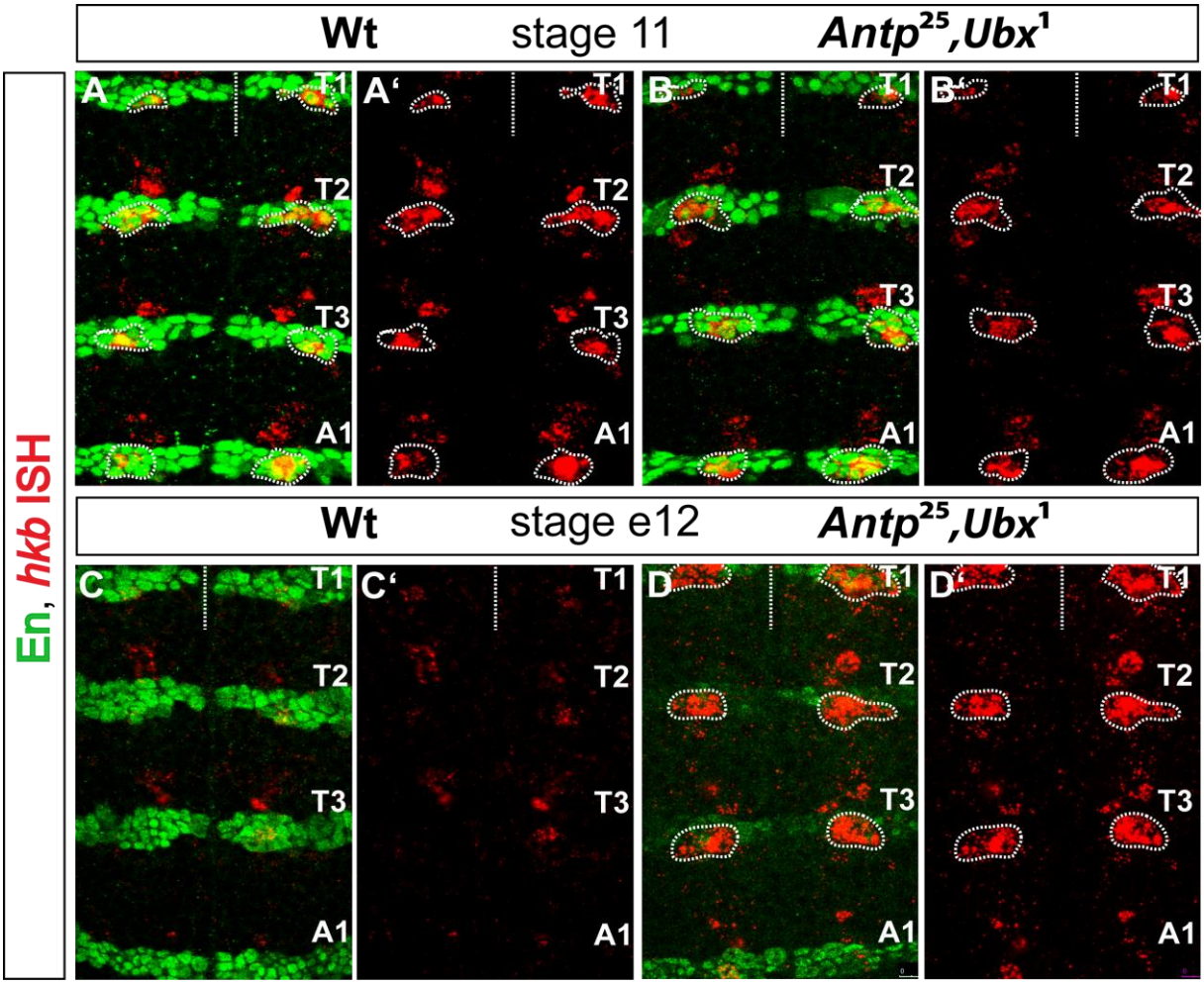

Fig. 25. The *hkb* RNA expression is maintained segment-specifically in *Antp* mutants.
Flat preparations of embryos focussing on the neuroectoderm at developmental stages 11 and 12 stained for En and *hkb* RNA in Wt (A, C) and *Antp*^{25},*Ubx*^{1} (B, D) (Bloomington) double mutants. Anterior is up in all images. The midline is marked with a dotted straight line. The segments in view are always indicated on the right hand side. The neuroectodermal cluster of NB7-3 is marked with a dotted outline. The single channel of *hkb* RNA expression pattern for each image is shown. (A, A') At early stage 11 in Wt, *hkb* RNA is expressed in 5 to 6 cells within the En-positive neuroectoderm. (B, B') Similar to the Wt neuroectoderm at stage 11, the *hkb* RNA expression is observed in the En row of *Antp*^{25},*Ubx*^{1} (Bloomington) double mutant embryos. (C, C') *hkb* RNA expression in the ventral En-positive neuroectoderm is mostly down regulated after NB delamination in early stage 12. Occasionally one or two small cells still retain the expression in all segments at this stage. (D, D') Different from the Wt at early stage 12, the *hkb* RNA expression within the neuroectoderm is segment-specifically maintained in all three thoracic segments of the *Antp*^{25},*Ubx*^{1} (Bloomington) double mutant embryos even after NB7-3 delamination. The normal downregulation of *hkb* expression within the neuroectoderm of the first abdominal segment (A1) can be noticed.

Shortly after NB delamination, the Hkb and L'sc expression cease in the proneural cluster, although Hkb expression is maintained in the complete NB7-3 lineages (Fig. 26B, B'). In contrast, L'sc expression remains for a while in the NB7-3, mostly until it divides once, and is then completely downregulated. Most interestingly, upon NB delamination at stage 11 (Fig. 26C, E, G), expression of neither L'sc nor Hkb ceased

in the neuroectodermal region of *Antp* mutants until mid stage 12. Essentially, all the *Antp* mutants analyzed, *Antp*^{25} (Fig. 26D, D'), *Antp*^{25seg18} (Fig. 26F, F') and the *Antp*^{25},*Ubx*^{1} (Bloomington) double mutant (Fig. 26H, H'), irrespective of their duplication phenotype frequency, exhibit similar proneural cluster maintenance ability after NB delamination. Within the VNC of early to mid stage 12 embryos, the primary NB7-3 and its lineage are found in a dorsal position (Fig. 26B1, D1, F1, H1). From the prolonged proneural cluster, a second NB7-3 was segregated at mid-stage 12. Following segregation of the second NB, Hkb and L'sc expression was downregulated within the thoracic neuroectoderm of *Antp* mutants (Fig. 27A, A, A"). The segregated second NB7-3 can be identified within the VNC by co-staining for L'sc and Hkb (Fig. 27A1, A1', A1"). In contrast, only Hkb expression was observed in the first NB and the lineage it generated (Fig. 27A2, A2', A2"). These observations show that the NB7-3 proneural cluster is maintained in a segment-specific manner and allows for second neuroblast segregation in *Antp* mutants. Segregation of two NBs from a single proneural cluster may suggest a defect in the lateral inhibition process within the NB7-3 proneural cluster. Lateral inhibition denotes the singling out of neuroblasts from the proneural cluster and is accomplished by a group of neurogenic genes (Cabrera, 1990). A single cell is selected as an NB through the interaction of neurogenic genes *Notch* and *Delta*, while other competent cells in the proneural cluster retain their undifferentiated state. Loss of any neurogenic gene disrupts the lateral inhibition process, which ultimately leads to segregation of 3 to 5 NBs from the equipotent proneural cluster. In order to find out whether the duplication of NB7-3 neuroblasts arises through a defect in lateral inhibition, expression of neurogenic gene *E(spl)* was analyzed and the results are discussed in the next section.

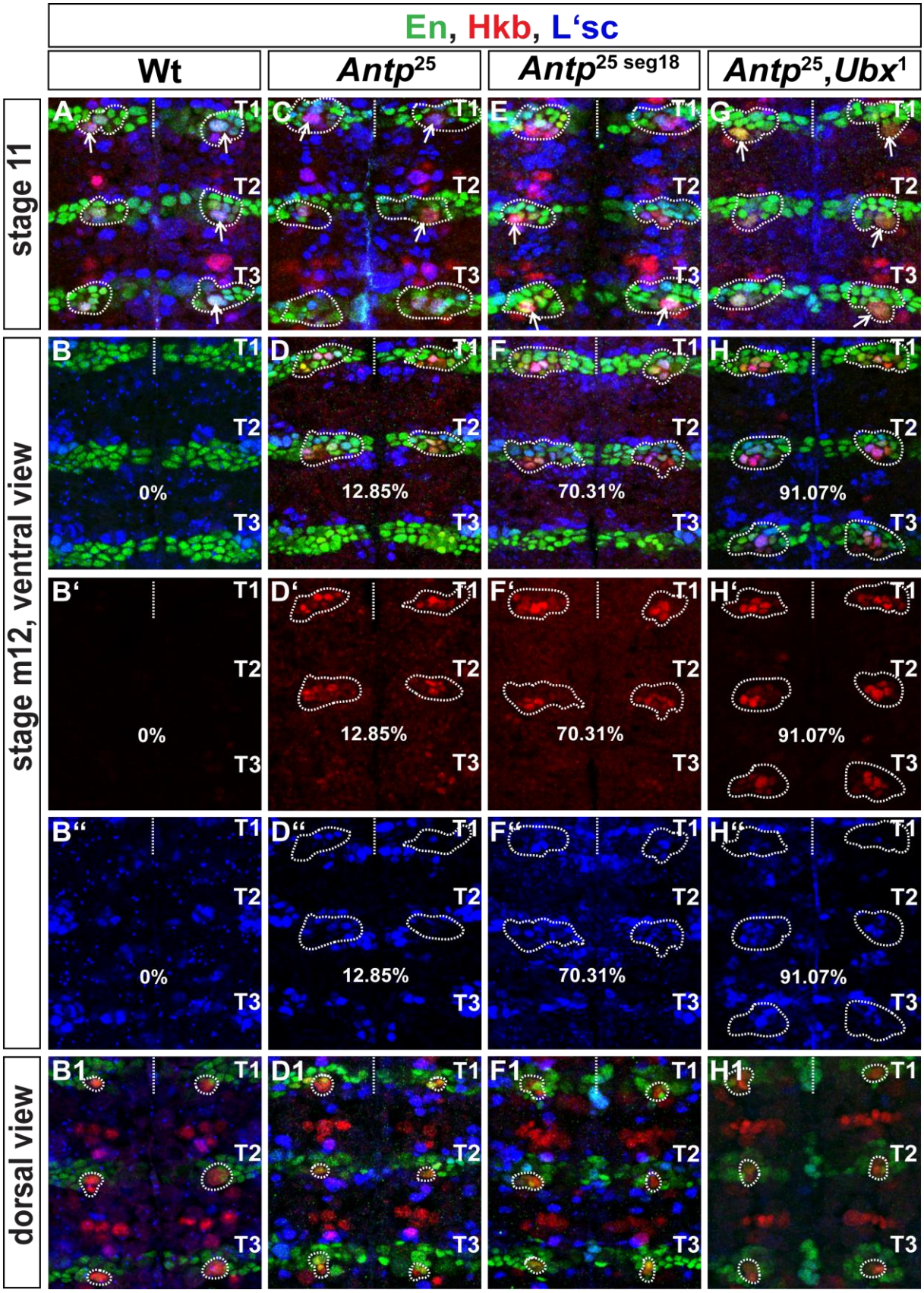

Fig. 26. Segment-specific proneural cluster maintenance in *Antp* mutants.
Confocal sections focusing on the ventral neuroectoderm (ventral focal view) and VNC (dorsal focal view) of the same embryo stained for En, Hkb and L'sc at embryonic stages 11 and 12 in Wt (A, B, B1), *Antp*^{25} (C, D, D1), *Antp*$^{25\ seg18}$ (E, F, F1) and *Antp*^{25},*Ubx*^{1} (G, H, H1) mutants. The midline is

marked with a dotted straight line and the segments in view are always indicated on the right hand side of the image. The single channel of Hkb and L'sc staining is seen below each genotype of stage 12 embryos. The proneural cluster of NB7-3 or its lineage is marked with a dotted outline. (A, C, E, G) From the proneural cluster of NB7-3, which can be identified by Hkb and L'sc co-expression in the En domain, one strongly double positive cell delaminates into VNC at stage 11 in Wt and in all *Antp* mutants (indicated by arrow). (B, B', B") Shortly after NB delamination in Wt, proneural gene expression diminishes and is lost in the ventral neuroectoderm. (B1) Only Hkb expression is noticed in the delaminated NB7-3 and its lineage in the VNC. (D, F, H) The NB7-3 proneural cluster, which is clearly distinguished by the single channels of Hkb and L'sc, is maintained in T1-T2 segments of single *Antp* mutants as well as in the T3 segment of $Antp^{25}$,Ubx^{1} double mutant until mid-stage 12. (D1, F1, H1) In the dorsal VNC views of the same embryos, the delaminated primary NB7-3 lineage can be seen.

3.6. Sequential Notch activity allows delamination of two 7-3 NBs from the maintained proneural cluster

The neural competence conferred to all cells in the cluster by proneural genes is finally restricted to a single cell by action of neurogenic genes (Cabrera, 1987; Cubas et al., 1991; Martin-Bermudo et al., 1991). In the VNC development, neurogenic genes include *Notch* (*N*), *Delta* (*Dl*), *bigbrain* (*bib*), *mastermind* (*mam*), *neuralized* (*neur*) and *Enhancer of split Complex* (*E(spl)-C*). A slight refinement of proneural gene expression in one of the cells in the cluster activates *Dl* expression, which ultimately leads to cleavage of Notch in the neighbouring cells. The localization of the cleaved Notch intracellular domain to the nucleus results in an accumulation of the products of the *E*(*spl*)*-C* genes, which are initially expressed in all cells of the proneural cluster (Technau and Campos-Ortega, 1987; de la Concha et al., 1988; Lieber et al., 1993). The E(spl)-C protein products antagonize the maintenance of proneural gene expression and promote the adoption of the non-neural fate (Martin-Bermudo et al., 1995). The segregated neuroblasts no longer express E(spl)-C proteins. The remaining cells, however, continue to express the E(spl)-C and terminate proneural gene expression. As *E(spl)* loci is one downstream target of Notch activity, its expression was examined as a readout for defects in lateral inhibition in the NB7-3 proneural cluster of *Antp* mutants. Within the Wt 7-3 proneural cluster at stage 11, a single specified NB was free from E(spl) protein expression while the remaining cells in the cluster show strong staining, suggesting that the Notch signaling pathway was activated in these cells (Fig. 28A, A', A''). After delamination of the NB, expression of both proneural genes and E(spl) was downregulated within the En-positive Wt ectoderm at stage 12 (Fig. 28B, B', B'').

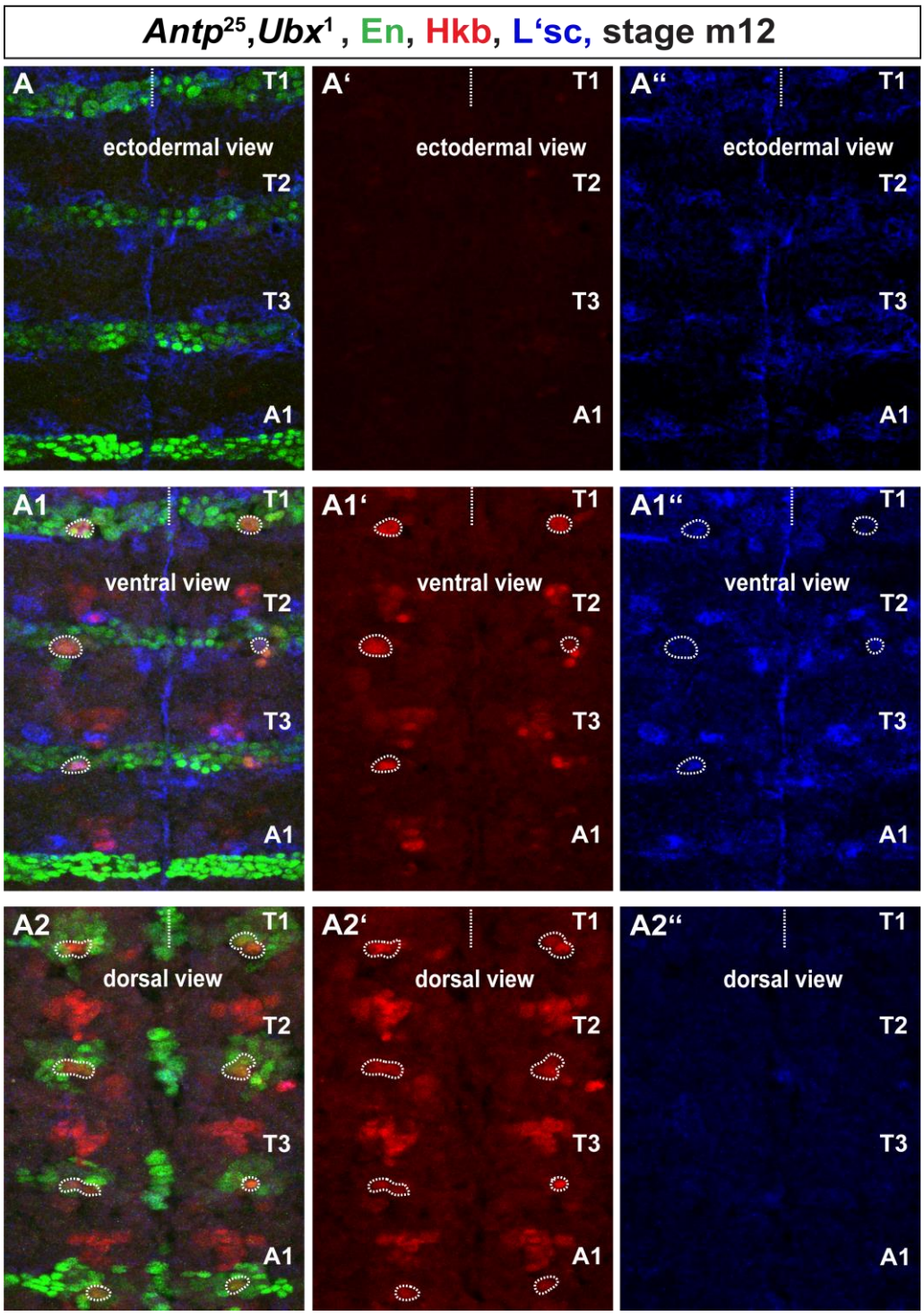

Fig. 27. Proneural cluster in *Antp* mutants is maintained until second NB segregation.
Confocal sections focusing on the ectoderm (A), ventral view of the VNC (A1) and dorsal view of the VNC (A2) of the same embryo stained for En, Hkb and L'sc at embryonic mid stage 12 in *Antp*^{25},*Ubx*^{1} (Bloomington) mutants. Anterior is up in all images. The midline is marked with a dotted straight line and the segments in view are always indicated on the right hand side of the image. The NB7-3 lineage is marked with a dotted outline. (A, A', A'') After the second NB segregation in the *Antp*^{25},*Ubx*^{1} (Bloomington) mutant embryos, the L'sc and Hkb expression in the En-positive ectoderm is downregulated. (A1, A1', A1'') The segregated second NB7-3, which can be identified through Hkb and L'sc co-expression in the En-positive VNC, is found only in the thoracic hemisegments but not in the abdominal segment. (A2, A2', A2'') Only Hkb expression can be noted in the primary NB7-3 lineage in the dorsal sectional view of the VNC.

Similar to Wt embryos at stage 11, in *Antp* mutants E(spl) protein expression is initially expressed in all L'sc-positive cells in the En row. Later, it is maintained in a single strongly L'sc-positive cell, while its expression is almost completely downregulated in the cluster (Fig. 29A, A', A''). Within the prolonged proneural clusters in *Antp* mutants, E(spl) staining was observed in all the cells until mid-stage 12 (Fig. 29B, B', B''). Eventually, one cell in the cluster downregulated E(spl) and delaminated into the VNC (Fig. 29C, C', C'').

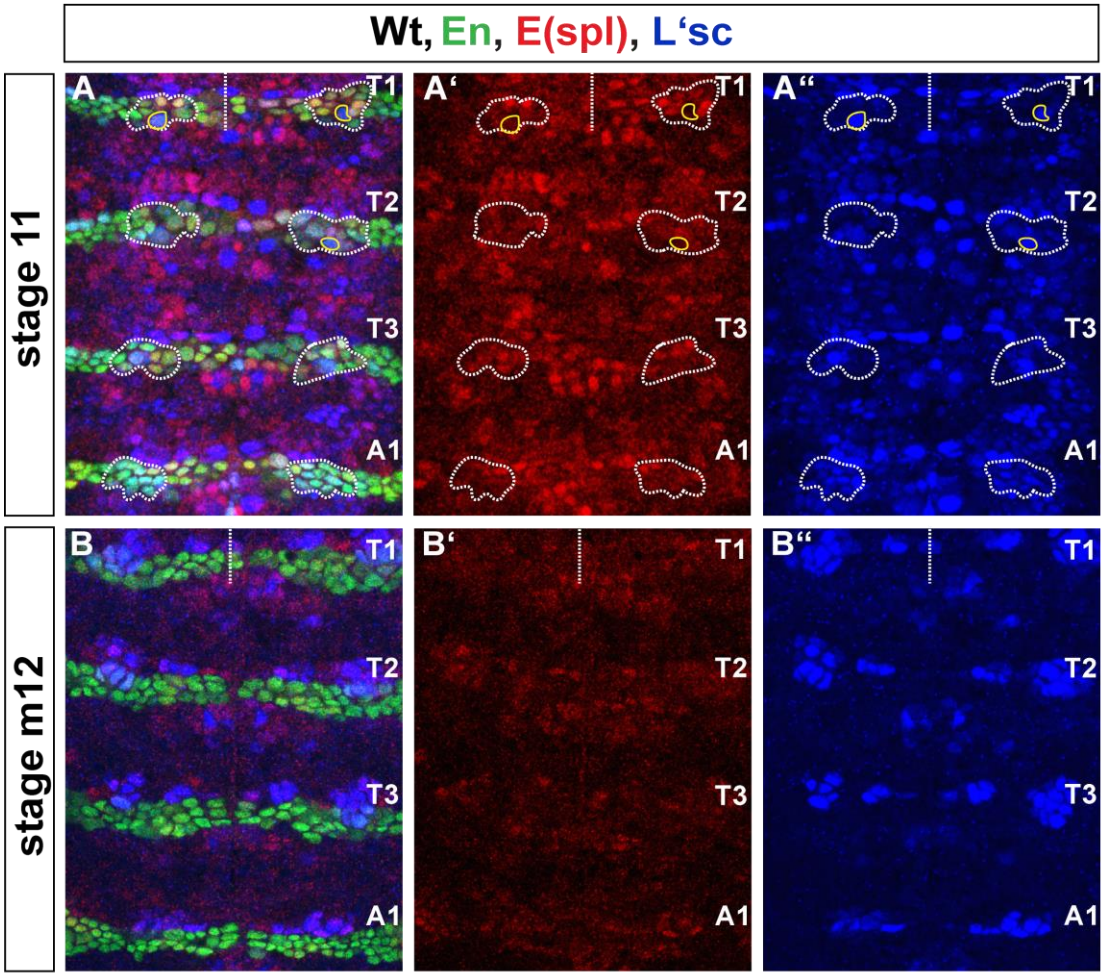

Fig. 28. E(spl) is the downstream target of the Notch pathway in the NB7-3 proneural cluster. Confocal sections focusing on the ventral neuroectoderm stained for En, E(spl) and L'sc at embryonic stages 11 and mid 12 in Wt (A, B). Anterior is up in all images. The midline is marked with a dotted straight line and the segments in view are always indicated on the right hand side. The single channel of E(spl) (A', B') and L'sc (A", B") staining is shown for each image. The proneural cluster of NB7-3 is marked with a dotted outline. (A, A', A") Activation of the Notch signaling pathway in the NB7-3 proneural cluster is identified with E(spl) staining, which is exclusively present in non-neural cells of the cluster. At stage 11 in Wt, one large segregated cell in the proneural cluster (outlined in yellow), the presumptive NB, shows strong L'sc expression and is free of E(spl). (B, B', B") After the NB delamination at stage 12, L'sc and E(spl) expression within the En-positive ectoderm is clearly lost in all segments.

Thus, unchanged E(spl) staining demonstrates that lateral inhibition was not defective in *Antp* mutants and sequential Notch activity allows segregation of two 7-3 neuroblasts one after the other.

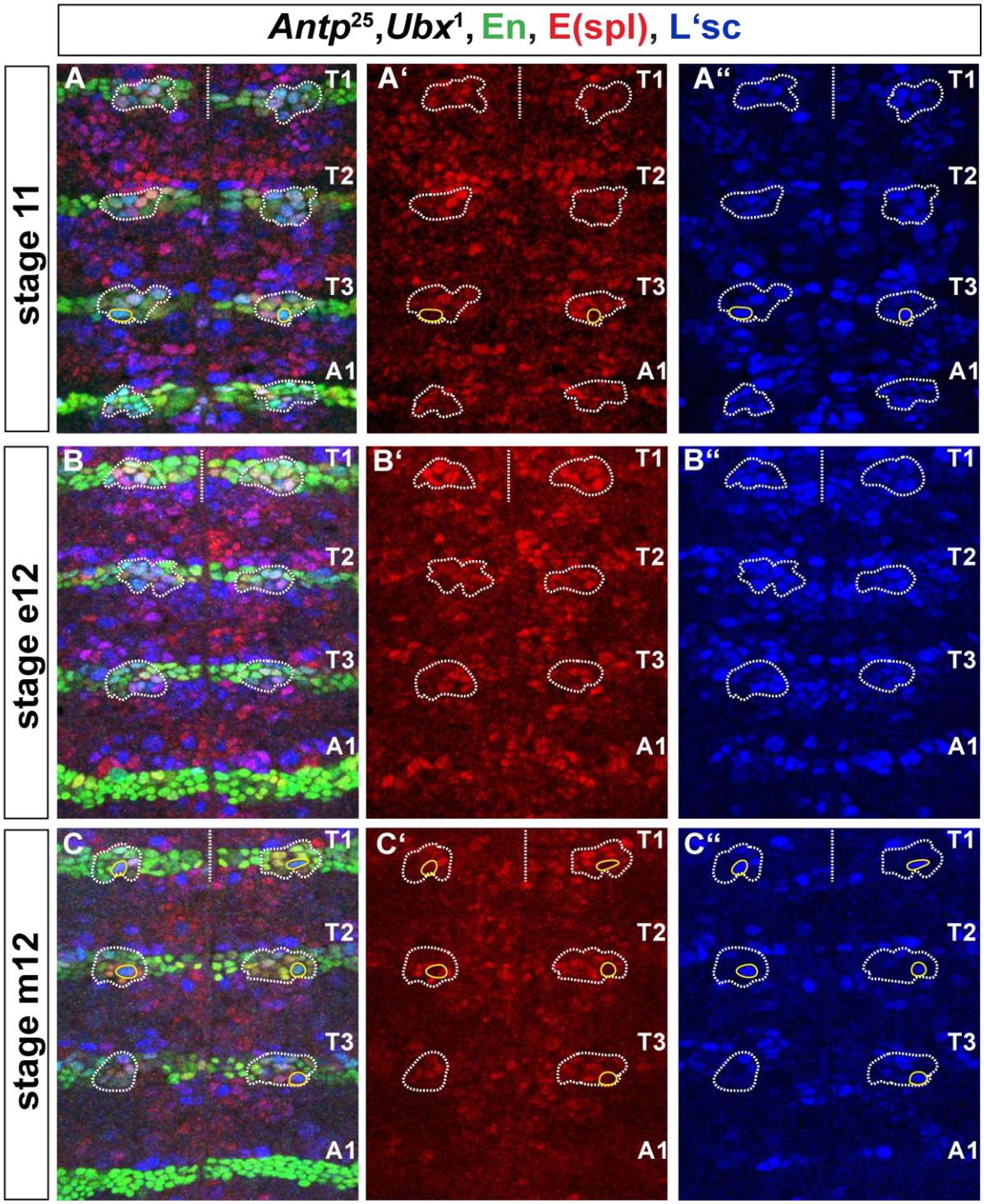

Fig. 29. Sequential Notch activity allows segregation of two NBs in *Antp* mutants.
Confocal sections focusing on the ventral neuroectoderm stained for En, E(spl) and L'sc at embryonic stages 11, early 12 and mid 12 in *Antp*^{25},*Ubx*^{1} (Bloomington) (G, H, H1) double mutants. Anterior is up in all images. The midline is marked with a dotted straight line and the segments in view are always indicated on the right hand side. The single channel of E(spl) (A', B', C') and L'sc (A'', B'', C'') staining

is shown for each image. The proneural cluster of NB7-3 is marked with a dotted outline. (A, A', A") At stage 11, all cells in the proneural cluster express E(spl) staining except a single segregated NB7-3 (outlined in yellow). (B, B', B") In the maintained proneural cluster of thoracic hemisegments in *Antp*^{25},*Ubx*^{1} (Bloomington) double mutant embryos, all cells still exhibit E(spl) expression at early stage 12, while the abdominal segment in the same embryo shows neither L'sc nor E(spl) expression. (C, C', C") During mid-stage 12, the strongly L'sc-positive second NB7-3 (outlined in yellow) is free from E(spl) staining while the other adjacent cells within the proneural cluster show strong E(spl) staining.

After segregation of the second NB7-3, Notch-mediated lateral inhibition represses proneural gene expression in the cluster. These observations strongly suggest that, in *Antp* mutants, either the proneural genes were not efficiently repressed by E(spl) protein products after the first NB segregation, or the proneural genes were reactivated and could override the effect of E(spl) proteins. The maintenance of the NB7-3 proneural cluster and the sequential specification of a second NB7-3 in *Antp* mutants are surprising and may suggest a lineage relationship of the second neuroblast to the primary neuroblast. The existing lineage tracing experiments performed in the Wt indicate that the NB7-3 neuroectodermal precursor (NEP) always undergoes a division in the neuroectoderm prior to its specification as a NB (Bossing et al., 1996). The neuroectodermal division generates two cells, which subsequently attain a neural and an epidermoblast identity. The specified NB delaminates into the VNC and generates the neural lineage, whereas its sister epidermoblast is retained in the ectoderm and generates a 3-4 cell epidermal subclone (Bossing et al., 1996; Schmid et al., 1999).

Sequential segregation of only one additional NB from the maintained proneural cluster in *Antp* mutants suggests that there might be a cell fate change of the sibling epidermoblast to a second NB7-3, resulting in lineage duplication. The lineage relationship between the two NBs was therefore analyzed in the next section.

3.7. The 7-3 neuroectodermal precursor in *Antp* mutants gives rise to the duplicated neuronal lineage and an epidermal subclone

Evaluation of a possible cell fate change of an epidermoblast to a second NB7-3 in *Antp* mutants requires identification of the sister epidermal subclone in the ectoderm. As there are no known antibody markers available to visualize the epidermal subclone of NB7-3, the DiI labelling technique was employed, which allows tracing of

each individually labelled NEP cell throughout embryonic development by observing the morphology of its fully differentiated cell progeny (Udolph et al., 1995; Lüer-Kirsch and Technau, 2009). Karin Lüer-Kirsch performed the lineage tracing experiments. Owing to a complete penetration and stronger expressivity of the NB7-3 lineage duplication phenotype from Lab-T3 segments in the *Antp*^{25},*Ubx*^{1} (Bloomington) double mutant, it was chosen for labelling. A comparative analysis of the lineages generated by the 7-3 NEP in Lab-T2 segments of the Wt and the *Antp*^{25},*Ubx*^{1} mutants revealed interesting results. In all seven clones obtained in Lab-T2 segments of Wt, a normal neuronal lineage of 4 to 6 cells was observed, and only three clones comprised a 2-cell epidermal subclone (Fig. 30A, B, C). The 2-cell epidermal sub-lineage observed in all three aforementioned clones showed mostly round cells instead of extended epidermal cells indicating that they might be undifferentiated. In contrast, in the *Antp*^{25},*Ubx*^{1} double mutant embryos, a single labelled 7-3 NEP from Lab-T2 segments generated a 12-14 cell 7-3 lineage and a 2-4 cell ectodermal subclone (Fig. 30D, E, F) by late embryonic stages. The three clones obtained in the T3 segment of Wt generated a 4 to 5 cell neuronal clone and a typical 4-cell epidermal sub-lineage (Fig. 31). These observations clearly ascertain that there was no cell fate change of an epidermoblast to a second NB7-3 in *Antp* mutants. In Wt anterior thoracic segments, the 7-3 NEP is either directly specified as NB or it divides once and gives rise to two cells, which subsequently develop as NB and an epidermoblast (Fig. 32A). In *Antp* mutants with duplicated lineage, a single NEP generates an epidermoblast and two 7-3 neuroblasts, which delaminate sequentially. This can only be attained with an additional division of the NEP derivatives within the neuroectoderm. Two possible modes of additional division in NEP derivatives could generate two 7-3 neuroblasts in *Antp* mutants. In the first possibility, the NEP would generates two cells, one of which would develop as an NB and delaminate into the VNC, while the other cell would attain the NEP identity, subsequently divide once and generates an epidermoblast and a second NB (Fig. 32B). In the second possibility, the NEP would produce two cells, which develop as NB and an epidermoblast. An additional division of the potential NB cell within the neuroectoderm, before it attains the complete neural potential would produce two cells with neural identities (Fig. 32B). In order to follow the division pattern of the NEP, it is necessary to identify that cell well in advance of its specification as NB.

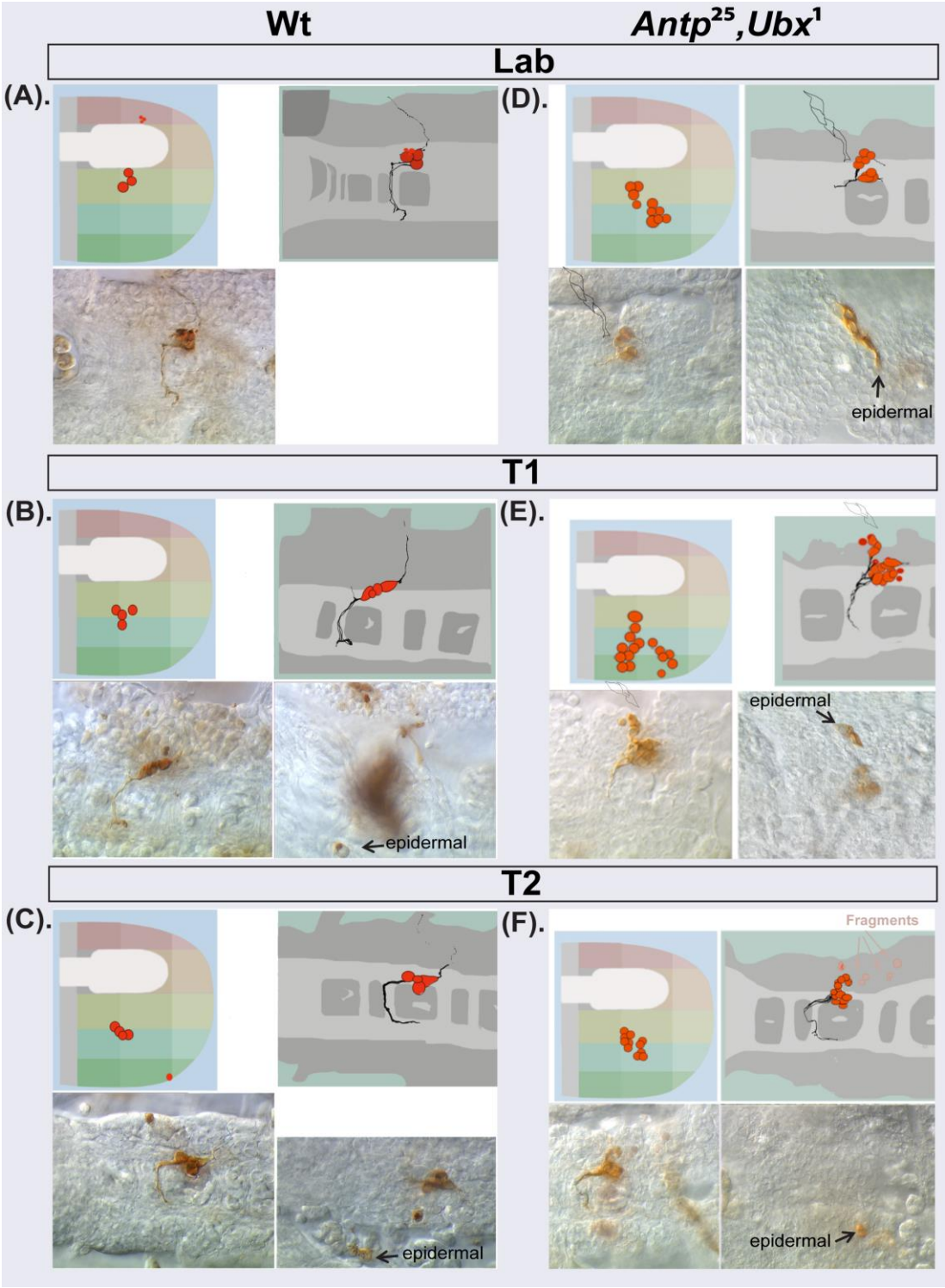

Fig. 30. A single 7-3 neuroectodermal precursor in *Antp* mutants gives rise to the duplicated neuronal lineage and an ectodermal sublineage.
DiI labelling of 7-3 NEP performed in Wt and *Antp*^{25},*Ubx*^{1} mutants from Lab to T2 segments was compared at stage 16. The dorsoventral position of the clone and the projection pattern of the neurons are presented schematically. The neuronal lineage and its ectodermal sub-lineage, if present, are shown for each clone. (A, B, C) Labelled 7-3 NEP in Wt from Lab to T2 segments generates a 4 to 5 cell neuronal lineage and an occasional 2-cell epidermal part. Some apoptotic neurons are typically observed laterally with respect to the clone. (D, E, F). In *Antp*^{25},*Ubx*^{1} (Bloomington) double mutants, the same NEP produces a 12-14 cell neuronal lineage and an epidermal subclone. The epidermal

sublineage part consists either of typical 3 to 4 cells or 2 cells. Images kindly provided by Karin Lüer-Kirsch.

However, the NB selection is a random choice from equally competent proneural cluster cells and there are no known marker genes to identify it before specification. Thus, to test for a possible cell cycle dysregulation in *Antp* mutants, the loss of function and gain of function of cell cycle genes in *Antp* mutants were examined.

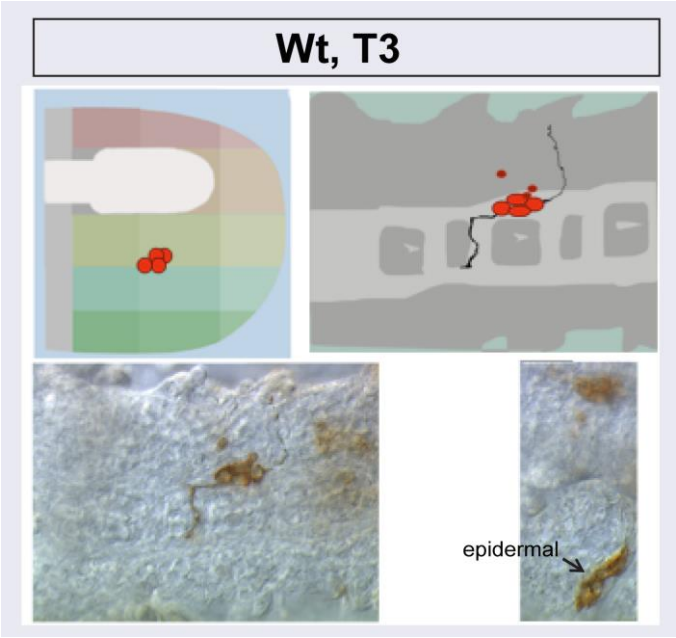

Fig. 31. DiI labelling of 7-3 NEP in segment T3 shows a 4-cell epidermal subclone.
DiI labelling of 7-3 NEP performed in Wt T3 segment shows a 4-5 cell neuronal lineage. Its epidermal subclone always comprises 4-cells. The DV position of the clone and the projection pattern of the neurons are presented schematically. Images kindly provided by Karin Lüer-Kirsch.

3.8. An additional cell division leads to NB7-3 duplication

To investigate whether the pattern of cell divisions in the neuroectoderm is altered in *Antp* mutants, experiments were performed where the cell cycle progression rate in *Antp* mutants was either increased or decreased. In *Drosophila*, after fertilization, 13 rapid synchronous nuclear divisions occur without cytokinesis and detectable gap phases, resulting in the formation of a syncytium. The cell-cycle regulatory components are synthesized from maternal products until 13 divisions (Foe, 1989). Divisions 14-16 occur after gastrulation and acquire a G2 phase. As a result, the divisions in cycle 14-16 are not synchronous, but instead occur in programmed spatial and temporal patterns depending on the zygotic expression of cell-cycle regulators (Edgar and Datar, 1996).

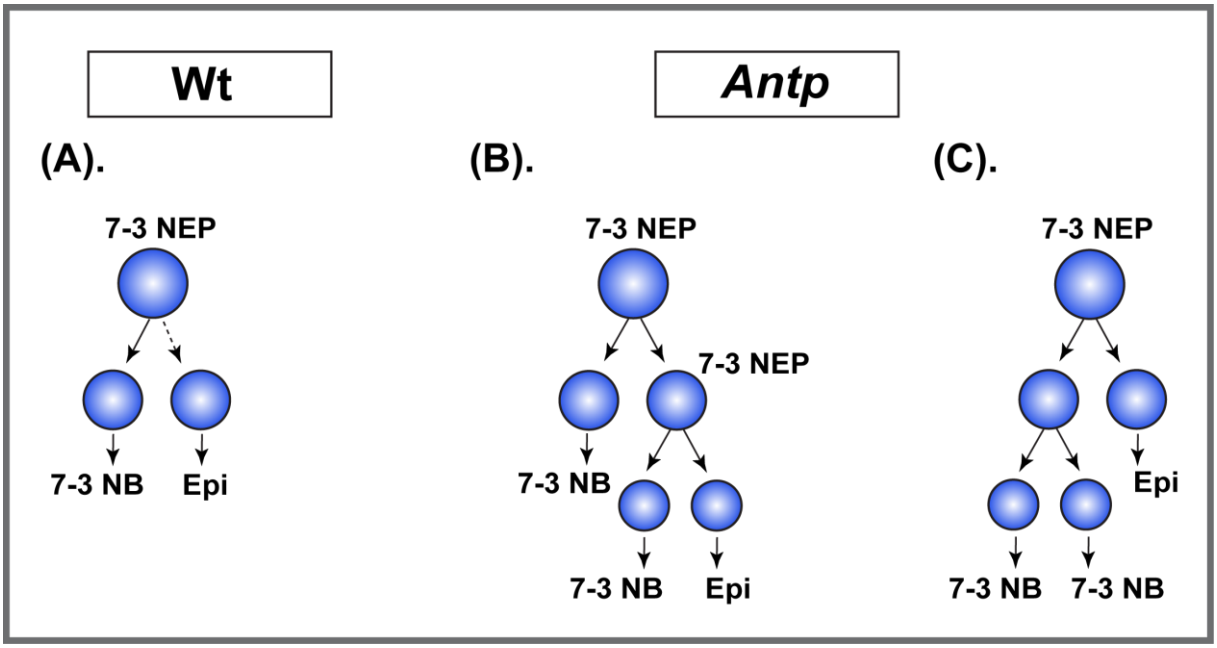

Fig. 32. Possible division modes of 7-3 NEP in *Antp* mutants.
Schematic model showing possible 7-3 NEP division modes within the neuroectoderm of Wt and *Antp* mutants exhibiting the duplication phenotype. (A) The 7-3 NEP in Wt anterior thoracic segments is either directly specified as an NB or divides and gives rise to one NB and an epidermoblast (Epi). (B, C) The duplicated 7-3 NBs in *Antp* mutants arise through an ectopic division of one of the NEP derivatives within the neuroectoderm. (B) The first division of the NEP could generate one NB and a renewed NEP. Subsequently, the NEP would divide and give rise to a second NB and an epidermoblast. (C) Alternatively, the first division of the NEP may be normal and generate two cells, one of which would have NB potential, while the other would develop as an epidermoblast. The cell with NB potential would then divide within the neuroectoderm before it attains the final NB identity and would thus generate two NBs, which delaminate one after the other.

The S1 and S2 NB segregation occurs from G2 arrested neuroectodermal cells at division 14. Regulated String (Stg), a Cdc25-type phosphatase that activates the mitotic kinase Cdk1 (Cdc2), expression in specific domains results in slow progression of division 14 in neuroectodermal cells, thus allowing some S3 and all S4 and S5 NEP cells to undergo one more division before their specification as neural stem cells (Edgar and Farrell, 1990; Hartenstein et al., 1994). The key G1/S regulator, Cyclin E (CycE) continues to be produced from maternal mRNA during division 14 to 16 and later relies exclusively on the regulated zygotic expression. Available evidence indicates that *Hox* genes, along with other factors, repress the cell cycle gene *CycE* to restrict the cell divisions in the embryonic VNC (Berger et al., 2005; 2010; Kannan et al., 2010; Baumgardt et al., 2014). Thus, it was interesting to examine how *CycE* loss of function and gain of function would affect neuroectodermal divisions in the 7-3 NEP of *Antp* mutants. In *CycE* loss of function mutants, the available maternal protein products allow the embryonic cell divisions

until division 16 or 17. However, these divisions in *CycE* mutants are typically slower than those noted in Wt (Knoblich et al., 1994; Jones et al., 2000). The NB7-3 lineages in anterior thoracic segments of *CycE*^{AR95} mutant embryos show 2 to 3 Eg-positive cells with mostly only one Hb co-expressing cell, suggesting it to be GMC-1 (Fig. 33A, A'). Occasionally, this GMC-1 also divides and generates two Hb-positive progeny. Slowing down cell cycle progression by combining the *CycE*^{AR95} mutation with the highly penetrant *Antp*$^{25\ seg18}$ mutation significantly reduced the NB7-3 duplication frequency from 70.31% to 38.63% (n = 44) (Fig. 33B, B', F). Similarly, in recombinants of *CycE*^{AR95} and *Antp*^{25}*,Ubx*^{1} (Bloomington) triple mutants, the NB7-3 duplication frequency was substantially reduced to 40% (n = 72) with a high statistical significance ($p<0.0001$) (Fig. 33F). However, the neuroectoderm of *CycE*^{AR95} and *Antp*$^{25\ seg18}$ double mutants retained proneural gene expression even after NB delamination in all anterior thoracic hemisegments, irrespective of their duplication frequency (Fig. 33C, C', C'' C1). This observation shows that proneural cluster maintenance and the additional cell division in the NEP are independent of one another. Overexpression of *CycE* using *en* GAL4 has no effect on NB7-3 lineage (Fig. 33D). Increasing the cell cycle rate by ectopic expression of *CycE* in low-penetrant single *Antp*^{25} mutant significantly augmented the NB7-3 duplication frequency from 12.85% to 38.88% ($p=0.0001$, n = 72) (Fig. 33E). However, overexpression of G2 to M promoting factors *Cyclin B* (20%, n = 40, $p=0.1824$) and *string* (*stg*) (11.11%, n = 36, $p=0.6634$) was not sufficient to significantly enhance the duplication phenotype in the same genetic background, suggesting that the G1 to S regulator *CycE* plays an important role in this division (Fig. 33E). Indeed, overexpression of proneural genes *l'sc* or *hkb* or any other cell cycle genes individually using *en* GAL4 in Wt background could not generate additional NBs (Table-3.2). This observation suggests that any additional division in the derivatives of NEP alone was likely insufficient to generate further NBs. Concomitant additional division with the overexpression of *CycE* in *Antp*^{25} mutation, which exhibits prolonged proneural cluster maintenance, enhanced segregation of the second NB. This conveys that convergence of these two phenomena results in duplication of the NB7-3 lineage.

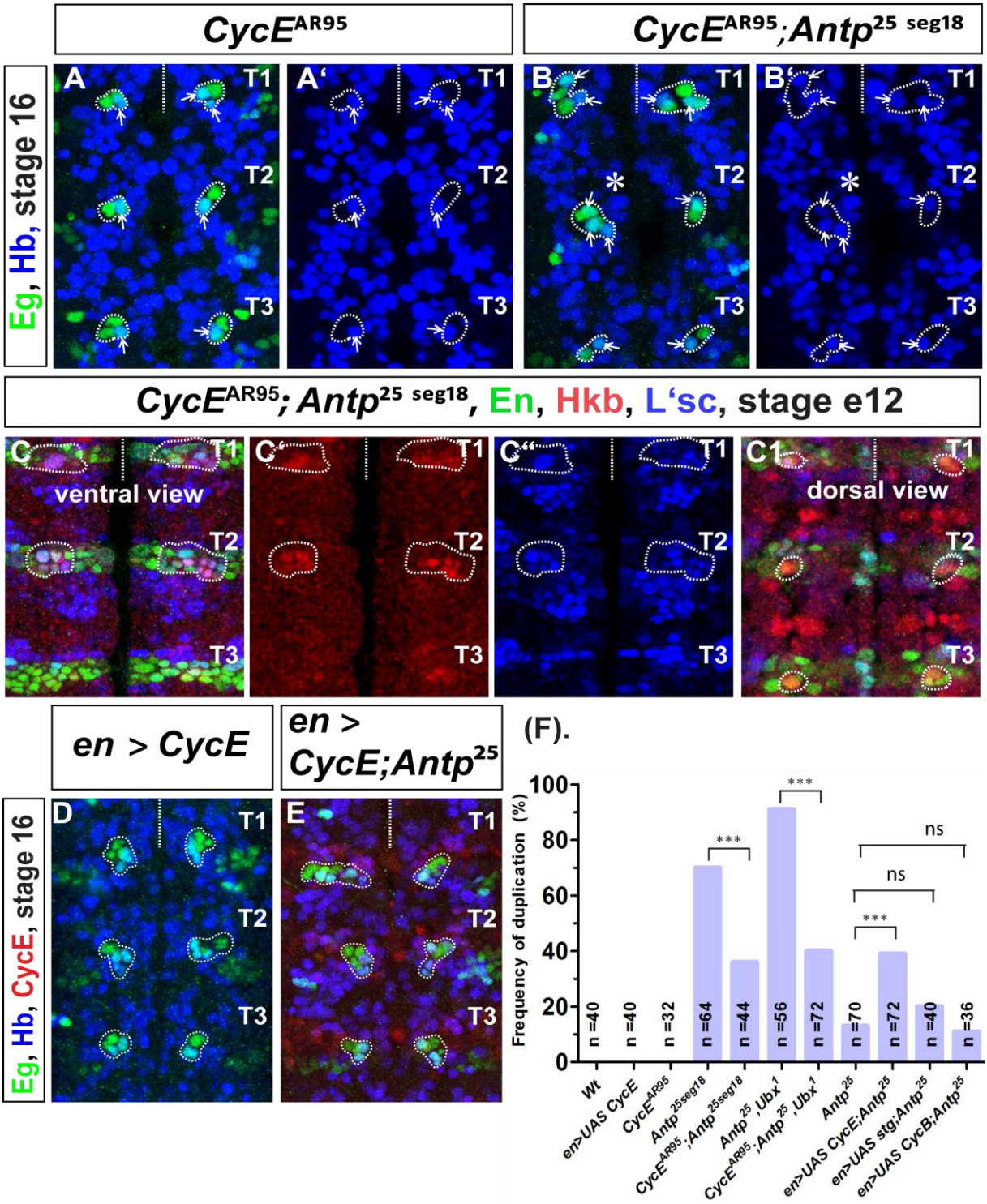

Fig. 33. Duplication frequency of NB7-3 is dependent on an additional neuroectodermal division.

Confocal sections stained for Eg and Hb (A, B, D, E) or Eg, L'sc and Hkb (C). Anterior is up in all images. The midline is marked with a dotted straight line and the segments in view are always indicated on the right hand side. The NB7-3 lineages in (A, B, D, E) or NB7-3 proneural cluster in (C) images are outlined with a dotted line. The single channel of Hb expression is shown for (A, B) images. The single channel of E(spl) and L'sc staining is shown for ventral view image of (C). (A, A') In *CycE*^{AR95} mutants, NB7-3 lineage is reduced to 2-3 Eg-positive cells, comprising one or two Hb-positive cells (indicated by arrow). (B, B') Recombination of *CycE*^{AR95} mutation to the strongly penetrant *Antp*$^{25\ seg18}$ mutant resulted in a significantly reduced duplication frequency. In

hemisegments with duplication phenotype (denoted by *), the 7-3 lineage shows 5 to 6 Eg-positive cells with 3 to 4 Hb co-expressing cells (indicated by arrow). (C, C', C'', C1) In *CycE*^{AR95};*Antp*$^{25\ seg18}$ double mutants, the proneural cluster is still maintained in all the anterior thoracic hemisegments even after NB delamination. (D) Overexpression of *CycE* using *en* GAL4 has no effect on NB7-3 lineage. (E) Overexpression of *CycE* in low-penetrant *Antp*^{25} mutant background increased the duplication frequency significantly. The CycE expression pattern in the En domain confirms the overexpression. (F) Graphical representation of duplication occurence variability in *Antp* mutants combined with *CycE* mutation and in *Antp*^{25} mutants overexpressing *CycE*, *stg* or *CycB*. The Chi-squared test (χ^2) was applied for statistical significance analysis. Both in *CycE*^{AR95} mutants and *CycE* overexpression using *en* GAL4, the NB7-3 duplication is not observed. The duplication frequencies were significantly reduced with $p<0.0001$ in combined *CycE*^{AR95};*Antp*$^{25\ seg18}$ and *CycE*^{AR95};*Antp*^{25},*Ubx*^{1} mutants compared to the *Antp*$^{25\ seg18}$ and *Antp*^{25},*Ubx*^{1} mutants, respectively. Only *CycE* overexpression in *Antp*^{25} mutant has significantly ($p<0.0001$) increased the duplication frequency. In contrast, overexpression of *stg* and *CycB* in *Antp*^{25} mutant could not enhance the frequency.

Collectively, these findings suggest that an additional cell division determines the duplication frequency across different *Antp* mutants. Further experiments were conducted in order to ascertain why the same *Antp*^{25} mutation shows different 7-3 NEP division frequencies within the neuroectoderm.

Genotype	Frequency (%)	(n)
en > UAS *CycA*	0%	20
en > UAS *CycB*	0%	32
en > UAS *CycD* (818)	0%	27
en > UAS *CycD* (820)	0%	28
en > UAS *CycD;*UAS *CDK4*	0%	40
en > UAS *CycE*	0%	36
en > UAS *dE2f*	0%	40
en > UAS *hkb*	0%	56
en > UAS *lsc*	0%	20
en > *UAS stg*	0%	72
sca > UAS *CycE*	0%	48

Table-3.2. NB7-3 duplication phenotype is not observed by overexpression of *l'sc*, *hkb* or any cell cycle regulator genes in NB7-3 neuroectodermal cluster. The number of anterior thoracic hemisegments analyzed is shown (n).

3.9. Molecular mapping of the *Antp*^{25} mutation

In order to explore the duplication frequency variation between single *Antp*^{25} and *Antp*^{25},*Ubx*^{1} (Bloomington) mutants, the *Antp* coding sequence of these two mutants was compared to that of Wt. Structurally, the *Antp* gene shows a complex pattern consisting of two functionally independent promoters, two polyadenylation sites, eight

exons and very long intronic regions totally covering nearly 103 kb in total on *3R* chromosome (Fig. 34A) (Scott et al., 1983; Schneuwly et al., 1986; Laughon et al., 1986; Wirz et al., 1986; Stroeher et al., 1988). Four classes of *Antp* transcripts synthesized from two promoters differ from each other at their 5' and 3' untranslated sequences but share a common open reading frame (ORF) of 1137 bp length positioned from exon5 to exon8 (Fig. 34A). The *Antp*^{25} mutant is genetically classified as an amorphic loss of function allele (Abbott and Kaufman, 1986), which elicits the same phenotype when homozygous and when heterozygous to a chromosomal deficiency that disrupts the same gene. For identifying whether a similar mutation in the *Antp* gene is present in single *Antp*^{25} and the *Antp*^{25},*Ubx*^{1} (Bloomington) double mutants, the complete *Antp* coding region was sequenced and thoroughly checked in comparison to the Wt and reported sequence in FlyBase. The results revealed that, at specific base positions of 5' and 3' untranslated regions of the RNA transcripts in the Wt, *Antp*^{25} and *Antp*^{25},*Ubx*^{1} (Bloomington) mutants, mostly similar polymorphisms are found compared to the FlyBase sequence (Fig. 34B). Importantly, in both single *Antp*^{25} and the *Antp*^{25},*Ubx*^{1} (Bloomington) double mutants, a single nonsense point mutation of C to T at the 370 bp in the *Antp* ORF was observed (Fig. 34B). Additionally, a silent point mutation of A to G at the 909 bp was noted in the ORF of the *Antp*^{25} and the *Antp*^{25},*Ubx*^{1} (Bloomington) mutants (Fig. 34B). Three individual replicate sequencing tests of Wt and *Antp*^{25} and the *Antp*^{25},*Ubx*^{1} (Bloomington) mutants showed identical observations. In Wt, the common ORF encodes a 378 aa long Antp protein (Stroeher et al., 1986) (Fig. 34C). In the amino terminal end of the Antp protein, two Glutamine rich (OPA repeat) domains are present while in the carboxyl terminal end an important Antp-specific hexapeptide linker region is lying adjacent to the 61 aa long homeodomain (Billeter et al., 1990; Qian et al., 1993; Fraenkel and Pabo, 1998). The homeodomain of the *Hox-C* genes have been shown to bind specific DNA sequences and regulate the transcription of the down-stream genes (Beachy et al., 1988; Kuziora and McGinnis, 1988; Affolter et al., 1990; Ekker et al., 1991). The C to T non-sense point mutation at 370 bp position within the ORF of both *Antp* mutants substitutes for a stop codon at 123 aa in the protein (Fig. 34C). The truncated 122 aa long Antp protein in single *Antp*^{25} and the *Antp*^{25},*Ubx*^{1} (Bloomington) double mutants lacks the important DNA-binding domain and Antp signature hexapeptide regions. These experiments clarify that both mutants carry the same mutation in the ORF of *Antp*.

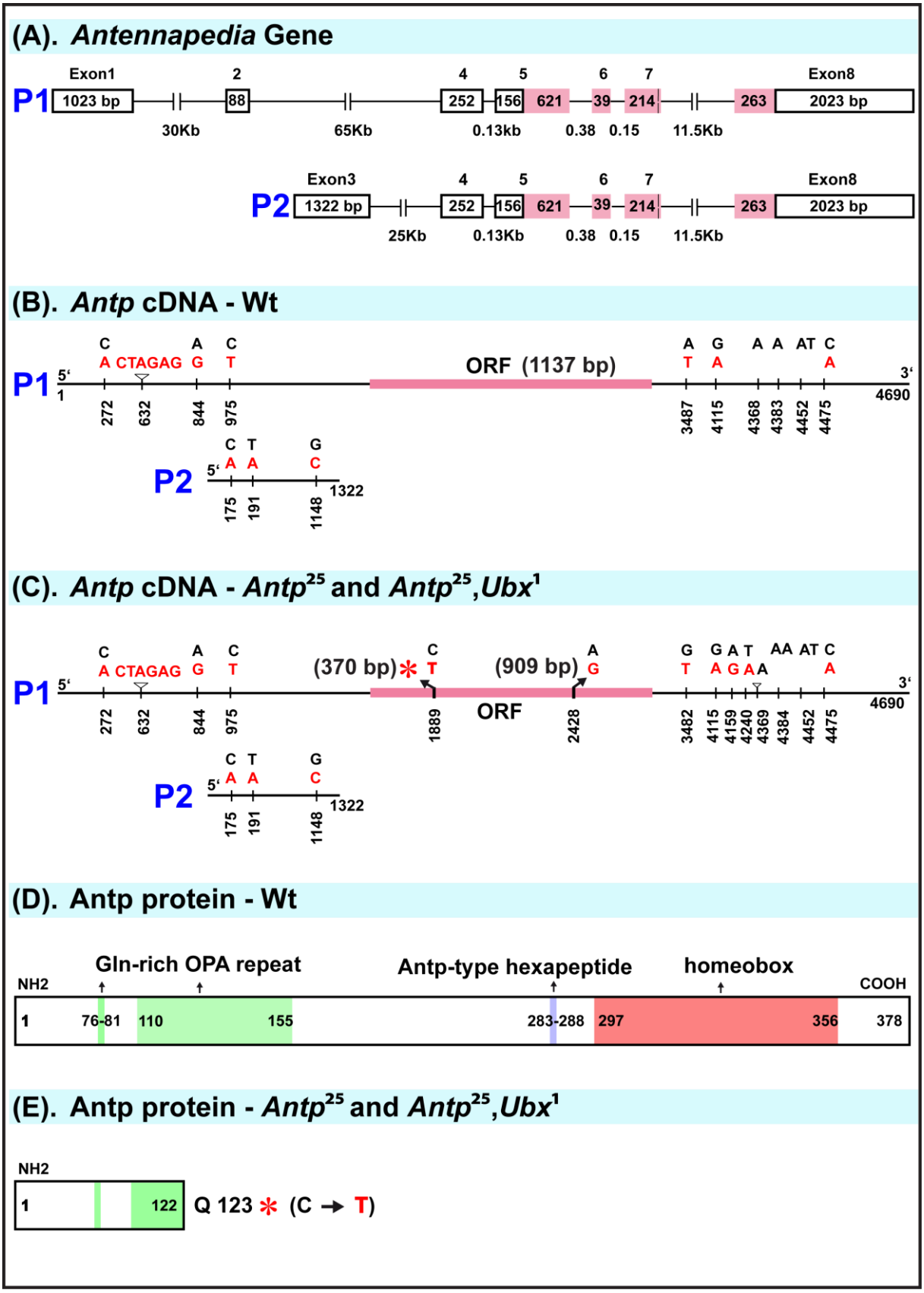

Fig. 34. Molecular mapping of the *Antp*^{25} mutation.
Schematic drawing of the *Antp* gene structure, longest transcripts synthesized from two promoters and the translated protein products in Wt and in *Antp*^{25} and *Antp*^{25},*Ubx*^{1} (Bloomington) mutants. (A) Schematic *Antp* gene structure with two promoters (P1, P2), 8 exons (box) and connecting intronic

regions. The base pairs (bp) of each exon and introns are given in numbers. The exon regions, which specify open reading frame (ORF), are filled with pink colour. (B, C) P1 and P2 promoter-specific long transcripts sequenced from Wt (B) and homozygous *Antp*^{25} and *Antp*^{25},*Ubx*^{1} (C) mutants is compared with FlyBase *Antp* transcripts. (B) The polymorphisms observed at certain base positions (red) in 5' and 3' ends of Wt transcripts compared to the FlyBase sequence are shown. No polymorphisms were observed in 1137 bp (pink) ORF of Wt. (C) Apart from the most common polymorphisms in the 5' and 3' ends, in *Antp*^{25} and *Antp*^{25},*Ubx*^{1} (Bloomington) double mutant ORF, two point mutations are observed at 370 (C to T) and 909 (A to G) bp locations (indicated with an asterisk). (D) The 378 aa long Wt-Antp protein possesses two glutamine-rich OPA repeats (filled with green) in the amino (NH2) terminal end whereas the Antp-type hexapeptide (filled with purple), and homeodomain (filled with brick red) are observed at the carboxyl (COOH) terminal end. (E) Point mutation observed at 370 bp in the ORF of both *Antp*^{25} mutants leads to a stop codon (indicated with an asterisk) at the 123 aa instead of glutamine in the protein. The truncated version of the protein in the mutants is deficient of important DNA-binding regions of the protein homeobox and the linking Antp signature hexapeptide regions.

It is surprising that the single *Antp*^{25} and the *Antp*^{25},*Ubx*^{1} (Bloomington) mutants exhibit extreme NB7-3 duplication frequency differences when they carry the same mutation in the *Antp* gene. These differences suggest an additional mutation in other *Antp* genomic regions of the *Antp*^{25},*Ubx*^{1} (Bloomington) mutants and its derivative *Antp*$^{25\ seg}$ mutants. If there is any second site mutation in *Antp*^{25},*Ubx*^{1} (Bloomington) double mutant, it must be lying in close vicinity of *Antp* as all the segregation mutants were also strongly penetrant compared to single *Antp*^{25} mutant.

To narrow down the possible affected genomic region in close vicinity of *Antp*, a complementation assay was performed using the deficiencies covering *3R*: 84A5-96B17 chromosomal regions. Among the 61 molecularly mapped deficiencies covering the genomic region of 84A5-96B17, the lethality of *Antp*$^{25\ seg18}$ was noted only *in trans* with one deficiency line, *Df(3R)BSC422* (Fig. 35A). It covers the genomic region of 84A5-84B2, in which the complete *Antp* gene and the remaining ANT-C genes *Dfd* and *Scr* are also found (Christensen et al., 2008.4.15) (Fig. 35A). The other cytologically mapped *Antp* deficiencies within the 84A5-84D14 chromosomal regions also produced non-complementation results (Fig. 35B). However, a cytologically mapped *Df(3R)9A99*, which covers *Dfd*, *Scr* and *fushi tarazu* (*ftz*) genomic fragments of 84A1-84A6 was not lethal *in trans* with *Antp*$^{25\ seg18}$ and *Antp*^{25},*Ubx*^{1} (Bloomington) double mutant. Thus, this region can be excluded as a possible location of the additional mutation (Fig. 35B). The remaining affected genomic region of *Df(3R)BSC422* with the coordinates from *3R*:6866245..6999049 (84A6-84B2) include the complete *Antp* gene, with the exception of 179 bp in its 5' region.

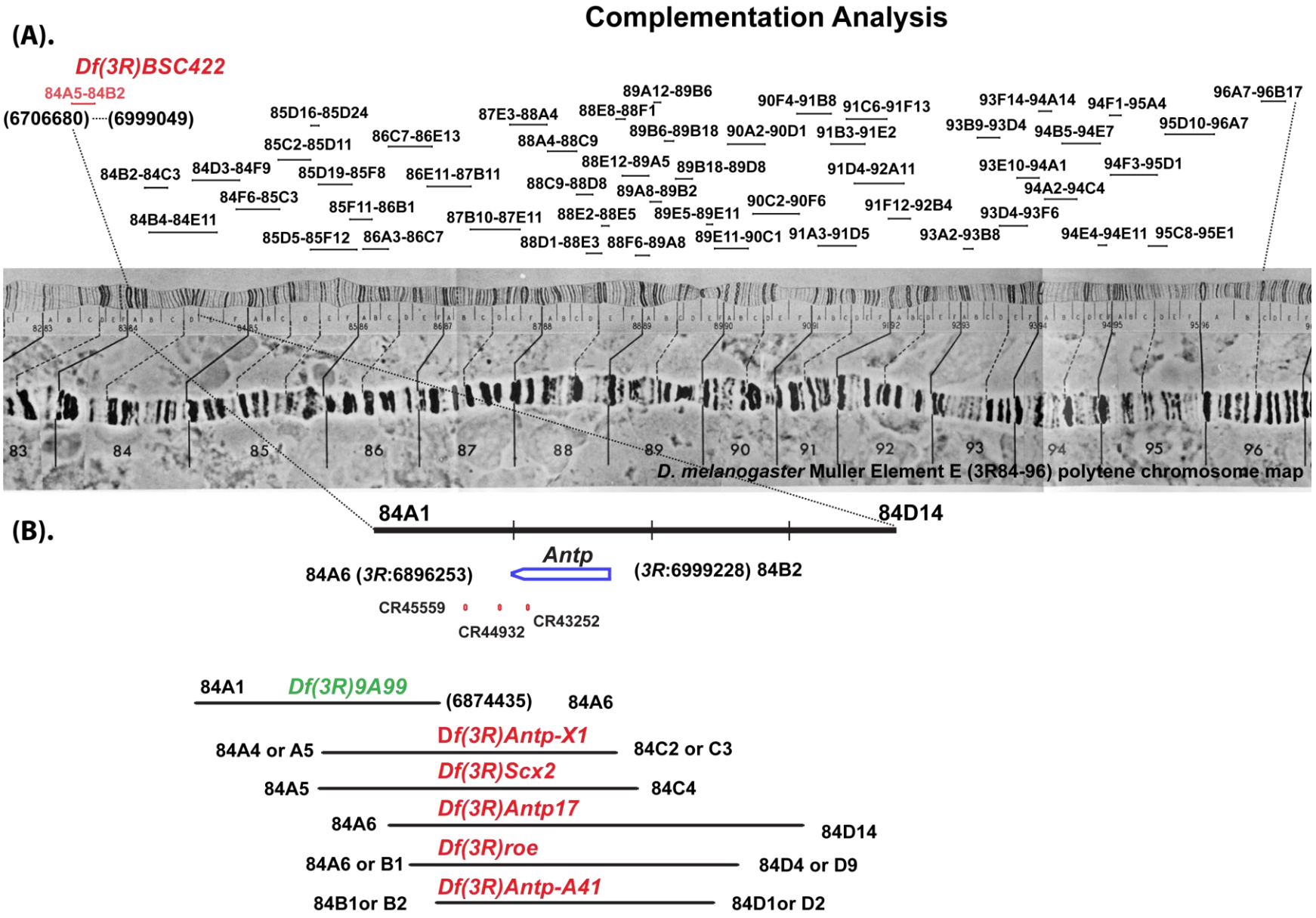
Complementation Analysis
(A).
Df(3R)BSC422
84A5-84B2
(6706680)
(6999049)
85D16-85D24
87E3-88A4
88E8-88F1
89A12-89B6
90F4-91B8
91C6-91F13
93F14-94A14
94F1-95A4
96A7-96B17
85C2-85D11
86C7-86E13
88A4-88C9
89B6-89B18
90A2-90D1
91B3-91E2
93B9-93D4
94B5-94E7
95D10-96A7
84B2-84C3
84D3-84F9
85D19-85F8
86E11-87B11
88E12-89A5
89B18-89D8
91D4-92A11
93E10-94A1
94F3-95D1
84F6-85C3
88C9-88D8
89A8-89B2
94A2-94C4
84B4-84E11
85F11-86B1
87B10-87E11
88E2-88E5
89E5-89E11
90C2-90F6
91F12-92B4
93D4-93F6
85D5-85F12
86A3-86C7
88D1-88E3
88F6-89A8
89E11-90C1
91A3-91D5
93A2-93B8
94E4-94E11
95C8-95E1
83
84
85
86
87
88
89
90
91
92
93
94
95
96
D. melanogaster Muller Element E (3R84-96) polytene chromosome map
(B).
84A1
84D14
Antp
84A6 (3R:6896253)
(3R:6999228) 84B2
CR45559
CR44932
CR43252
84A1
Df(3R)9A99
(6874435)
84A6
84A4 or A5
Df(3R)Antp-X1
84C2 or C3
Df(3R)Scx2
84A5
84C4
84A6
Df(3R)Antp17
84D14
84A6 or B1
Df(3R)roe
84D4 or D9
84B1or B2
Df(3R)Antp-A41
84D1or D2

Fig. 35. Complementation analysis for identifying the second mutation in strongly penetrant *Antp*^{25} mutants.
Schematic of the complementation analysis tested against *Antp*$^{25\ seg18}$ and 61 molecularly mapped deficiencies covering *3R*:84A5-96B17 (A) or cytologically mapped deficiencies falling in the region *3R*:84A1-84D14 (B). *Drosophila melanogaster* Muller 3R polytene chromosome map 84-96 was adopted in the scheme to locate the regions. *Antp* gene with its coordinates (blue, not drawn to scale) and three non-coding RNAs (red), two (CR44932, CR45559) lying in close vicinity of it and one lying within the intron (CR43252), were also shown. (A) Among the 61 tested deficiencies (each indicated with a line and the deleted region relative to map), only a deficiency (*Df(3R)BSC422*) covering 84A5 to 84B2 (indicated in red color) complements the *Antp*$^{25\ seg18}$ mutant. (B) Complementation analysis performed between *Antp*$^{25\ seg18}$ and the cytologically mapped deficiencies covering the 84A5-84D14 region, all the deficiencies are complementing except the *Df(3R)9A99* (green) covering the 84A1 to 84A6.

Three non-coding RNAs were lying in close vicinity of *Antp*, two are located near to 3' end (CR45559 and CR44932) and one within an intron (CR43252) (Fig. 35B). The expression pattern and function of these non-coding RNAs has not been studied so far. To exclude the possible second site mutation within the CR43252 of *Antp*$^{25\ seg18}$ and *Antp*^{25},*Ubx*^{1} (Bloomington) mutants genomic sequences, sequencing analysis was performed. However, no differences in the genomic sequence of CR43252 was observed in homozygous *Antp*$^{25\ seg18}$ and *Antp*^{25},*Ubx*^{1} (Bloomington) mutants relative to the Wt and single homozygous *Antp*^{25} mutant sequence. In order to analyze how strongly the phenotype is penetrant in the *trans*-heterozygotes of the *Antp*^{25},*Ubx*^{1} (Bloomington) and the lethal deficiencies, duplication frequencies were analyzed. The frequency of duplication in *trans*-heterozygotes of five deficiencies and *Antp*^{25},*Ubx*^{1} (Bloomington) double mutant is also stronger with an average of at least 60% (Fig. 36). The frequency was stronger *in trans* with the deficiencies covering anterior to the 3' end of the *Antp* gene. In *trans*-heterozygotes of *Antp*^{25},*Ubx*^{1} (Bloomington) and the molecularly mapped non-complementing deficiency *Df(3R)BSC422*, 64% duplication frequency was observed (Fig. 36). It was comparable to the evaluated frequency of the segregation mutants and the strongly penetrant single *Antp*^{14} mutant. Additionally, the duplication frequency of single *Antp*^{25} mutant significantly increased to 29.54% (n = 44, p=0.031) *in trans* with the *Df(3R)BSC422* (Fig. 36). Together, these results suggest that there must be an additional mutation in the *Antp*^{25},*Ubx*^{1} (Bloomington) double mutant and its derivative segregation mutants, which enhances the 7-3 NEP neuroectodermal divisions. To map the additional mutation, genomic sequencing analysis of the complete 103 Kb long *Antp* gene, and it's neighbouring regions would have to be performed, which was not possible for time reasons.

To determine whether any promoter-specific transcriptional variations or translational efficiency differences between the two mutants exist, the *Antp* RNA and antibody expression patterns were examined in the single *Antp*^{25} and *Antp*^{25},*Ubx*^{1} (Bloomington) double mutants.

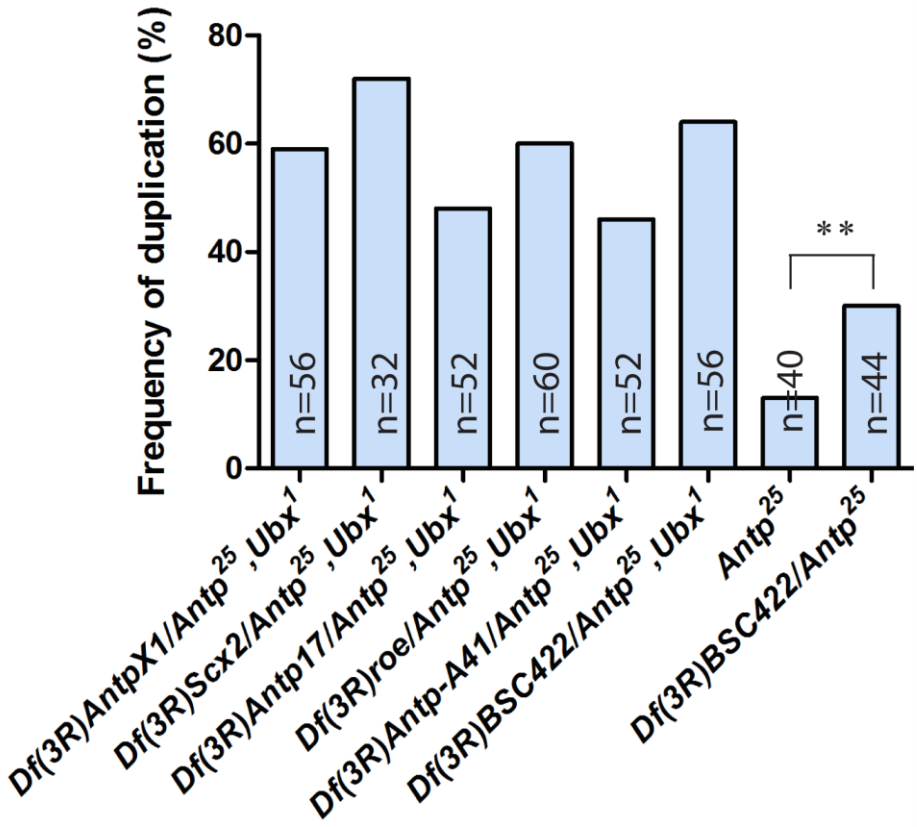

Fig. 36. Duplication frequency is average in *trans*-heterozygotes of *Antp*^{25},*Ubx*^{1} (Bloomington) and lethal deficiencies.
Graphical representation of duplication frequency in the *trans*-heterozygotes of *Antp*^{25},*Ubx*^{1} (Bloomington) and lethal deficiencies. The strength of duplication frequency in all the *trans*-heterozygotes was observed on average of atleast 60%. The frequency in *trans*-heterozygotes of single *Antp*^{25} mutant and *Df(3R)BSC422* exhibit significant increase compared to the homozygous single mutant (P = 0.0031).

3.10. RNA and protein expression analysis in *Antp* mutants

The transcripts synthesized from the two promoters differ in encompassing specific 5' exons. Exon1 and 2 are exclusively present in the P1-promoter (P1) specific transcripts and exon3 only in the transcripts synthesized from the P2-promoter (P2) (Fig. 34A) (Scott et al., 1983; Wirz et al., 1986; Stroeher et al., 1988). Transcriptional efficiency differences between the two mutants were examined by RNA expression analysis. The observed promoter-specific transcript pattern in the Wt neuroectoderm at stage 11 is consistent with the previous results of Bermingham et al., 1990. The

P1 specific RNA expression was observed in the neuroectoderm from posterior T1 to the anterior A7 segment at stage 11, with a stronger expression domain restricted from posterior T1 to anterior T3 segment (Fig. 37A, B, B'). Similar to Wt, the strong expression domain of P1-specific RNA is noted from posterior T1 to anterior T3 segment within the neuroectoderm of single *Antp*^{25} mutant embryos at stage 11 (Fig. 37C, C'). In the neuroectoderm of double mutants at stage 11, the stronger expression domain of *Antp* was extended until the anterior A1 segment (Fig. 37D, D'). This is consistent with the previous observations stating that Ubx protein represses *Antp* transcription in parasegment 6 (Wirz et al., 1986; Appel and Sakonju, 1993). Thus, in the absence of Ubx protein in double mutants, the expression domain of *Antp* extended until anterior A1. Apart from changes in the expression domain, quantitative levels of the RNA expression in both mutants do not seem to vary between *Antp* mutants and Wt. *Antp* transcripts synthesized from the P2 possess only exon3 (Fig. 34A) (Scott et al., 1983; Wirz et al., 1986; Stroeher et al., 1988). In Wt neuroectoderm at stage 11, P2-specific RNA expression was noted from posterior Lab to the A9 segment, with slightly stronger expression from posterior T1 to anterior T3 segment (Fig. 37E, F, F'). P2-specific RNA *in situ* analysis within the neuroectoderm of *Antp*^{25} and double mutants did not exhibit any significant changes in the expression levels compared to Wt thoracic segments (Fig. 37G, G', H, H'). As there were no significant changes in expression of *Antp* transcripts, protein expression in *Antp*^{25} and *Antp*^{25},*Ubx*^{1} mutants was analyzed and compared to Wt. Comparative analysis of Antp protein expression in early embryonic stages revealed discrepancies between *Antp*^{25} and *Antp*^{25},*Ubx*^{1} (Bloomington) mutants. In Wt, strong Antp expression is noted from posterior T1 to anterior T3 segment within the neuroectoderm and also in the late VNC (Fig. 38A, A') (Wirz et al., 1986). Relative to the Wt embryos, substantially reduced Antp protein levels were detected at stage 11 in the neuroectoderm and in the late VNC of single *Antp*^{25} mutants (Fig. 38B, B'). However, in the early embryos of the double mutant, as well as in the *Antp*$^{25\ seg}$ mutants derived from it, no detectable amounts of protein could be observed (Fig. 38C, D). Later, in the VNC, very faint Antp expression was noted in the double mutant and *Antp*$^{25\ seg}$ mutants (Fig. 38C', D'). Altogether, sequencing and RNA expression analysis suggest that a single point mutation and similar RNA expression in both mutants generate quantitatively different amounts of a truncated 122 aa Antp protein in early embryonic stages.

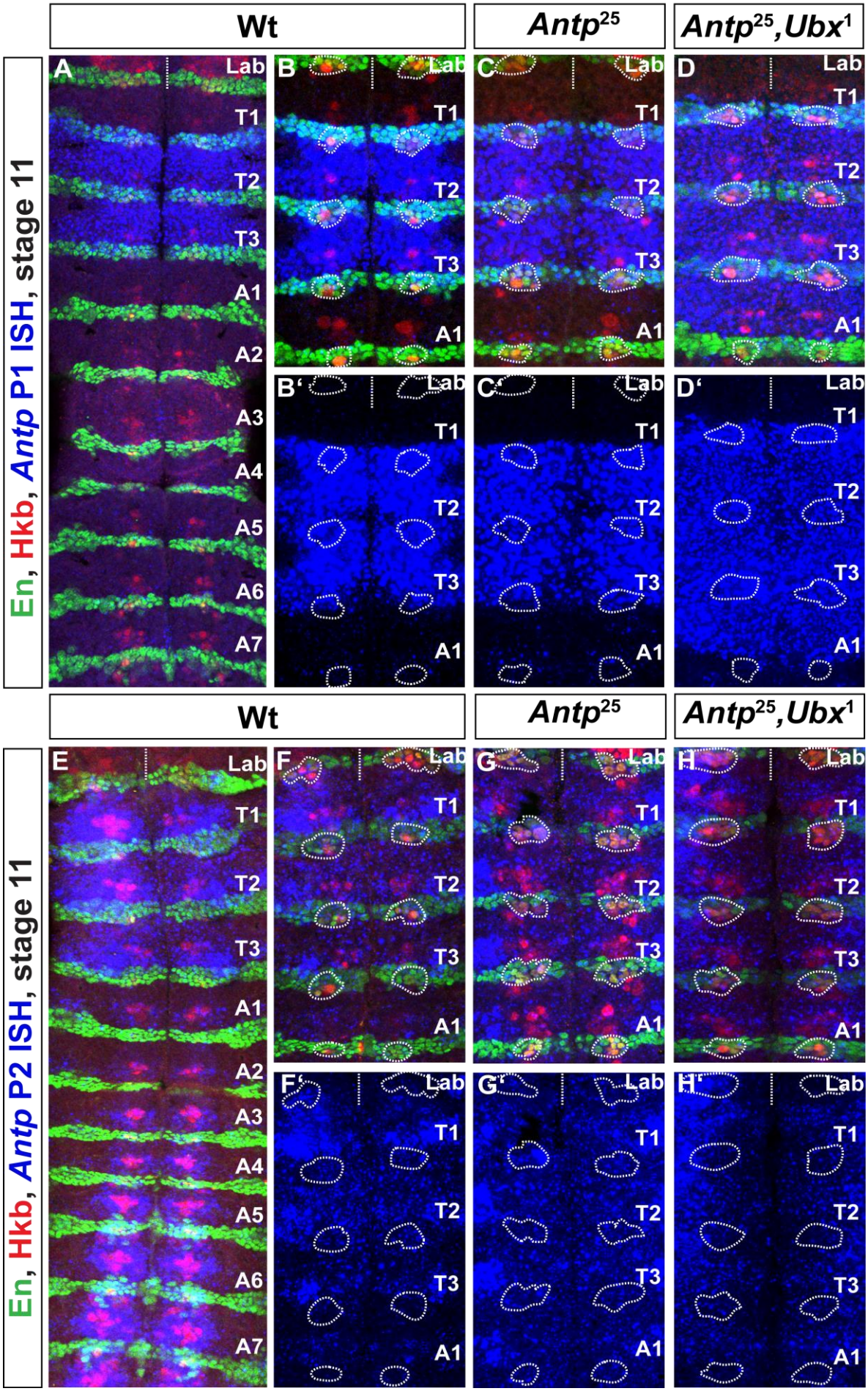
Wt
Antp25
Antp25,Ubx1
En, Hkb, Antp P1 ISH, stage 11
En, Hkb, Antp P2 ISH, stage 11
A
B
B'
C
C'
D
D'
E
F
F'
G
G'
H
H'
Lab
T1
T2
T3
A1
A2
A3
A4
A5
A6
A7

Fig. 37. Analogous *Antp* RNA expression in single *Antp*^{25} and *Antp*^{25},*Ubx*^{1} double mutants.
Confocal sections focusing on the ventral neuroectoderm stained with En and Hkb antibodies and *Antp Exon1* (A, B, C, D) or *Exon3* (E, F, G, H) specific *in situ* probes at embryonic stages 11 in Wt (A, B, E, F), *Antp*^{25} (C, G) and *Antp*^{25},*Ubx*^{1} (D, H) (Bloomington) double mutants. Anterior is up in all images. The midline is marked with a dotted straight line and the segments in view are always indicated on the right hand side of the image. The single channel of RNA expression is shown for each genotype, and the proneural cluster of NB7-3 is marked with a dotted outline. (A) The expression of promoter-1 specific transcripts is observed from posterior T1 to anterior A7 segment in Wt neuroectoderm at stage 11. (B, B') In Wt, the strong promoter-1 specific RNA expression is observed from posterior T1 to anterior T3 segment. Specifically, the Hkb-positive NB7-3 proneural clusters in T1 and T2 segments are strongly positive for *Antp*. (C, C', D, D') The promoter-1 specific RNA expression does not seen different from Wt in the anterior thoracic NB7-3 proneural clusters of *Antp*^{25} and *Antp*^{25},*Ubx*^{1} (Bloomington) double mutants. The stronger expression domain is extended until anterior A1 in double mutants. (E) At stage 11, weak expression of promoter-2 specific RNA in the neuroectoderm can be observed from posterior Lab to A9 segment in Wt. (F, F') The strong promoter-2 specific RNA expression is noted in the T1 and T2 segments NB7-3 proneural clusters of Wt. (G, G', H, H') The expression level of promoter-2 specific RNA in *Antp*^{25} and *Antp*^{25},*Ubx*^{1} (Bloomington) double mutants is not different from Wt.

Variation in the duplication phenotype frequency across different *Antp*^{25} mutants, positively correlating with early embryonic protein expression, implies that the truncated Antp protein might efficiently repress the NB7-3 duplication. Coincidentally, *Antp*^{11} mutant, a loss of function allele, with low duplication penetration of only 16% shows detectable protein, whereas in the strongly penetrant, *Antp*^{14} mutant, no detectable protein was found at early embryonic stages (Fig. 38E, F). These results imply that, in *Antp*^{11}, the mutation in *Antp* might be generating a truncated protein product. In addition, NB7-3 duplication frequency seems to be correlated with early protein expression in the mutants. These results raise two questions:

1. How do the differences in Antp protein levels between Wt and *Antp*^{25} on one hand, and *Antp*^{25},*Ubx*^{1} and the segregation mutants on the other hand arise?
2. Does Antp require its homeodomain to suppress additional NEP divisions in the neuroectoderm?

I attempted answering these questions aimed at determining whether the protein observed in single *Antp*^{25} mutants is indeed truncated or whether a read-through of the mutation leads to expression of a protein of normal length. To analyze this a western blot analysis was performed. The role of early embryonic truncated HD-less Antp protein in influencing the neuroectodermal divisions across the different *Antp*^{25} mutants was analyzed by overexpression of the truncated protein in *Antp* mutants. The results of these experiments are discussed in the next section.

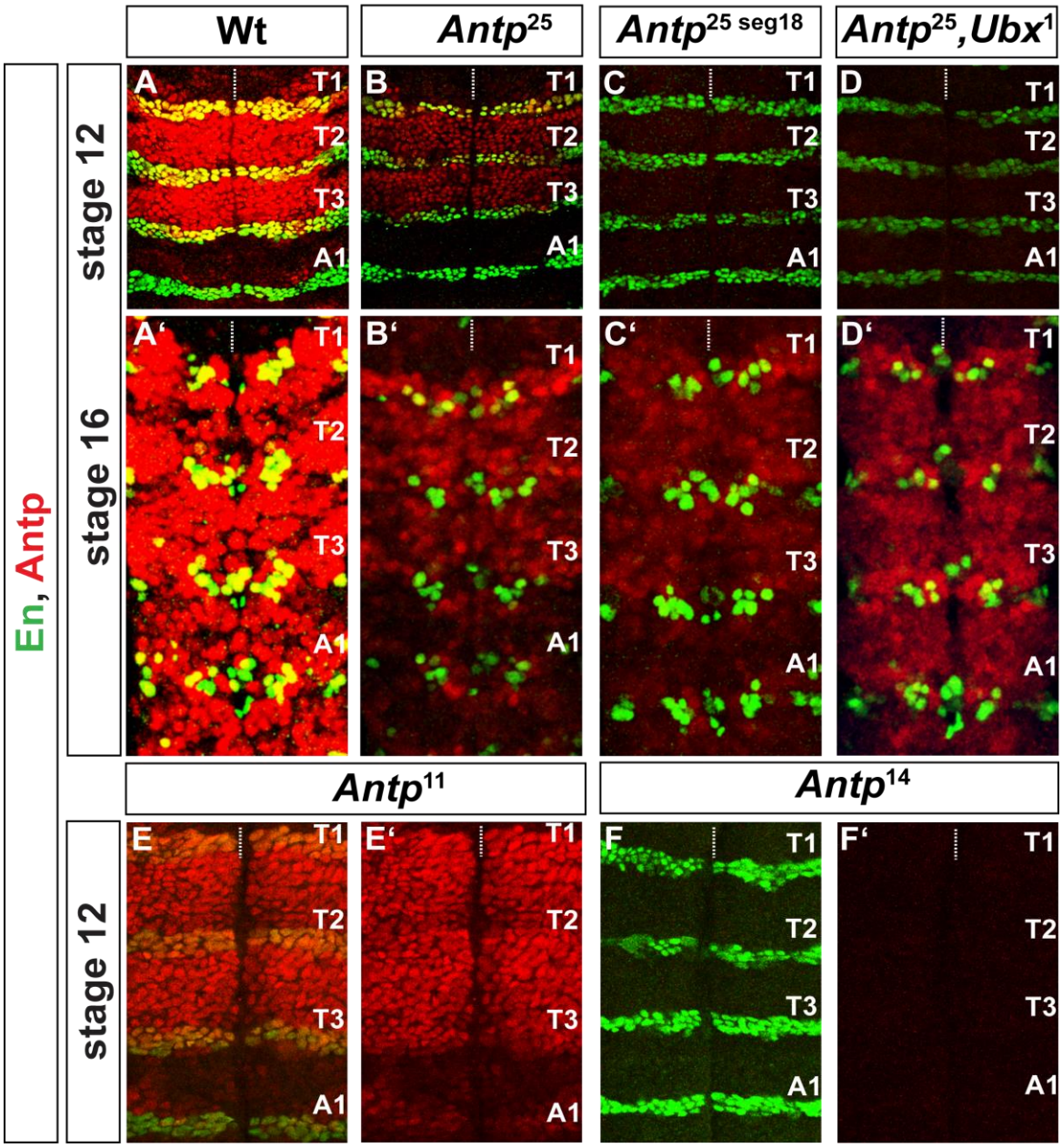

Fig. 38. Correlation of NB7-3 duplication frequency and early Antp protein expression levels in the mutants.

Confocal sections focusing on the ventral neuroectoderm stained for En and Antp at embryonic stages 12 and 16 in Wt (A, A') and in *Antp*^{25} (B, B'), *Antp*$^{25\ seg18}$ (C, C'), *Antp*^{25},*Ubx*^{1} (Bloomington) (D, D'), and only at stage 12 in *Antp*^{11} (E) and *Antp*^{14} (F) mutants. Anterior is up in all images. The midline is marked with a dotted straight line and the segments in view are always indicated on the right hand side. (A, A') The strong Antp expression is observed from posterior T1 to anterior T3 segments within the neuroectoderm of early stage 12 embryos (A). Very similar pattern but stronger expression is observed in the VNC at stage 16 (A'). (B, B') Compared to Wt, the weakly penetrant *Antp*^{25} mutant shows weak expression of the protein in the neuroectoderm at stage 12 (B) and in the late stage VNC (B'). (C, C') In the strongly penetrant *Antp*$^{25\ seg18}$, no detectable protein expression is noticed within the neuroectoderm at stage 12 (C) while it is observed in the same pattern like in single *Antp*^{25} mutant at late stage VNC (C'). (D, D') Similarly, the Antp expression is not observed in the neuroectoderm (D) of *Antp*^{25},*Ubx*^{1} (Bloomington) double mutant, but is noticeable in the VNC (D'). The extended expression domain of Antp until anterior A1 is observed in the VNC (D'). (E, E') At stage 12, Antp expression in *Antp*^{11} mutant looks like in Wt. (F, F') In the highly penetrant *Antp*^{14} mutant, Antp expression is not observed at stage 12.

3.11. The truncated Antp protein is not able to rescue the NB7-3 duplication phenotype

First, to clarify whether the observed *in vivo* Antp protein in the single *Antp*^{25} mutant is a truncated protein or not, a western blot analysis was performed. Due to the lack of epitope information for the available monoclonal Antp 8C11 and 4C3 antibodies, analysis was conducted in *Drosophila* S2R+ cells. The first 370 bp sequence, coding for the truncated *Antp* protein, was cloned into the pUAST *attB* vector by applying Gateway cloning method to generate a pUAST_*Antp1-123*.*attB* vector (Fig. 9A, B). Overexpression of the combination of plasmids carrying the truncated pUAST_*Antp1-123.attB*, and the control pUAST_Histone GFP driven by Act-GAL4 in *Drosophila* S2R+ cells was carried out by transient transfection. Subsequently, immunofluorescence analysis of the transfected S2R+ cells using the Antp 8C11 and 4C3 antibodies was performed. The cells overexpressing the truncated protein were detectable with both antibodies (Fig. 39A, A', C, C'). No specific detection was observed with either antibody in the control transfection experiments overexpressing only Histone GFP (Fig. 39B, B', D, D'). Hence, these findings confirm that the epitope regions of both antibodies were situated in the amino terminal 122 aa region of the Antp protein. Western blot analysis of the nuclear extracts prepared from Wt and homozygous *Antp*^{25} mutant embryos exhibit detectable protein size variation. The full-length Wt Antp protein was detected in the range of nearly 55 KD, whereas the truncated protein in *Antp*^{25} mutant embryos shows two bands close to 21 KD. Indeed, the complete S2R+ cell extract overexpressing pUAST_*Antp1-123.attB* using Act-GAL4 rather shows two bands close proximity to 21 KD (Fig. 39E). These results confirm that the detected Antp protein in *Antp*^{25} mutant embryos is a truncated 122 aa protein. Hence, further experiments with overexpression of the truncated Antp protein in mutants aimed to test whether truncated Antp protein is really influencing neuroectodermal divisions across the different *Antp*^{25} mutants. Fly stocks carrying the UAS *Antp1-123* were generated. Two different lines were combined with different *Antp* mutants and overexpressed using *en* GAL4. The artificially provided truncated Antp protein in the single *Antp*^{25} mutant did not change the duplication phenotype (n = 36) (Fig. 40). Overexpression of the truncated protein in the strongly penetrant *Antp*$^{25\ seg18}$ mutants, which do not show early expression, did not rescue the duplication phenotype (Fig. 40). Similarly, rescue experiments tested using UAS

Antp1-123 (3) line and UAS *Antp1-123* (4) line in *Antp*$^{25\ seg\ 11}$ also did not rescue the phenotype (Fig. 40). These results clearly suggest that the truncated Antp expression has no influence on the duplication frequency in different mutants.

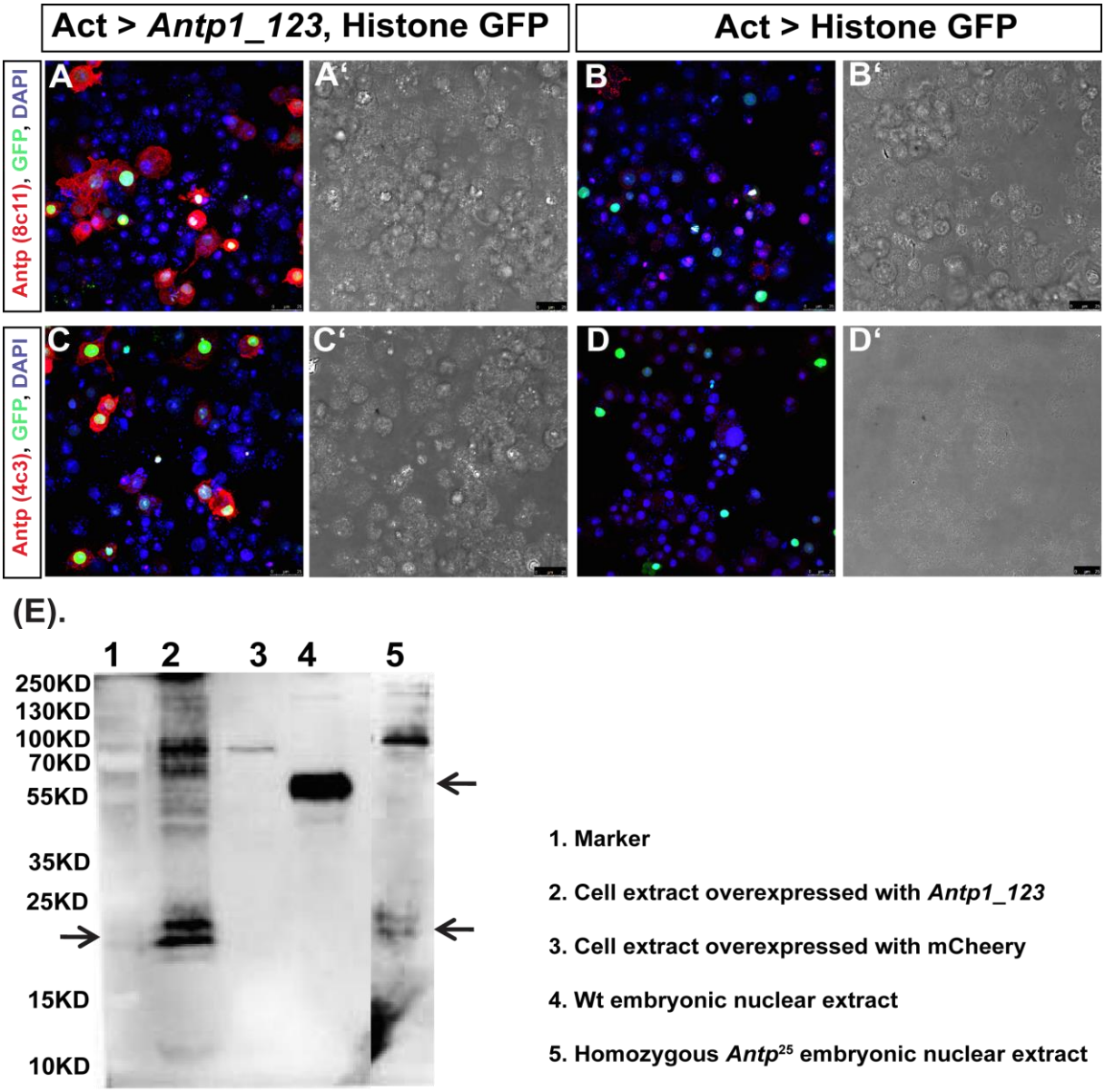

Fig. 39. Antp protein in *Antp*^{25} mutants is a truncated protein.
(A-D). Confocal sections of S2R+ cells stained either for Antp 8C11 (A, B) or Antp 4C3 (C, D), GFP and DAPI. The cells were co-transfected with UAS constructs that code for the truncated 123 aa Antp protein, Histone-GFP driven by Act-GAL4 (A, C) or in control experiments only with histone-GFP and Act-GAL4 (B, D). The single channel of cells in focus is shown for each image. Both antibodies specifically detect the truncated Antp protein, and no specific detection was observed in control experiments transfected with only Histone-GFP and driver GAL4 constructs. (E). Immunoblot analysis aimed at detecting Antp in the cell extract (lane 2), in which truncated protein encoding the *Antp* ORF is overexpressed, control cell extract (lane 3) with overexpressed mCherry, and *in vivo* protein extracts from Wt (lane 4) and homozygous *Antp*^{25} mutant embryos (lane 5). The truncated protein shows two bands around 22 KD in lanes 2 and 5. The Wt-Antp protein is detected at around 55 KD and no specific bands are noted in the control.

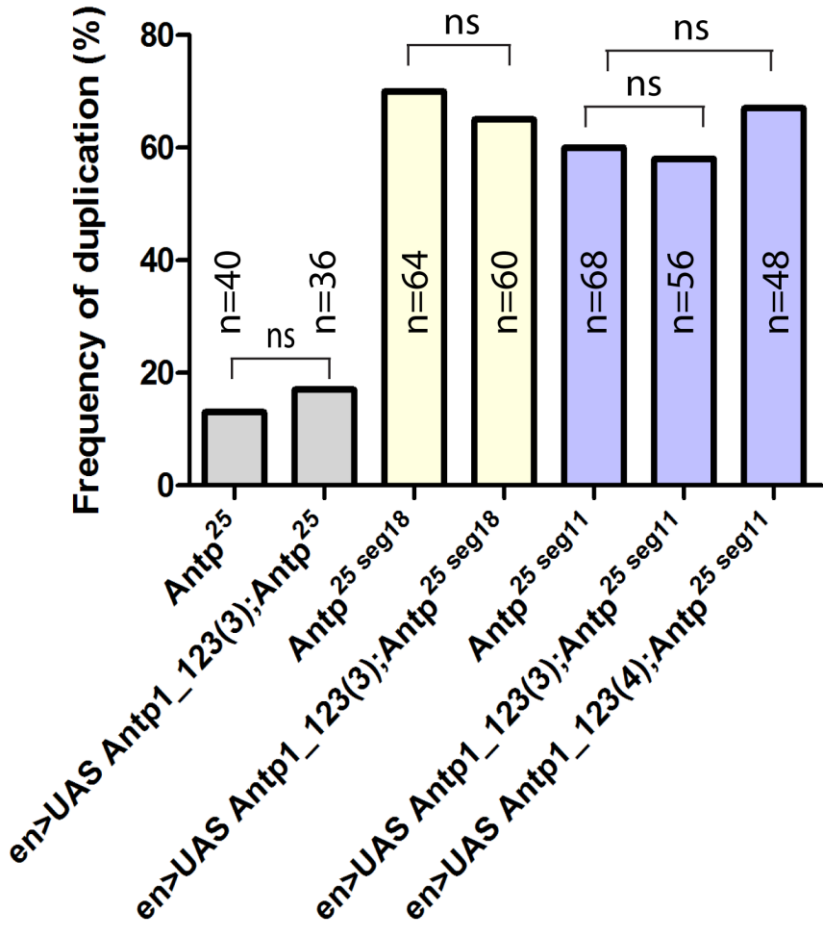

Fig. 40. Truncated Antp protein is not able to repress NB7-3 duplication.
Graphical representation of NB7-3 duplication frequency in mutant genetic backgrounds with the overexpression of the truncated *Antp*. The duplication occurrence is not significantly (ns) altered in all three genotypes tested. The significance (p) values are calculated using Chi-square analysis.

3.12. Functional HD of the Antp is not required for preventing the NB7-3 duplication.

To further explore how the different duplication frequencies arise in different *Antp* mutants, rescue experiments were performed in Wt, single *Antp*^{25}, *Antp*$^{25\ seg18}$ and *Antp*^{25},*Ubx*^{1} (Bloomington) double mutants. Unlike the *Hox* gene *Abd*-B, which suppressed the NB7-3 formation when overexpressed using *en* GAL4 (Birkholz et al., 2013b), early overexpression of *Antp* in the Wt could not show any missing NB7-3 lineages at stage 16 (n = 180). However, only three Eg-positive cells with two Hb co-expressing cells were noted in 7-3 lineages of the posterior thoracic and abdominal segments at early stage 16 (Fig. 41A, A'). The *dSer*T RNA expression analysis revealed that the missing neuron in *Antp* overexpression is the EW3 neuron (Fig. 41B, B'). Compared to the control rescue experiment using UAS mCD8::GFP

(20.8%, n = 24, p=0.131), overexpression of UAS *Antp* in weakly penetrant *Antp*^{25} mutant completely rescued the duplication phenotype (0%, n = 44, p <0.0001) (Fig. 42, Table-3.3). It also completely rescued the cell survival phenotype observed in anterior thoracic NB7-3 lineages (Fig. 43A, A'). In the control rescue experiment using UAS mCD8::GFP in the *Antp*$^{25\ seg18}$ mutant, 79.16% (n = 48, p=0.1443) duplication phenotype was noted (Fig. 42, Table-3.3). With overexpression of UAS *Antp* in strongly penetrant *Antp*$^{25\ seg18}$ mutant, the duplication phenotype was reduced to 3.57% (n = 56, p<0.0001) (Fig. 42, Table-3.3) while the cell survival phenotype was also completely removed (Fig. 43B, B'). Similarly, the duplication phenotype in *Antp*^{25},*Ubx*^{1} (Bloomington) double mutants was suppressed to 6% (n = 50, p<0.0001), and the cell survival phenotype completely (Fig. 42, Table-3.3). Together, rescue experiments confirmed the direct role of Antp in controlling 7-3 NBs number, as well as for regulating the proper apoptosis in the 7-3 lineages of anterior thoracic segments.

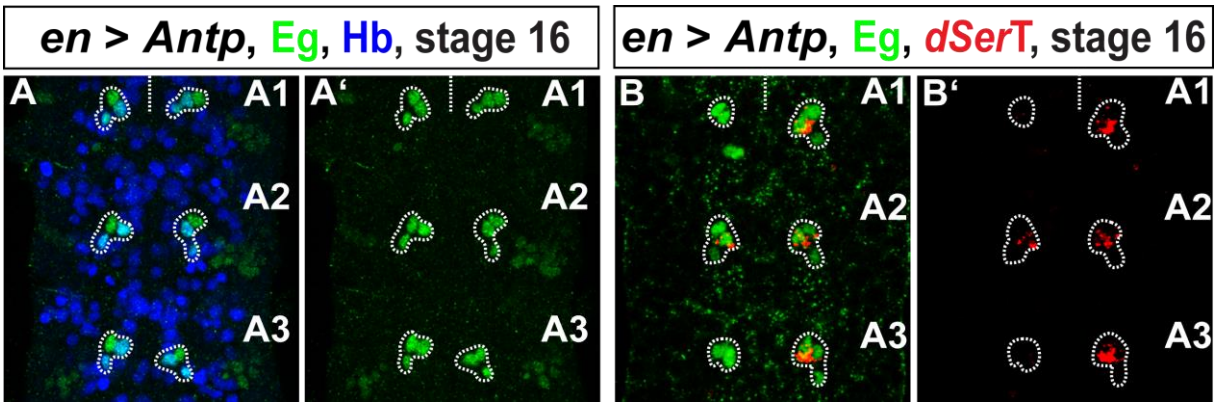

Fig. 41. Overexpression of *Antp* does not repress the NB7-3 formation.
Confocal sections focusing on NB7-3 lineages (outlined) stained either for Eg and Hb or Eg antibody and *dSer*T RNA probe at the embryonic stage 16. Anterior is up in all images. The midline is marked with a dotted straight line, and the segments in view are always indicated on the right hand side of the image. The single channel of Eg expression pattern and *dSer*T expression is shown next to each image. (A, A') Overexpression of Wt-*Antp* shows only three Eg-positive cells including Hb co-expressing cells GW and EW1 in abdominal segments at stage 16. (B, B') Among three Eg-positive cells, *dSer*T RNA expression analysis shows the presence of EW1 and EW2 neurons.

To understand if any non DNA-binding activity of Antp was also involved in thoracic NB7-3 lineage patterning, a mutated form of the Antp carrying an aminoacid substitution in the HD at important 50th position, (Antp K50Q), and thus lacks DNA-binding activity (Plaza et al., 2001, 2008) was overexpressed in *Antp* mutants. Surprisingly, the duplication phenotype was rescued significantly in all *Antp* mutants.

Moreover, this mutated HD construct cannot rescue the late cell survival phenotype observed in anterior thoracic segments of *Antp* mutants. Overexpression of UAS *AntpK50* in single *Antp*^{25} mutant shows significant rescue of the duplication phenotype (1.92%, n = 52, p<0.0001) (Fig. 42, Table-3.3). However, the cell survival phenotype was still observed in the anterior thoracic segments (Fig. 43C, C'). Similar results were noted with overexpression of UAS *AntpK50* in *Antp*$^{25\ seg18}$ mutants, which rescued the duplication phenotype to 21.42% (n = 56, p<0.0001) (Fig. 42, Table-3.3) without rescue of the cell survival phenotype (Fig. 43D, D'). Rescue experiments with mutated HD construct in *Antp*^{25}, *Ubx*^{1} (Bloomington) double mutant also reduced the duplication phenotype to 26.66% (n = 60, p<0.0001) (Fig. 42, Table-3.3). A series of similar experiment using another mutated *Antp* construct with aminoacid replacement at two positions in the HD 50 and 51 (*Antp A50, A51*) thus lost DNA-binding activity (Plaza et al., 2001, 2008), in *Antp*$^{25\ seg11}$ mutant, also yielded significantly reduced duplication phenotype to 34.37% (n = 64, p<0.0001) (Fig. 42, Table-3.3). In spite of the complete absence of DNA-binding activity in these two mutated HD versions of Antp (Plaza et al., 2008), their ability to efficiently rescue the duplication phenotype clearly demonstrates that this function is independent of a functional HD. The DNA-binding independent Hox function strongly suggests possible direct protein-protein interactions. *Antp* has been shown to inhibit the activity of the eye selector gene *eyeless* (*ey*) at posttranslational level through protein-protein interaction (Plaza et al., 2001). Through an interaction assay performed by Plaza et al., 2008 confirmed that Antp interact with Eyeless (Ey) paired domain and represses its function. DNA-binding activity of Antp is not necessarily needed to execute this function. Coincidently, Ey is also expressed in the NB7-3 lineage (Deshpande et al., 2001). Hence, for evaluating the Ey and Antp protein interaction in the context of NB7-3 duplication, this lineage was examined in *ey* loss of function and gain of function situations. In *ey*$^{J5.71}$ (Kammermeiner et al., 2001; Punzo et al., 2001) mutants, the anterior thoracic NB7-3 lineage comprises 7 to 10 Eg-positive cells, including typical two Hb co-expressing cells (Fig. 44A).

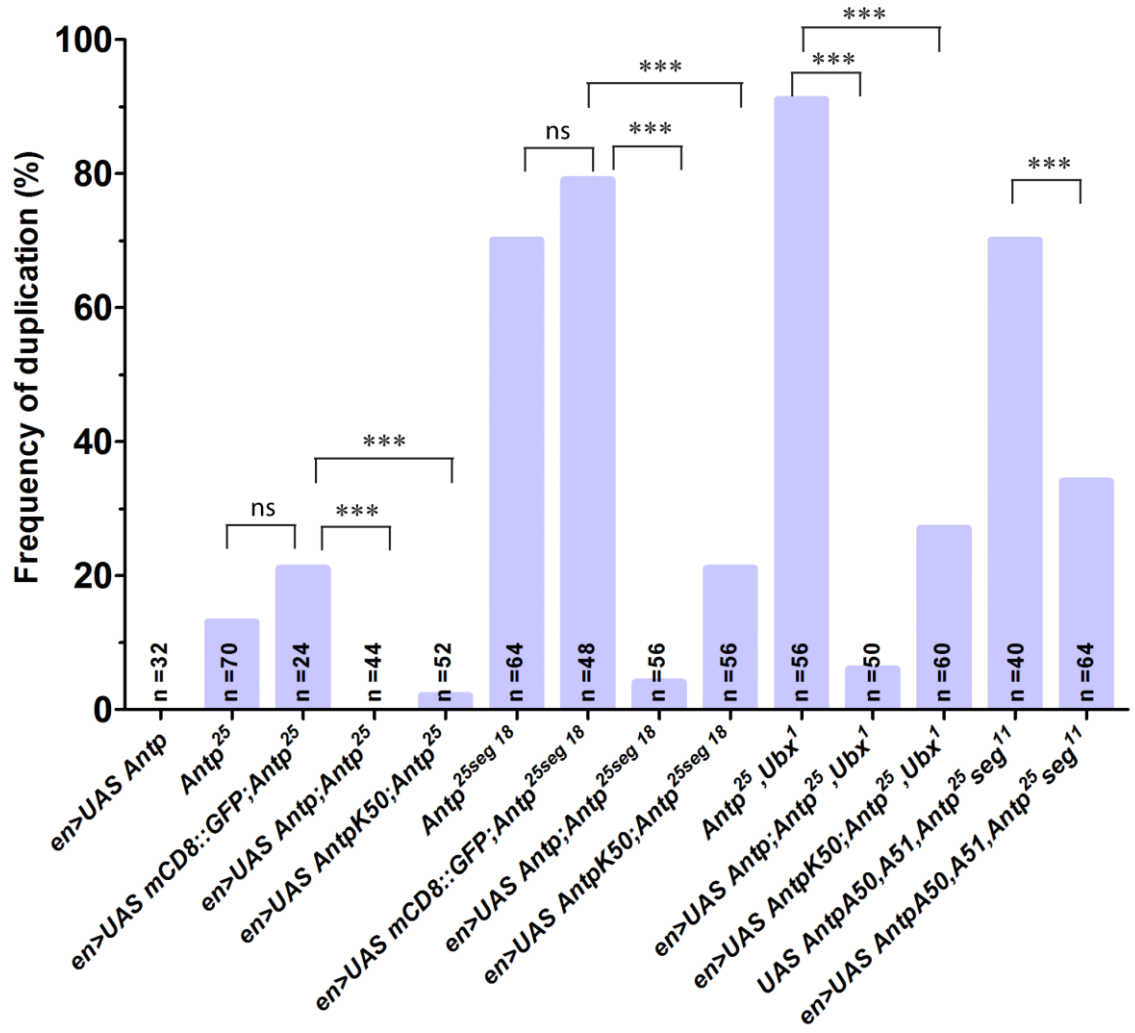

Fig. 42. Functional HD of Antp is not required for repressing the NB7-3 duplication.
Graphical representation of duplication frequency in rescue experiments performed using Wt-*Antp* and mutated HD constructs (UAS *AntpK50* and UAS *AntpA50,A51*) in various *Antp* mutants. Overexpression of Wt-*Antp* in both weakly and strongly penetrant mutants rescued the phenotype almost completely compared to control experiments driving mCD8::GFP. Overexpression of mutated HD constructs *K50*and *A50,A51* also significantly reduced the phenotypes in both weak and strong mutants. Chi-squared P values are shown in Table-3.3.

Genotype	Frequency (%)	X^2 P
Antp^{25}	12.85%	
en > UAS mCD8::GFP;*Antp*^{25}	20.8%	0.1321 (ns)
en > UAS *Antp;Antp*^{25}	0%	<0.0001
en > UAS *AntpK50;Antp*^{25}	1.92%	<0.0001
Antp$^{25\ seg18}$	70%	20
en > UAS mCD8::GFP;*Antp*$^{25\ seg18}$	79.16%	0.1443 (ns)
en > UAS *Antp;Antp*$^{25\ seg18}$	3.57%	<0.0001
en > UAS *AntpK50;Antp*$^{25\ seg18}$	21.42%	<0.0001

Antp^{25},*Ubx*^{1} (Bloomington)	91.07%	
en > UAS *Antp;Antp*^{25},*Ubx*^{1}(Bloomington)	6%	<0.0001
en > UAS *AntpK50;Antp*^{25},*Ubx*^{1}(Bloomington)	26.66%	<0.0001
UAS *AntpA50,A51;Antp*$^{25\ seg11}$	70%	
UAS *AntpA50,A51*;*Antp*$^{25\ seg11}$	34.37%	<0.0001

Table-3.3. The frequencies of duplication in rescue experiments and the Chi-squared P values are shown.

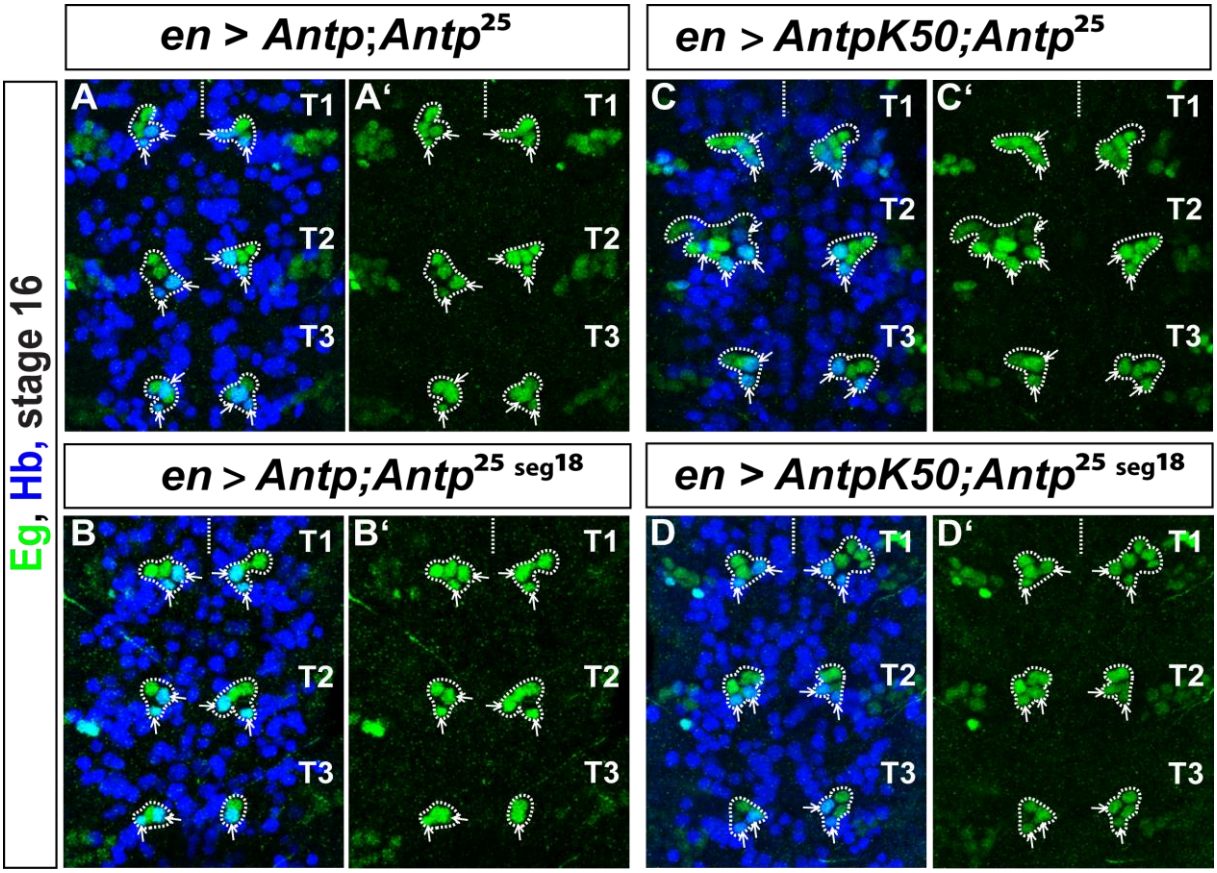

Fig. 43. DNA-binding activity of Antp is necessary to suppress cell survival in NB7-3 lineage. (A-D) Confocal sections focusing on NB7-3 lineages (outlined) stained for Eg and Hb at the embryonic stage 16. Anterior is up in all images. The midline is marked with a dotted straight line, and the segments in view are always indicated on the right hand side of the image. The single channel of Eg expression is shown next to each image. Arrows indicate the Hb-positive cells of NB7-3 lineage. (A, A') Overexpression of Wt-*Antp* rescues the duplication and prolonged cell survival phenotype observed in single *Antp*^{25} mutants. Only four Eg-positive cells are observed in anterior thoracic NB7-3 lineages at stage 16. (B, B') In strongly penetrant *Antp*$^{25\ seg18}$ mutants, both the duplication phenotype and the cell phenotype are completely repressed by overexpression of Wt-*Antp*. (C, C') Contrarily, only duplication phenotype was rescued, but not the cell survival phenotype, with overexpression of *AntpK50* in single *Antp*^{25} mutants. (D, D') The mutated HD constructs significantly suppressed the duplication occurrence in *Antp*$^{25\ seg18}$ mutants but not the cell survival phenotype. The anterior thoracic hemisegments with 6 to 7 Eg-positive cells can be observed.

This suggests that NB7-3 is surviving longer and generating additional cells as in *H99* mutants. Conversely, overexpression of *ey* using *en* GAL4 reduces the 7-3 lineages to three cells. Moreover, occasionally the complete NB7-3 lineage was absent with overexpression of *ey* only in late embryonic stages, which suggest that Ey plays a role in embryonic NB7-3 apoptosis (Fig. 44B, B'). These observations exclude the possible Antp and Ey interaction for controlling early NB7-3 segregation. For identifying the Antp protein interaction partner involved in controlling early NB7-3 duplication, a protein-protein interaction screen would be required, which is a subject of interest for future work. Considering the fact that the rescue efficiency of duplication phenotype by mutated HD constructs was lower than that noted with the Wt-*Antp* construct, an attempt was made to elucidate their functional differences through analyzing the proneural cluster in rescue experiments.

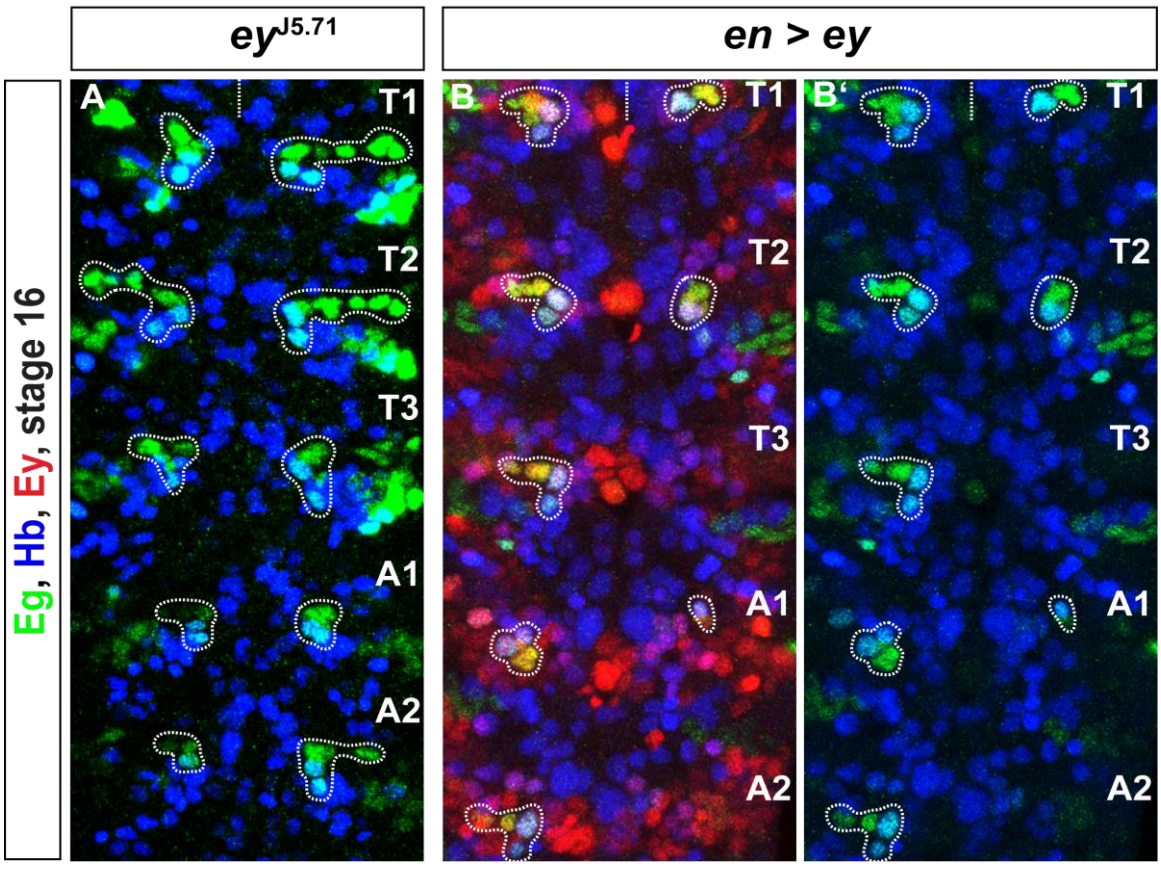

Fig. 44. Ey does not regulate NB7-3 formation.
Confocal sections focusing on NB7-3 lineages (outlined) stained for Eg, Hb and Ey at the embryonic stage 16 in *ey*$^{j5.71}$ (A) mutants and overexpression of *ey* using *en* GAL4 (B, B'). Anterior is up in all images. The midline is marked with a dotted straight line and the segments in view are always indicated on the right hand side of the image. (A) In *ey* mutants, the thoracic NB7-3 lineage shows 8 to 10 Eg-positive cells with typical 2 Hb co-expressing cells. (B, B') Overexpression of *ey* using *en* GAL4 causes fewer cells in NB7-3 lineage and an occasional absence of the complete lineage. The NB7-3 lineages in T3 and A2 right hemisegments are missing.

3.13. DNA-binding activity of Antp is needed for repressing the proneural gene expression but not for neuroectodermal divisions

Previous results in sections 3.5 and 3.7 suggest that the duplication phenotype in *Antp* mutants arises through a combination of proneural cluster maintenance mechanisms and neuroectodermal additional division in the 7-3 NEP derivatives. In order to evaluate in which of these two functions Wt-*Antp* and mutated HD (*AntpK50*) constructs functionally vary proneural gene expression was analyzed. In rescue experiments, overexpression of Wt-*Antp* in *Antp*$^{25\ seg18}$ mutants shows repression of proneural clusters at early stage 12 in 92.31% of hemisegments (n = 52) (Fig. 45A, A', A''). The proneural gene expression in the En-positive neuroectoderm at early stage 12 resembles the Wt pattern. The Hkb expression in the En-positive dorsal sectional view in the VNC confirms the delaminated primary NB7-3 (Fig. 45A1). In contrast, in rescue experiments using *AntpK50* in *Antp*$^{25\ seg18}$ mutants, the proneural gene expression was still maintained in 90.90% of hemisegments (n = 44) at early stage 12 in anterior thoracic hemisegments (Fig. 45B, B', B''). The delaminated primary NB7-3 at this stage was identified with Hkb expression within the En-positive VNC (Fig. 45B1). This observation correlates with the proneural gene expression observed in *CycE*^{AR95};*Antp*$^{25\ seg18}$ double mutants, in which the duplication frequency was rescued due to slower cell divisions (Fig. 33C). Similar results were observed in comparative rescue experiments with Wt-*Antp* (Fig. 45C, C', C'', C1) and *AntpK50* in single *Antp*^{25} mutants (Fig. 45D, D', D", D1). The discrepancies in proneural gene repression after the NB delamination by Wt and mutated Antp protein explain the efficiency of duplication variations. However, both the constructs could not affect the proneural gene expression at stage 11, and primary NB formation. These observations clearly indicate that the DNA-binding activity of Antp is necessary to accomplish proneural gene repression in the NB7-3 proneural cluster after the primary NB segregation. Rescue experiments using mutated HD *Antp* clearly suggest that it could rescue additional cell division in 7-3 NEP derivatives but not the proneural gene repression. The cell survival phenotype suppression needs a functional homeodomain. Altogether, these results reveal that regulation of NBs arising from the NB7-3 proneural cluster involves both Antp DNA-binding dependent and independent functions.

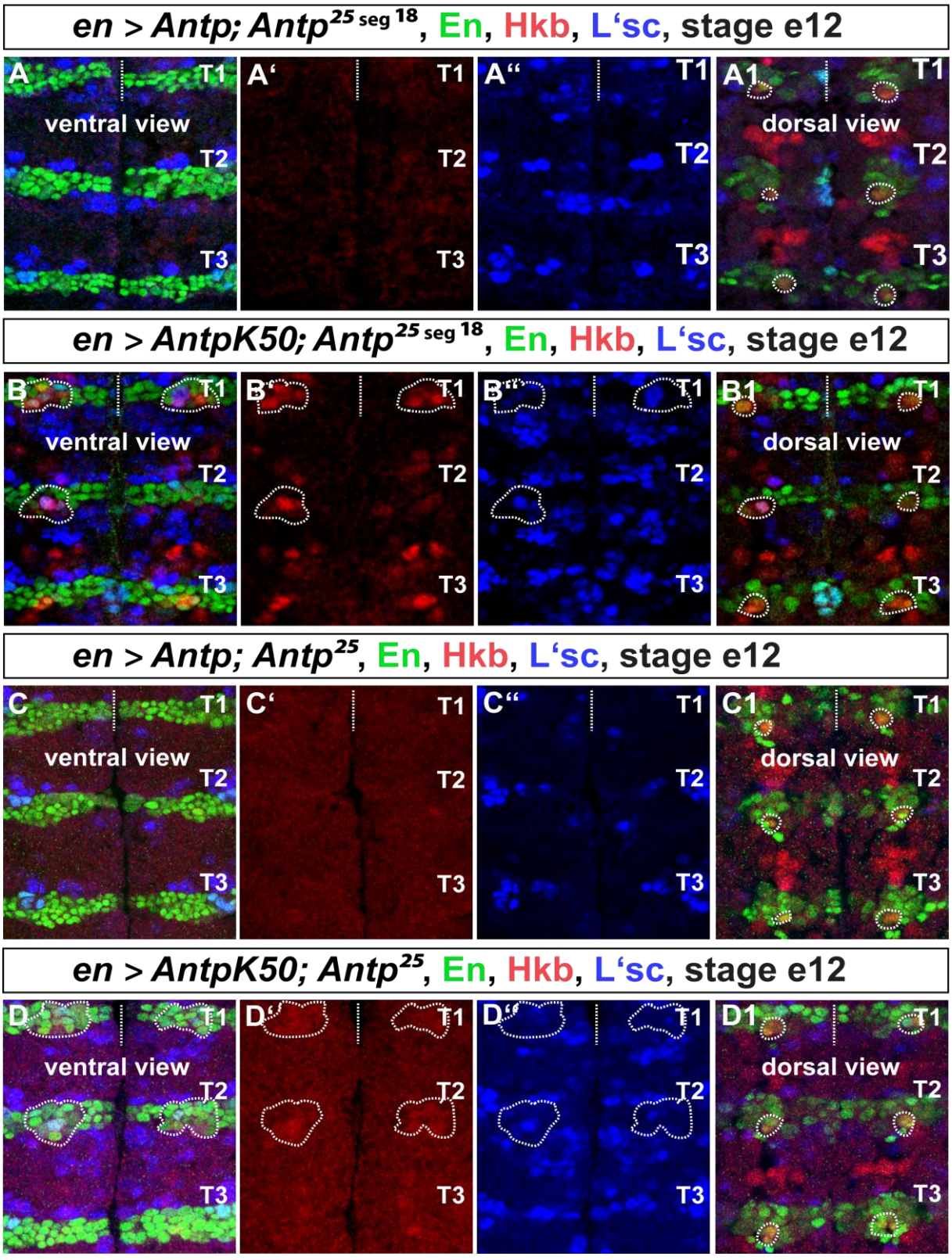

Fig. 45. DNA-binding activity of Antp is necessary for proneural cluster repression but not for neuroectodermal divisions.
Confocal sections focused on the ventral neuroectoderm and dorsal VNC of the same embryos stained for En, Hkb and L'sc in rescue experiments using Wt-*Antp* and mutated *AntpK50* in *Antp*$^{25\ seg18}$ (A, B) and *Antp*^{25} mutants (C, D) at the embryonic early stage 12. Anterior is up in all images. The midline is marked with a dotted straight line, and the segments in view are always indicated at the right hand side of the image. The single channel of Hkb and L'sc staining for ventral sectional views are

shown. The proneural cluster of NB7-3 or its lineage is marked with a dotted outline. (A, A', A") Overexpression of Wt-*Antp* completely repressed the proneural gene expression observed at early stage 12 in *Antp*$^{25\ seg18}$ mutants. (A1) The Hkb expression in the En-positive VNC of the same embryo confirms the presence of delaminated primary NB7-3. (B, B', B") The mutated HD construct overexpression did not rescue the proneural cluster maintenance observed in *Antp*$^{25\ seg18}$ mutants at early stage 12. (B1) Observation of Hkb-positive cells in En domain within the VNC of the same embryo confirms the presence of delaminated primary NB7-3. (C, C', C", C1) Overexpression of Wt-*Antp* completely rescued the proneural gene expression observed in *Antp*^{25} mutants at early stage 12. (D, D', D", D1) However, the mutated *AntpK50* could not rescue proneural gene maintenance observed in single *Antp*^{25} mutants at early stage 12.

To confirm further the role of HD in proneural cluster maintenance, *Dfd* and *Scr* mutants lacking the HD were analyzed. The results are described in the next section.

3.14. The NB7-3 Proneural cluster is also maintained segment-specifically in HD-deficient *Dfd* and *Scr* mutants

Since mutants for two other ANT-C genes, *Dfd* and *Scr*, also exhibit the segment-specific NB7-3 duplication phenotype, I examined whether they also maintained the proneural cluster longer than normal. The mutations in the analyzed *Dfd*^{16}, *Scr*^{17} and *Scr*^{4} mutants lead to production of truncated Dfd and Scr proteins that lack the homeodomain. The *Dfd*^{16} mutant carries a point mutation, which leads to truncation of the protein at 346 aa in Dfd protein, which is normally 586 aa long (Zeng et al., 1994). Point mutations in *Scr* gene of *Scr*^{17} and *Scr*^{4} mutants lead to truncation of the Scr protein at 242 aa and 131 aa respectively (Sivanantharajah and Percival-Smith, 2009). The Wt Scr protein is 417 aa long. Since Hkb is broadly expressed in salivary gland body primordia located in the gnathal maxillary region (Bronner et al., 1994), only L'sc expression could be analyzed with respect to the NB7-3 proneural cluster in Md and Mx segments. In Wt embryos after NB7-3 delamination, L'sc expression was downregulated immediately (Fig. 46A, A'). The Md segment of *Dfd*^{16} mutants shows maintained L'sc expression in the NB7-3 proneural cluster even after the NB delamination (n = 14) (Fig. 46B, B'). Observation of Mx segment in *Scr*^{4} mutants at early stage 12 also clearly shows maintained NB7-3 proneural gene expression in the NB7-3 proneural cluster (n = 20). In addition, one of the Md hemisegments in these mutants very often shows the maintained cluster. These results clarify that *Dfd* and *Scr* mutants, with homeodomain-less protein, also exhibit prolonged NB7-3 proneural cluster maintenance. Altogether, these results strongly support the notion that the HD of the Dfd, Scr and Antp proteins plays a key role in regulating the

prolonged NB7-3 neurogenic potential. Through these observations, novel functions of anterior *Hox* genes in neuroectodermal specification mechanisms are uncovered. These results give clear insights into a combination of homeodomain-dependent and homeodomain-independent functions of anterior Hox proteins, and show that they are involved in regulating the neural stem cells arising from the NB7-3 proneural cluster. An activation or repression mechanism of down stream targets by homeodomain of Hox proteins is involved in prolonged proneural cluster maintenance. An additional neuroectodermal cell division plays a role in regulating the number of NBs produced and a functional HD is not required to regulate this function.

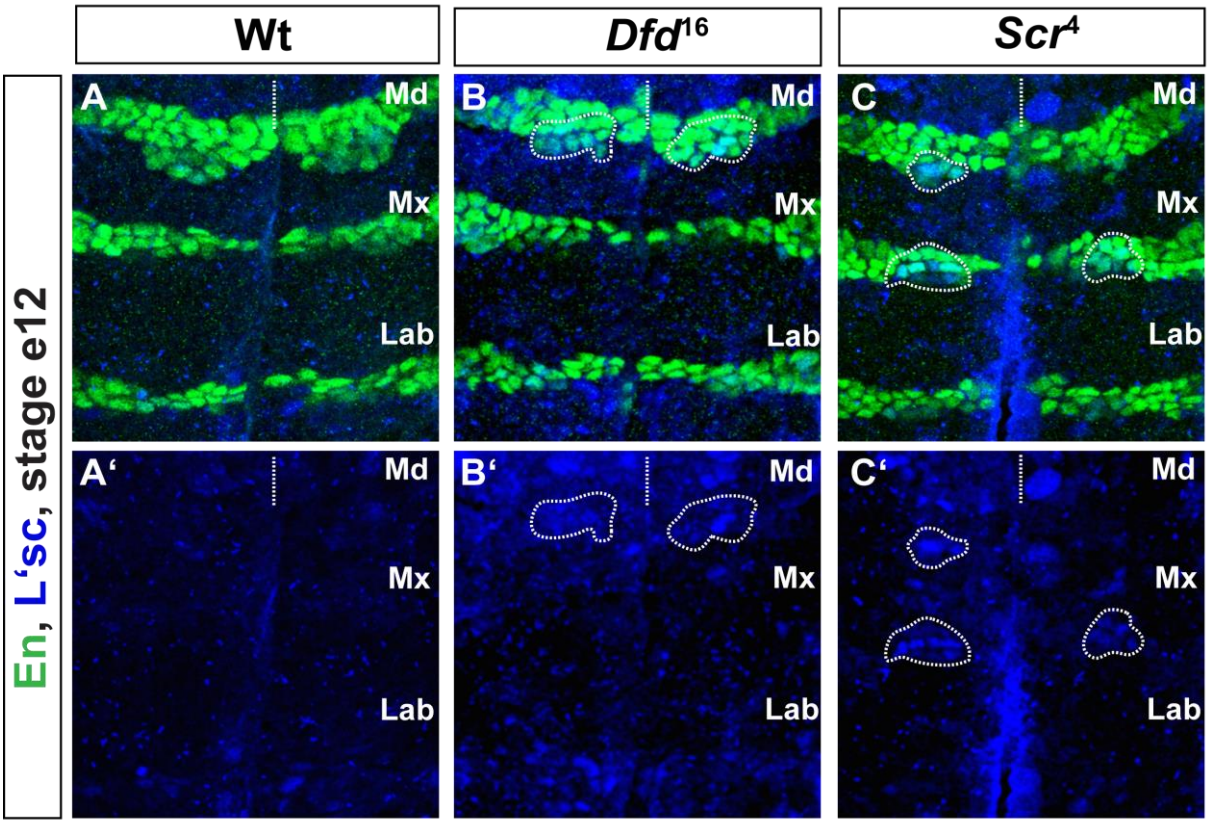

Fig. 46. Proneural cluster is also maintained segment-specifically in *Dfd* and *Scr* mutants.
Confocal sections focused on the ventral neuroectoderm of Wt embryos stained for En and L'sc (A) and in *Dfd*^{16} (B) and *Scr*^{4} mutants (C) at embryonic early stage 12. Anterior is up in all images. The midline is marked with a dotted straight line, and the segments in view are always indicated on the right hand side of the image. The single channel of L'sc staining is shown for each image. The proneural cluster of NB7-3 is marked with a dotted outline. (A, A') In Wt, L'sc expression in Md and Mx segments is downregulated by early stage 12. (B, B') The proneural cluster is still observed in the Md segment of *Dfd*^{16} mutants at early stage 12. (C, C') Segment-specifically maintained proneural gene expression is observed in Mx segment of *Scr*^{4} mutants at early stage 12. Very often one cluster in the Md segment also shows maintanance of L'sc in these mutants.

4. Discussion

Multicellular organism growth and development must be coordinated with cell proliferation, specification, differentiation and maintenance of different cell types. This is achieved through proper inductive and inhibitory cell-cell communication mechanisms, which then translate into spatial and temporal developmental responsive cues. Signalling mechanisms regulating these decisions generate different cellular responses in different cell and developmental contexts. Many reports on *Drosophila* nervous system development provided an immense knowledge about these mechanisms in several cell-contexts. In my thesis, I provide new insights into how early embryonic developmental cues incurred by *Hox* genes within the neuroectoderm ultimately control the number of specific neural stem cells formed. Identical neural fate acquisition by two cells instead of one is accomplished through concomitant additional cell division in the predetermined neuroectodermal precursor and sequential delamination of these cells through providing prolonged neural competence to neuroectodermal cells. In the late embryonic developmental stages they also pattern the neural lineages along the anterior posterior (AP) axis in the ventral nerve cord (VNC). The observations in my thesis contributed to the current understanding of segment-specific patterning of the neural lineages in the VNC through *Hox* gene-dependent apoptosis.

4.1. Each ANT-C gene distinctly patterns neural lineages in the VNC

Extensive molecular and genetic studies have identified gene cascades that are involved in embryonic central nervous development (CNS) development. First, the consecutive action of maternal, gap and pair-rule genes defines the segmental and parasegmental boundaries by initiating segment-polarity gene transcription (Nusslein-Volhard et al., 1987). Second, the complete cascade including the segment-polarity genes, in turn, activates the collinear pattern of *Hox* gene expression in specific parasegmental domains, which provides the morphological diversity along the AP axis (Akam, 1987; Scott and Carroll, 1987; Ingham, 1988). The tagma-specific diversity imposed by *Hox* genes in the VNC has been extensively studied at multiple embryonic neurogenesis steps, including neuroblast (NB) formation, specification, proliferation and apoptosis. NB delamination occurs in five

sequential temporal waves and generates serial homologs of 30 NBs in three thoracic and eight abdominal segments (Doe, 1992; Broadus et al., 1995). Patterning mediated by the posterior *Hox* gene Abdominal-B hones the terminal abdominal A9 and A10 segments by regulating formation of fewer NBs (Birkholz et al., 2013a, b). Similar deviations to the serial homologous pattern were noted in gnathal maxillary (Mx), mandibular (Md) and labial (Lab) segments controlled by *Deformed* (*Dfd*) and *Sex combs reduced* (*Scr*) genes (Urbach et al., 2016). These reports infer how *Hox* genes shape the head and tail regions of the VNC by regulating NBs formation. Most of the NBs generate invariant lineages in serially homologous thoracic and abdominal segments. However, a few NBs generate either smaller lineages in abdominal segments compared to thoracic ones, or the cell type composition of the lineages diverges between the tagma (Bossing et al., 1996; Schmidt et al., 1997). Single cell culture and transplantation experiments clarified that specific capacities for proliferation are conferred to embryonic NBs already in the neuroectoderm (Lüer and Technau, 1992). NBs express these capacities in a cell-autonomous manner, and segmental differences in proliferation patterns are under the control of *Hox* genes (Prokop and Technau, 1994; Prokop et al., 1998). The composition of the thoracic lineages generated by NB1-1 and NB6-4 represents the ground state, which does not require input from any homeotic genes (Prokop and Technau, 1994; Prokop et al., 1998; Berger et al., 2005). On the other hand, *Ultrabithorax* (*Ubx*) and *abdominal-A* (*abd-A*) impose an abdominal fate upon these NBs in the pertinent domains. In respective abdominal fate specifying *Hox* gene mutants, these NBs gain the thoracic identity. A pulse of the abd-A in mid embryonic development schedules the end of neural proliferation in abdominal segments by inducing NB apoptosis (Bello et al., 2003). The thoracic and abdominal NB5-6 lineage divergence is mediated through regulating cell cycle exit and apoptosis of the NB in the abdomen by bithorax complex (BX-C) along with co-factors (Karlson et al., 2010). Most NBs in the thorax exit the cell cycle in mid embryonic stages and enter quiescence until the larval stage, which is influenced by *Antp* (Tsuji et al., 2008; Birkholz et al., 2015). Detailed studies focusing on NB7-3 revealed that cell death played an important role in controlling the size of this lineage along the AP axis. First, a Notch-mediated apoptotic mechanism removes two progeny cells EW2 and EW3 sib neurons from a six cell NB7-3 lineage in the early developmental stages (Lundell et al., 2003). However, thus far, the manner in which Notch induces apoptosis of these neurons

has not been extensively investigated. Later in development, an *Ubx*-mediated apoptotic mechanism segment-specifically removes the GW neuron of NB7-3 lineage from T3 to A8 segments as well as in the gnathal Lab segment. In the anterior thoracic segments (T1-T2), the GW neuron was rescued only if sufficient Antp expression levels are present (Rogulja-Ortmann et al., 2008, Rogulja-Ortmann and Technau, 2008). Analysis of the NB7-3 lineage in Antennapedia complex (ANT-C) mutants performed in this study shows additional *Hox*-directed refinement of this lineage along the AP axis. The NB7-3 lineages of the Md segment in Wt also removed the EW3 neuron, thus are reduced to two cells by late embryonic stages. Unlike *Ubx* mutants, the NB7-3 lineages in the respective segments of *Antp*, *Scr* and *Dfd* mutants were not transformed to their posterior or anterior segmental identities. In these mutants, the NB7-3 lineages retained the basic ground state. Thus, it is possible to study direct *Hox* gene functions in generating morphological diversity of the lineages in the VNC. The 7-3 lineage in *Hox*-free ground states exhibits duplication of the complete lineage and lack of apoptosis. Prolonged survival of Notch-mediated apoptotic EW2sib and EW3sib neurons in ANT-C mutants suggest the role of *Hox* genes in this apoptotic mechanism. Rescue experiments further confirmed that apoptosis of these neurons is contingent on the Hox proteins DNA-binding activity. This observation suggests that ANT-C genes may be regulating the transcriptional activation of apoptotic genes in EW2sib and EW3sib neurons. Further genetic and molecular studies are needed in order to establish the point in this cascade at which ANT-C genes are involved. Nevertheless, the results reported in this work suggest that GW neuron apoptosis in the gnathal segments is also *Hox* dependent. Specifically, EW3 neuron removal by a *Dfd*-dependent mechanism appears to be part of the more refinement in this segment. More extensive analysis of the other lineages in gnathal and tail regions is required to examine whether similar mechanisms are employed in additional lineages. It is likely that BX-C gene mutants also exhibit similar phenotypes. However, an overlapping expression of other *Hox* genes and the posterior prevalence mechanism from T3 to A8 segments may conceal their effects.

4.2. *Hox* genes control neural stem cell number by regulating cell divisions within the neuroectoderm

The first population of S1 and S2 neuroblasts delaminates from the G2 arrested ventral neuroectoderm shortly after gastrulation (Weigmann and Lehner, 1995; Cui and Doe, 1995). BrdU labelling experiments confirmed the association of NB delamination and mitosis. More specifically, after the first two waves of delamination, patches of mitotic activity were observed in the neuroectodermal cells (Hartenstein et al., 1994). Single cell DiI lineage tracing experiments also revealed the same phenomenon (Bossing et al., 1996; Schmidt et al., 1997). Unlike S1 and S2 NBs, the late delaminating S4, S5 and some S3 NBs exhibit an epidermal sister clone, due to one postblastodermal division of the respective neuroectodermal progenitor (NEP) within the neuroectoderm. One of the cells subsequently delaminates as the NB, whereas the other remains in the ectoderm and develops as an epidermoblast (Bossing et al., 1996). However, NB fate has been proved independent of this division (Berger et al., 2001). NEP labellings of NB4-3 and NB4-4 produce, in addition to the neuronal lineage, an epidermal sister clone and a sensory neuronal lineage (Schmidt et al., 1997). Since it is specified in the S5 phase, NB7-3 mostly shows an epidermal subclone (Bossing et al., 1996). My analysis of the NB7-3 lineage in a *Hox*-free ground state through intense lineage specific molecular marker analysis revealed frequent duplication of the complete lineage. Analysis of early developmental stages infers that two sequentially specified 7-3 NBs produce the duplicated lineage. Single cell lineage tracing experiments carried out through DiI labelling method in the Wt anterior thoracic segments point to segment-specific proliferation differences within the neuroectoderm. Only 50% of the 7-3 NEP clones from Lab to T2 segments possess a 2-cell sister epidermal clone, whereas in the T3 it always produces a 4-cell sister clone. In contrast, the labelled single 7-3 NEP cells in *Antp* mutants mostly possess a 3- to 4-cell epidermal sub clone in anterior thoracic segments and a duplicated neuronal lineage. These results clearly indicate that the duplication is not resulting from a possible cell fate change of the sister epidermal cell to a NB or from a lateral inhibition defect. Rather, it arises through one additional early division in the neuroectoderm, either of the potential neural precursor or of the epidermal precursor of 7-3. This process resembles the assumed division pattern described for NB4-3 and NB4-4 NEP, in which the first neuroectodermal division

generates the NBs. Following the NB delamination, the sister ectodermal cell divides again, giving rise to the epidermal and sensory sub clones (Schmidt et al., 1997). Despite employing the DiI labelling method in the *Antp* mutants, the division mode of the 7-3 NEP within the ectoderm could not be clarified. Thus, a genetic approach was taken with the aim of altering the cell cycle rate via overexpression and loss of function of *Cyclin E* (*CycE*) in *Antp* mutants. The results yielded through these experiments confirmed that proliferation plays a key role in determining the duplication frequency across different *Antp* mutants. Reducing the cell division speed by recombining *CycE* mutation to strongly penetrant *Antp* mutants significantly reduced the duplication frequency. Interestingly, in a low-penetrant *Antp* mutant, overexpression of the G1/S promoting *CycE* gene significantly increased the duplication occurrence. However, the same was not true for the G2/M promoting genes *string* (*stg*) or *Cyclin B* (*CycB*). This observation suggests that either *CycE* transcription or function acts as a rate-limiting factor to induce precocious mitosis in the 7-3 NEP derivatives across different *Antp* mutants. These findings are not in agreement with the results reported by Edgar and O'Farrell (1989, 1990), who noted that the regulations of cycles 14 to 16 in the ectoderm is mediated by the transcriptional regulation of *stg*. However, the duplication of NB7-3 is not dependent on *stg* regulation, indicating that during the complex events of cycles 14-16, regulations is mediated differently and is dependent on the distinct developmental contexts in the epidermal cells. In sum, ectopic expression of any cell cycle regulator, including *CycE*, in the Wt was unable to cause duplication of NB7-3 lineage. This suggests that, apart from an additional division in the neuroectoderm, additional extrinsic or intrinsic factors must be involved in providing neural potential to the progeny of this division, leading to NB duplication.

4.3. HD-dependent 7-3 proneural cluster maintenance allows sequential segregation of two NBs

Controlled and tight regulatory mechanisms allow specification of only one third of cells in the bipotent neuroectodermal cells into neural stem cells, whereas the remaining ones develop into ectodermal cells. Neural potential with respect to the patches of cells within the neuroectoderm is exhibited through proneural gene expression (Cabrera et al., 1987). Proneural clusters of S1 and S2 NBs were traceable due to a well-separated grid-like patchy expression of proneural genes

within the neuroectoderm (Skeath and Thor, 2003). For S3 to S5 NBs, the same was not possible because of their interdigitated position relative to the first-formed clusters. Fortunately, owing to the exclusive *huckebein* (*hkb*) expression being restricted only to the NB7-3 proneural cluster within the En domain, it could unambiguously be identified using double staining (Mc Donald and Doe, 1997). I could thus confirm that the NB7-3 proneural cluster expresses the proneural gene *lethal of scute* (*l'sc*). Assessment of the comparative dynamics of Hkb and Lsc protein expression in the NB7-3 proneural cluster in the Wt and *Antp* mutants revealed that the cluster is maintained even after NB delamination in a segment-specific manner in *Antp* mutants. This phenomenon is equal across all the *Antp* mutants, irrespective of the duplication frequency that they exhibit. In the double mutants of *CycE* and strongly penetrant *Antp*, in which the duplication frequency significantly reduced due to slower divisions, the proneural cluster is still strongly maintained. These observations elucidate that neuroectodermal division and prolonged proneural gene expression involved in duplication of NB7-3 are not interrelated mechanisms. The NB7-3 proneural cluster is also maintained in HD-deficient *Dfd* and *Scr* mutants. Proneural gene expression provides the neural potential to the group of neuroectodermal cells (Jimenez and Campos-Ortega, 1979, 1987, 1990; White, 1980; White et al., 1983; Brand and Campos-Ortega, 1988; Caudy et al., 1988a). The Notch lateral signalling pathway ultimately activates expression of *E(spl)-C* genes, which antagonize the function of the proneural proteins in these cells (Jennings et al., 1994). These assertions suggest that a predetermined cell at a specific position would be able to overcome this repression perhaps due to a higher level of proneural proteins produced by an extrinsic signal (P. Simpson, 1990). Mutation in any Notch signaling pathway genes leads to absence of lateral inhibition, as a consequence, all cells in the proneural cluster attain the neural identity (Lehmann et al., 1983; Brand and Campos-Ortega, 1988; Skeath and Carroll, 1992). Conversely, loss of *AS-C* proneural genes leads to only 20% loss of VNC NBs, suggesting involvement of further unidentified redundant genes in this process (Seugnnet et al., 1997). Analysis of E(spl) protein expression in *Antp* mutants confirms that a sequential Notch activity segregates two NBs. Notch-mediated second NB segregation from the proneural cluster always occurs after the first NB has undergone at least one or two divisions within the VNC. Identical neural fate acquisition by two cells instead of one is accomplished through concomitant

additional cell division in the predetermined neuroectodermal precursor and sequential delamination of these cells through providing prolonged neural competence to neuroectodermal cells (Fig. 47). The segregated neural precursor cells normally maintain contact with the apical proneural cells before dividing, thus maintaining lateral inhibition (Doe, 1992). The first division results in a complete loss of contact. In anterior *Hox* gene mutants, the second NB appears to overcome lateral inhibition by the primary NB, perhaps due to its predetermined neural state. Maintenance of proneural gene expression, even after delamination of the first NB allows subsequent segregation of the second NB.

4.4. Functional DNA-binding activity of Antp is necessary for repressing the proneural gene expression but not for regulating divisions in the neuroectoderm

Hox genes code for proteins that contain a conserved DNA-binding domain of 60 aa, known as homeodomain (HD), through which they bind to promoter recognition elements (PRE) and either activate or repress the downstream target genes (Chang et al., 1995; Mann and Hogness, 1990). However, a mutated Antp HD, which exhibits no DNA-binding activity, has been shown to repress the Ey function in eye discs through direct protein-protein interaction (Plaza et al., 2008). The experiments aimed at elucidating the *in vivo* non DNA-binding functions of Antp using mutated *Antp* constructs, surprisingly significantly repressed the NB7-3 duplication phenotype observed in *Antp* mutants. However, the cell survival phenotype observed in anterior thoracic segments could not be rescued by these constructs. Both the phenotypes observed in *Antp* mutants were completely rescued using Wt-*Antp* expression. These observations confirm that Notch-mediated apoptosis of EW2sib and EW3sib neurons requires the functional HD with DNA-binding activity. Similar to the molecular mechanism of direct activation of the proapoptotic gene *reaper* (*rpr*) by *Dfd* in the ectoderm (Lohmann et al., 2002), the EW2sib and EW3sib neuron apoptosis in the NB7-3 lineage might involves *Hox*-dependent activation of proapoptotic gene. It is however not clear whether this effect is direct or not. The significant degree of duplication phenotype rescue in *Antp* mutants following overexpression of mutated HD versions, *AntpK50* and *AntpA50,A51*, that lost the DNA-binding activity due to a

key amino acid change at 50th position in the HD (Trelsman et al., 1989), suggests the involvement of a non DNA-binding function of Antp.

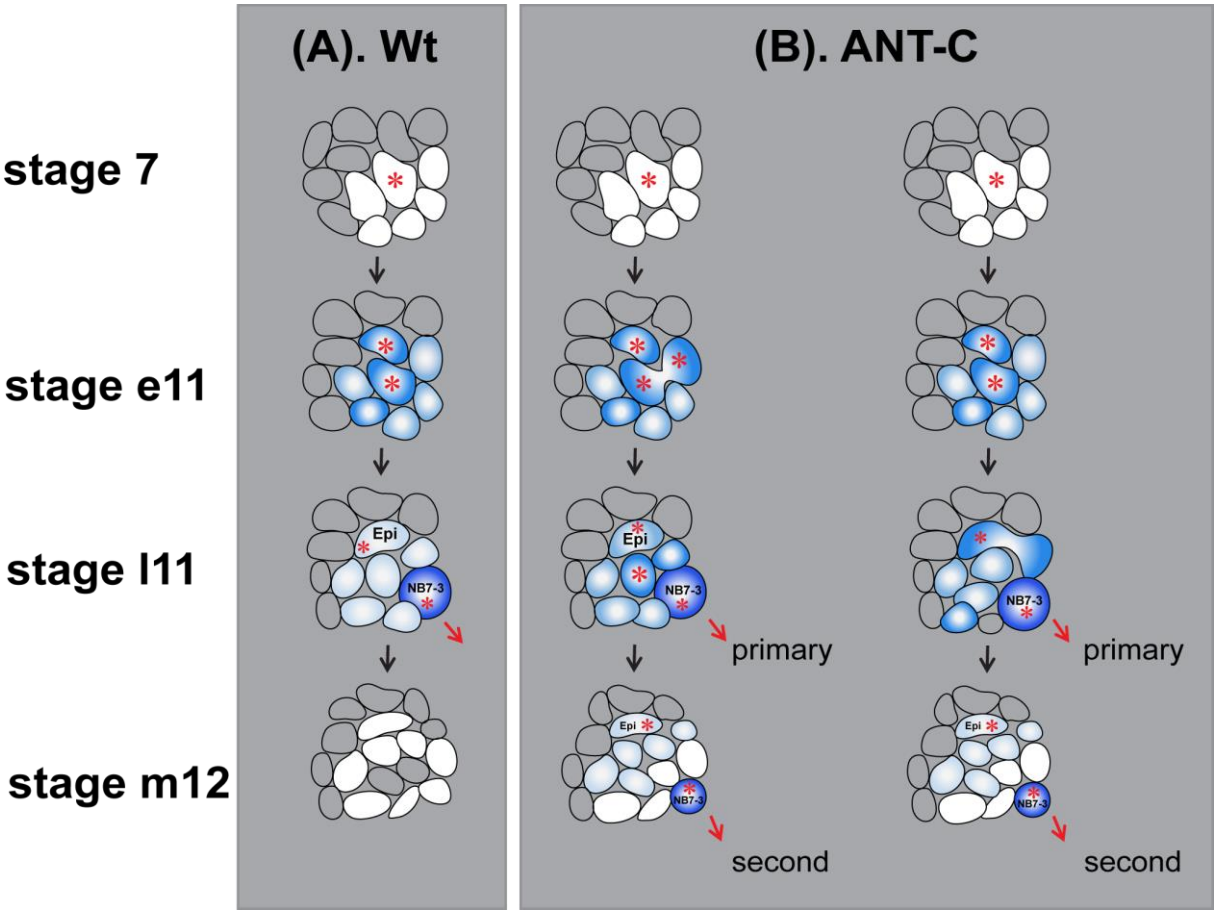

Fig. 47. Schematic model showing possible division modes of the 7-3 proneural precursor in ANT-C mutants with duplication phenotype.
Scematic model explaining the possible NB7-3 formation modes in anterior thoracic segments of Wt (A) and ANT-C mutants (B) with duplication phenotype. The 7-3 NEP and its derivatives are denoted with an asterisk (*) and the delaminating NBs is marked with a red arrow. The dynamic expression pattern of proneural genes in the 7-3 neuroectodermal cluster is shown with different shades of blue. (A) In Wt, 7-3 NEP often divides once before specification and gives rise to two cells, one of which differentiates as a NB and another as an epidermoblast. The specification and delamination of the NB7-3 from the proneural cluster occurs at late stage 11. Shortly after NB delamination, proneural gene expression within the neuroectoderm is diminished and lost. (B) In ANT-C mutants with NB7-3 duplication, the 7-3 NEP divides one more time within the neuroectoderm and allows sequential segregation of two NBs instead of one by maintaing proneural gene expression. This abnormal aditional division can take place in one of the two modes shown. In the first mode, the normal division of the 7-3 NEP generates two cells, which subseuently develop as epidermoblast and neuroblast. An aberrant additional division in a cell with higher neural potential leads to the formation of two NBs, one of which delaminates at the normal developmental stage, whereas the second one delaminates later. Otherwise, the first division leads to the formation of an NB and an NEP, wherby the latter divides after the NB segregation and give rise to the second NB and an epidermoblast. The proneural cluster is segment-specifically maintained in the mutants until mid stage 12 to allow segregation of the second NB.

Duplication of 7-3 NBs certainly takes place through the convergence of two independent mechanisms regulating additional division and proneural gene expression maintenance in the neuroectoderm. Further functional dissection using Wt-*Antp* and *AntpK50* clarified that a functional HD is needed to repress proneural gene expression after segregation of the primary NB7-3. Thus, the duplication phenotype rescue using *AntpK50* overexpression is most likely achieved by controlling the additional division within the neuroectoderm. The possible Ey interaction with Antp in regulating neuroectodermal cell division was ruled out by analyzing the *ey* loss- and gain-of-function. It has been shown that the segment-polarity gene *wingless* (*wg*) regulates the neuroectodermal divisions (Hartenstein et al., 1994). A possible direct interaction of the Antp protein with segment-polarity proteins Engrailed (En) or Hedgehog (Hh) might regulate additional division in the neuroectoderm. Across the tested *Antp* mutants, proneural gene expression is equally and segment-specifically maintained, irrespective of the duplication frequency that they exhibit. Similarly, the NB7-3 proneural cluster is also segment-specifically maintained in HD-deficient *Dfd* and *Scr* mutants. The rescue experiments using mutated HD construct *AntpK50* could not repress proneural gene expression after delamination of the primary NB. These observations confirm that a *Hox*-dependent transcriptional regulation is needed for this function. However, these assertions still do not help to elucidate why *Antp*, *Scr* and *Dfd* gene loss retains proneural gene expression in 7-3 clusters. Are they reactivating proneural genes or maintaining their expression? Ectopic *Antp* experiments in Wt show that it represses neither NB7-3 proneural gene expression within the neuroectoderm nor the NB formation. Thus, it is possible that it acts through E(spl) proteins to repress proneural gene expression after NB segregation. The E(spl)-C proteins repress proneural genes by sequestering their transcriptional activators of the proneural genes in 'poisoned' heterodimers (Benezra et al., 1990; Ellis et al., 1990; Garrell and Modolell, 1990), making them incapable of transcriptional activation. Alternatively, they could block proneural gene transcription directly by binding to the control regions of these genes. None of the E(spl)-C proteins accumulate, if the signalling is disrupted in *Notch*, *Delta* and *neuralised* mutations (Knust et al., 1992). However, in *Antp* mutants E(spl) expression is observed in all cells of the proneural cluster, except in the two segregated 7-3 NBs, suggesting that its expression is not defective. This observation could favor the reactivation of the proneural gene expression in the cluster after

primary NB7-3 segregation. However, NB7-3 specific proneural gene expression is continuously seen within the neuroectoderm until the second NB7-3 segregation takes place. Segment polarity proteins Gooseberry and Naked have been shown to act on the cis-regulatory regions of proneural genes *achaete* and *scute* and repress them to maintain their expression domains (Skeath et al., 1992). It is possible that reduced En expression in the neuroectoderm of *Antp* mutants results in prolonged expression of the proneural gene *l'sc*. A detailed study in this direction may help to elucidate how *Hox* genes regulate proneural gene expression.

4.5. Duplication frequency is not dependent on expression of the truncated Antp protein

Analyzed *Antp* mutants in this study exhibit duplication frequencies in two ranges, some with 10 to 20% and the others with at least 60% occurrence. The frequency was observed much stronger with atleast 90% of the anterior thoracic segments in *Antp*^{25},*Ubx*^{1} (Bloomington) double mutants. The anterior *Hox* gene *Scr* and the posterior *Hox* gene *Ubx* expression patterns were not significantly different from the Wt pattern in different *Antp* mutants with low and high duplication frequencies. In addition, posteriorly extended expression of Scr in the Lab and T1 segment at stage 11 and 12 of *Antp* mutants could not rescue the phenotype in that segment, suggesting that only early and sufficient amounts can rescue this phenotype. Recombination of different *Ubx* mutants with the weakly penetrant *Antp*^{25} and *Antp*^{11} mutants has no profound effect on duplication phenotype strength. Conversely, all the single *Antp*$^{25\ seg}$ mutants segregated from the *Antp*^{25},*Ubx*^{1} (Bloomington) double mutant maintain the high duplication frequency, suggesting that *Ubx* does not play a role in enhancing this phenotype. Molecular mapping analysis of *Antp* coding regions in single *Antp*^{25} and *Antp*^{25},*Ubx*^{1} (Bloomington) double mutants shows the identical non-sense point mutation that leads to protein truncation at 123 aa. Promoter-specific *Antp* RNA expression analysis revealed no distinguishable differences between the *Antp* mutants. However, the *Antp*^{25} and *Antp*^{11} mutants that are characterized by lower duplication frequency show certain amount of early embryonic Antp protein expression, as opposed to mutants with high duplication frequencies. Early protein expression differences in these two mutants suggest that an additional mutation is

present in *Antp*^{25},*Ubx*^{1} (Bloomington) and its derivative *Antp*$^{25\ seg}$ mutants. This assertion can, however, only be investigated through sequencing of the complete *3* chromosome analysis in both *Antp* mutants. The attempts made through complementation analysis to idenitfy any additional lethal mutation lying on the *3R* chromosome in strongly penetrant mutant revealed none. The additional mutation is likely to play a regulatory role, acting either through repressing translation or degrading the truncated protein. However, rescue experiments with the truncated protein could not suppress the duplication phenotype, thus defying the hypothesis that early protein expression and phenotype strength are correlated. Alternatively, it can be postulated that additional co-factors that are involved in regulating the early neuroectodermal divisions are differently impaired. It has been shown that the accumulation of additional region-specific homeotic gene products or accessory proteins (e.g. *extradenticle, cap n*' *collar*, *teashirt*, *spalt, homothorax*) has a profound effect on the phenotypic consequences of *Hox* gene function (Andrew et al., 1994; Kuhnlein et al., 1994; Gonzalez-Crespo and Morata, 1995; Mohler et al., 1995; Ryoo and Mann, 1999). It is likely that accessory proteins are incapable of functioning efficiently in strongly penetrant *Antp* mutants. It would be interesting to identify those co-factors involved in additional neuroectodermal division.

5. Summary

The homeotic (*Hox*) genes specify the segmental identities along the anterior-posterior body axis. During *Drosophila* ventral nerve cord development, the *Hox* genes play a major role in many aspects of neurogenesis like neural cell fate specification, cell number, apoptosis and proper differentiation of the neurons at embryonic and post-embryonic development in a segmental manner. This study informed that Antennapedia complex (ANT-C) genes *Deformed* (*Dfd*), *Sex combs reduced* (*Scr*) and *Antennapedia* (*Antp*) control the number and size of NB7-3 lineages in a segment-specific manner. Analysis of NB7-3 lineages in these mutants shows a two-step *Hox* gene control at early and late embryonic phases of development. They exhibit prolonged survival of early dying neurons within this lineage until late developmental stages and importantly complete lineage duplication phenotype in a segment-specific way. Detailed study of the duplication phenotype in *Antp* mutants reveals that it arises from two sequentially delaminating neural stem cells (neuroblasts, NBs). In early *Antp* mutant embryos the neuroectodermal precursor (NEP) of NB7-3 performs an additional cell division before it attains neural identity. Both daughter cells subsequently delaminate as

NB7-3 in a segment-specific manner due to prolonged proneural gene expression in the mutant. The study reveals that a *Hox* mediated simultaneous cell division and specification program can intersect in the neuroectoderm to control the number of delaminating neural stem cells.

The *Hox* genes encode transcription factors that control the expression of downstream target genes through a common 60 amino acid domain, the homeodomain, which is involved in DNA-binding. The results in this study revealed that a combination of novel *in vivo* DNA-binding activity-dependent and -independent functions of ANT-C proteins are involved in regulating the neural stem cells arising from the NB7-3 proneural cluster. Regulation of cell division within the 7-3 NEP does not require the Hox DNA-binding function, but this function is necessary for prompt repression of proneural gene expression after NB delamination and, subsequently, for execution of proper apoptosis of NB7-3 progeny cells.

6. References

Abbott, M.K. and Kaufman, T.C. (1986). The relationship between the functional complexity and the molecular organization of the Antennapedia locus of Drosophila melanogaster. *Genetics* **114**, 919-942.

Affolter, M., Percival-Smith, A., Müller, M., Leupin, W., Gehring, W.J. (1990). DNA binding properties of the purified Antennapedia homeodomain. *Proc. Natl. Acad. Sci. USA* **87**, 4093-4097.

Akam, M. (1987). The molecular basis for metameric pattern in the Drosophila embryo. *Development* **101**, 1-22.

Alberts, B., Johnson, A., Lewis, J., Raff, M., Roberts, K., Walter. P. (2002). Homeotic selector Genes and the Patterning of the Anteroposterior Axis. *Molecular Biology of the Cell*. **4**th edition.

Andrew, D.J., Horner, M.A., Petitt, M.G., Smolik, S.M., Scott, M.P. (1994). Setting limits on homeotic gene function: restraint of Sex combs reduced activity by teashirt and other homeotic genes. *EMBO J.* **13,** 1132-1144.

Appel, B. and Sakonju, S. (1993). Cell-type-specific mechanisms of transcriptional repression by the homeotic gene products Ubx and abd-A in Drosophila embryos. *EMBO J.* **12**, 1099-1109.

Bateman, J.R., Lee, A.M., Wu, C.T. (2006). Site-specific transformation of Drosophila via phiC31 integrase-mediated cassette exchange. *Genetics* **173**, 769-777.

Baumgardt, M., Karlsson, D., Salmani, B.Y., Bivik, C., MacDonald, R.B., Gunnar, E., Thor, S. (2014). Global Programmed Switch in Neural Daughter Cell Proliferation Mode Triggered by a Temporal Gene Cascade. *Dev. Cell* **30**, 192-208.

Beachy, P.A., Krasnow, M.A., Gavis, E.R., Hogness, D.S. (1988). An Ultrabithorax protein binds sequences near its own and the Antennapedia P1 promoters. *Cell* **55**, 1069-1081.

Bello, B.C., Hirth, F., Gould, A.P. (2003). A pulse of the Drosophila Hox protein Abdominal-A schedules the end of neural proliferation via neuroblast apoptosis. *Neuron* **37**, 209-219.

Benezra, R., Davis, R.L., Lockshon, D., Turner, D.L., Weintraub, H. (1990). The protein Id: a negative regulator of helix-loop-helix DNA binding proteins. *Cell* **61**, 49-59.

Berger, C., Kannan, R., Myneni, S., Renner, S., Shashidhara, L.S., Technau, G.M. (2010). Cell cycle independent role of Cyclin E during neural cell fate specification in Drosophila is mediated by its regulation of Prospero function. *Dev*. *Biol*. **337**, 415-24.

Berger, C., Pallavi, S.K., Prasad, M., Shashidhara, L.S., Technau, G.M. (2005). A critical role for Cyclin E in cell fate determination in the central nervous system of Drosophila melanogaster. *Nat. Cell Biol.* **7**, 56-62.

Berger, C., Urban, J., Technau, G.M. (2001). Stage-specific inductive signals in the Drosophila neuroectoderm control the temporal sequence of neuroblast specification. *Development* **128**, 3243-3251.

Bermingham, J.R., Martinez Arias, A., Petitt, M.G., Scott, M.P. (1990). Different patterns of transcription from the two Antennapedia promoters during Drosophila embryogenesis. *Development* **109**, 553-66.

Bhat, K.M. (1996). The patched signaling pathway mediates repression of gooseberry allowing neuroblast specification by wingless during Drosophila neurogenesis. *Development* **122**, 2921-32.

Bhat, K.M. (1999). Segment polarity genes in neuroblast formation and identity specification during Drosophila neurogenesis. *Bioessays* **21**, 472-85.

Bhat, K.M. and Schedl, P. (1997). Requirement for engrailed and invected genes reveals novel regulatory interactions between engrailed/invected, patched, gooseberry and wingless during Drosophila neurogenesis. *Development* **124**,1675-88.

Bier, E., Vaessin, H., Younger-Shepherd, S., Jan, L.Y., Jan, Y.N. (1992). deadpan, an essential pan-neural gene in Drosophila, encodes a helix-loop-helix protein similar to the hairy gene product. *Genes Dev.* **6**, 2137-51.

Billeter, M., Qian, Y.Q., Otting, G., Mfiller, M., Gehring, W.J., Wfithrich, K. (1990). Determination of the three-dimensional structure of the Antennapedia homeo domain from Drosophila in solution by 1H nuclear magnetic resonance spectroscopy. *J*. *Mol*. *Biol*. **214**, 183-197.

Birkholz, O., Rickert, C., Berger, C., Urbach, R., Technau, G.M. (2013a). Neuroblast pattern and identity in the Drosophila tail region and role of doublesex in the survival of sex-specific precursors. *Development* **140**, 1830-42.

Birkholz, O., Rickert, C., Nowak, J., Coban, Ivo C., Technau G.M. (2015). Bridging the gap between postembryonic cell lineages and identified embryonic neuroblasts in the ventral nerve cord of Drosophila melanogaster. *Biol. open* **4**, 420-434.

Birkholz, O., Vef, O., Rogulja-Ortmann, A., Berger, C., Technau, G.M. (2013b). Abdominal-B and caudal inhibit the formation of specific neuroblasts in the Drosophila tail region. *Development* **140**, 3552-64.

Bischof, J., Maeda, R.K., Hediger, M., Karch, F., Basler, K. (2007). An optimized transgenesis system for Drosophila using germ-line-specific φC31 integrases. *Proc*. *Natl. Acad. Sci. USA* **104**, 3312-17.

Bossing, T. and Technau, G.M. (1994). The fate of the CNS midline progenitors in Drosophila as revealed by a new method for single cell labelling. *Development* **120**, 1895-06.

Bossing, T., Technau, G.M., Doe, C.Q. (1996). huckebein is required for glial development and axon pathfinding in the neuroblast 1-1 and neuroblast 2-2 lineages in the Drosophila central nervous system. *Mech. Dev.* **55**, 53--64.

Bossing, T., Udolph, G., Doe, C.Q., Technau, G.M. (1996). The embryonic central nervous system lineages of Drosophila melanogaster. I. Neuroblast lineages derived from the ventral half of the neuroectoderm. *Dev. Biol.* **179**, 41-64.

Boulianne, G.L., de la Concha, A., Campos-Ortega, J.A., Jan, L.Y., Jan, Y.N. (1991). The Drosophila neurogenic gene neuralized encodes a novel protein and is expressed in precursors of larval and adult neurons. *EMBO J.* **10**, 2975-83.

Brand, A.H. and Perrimon, N. (1993). Targeted gene expression as a means of altering cell fates and generating dominant phenotypes. *Development* **118**, 401-415.

Brand, M. and Campos-Ortega, J.A. (1988). Two groups of interrelated genes regulate early neurogenesis in Drosophila melanogaster. *Roux's Arch. Dev. Biol.* **197**, 457-470.

Bray, S.J., Burke, B., Brown, N.H., Hirsh, J. (1989). Embryonic expression pattern of a family of Drosophila proteins that interact with a central nervous system regulatory element. *Genes Dev*. **3**, 1130-1145.Peterson, C., Carney, G.E., Taylor, **B.J., White, K.** (2002). reaper is required for neuroblast apoptosis during Drosophila development. *Development* **129,** 1467-1476.

Broadus, J., Skeath, J.B., Spana, E.P., Bossing, T., Technau, G., Doe, C.Q. (1995). New neuroblast markers and the origin of the aCC/pCC neurons in the Drosophila central nervous system. *Mech. Dev.* **53***,* 393-402.

Brodu, V., Elstob, P.R., Gould, A.P. (2002). abdominal A specifies one cell type in Drosophila by regulating one principal target gene. *Development* **129**, 2957-2963.

Bronner, G., Chu-LaGraff, Q., Doe, C.Q., Cohen, B., Weigel, D., Taubert, H., Jaeckle, H. (1994). Sp1/egr-like zinc-finger protein required for endoderm specification and germ-layer formation in Drosophila. *Nature* **369**, 664-668.

Cabrera, C.V. (1990). Lateral inhibition and cell fate during neurogenesis in Drosophila: the interactions between scute, Notch and Delta. *Development* **109**, 733-42.

Cabrera, C.V., Martinez Arias, A., Bate, M. (1987). The expression of three members of the achaete-scute gene complex correlates with neuroblast segregation in Drosophila. *Cell* **50**, 425-433.

Capovilla, M., Brandt, M., Botas, J. (1994). Direct regulation of decapentaplegic by Ultrabithorax and its role in Drosophila midgut morphogenesis. *Cell* **76**, 461-475.

Carroll, S.B., Laymon, R.A., McCutcheon, M.A., Riley, P.D., Scott, M.P. (1986). The localization and regulation of Antennapedia protein expression in Drosophila embryos. *Cell* **47**, 113-122.

Castelli-Gair, J.E., Greig, S., Micklem, G., Akam, M.E. (1994). Dissecting the temporal requirements for homeotic gene function. *Development* **120,** 1983-1995.

Castelli-Gair, J.E., Micol, J.L., Garcia-Bellido, A. (1990). Transvection in the Drosophila Ultrabithorax gene: a Cbx^1mutant allele induces ectopic expression of a normal allele in trans. *Genetics* **126**, 177-184.

Caudy, M., Vassin, H., Brand, M., Tuma, R., Jan, L.Y., Jan, Y.N. (1988a). daughterless, a Drosophila gene essential for both neurogenesis and sex determination, has sequence similarities to myc and the achaete-scute complex. *Cell* **55**, 1061-1067.

Cenci, C. and Gould, A.P. (2005). Drosophila Grainyhead specifies late programmes of neural proliferation by regulating the mitotic activity and Hox-dependent apoptosis of neuroblasts. *Development* **132**, 3835-3845.

Chang, Y.L., King, B.O., O'Connor, M., Mazo, A., Huang, D.H. (1995). Functional reconstruction of trans regulation of the Ultrabithorax promoter by the products of two antagonistic genes, trithorax and Polycomb. *Mol. Cell. Biol.* **15**, 6601-6612.

Christensen, S., Cook, K., Cook, K. (2008). Isolation and characterization of Df(2R)BSC422. *FlyBase* report.

Chu-LaGraff, Q. and Doe, C.Q. (1993). Neuroblast specification and formation regulated by wingless in the Drosophila CNS. *Science* **261**, 1594-1597.

Chu-LaGraff, Q., Schmid, A., Leidel, J., G., B., Jäckle, H. and Doe, C. Q. (1995). huckebein specifies aspects of CNS precursor identity required for motoneuron axon pathfinding. *Neuron* **15**, 1041-51.

Cubas, P., de Celis, J.F., Campuzano, S., Modolell, J. (1991). Proneural clusters of achaete-scute expression and the generation of sensory organs in the Drosophila imaginal wing disc. *Genes Dev***. 5**, 996-1008.

Cui, X. and Doe, C.Q. (1995). The role of the cell cycle and cytokinesis in regulating neuroblast sublineage gene expression in the Drosophila CNS. *Development* **121**, 3233-3243.

de la Concha, A., Dietrich, U., Weigel, D., Campos-Ortega, J.A. (1988). Functional interactions of neurogenic genes of Drosophila melanogaster. *Genetics* **118**, 499-508.

Deshpande, N., Dittrich, R., Technau, G.M., Urban, J. (2001). Successive specification of Drosophila neuroblasts NB 6-4 and NB 7-3 depends on interaction of the segment polarity genes wingless, gooseberry and naked cuticle. *Development* **128**, 3253-3261.

Dittrich, R., Bossing, T., Gould, A.P., Technau, G.M., Urban, J. (1997). The differentiation of the serotonergic neurons in the Drosophila ventral nerve cord depends on the combined function of the zinc finger proteins Eagle and Huckebein. *Development* **124**, 2515-2525.

Doe, C.Q. (1992). Molecular markers for identified neuroblasts and ganglion mother cells in the Drosophila central nervous system. *Development* **116**, 855-863.

Doe, C.Q. and Goodman, C.S. (1985). Early events in insect neurogenesis. II. The role of cell interactions and cell lineages in the determination of neuronal precursor cells. *Devi Biol*. **III** , 206-219.

Doe, C.Q. and Scott, M.P. (1988). Segmentation and homeotic gene function in the developing nervous system of Drosophila. *Trends Neurosci*. **11**, 101-106.

Duboule, D. and Morata, G. (1994). Colinearity and functional hierarchy among genes of the homeotic complexes. *Trends Genet*. **10**, 358-364.

Edgar, B.A. and Datar, S.A. (1996). Zygotic degradation of two maternal Cdc25 mRNAs terminates Drosophila's early cell cycle program. *Genes Dev.* **10**, 1966-1977.

Edgar, B.A. and O'Farrell, P.H. (1989). Genetic control of cell division patterns in the Drosophila embryo. *Cell* **57**, 177-187.

Edgar, B.A. and O'Farrell, P.H. (1990). The three postblastoderm cell cycles of Drosophila embryogenesis are regulated in G2 by string. *Cell* **62**, 469-480.

Edgar, B.A., Lehman, D.A., O'Farrell, P.H. (1994). Transcriptional regulation of string (cdc25): a link between developmental programming and the cell cycle. *Development* **120**, 3131-3143.

Ekker, S.C., Young, K.E., Von Kessler, D.P., Beachy, P.A. (1991). Optimal DNA sequence recognition by the Ultrabithorax homeodomain of Drosophila. *EMBO J.* **10**, 1179-1186.

Ellis, H.M., Spann, D.R., Posakony, J.W. (1990). extramacrochaetae, a negative regulator of sensory organ development in Drosophila, defines a new class of helix-loop-helix proteins. *Cell* **61**, 27-38.

Foe, V.E. (1989). Mitotic domains reveal early commitment of cells in Drosophila embryos. *Development* **107**, 1-22.
Fraenkel, E. and Pabo, C.O. (1998). Comparison of X-ray and NMR structures for the Antennapedia homeodomain-DNA complex. *Nat Struct. Biol.* **5**, 692-7.
Garrell, J. and Modolell, J. (1990). The Drosophila extramacrochaetae locus, an antagonist of proneural genes that, like these genes, encodes a helix-loop-helix protein. *Cell* **61**, 39-48.
Gebelein, B., McKay, D.J., Mann, R.S. (2004). Direct integration of Hox and segmentation gene inputs during Drosophila development. *Nature* **431**, 653-659.
Gehring, W.J. (1993). The homeobox in perspective. *Trends Biochem Sci*. **17**, 277-80.
Gehring, W.J., Kloter, U., Suga, H. (2009). Evolution of the Hox gene complex from an evolutionary ground state. *Curr. Top. Dev. Biol*. **88**, 35–61
Gonzalez-Crespo, S. and Morata, G. (1995). Control of Drosophila adult pattern by extradenticle. *Development* **121,** 2117-2125.
Gonzalez-Reyes, A. and Morata, G. (1990). The developmental effect of overexpressing a Ubx product in *Drosophila* embryos is dependent on its interactions with other homeotic products. *Cell* **61**, 515-522.
Grienenberger, A., Merabet, S., Manak, J., Iltis, I., Fabre, A., Berenger, H., Scott, M.P., Pradel, J., Graba, Y. (2003). Tgfbeta signaling acts on a Hox response element to confer specificity and diversity to Hox protein function. *Development* **130**, 5445-5455.
Hafen, E., Kuroiwa, A., Gehring, W.J. (1984). Spatial distribution of transcripts from the segmentation gene fushi tarazu during Drosophila embryonic development. *Cell* **37**, 833-841.
Harding, K. and Levine, M. (1998). Gap genes define the limits of antennapedia and bithorax gene expression during early development in Drosophila. *EMBO J*. **7**, 205-14.
Harding, K., Wedeen, C., McGinnis, W., Levine, M. (1985). Spatially regulated expression of homeotic genes in Drosophila. *Science* **229**, 1236-1242.
Hartenstein, V. and Campos-Ortega, J.A. (1984). Early neurogenesis in wild-type Drosophila melanogaster. *Rouxs Arch. Dev. Biol.* **193**, 308-325.
Hartenstein, V. and CamposOrtega, J. A. (1985). Fate-mapping in wild-type Drosophila melanogaster. *Roux's Arch. of Dev. Bio.* **194**, 181-195.
Hartenstein, V. and Wodarz, A. (2013). Initial neurogenesis in Drosophila. *Wiley Interdiscip Rev. Dev. Biol*. **2**, 701–721.
Hartenstein, V., Rudloff, E., and Campos-Ortega, J.A. (1987). The pattern of proliferation of the neuroblasts in the wild-type embryo of Drosophila melanogaster. *Rouxs Arch. Dev. Biol.* **196**, 473-485.
Hartenstein, V., Younossi-Hartenstein, A., Lekven, A. (1994). Delamination and division in the Drosophila neurectoderm: spatiotemporal pattern, cytoskeletal dynamics, and common control by neurogenic and segment polarity genes. *Dev. Biol.* **165**, 480-499.
Hersh, B.M. and Carroll, S.B. (2005). Direct regulation of knot gene expression by Ultrabithorax and the evolution of cis-regulatory elements in Drosophila. *Development* **132**, 1567-1577.
Higashijima, S., Shishido, E., Matsuzaki, M., Saigo, K. (1996). eagle, a member of the steroid receptor gene superfamily, is expressed in a subset of neuroblasts and regulates the fate of their putative progeny in the Drosophila CNS. *Development* **122**, 527-536.
Hirth, F., Hartmann, B., Reichert, H. (1998). Homeotic gene action in embryonic brain development of Drosophila. *Development* **125**, 1579-1589.
Ingham, P.W. (1988). The molecular genetics of embryonic pattern formation in Drosophila. *Nature* **335**, 25-34.
Irish, V.F., Martinez Arias, A., Akam, M. (1989). Spatial regulation of the Antennapedia and Ultrabithorax homeotic genes during Drosophila early development. *EMBO J.* **8**, 1527-1537.
Isshiki, T., Pearson, B., Holbrook, S., Doe, C.Q. (2001). Drosophila neuroblasts sequentially express transcription factors which specify the temporal identity of their neuronal progeny. *Cell* **106**, 511-521.
Isshiki, T., Takeichi, M., Nose, A. (1997). The role of the msh homeobox gene during Drosophila neurogenesis: implication for the dorsoventral specification of the neuroectoderm. *Development* **124**, 3099-3109.

Jennings, B., Preiss, A., Delidakis, C., Bray, S. (1994). The Notch signalling pathway is required for Enhancer of split bHLH protein expression during neurogenesis in the Drosophila embryo. *Development* **120**, 3537-3548.
Jimenez, F. and Campos-Ortega, J.A. (1979). A region of the Drosophila genome necessary for CNS development. *Nature* **282**, 310-312.
Jiménez, F. and Campos-Ortega, J.A. (1987). Genes in subdivision 1B of the Drosophila *melanogaster* X-chromosome and their influence on neural development. *J. Neurogenet.* **4**,179-200
Jiménez, F. and Campos-Ortega, J.A. (1990). Defective neuroblast commitment in mutants of the *achaete-scute* complex and adjacent genes of D. melanogaster. *Neuron* **5**, 81-89.
Johnston, L.A., Ostrow, B.D., Jasoni, C., Blochlinger, K. (1998). The homeobox gene cut interacts genetically with the homeotic genes proboscipedia and Antennapedia. *Genetics* **149**, 131-142.
Jones, L., Richardson, H., Saint, R. (2000). Tissue-specific regulation of cyclin E transcription during Drosophila melanogaster embryogenesis. *Development* **127**, 4619-4630.
Kammermeier, L., Leemans, R., Hirth, F., Flister, S., Wenger, U., Walldorf, U., Gehring, W.J., Reichert, H. (2001). Differential expression and function of the Drosophila Pax6 genes eyeless and twin of eyeless in embryonic central nervous system development. *Mech. Dev.* **103**, 71-78.
Kannan, R., Berger, C., Myneni, S., Technau, G.M., Shashidhara, L.S. (2010). Abdominal-A mediated repression of Cyclin E expression during cell-fate specification in the Drosophila central nervous system. *Mech. Dev*. **127**, 137-145.
Karcavich, R. and Doe, C.Q. (2005). Drosophila neuroblast 7-3 cell lineage: a model system for studying programmed cell death, Notch/Numb signaling, and sequential specification of ganglion mother cell identity. *J Comp. Neurol.* **481**, 240-51.
Karlsson, D., Baumgardt, M., Thor, S. (2010). Segment-specific neuronal subtype specification by the integration of anteroposterior and temporal cues. *PLoS Biol.* **8**, e1000368.
Kassis J.A. (1990). Spatial and temporal control elements of the Drosophila engrailed gene. *Genes Dev.* **4**, 433-43.
Kaufman, T.C., Seeger, M.A., Olsen, G. (1990). Molecular and genetic organization of the Antennapedia gene complex of Drosophila melanogaster. *Adv. Genet*. **27**, 309-362.
Kidd, S., Kelley, M.R., Young, M.W. (1986). Sequence of the Notch locus of Drosophila melanogaster: relationship of the encoded protein to mammalian clotting and growth factors. *Mol. Cell. Biol.* **6**, 3094-3108.
Klambt, C., Knust, E., Tietze, K., Campos-Ortega, J.A. (1989). Closely related transcripts encoded by the neurogenic gene complex Enhancer of split of Drosophila melanogaster. *EMBO J.* **8**, 203-210.
Knoblich, J.A., Sauer, K., Jones, L., Richardson, H., Saint, R., Lehner, C.F. (1994). Cyclin E controls S phase progression and its down-regulation during Drosophila embryogenesis is required for the arrest of cell proliferation. *Cell* **77**, 107-120.
Knust, E., Bremer, K.A., Vassin, H., Ziemer, A., Tepass, U., Campos-Ortega, J.A. (1987). The Enhancer of split locus and neurogenesis in Drosophila melanogaster. *Dev. Biol*. **122**, 262-273.
Knust, E., Schrons, H., Grawe, F. and Campos-Ortega, J. A. (1992). Seven genes of the Enhancer of split complex of Drosophila melanogaster encode helix-loop-helix proteins. *Genetics* **132**, 505-518.
Kopczynski, C.C., Alton, A.K., Fechtel, K., Kooh, P.J., Muskavitch, M.A. (1988). Delta, a Drosophila neurogenic gene, is transcriptionally complex and encodes a protein related to blood coagulation factors and epidermal growth factor of vertebrates. *Genes Dev*. **2**, 1723-1735.
Kuhnlein, R.P., Frommer, G., Friedrich, M., Gonzalez-Gaitan, M., Weber, A., Wagner-Bernholz, J.F., Gehring, W.J., Jackle, H., Schuh, R. (1994). spalt encodes an evolutionarily conserved zinc finger protein of novel structure which provides homeotic gene function in the head and tail region of the Drosophila embryo. *EMBO J.* **13,** 168-179.

Kunisch, M., Haenlin, M., Campos-Ortega, J.A. (1994). Lateral inhibition mediated by the Drosophila neurogenic gene Delta is enhanced by proneural proteins. *Proc. Natl. Acad. Sci. USA* 91, 10139-10143.
Kuroiwa, A., Kloter, U., Baumgartner, P., Gehring, W.J. (1985). Cloning of the homeotic Sex combs reduced gene in Drosophila and in situ lacatization of its transcripts. *EMBO J.* **4**, 3757-3764.
Kuziora, M.A. and McGinnis, W. (1988). Autoregulation of a Drosophila homeotic selector gene. *Cell* **55**, 477-485.
Laughon, A., Boulet, A.M., Bermingham, J.R., Laymon, R.A., Scott, M.P. (1986). Structure of transcripts from the homeotic Antennapedia gene of Drosophila melanogaster: two promoters control the major protein-coding region. *Mol. Cell. Biol*. **6**, 4676-4689.
Lee, H.K. and Lundell, M.J. (2007). Differentiation of the Drosophila serotonergic lineage depends on the regulation of Zfh-1 by Notch and Eagle. *Mol. Cell. Neurosci.* **36**, 47-58.
Lehmann, R., Jimenez, F., Dietrich, U., Campos-Ortega, J.A. (1983). On the phenotype and development of mutants of early neurogenesis in Drosophila melanogaster. *Roux's Arch. Dev. Biol.* **192**, 62-74.
Lewis, E.B. (1978). A gene complex controlling segmentation in Drosophila. *Nature* **276**, 565-570.
Lewis, E.B., Knafels, J.D., Mathog, D.R., Celniker, S.E. (1995). Sequence analysis of the cis-regulatory regions of the bithorax complex of Drosophila. *Proc. Natl. Acad. Sci. USA* 92, 8403-8407.
Lieber, T., Kidd, S., Alcamo, E., Corbin, V., Young, M.W. (1993). Antineurogenic phenotypes induced by truncated Notch proteins indicate a role in signal transduction and may point to a novel function for Notch in nuclei. *Genes Dev.* **7**, 1949-1965.
Lohmann, I., McGinnis, N., Bodmer, M., McGinnis, W. (2002). The Drosophila Hox gene Deformed sculpts head morphology via direct regulation of the apoptosis activator reaper. *Cell* **110**, 457-466.
Lüer, K. and Technau, G.M. (1992). Primary culture of single ectodermal precursors of Drosophila reveals a dorsoventral prepattern of intrinsic neurogenic and epidermogenic capabilities at the early gastrula stage. *Development* **116**, 377-85.
Lüer, K. and Technau, G.M. (2009). Single cell cultures of Drosophila neuroectodermal and mesectodermal central nervous system progenitors reveal different degrees of developmental autonomy. *Neural Dev.* **4**, 30.
Lundell, M.J. and Hirsh, J. (1992). The zfh-2 gene product is a potential regulator of neuron-specific dopa decarboxylase gene expression in Drosophila. *Dev. Biol*. **154**, 84-94.
Lundell, M.J. and Hirsh, J. (1994). Temporal and spatial development of serotonin and dopamine neurons in the Drosophila CNS. *Dev. Biol*. **165**, 385-96.
Lundell, M.J. and Hirsh, J. (1998). Eagle is required for the specification of serotonin neurons and other neuroblast 7-3 progeny in the Drosophila CNS. *Development* **125**, 463-472.
Lundell, M.J., Chu-LaGraff, Q., Doe, C.Q., Hirsh, J. (1996). The *engrailed* and *huckebein* genes are essential for development of serotonin neurons in the Drosophila CNS. *Mol. Cell. Neurosci.* **7**, 46-61.
Lundell, M.J., Lee, H.K., Perez, E., Chadwell, L. (2003). The regulation of apoptosis by Numb/Notch signaling in the serotonin lineage of Drosophila. *Development* **130**, 4109-4121.
Mahaffey, J.W. and Kaufman, T.C. (1987). Distribution of the Sex combs reduced gene products in Drosophila melanogaster. *Genetics* **117**, 51-60.
Mann, R.S and Hogness, D.S. (1990). Functional dissection of Ultrabithorax proteins in D. melanogaster. *Cell* **60**, 597-610.
Mann, R.S., Lelli, K.M., Joshi, R. (2009). Hox specificity unique roles for cofactors and collaborators. *Curr. Top. Dev. Biol.* **88**, 63-101.
Martin-Bermudo, M.D., Carmena, A., Jimenez, F. (1995). Neurogenic genes control gene expression at the transcriptional level in early neurogenesis and in mesectoderm specification. *Development* **121**, 219-224.

Martin-Bermudo, M.D., Martinez, C., Rodriguez, A., Jimenez, F. (1991). Distribution and function of the lethal of scute gene product during early neurogenesis in Drosophila. *Development* **113**, 445-454.
Martinez Arias, A. and White, R.A.H. (1988). Ultrabithorax and engrailed expression in Drosophila embryos mutant for segmentation genes of the pair-rule class. *Development* **102**, 325-338.
Martinez Arias, A., Ingham, P.W., Scott, M.P., Akam, M.E. (1987). The spatial and temporal deployment of Dfd and Scr transcripts throughout development of Drosophila. *Development* **100**, 673-683.
Matsuzaki, M. and Saigo, K. (1996). hedgehog signaling independent of engrailed and wingless required for post-S1 neuroblast formation in the *Drosophila* CNS. *Development* **122**, 3567-3575.
McDonald, J.A. and Doe, C.Q. (1997). Establishing neuroblast-specific gene expression in the Drosophila CNS: huckebein is activated by Wingless and Hedgehog and repressed by Engrailed and Gooseberry. *Development* **124**, 1079-1087.
McDonald, J.A., Holbrook, S., Isshiki, T., Weiss, J., Doe, C.Q., Mellerick, D.M. (1998). Dorsoventral patterning in the Drosophila central nervous system: the vnd homeobox gene specifies ventral column identity. *Genes Dev.* **12**, 3603-3612.
McGinnis, W. and Krumlauf, R. (1992). Homeobox genes and axial patterning. *Cell* **68**, 283-302.
McGinnis, W., Levine, M.S., Hafen, E., Kuroiwa, A., Gehring, W.J. (1984). A conserved DNA sequence in homoeotic genes of the Drosophila Antennapedia and bithorax complexes. *Nature* **308**, 428-433.
Merrill, V.K., Diederich, R.J., Turner, F.R., Kaufman, T.C. (1989). A genetic and developmental analysis of mutations in labial, a gene necessary for proper head formation in Drosophila melanogaster. *Dev. Biol.* **135**, 376-391.
Merrill, V.K., Turner, F.R., Kaufman, T.C. (1987). A genetic and developmental analysis of mutations in the Deformed locus in Drosophila melanogaster. *Dev. Biol.* **122**, 379-395.
Mettler, U., Vogler, G., Urban, J. (2006). Timing of identity: spatiotemporal regulation of hunchback in neuroblast lineages of Drosophila by Seven-up and Prospero. *Development* **133**, 429-437.
Mohler, J., Mahaffey, J.W., Deutsch, E., Vani, K. (1995). Control of Drosophila head segment identity by the bZIP homeotic gene cnc. *Development* **121,** 237-247.
Nakao, K. and Campos-Ortega, J.A. (1996). Persistent expression of genes of the Enhancer of Split complex suppresses neural development in Drosophila. *Neuron* **16**, 275-286.
Novotny, T., Eiselt, R., Urban, J. (2002). Hunchback is required for the specification of the early sublineage of neuroblast 7-3 in the Drosophila central nervous system. *Development* **129**, 1027-1036.
Nusslein-Volhard, C., Frohnhofer, H.G., Lehmann, R. (1987). Determination of anteroposterior polarity in Drosophila. *Science* **238**, 1675-1681.
Ohlen, V.T. and Doe, C.Q. (2000). Convergence of Dorsal, Dpp, and Egfr signaling pathways subdivides the Drosophila neuroectoderm into three dorsal-ventral columns. *Dev. Biol.* **224**, 362-372.
Plaza, S., Prince, F., Adachi, Y., Punzo, C., Cribbs, D.L., Gehring, W.J. (2008). Cross-regulatory protein-protein interactions between Hox and Pax transcription factors. *Proc. Natl. Acad. Sci. USA* **105**, 13439-13444.
Plaza, S., Prince, F., Jaeger, J., Kloter, U., Flister, S., Benassayag, C., Cribbs, D., Gehring, W.J. (2001). Molecular basis for the inhibition of Drosophila eye development by Antennapedia. *EMBO J.* **20**, 802-811.
Preiss, A., Hartley, D.A., Artavanis-Tsakonas, S. (1988). The molecular genetics of Enhancer of split, a gene required for embryonic neural development in Drosophila. *EMBO J.* **7**, 3917-3927.
Prokop, A. and Technau, G.M. (1994). Early tagma-specific commitment of Drosophila CNS progenitor NB1-1. *Development* **120**, 2567-2578.

Prokop, A., Bray, S., Harrison, E., Technau, G.M. (1998). Homeotic regulation of segment-specific differences in neuroblast numbers and proliferation in the Drosophila central nervous system. *Mech. Dev.* **74**, 99-110.
Punzo, C., Kurata, S., Gehring, W.J. (2001). The eyeless homeodomain is dispensable for eye development in Drosophila. *Genes Dev.* **15**, 1716-1723.
Qian, Y.Q., Otting, G., Billeter, M., Müller, M., Gehring, W.J., Wüthrich, K. (1993). Nuclear magnetic resonance spectroscopy of a DNA complex with the uniformly ^{13}C-labeled Antennapedia homeodomain and structure determination of the DNA-bound homeodomain. *J. Mol. Biol.* **234**, 1070-1083.
Rao, Y., Jan, L.Y., Jan, Y.N. (1990). Similarity of the product of the Drosophila neurogenic gene big brain to transmembrane channel proteins. *Nature* **345**, 163-167.
Rogulja-Ortmann, A. and Technau, G.M. (2008) Multiple roles for Hox genes in segment-specific shaping of CNS lineages. Fly (Austin) 6, 316-319.
Rogulja-Ortmann, A., Lüer, K., Seibert, J., Rickert, C., Technau, G.M. (2007). Programmed cell death in the embryonic central nervous system of Drosophila melanogaster. *Development* **134**, 105-116.
Rogulja-Ortmann, A., Renner, S., Technau, G.M. (2008). Antagonistic roles for Ultrabithorax and Antennapedia in regulating segment-specific apoptosis of differentiated motoneurons in the Drosophila embryonic central nervous system. *Development* **135**, 3435-3445.
Ryoo, H.D. and Mann, R.S. (1999). The control of trunk Hox specificity and activity by Extradenticle. *Genes Dev.* **13,** 1704-1716.
Schmid, A., Chiba, A., Doe, C.Q. (1999). Clonal analysis of Drosophila embryonic neuroblasts: neural cell types, axon projections and muscle targets. *Development* **126**, 4653-4689.
Schmidt, H., Rickert, C., Bossing, T., Vef, O., Urban, J., Technau, G.M. (1997). The embryonic central nervous system lineages of Drosophila melanogaster: II. Neuroblast lineages derived from the dorsal part of the neuroectoderm. *Dev. Biol.,* **189**, 186-204.
Schneuwly, S., Klemenz, R., Gehring, W.J. (1987). Redesigning the body plan of *Drosophila* by ectopic expression of the homoeotic gene Antennapedia. *Nature* **325**, 816-818.
Schneuwly, S., Kuroiwa, A., Baumgartner, P., Gehring, W.J. (1986). Structural organization and sequence of the homeotic gene Antennapedia of Drosophila melanogaster. *EMBO J.* **5**, 733-739.
Scott, M.P. and Carroll, S.B. (1987). The segmentation and homeotic gene network in early Drosophila development. *Cell* **51**, 689-98.
Scott, M.P. and Weiner, A.J. (1984). Structural relationships among genes that control development: sequence homology between the Antennapedia, Ultrabithorax, and fushi tarazu loci of Drosophila. *Proc. Natl. Acad. Sci. USA* **81**, 4115-9.
Scott, M.P., Weiner, A.J., Hazelrigg, T., Polisky, B.A., Pirrotta, V., Scalenghe, F., Kaufman, T.C. (1983). The molecular organization of the Antennapedia locus of Drosophila. *Cell* **35**, 763-776.
Simon, J.A. and Tamkun, J.W. (2002). Programming off and on states in chromatin: mechanisms of polycomb and trithorax group complexes. *Curr. Opin. Genet. Dev.* **12**, 210-218.
Simpson, p. (1990). Notch and the choice of cell fate in Drosophila neuroepithelium. *Trends Genet*. **6**, 343-345.
Sivanantharajah, L. and Percival-Smith, A. (2009). Analysis of the Sequence and Phenotype of Drosophila Sex combs reduced Alleles Reveals Potential Functions of Conserved Protein Motifs of the Sex combs reduced Protein. *Genetics* **182**, 191-203.
Skeath, J.B. (1998). The Drosophila EGF receptor controls the formation and specification of neuroblasts along the dorsal-ventral axis of the Drosophila embryo. *Development* **125**, 3301-3312.
Skeath, J.B. (1999). At the nexus between pattern formation and cell-type specification: the generation of individual neuroblast fates in the Drosophila embryonic central nervous system. *BioEssays* **21**, 922-931.

Skeath, J.B. and Carroll, S.B. (1992). Regulation of proneural gene expression and cell fate during neuroblast segregation in the Drosophila embryo. *Development* **114**, 939-946.
Skeath, J.B. and Thor, S. (2003). Genetic control of Drosophila nerve cord development. *Curr. Opin. Neurobiol.* **13,** 8-15.
Skeath, J.B., Panganiban, G., Carroll, S.B. (1994). The ventral nervous system defective gene controls proneural gene expression at two distinct steps during neuroblast formation in Drosophila. *Development* **120**, 1517-1524.
Skeath, J.B., Panganiban, G., Selegue, J., Carroll, S.B. (1992). Gene regulation in two dimensions: the proneural achaete and scute genes are controlled by combinations of axis-patterning genes through a common intergenic control region. *Genes Dev.* **6**, 2606-2619.
Skeath, J.B., Zhang, Y., Holmgren, R., Carroll, S.B., Doe, C.Q. (1995). Specification of neuroblast identity in the Drosophila embryonic central nervous system by gooseberry-distal. *Nature* **376,** 427-430.
Smoller, D.A., Friedel, C., Schmid, A., Bettler, D., Lam, L., Yedvobnick, B. (1990). The Drosophila neurogenic locus mastermind encodes a nuclear protein unusually rich in amino acid homopolymers. *Genes Dev.* **4**, 1688-1700.
Sprecher, S.G., Mueller, M., Kammermeier, L., Miller, D.F.B., Kaufman, T.C., Reichert, H., Hirth, F. (2004). Hox gene cross-regulatory interactions in the embryonic brain of Drosophila. *Mech. Dev.* **121**, 527-536.
Stroeher, V. L., Jorgensen, E.M., Garber, R. L. (1986). Multiple transcripts from the Antennapedia gene of Drosophila melanogaster. *Mol. Cell. Biol.* **6**, 4667-4675.
Stroeher, V.L., Gaiser, J.C., Garber, R.L. (1988). Alternative RNA splicing that is spatially regulated: generation of transcripts from the Antennapedia gene of Drosophila melanogaster with different protein-coding regions. *Mol. Cell. Biol.* **8**, 4143-4154.
Struhl, G. and White, R.A. (1985). Regulation of the Ultrabithorax gene of Drosophila by other Bithorax complex genes. *Cell* **43**, 507-519.
Struhl, G., Fitzgerald, K., Greenwald, I. (1993). Intrinsic activity of the Lin-12 and Notch intracellular domains in vivo. *Cell* **74**, 331-345.
Suska, A., Miguel-Aliaga, I., Thor, S. (2011). Segment-specific generation of Drosophila Capability neuropeptide neurons by multi-faceted Hox cues. *Dev. Biol.* **353**, 72-80.
Taghert, P.H., Doe, C.Q., Goodman, C.S. (1984). Cell determination and regulation during development of neuroblasts and neurones in grasshopper embryos. *Nature* **307**, 163-165.
Tata, F. and Hartley, D.A. (1995). Inhibition of cell fate in Drosophila by Enhancer of split genes. *Mech. Dev.* **51**, 305-315.
Technau, G.M. and Campos-Ortega, J.A. (1987). Cell autonomy of expression of neurogenic genes of Drosophila melanogaster. *Proc. Natl. Acad. Sci. USA* **84**, 4500-4504.
Treisman, J., Gonczy, P., Vashishtha, M., Harris, E., Desplan, C. (1989). A single amino acid can determine the DNA binding specificity of homeodomain proteins. *Cell* **59**, 553-562.
Truman, J.W., Bate, M. (1988). Spatial and temporal patterns of neurogenesis in the central nervous system of Drosophila melanogaster. *Dev. Biol*. **125,** 145-157.
Tsuji, T., Hasegawa, E., Isshiki, T. (2008). Neuroblast entry into quiescence is regulated intrinsically by the combined action of spatial Hox proteins and temporal identity factors. *Development* **135**, 3859-3869.
Udolph, G., Luer, K., Bossing, T., Technau, G.M. (1995). Commitment of CNS progenitors along the dorsoventral axis of Drosophila neuroectoderm. *Science* **269**, 1278-1281.
Udolph, G., Prokop, A., Bossing, T., Technau, G.M. (1993). A common precursor for glia and neurons in the embryonic CNS of Drosophila gives rise to segment-specific lineage variants. *Development* **118**, 765-775.
Urbach, R., Jussen, D., Technau, G.M. (2016). Gene expression profiles uncover individual identities of gnathal neuroblasts and serial homologies in the embryonic CNS of Drosophila. *Development* **143**, 1290-1301.
Vachon, G., Cohen, B., Pfeifle, C., McGuffin, M.E., Botas, J., Cohen, S.M. (1992). Homeotic genes of the Bithorax complex repress limb development in the abdomen of the Drosophila embryo through the target gene Distal-less. *Cell* **71**, 437-450.

Vaessin, H., Bremer, K.A., Knust, E., Campos-Ortega, J.A. (1987). The neurogenic Gene Delta of Drosophila melanogaster is expressed in neurogenic territories and encodes a putative transmembrane protein with EGF-like repeats. *EMBO J.* **6**, 3431-3440.
Wakimoto, B.T. and Kaufman, T.C. (1981). Analysis of larval segmentation in lethal genotypes associated with the Antennapedia gene complex in Drosophila melanogaster. *Dev. Biol.* **81**, 51-64.
Walsh, C.M. and Carroll, S.B. (2007). Collaboration between Smads and a Hox protein in target gene repression. *Development* **134**, 3585-3592.
Weigmann, K. and Lehner, C.F. (1995). Cell fate specification by even-skipped expression in the Drosophila nervous system is coupled to cell cycle progression. *Development* **121**, 3713-3721.
Weinzierl, R.O.J., Axton, J.M., Ghysen, A., Akam, M.E. (1987). Ultrabithorax mutations in constant and variable regions of the protein coding sequence. *Genes Dev.* 1, 386-397.
Weiss, J.B., Von Ohlen, T., Mellerick, D.M., Dressler, G., Doe, C.Q., Scott, M.P. (1998). Dorsoventral patterning in the Drosophila central nervous system: the intermediate neuroblasts defective homeobox gene specifies intermediate column identity. *Genes Dev*. **12**, 3591-3602.
Wharton, K.A., Johansen, K.M., Xu, T., Artavanis-Tsakonas, S. (1985). Nucleotide sequence from the neurogenic locus Notch implies a gene product that shares homology with proteins containing EGF-like repeats. *Cell* **43**, 567-581.
White, K. (1980). Defective neural development in Drosophila melanogaster embryos deficient for the tip of the X chromosome. *Dev. Biol.* **80**, 332-44.
White, K., De Celles, N.L., Enlow, T.C. (1983). Genetic and developmental analysis of the locus vnd in Drosophila melanogaster. *Genetics* **104**, 433-448.
White, K., Grether, M.E., Abrams, J.M., Young, L., Farrell, K., Steller, H. (1994). Genetic control of programmed cell death in Drosophila. *Science* **264**, 677-683.
White, R.A.H. and Wilcox, M. (1985). Distribution of Ultrabithorax proteins in Drosophila. *EMBO J.* **4**, 2035-2043.
Wirz, J., Fessler, L.I., Gehring, W.J. (1986). Localization of the Antennapedia protein in Drosophila embryos and imaginal discs. *EMBO J.* **5**, 3327-3334.
Zeng, C., Pinsonneault, J., Gellon, G., McGinnis, N., McGinnis, W. (1994). Deformed protein binding sites and cofactor binding sites are required for the function of a small segment-specific regulatory element in Drosophila embryos. *EMBO J.* **13**, 2362-2377.
Zhang, Y., Ungar, A., Fresquez, C., Holmgren, R. (1994). Ectopic expression of either the Drosophila gooseberry-distal or proximal gene causes alterations of cell fate in the epidermis and central nervous system. *Development* **120**, 1151-116.

7. Appendix

Abbreviation index

°C	centrigrade
aa	aminoacid
abd A	*abdominal-A*
Abd B	*Abdominal-B*
ANT-C	*Antennapedia* complex
Antp	*Antennapedia*
AP	alkaline phosphotase
AP	anterio-posterior
APS	ammonium per sulphate
AS-C	*achaete-scute* complex
*att*P	phase attachment site
bHLH	basic Helix-Loop-Helix
bp	basepair
BX-C	*bithorax* complex
*ccd*B	control of cell death
cDNA	complementary DNA
CNS	central nervous system
DAPI	4',6-Diamidino-2-Phenylindole, Dihydrochloride
Def	deficiency
DEPC	diethlpyrocarbonate
Dfd	*Deformed*
DGRC	Drosophila Genetic Resource Center
DIG	Digoxigenin
DiI	1,1'-Dioctadecyl-3,3,3',3'-tetramethylindocarbocyanideperchlorate
DNA	deoxyribonucleic acid
DSHB	Developmental Studies Hybridoma Bank
DTT	Dithiothreitol
DV	dorso-ventral
e.g.	exempli gratia
EDTA	Ethylenediaminetetraacetic acid
et al.	and others
F1	first filial generation
Fig.	Figure
GFP	green fluorescent protein
g	gram
GMC	ganglion mother cell
HD	homeodomain
Hox	homeotic
hrs	hours
Hyb	hybridization
kb	kilobases
KCH_3COO	potassium acetate

KCl	potassium chloride
KHCO3	potassium hydrogen carbonate
Lab	Labial
lacz	βgalactosidase
LiCl	Lithium chloride
L	liter
Md	mandibular
MES	mesoectoderm
MgCl2	Magnesium chloride
mg	milligram
min	minutes
ML	midline
ml	milliliter
mM	millimolar
M	molar
mRNA	messenger RNA
Mx	maxillary
Na2HPO4.2 H2O	Disodium phosphate
NaCl	Sodium chloride
NaH2PO4 · 1 H2O	Monosodium phosphate
NB	neuroblast
ORF	open reading frame
PBS	Phosphate-buffered saline
PCR	polymerase chain reaction
POD	peroxidase
RNA	ribonucleic acid
Rpm	revolutions per minute
RT	room temperature
S1-S5	segregation wave one to five
Scr	*sex combs reduced*
SDS	sodium dodecyl sulfate
SSC	saline sodium citrate
ssDNA	salmon sperm DNA
T1-T2	anterior thoracic segments
T1-T3	thoracic segment one to three
T3-A7	third thoracic to the seventh abdominal segments
Taq	thermostable DNA polymerase
TEMED	Tetramethylethylenediamine
UAS	upstream activating sequence
Ubx	*Ultrabithorax*
UTP	uridine triphosphate
UTR	untranslated region
VNC	ventral nerve cord
Wt	wild-type
YFP	yellow fluorescent protein
µg	microgram
µl	microliter

8. Figure list

9. Vectors

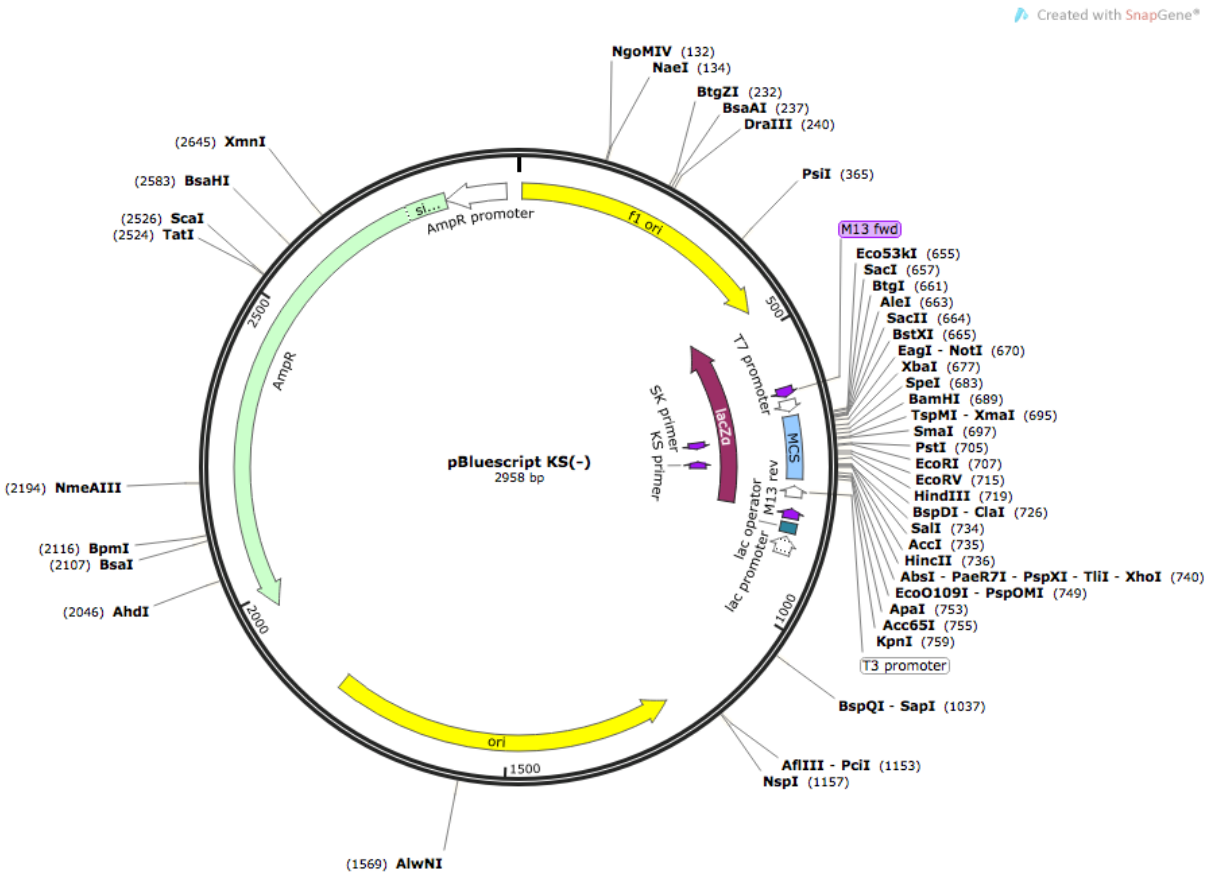
Created with SnapGene®
NgoMIV (132)
NaeI (134)
BtgZI (232)
BsaAI (237)
DraIII (240)
PsiI (365)
M13 fwd
Eco53kI (655)
SacI (657)
BtgI (661)
AleI (663)
SacII (664)
BstXI (665)
EagI - NotI (670)
XbaI (677)
SpeI (683)
BamHI (689)
TspMI - XmaI (695)
SmaI (697)
PstI (705)
EcoRI (707)
EcoRV (715)
HindIII (719)
BspDI - ClaI (726)
SalI (734)
AccI (735)
HincII (736)
AbsI - PaeR7I - PspXI - TliI - XhoI (740)
EcoO109I - PspOMI (749)
ApaI (753)
Acc65I (755)
KpnI (759)
T3 promoter
BspQI - SapI (1037)
AflIII - PciI (1153)
NspI (1157)
(1569) AlwNI
(2194) NmeAIII
(2116) BpmI
(2107) BsaI
(2046) AhdI
(2645) XmnI
(2583) BsaHI
(2526) ScaI
(2524) TatI
AmpR promoter
f1 ori
T7 promoter
MCS
lacZα
M13 rev
lac operator
lac promoter
SK primer
KS primer
AmpR
ori
pBluescript KS(-)
2958 bp
500
1000
1500
2000
2500

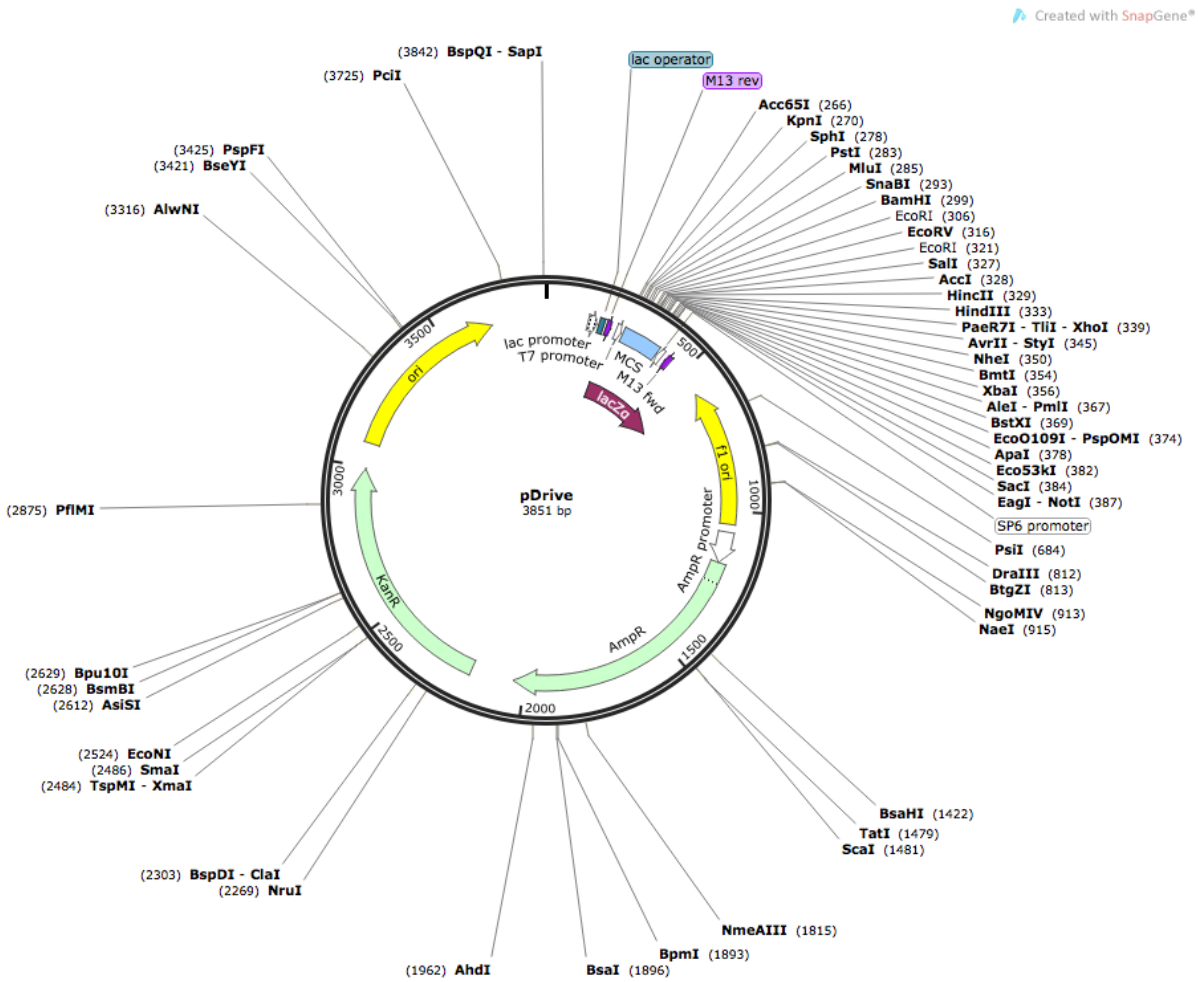
Created with SnapGene®
pDrive
3851 bp
lac promoter
T7 promoter
MCS
M13 fwd
lacZα
ori
f1 ori
AmpR promoter
AmpR
KanR
lac operator
M13 rev
SP6 promoter
(3842) BspQI - SapI
(3725) PciI
(3425) PspFI
(3421) BseYI
(3316) AlwNI
(2875) PflMI
(2629) Bpu10I
(2628) BsmBI
(2612) AsiSI
(2524) EcoNI
(2486) SmaI
(2484) TspMI - XmaI
(2303) BspDI - ClaI
(2269) NruI
(1962) AhdI
BsaI (1896)
BpmI (1893)
NmeAIII (1815)
ScaI (1481)
TatI (1479)
BsaHI (1422)
NaeI (915)
NgoMIV (913)
DraIII (812)
BtgZI (813)
PsiI (684)
Eco53kI (382)
SacI (384)
EagI - NotI (387)
ApaI (378)
EcoO109I - PspOMI (374)
BstXI (369)
AleI - PmlI (367)
XbaI (356)
BmtI (354)
NheI (350)
AvrII - StyI (345)
PaeR7I - TliI - XhoI (339)
HindIII (333)
HincII (329)
AccI (328)
SalI (327)
EcoRV (316)
EcoRI (321)
EcoRI (306)
BamHI (299)
SnaBI (293)
MluI (285)
PstI (283)
SphI (278)
KpnI (270)
Acc65I (266)

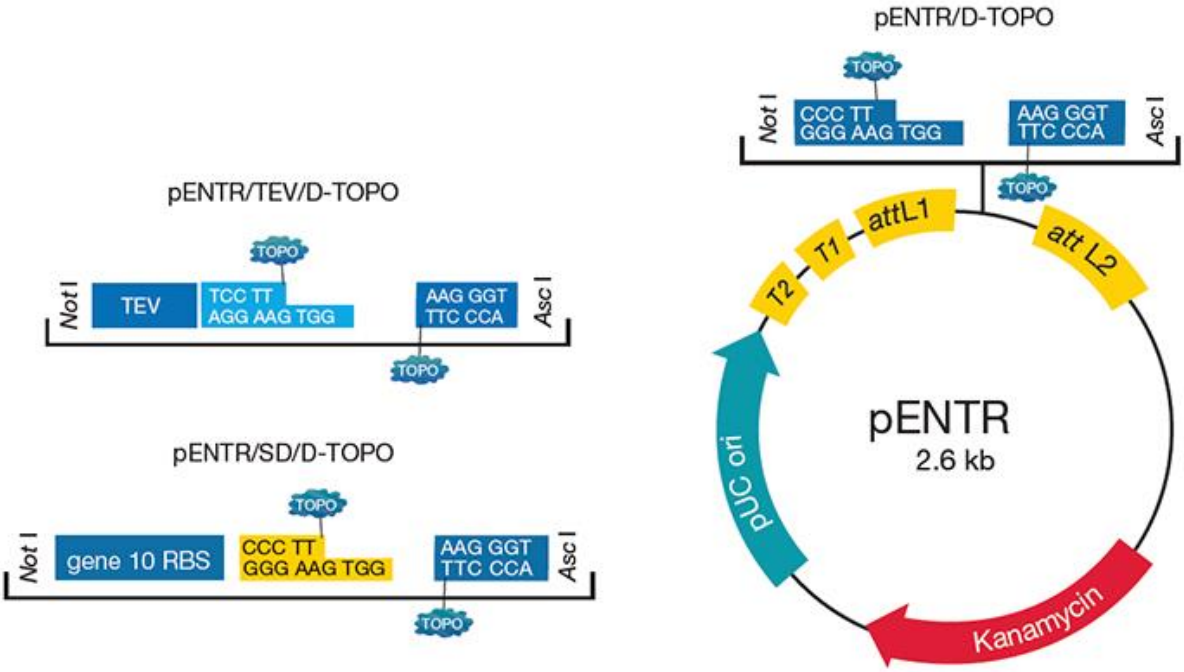
pENTR/TEV/D-TOPO
TOPO
Not I
TEV
TCC TT
AGG AAG TGG
AAG GGT
TTC CCA
Asc I
TOPO
pENTR/SD/D-TOPO
TOPO
Not I
gene 10 RBS
CCC TT
GGG AAG TGG
AAG GGT
TTC CCA
Asc I
TOPO
pENTR/D-TOPO
TOPO
Not I
CCC TT
GGG AAG TGG
AAG GGT
TTC CCA
Asc I
TOPO
attL1
T1
T2
att L2
pENTR
2.6 kb
pUC ori
Kanamycin

Declaration

Versicherung gemäß §11, Abs.3d der Promotionsordnung

1. Ich habe die als Dissertation vorgelegte Arbeit selbst angefertigt und alle benutzten Hilfemittel (Literatur, Apparaturen, Material) in der Arbeit angegeben.

2. Ich habe und hatte die als Dissertation vorgelegte Arbeit nicht als Prüfungsarbeit für eine staatliche oder andere wissenschaftliche Prüfung eingereicht.

3. Ich hatte weder die als Dissertation vorgelegte Arbeit noch Teile einer Abhandlung davon bei einer anderen Fakultät bzw. einem anderen Fachbereich als Dissertation eingereicht

Mainz,den Sudha Rani. Myneni

Appendix

Figure list